UNIVERSITY OF BIRMINGHAM

DEVELOPMENT OF KINETICS, MATHEMATICAL MODEL AND OPTIMIZATION OF FISCHER-TROPSCH SYNTHESIS ON COBALT-BASED CATALYST

By

Nima Moazami

MEng (Mechanical Engineering)

Thesis Submitted in Partial Fulfilment of Requirements for the Degree of

DOCTOR OF PHILOSOPHY

School of Mechanical Engineering
The University of Birmingham
Edgbaston, Birmingham, UK
November 2015

تقدیم

به پدرم که همواره برایم مظهر صبر، استقامت و شجاعت بود

او که در تمامی مراحل زندگی حامی و مشوق من بود

به مادرم که زیباترین شعر خداست، برایم دریای محبت بود

عشقش به مترله جان و روح من بود

به خواهر بهتراز جانم، یارو غمخوارم

کلمات نمی توانند بیان کنند چقدر اورا دوست می دارم، بی او زنده نیستم

نیما - پاییز ۹۴

ACKNOWLEDGEMENTS

Firstly, my deepest gratitude and appreciation goes to my lead supervisor, Professor Miroslaw Lech Wyszynski for the continuous encouragement, kindness, patience, support and guidance. I am tremendously thankful for his advice and direction that has enlightened me throughout the process of compiling this work.

I would like to express my sincere gratefulness to my co-supervisor, Dr Athanasios Tsolakis, not only for his useful comments and suggestions, but also for giving me an excellent opportunity to work as a teaching assistant.

I am thankful for the financial support and PhD scholarship provided by the School of Mechanical Engineering, the University of Birmingham, United Kingdom. This opportunity enables me to continue my research for the course of the doctoral studies. My thanks go to the College of Engineering and Physical Sciences, the University of Birmingham, for their partial fund for my travel to the International Conference on Applied Energy (ICAE) 2015 in Abu Dhabi, United Arab Emirates in 28-31 March 2015. My thanks go to the ProcessNet subject division Chemical Reaction Engineering, to support me for attending the ESCRE2015 conference in Fürstenfeldbruck, Germany in 27-30 October 2015.

I would like to express my deep gratitude to my friend, Kiyarash Rahbar, for his invaluable scientific support and advice. I am indebted to him for his motivation especially during my last two years of my PhD research when I was in hard time. I would like to extend an acknowledgment to my friend and colleague, Dr Hamid Mahmoudi, for his contribution in this research and especially for the willingness to entrust his experimental results. I would like

to mention that this thesis was copy edited for conventions of language, spelling and grammar by Janet's Proofreading Service.

Last, but absolutely not least, I am particularly grateful to my parents and my sister for their endless love, encouragement and support over the years. I am deeply thankful to them for enduring my absence during my research and helped me tremendously in all ways possible. They have always given me the inspiration and will always be my motivator. I would like to dedicate this work to them. This thesis is a sign of my love to them.

LIST OF PUBLICATIONS

List of Journals

I. N. Moazami, M. Wyszynski, and H. Mahmoudi, "Modelling of catalytic monolith reactor for reforming of hexadecane with exhaust gas," Elsevier, *International Journal of Hydrogen Energy,* vol. 38, pp. 11826-11839, 2013.

II. N. Moazami, M. L. Wyszynski, H. Mahmoudi, A. Tsolakis, Z. Zou, P. Panahifar, K. Rahbar, "Modelling of a fixed bed reactor for Fischer–Tropsch synthesis of simulated N_2-rich syngas over Co/SiO_2: Hydrocarbon production," Elsevier, *Fuel*, vol. 154, pp. 140-151, 8/15/2015.

III. N. Moazami, H. Mahmoudi, K. Rahbar, P. Panahifar, A. Tsolakis, and M. L. Wyszynski, "Catalytic performance of cobalt–silica catalyst for Fischer–Tropsch synthesis: Effects of reaction rates on efficiency of liquid synthesis," Elsevier, *Chemical Engineering Science*, vol. 134, pp. 374-384, 9/29/2015.

IV. N. Moazami, H. Mahmoudi, P. Panahifar, K. Rahbar, A. Tsolakis, and M. L. Wyszynski, "Mathematical Modelling and Performance Study of Fischer-Tropsch Synthesis of Liquid Fuel over Cobalt-silica," Elsevier, *Energy Procedia*, vol. 75, pp. 62-71, 8/2015.

V. N. Moazami, M. L. Wyszynski, H. Mahmoudi, K. Rahbar, A. Tsolakis, "A comprehensive kinetics study of Fischer-Tropsch synthesis mechanism over cobalt-based catalyst," Elsevier, *Chemical Engineering Science*, submitted.

VI. N. Moazami, M. L. Wyszynski, H. Mahmoudi, K. Rahbar, A. Tsolakis, "Parametric study and multi-objective optimization of hydrocarbon selectivity and syngas conversion in Fischer-Tropsch synthesis," Elsevier, *Chemical Engineering Science*, submitted.

List of Conferences

I. N. Moazami, H. Mahmoudi, P. Panahifar, K. Rahbar, A. Tsolakis, and M. L. Wyszynski, "Mathematical Modelling and Performance Study of Fischer-Tropsch Synthesis of Liquid Fuel over Cobalt-Silica," *7th International Conference on Applied Energy – ICAE2015*, Abu Dhabi, United Arab Emirates, 31/03/2015.

II. N. Moazami, H. Mahmoudi, A. Tsolakis, K. Rahbar, P. Panahifar, M. L. Wyszynski, "Mathematical modelling and chemical kinetics study of Fischer-Tropsch synthesis on a cobalt-silica catalyst," DECHEMA, *European Symposium on Chemical Reaction Engineering (ESCRE 2015)*, Fürstenfeldbruck, Germany, 28/10/2015.

III. N. Moazami, H. Mahmoudi, K. Rahbar, P. Panahifar, A. Tsolakis, and M. L. Wyszynski, "Study of three different kinetics approaches for Fischer-Tropsch synthesis over Co/SiO_2", IMechE*, Internal Combustion Engine*, Royal College of Physicians, London, United Kingdom, 03/12/2015.

IV. Nima Moazami, Miroslaw Wyszynski, Hamid Mahmoudi, Kiyarash Rahbar, Athanasios Tsolakis, "Kinetic Study and Multi-Objective Optimization of Fischer-Tropsch Synthesis Performance over Co-based Catalyst Using Evolutionary Optimization Algorithm", 251st ACS National Meeting & Exposition, San Diego, California, March 13-17, 2016, Division of Catalysis Science and Technology.

ABSTRACT

Liquid fuels produced from biomass via Fischer-Tropsch (FT) synthesis have great potential to produce high-performance, environmentally friendly clean and high-quality transportation fuels; mainly due to the absence of aromatic compounds, SO_x (sulphur oxides) and NO_x (nitrogen oxides). The description of kinetics of FT synthesis is crucial for the process design, simulation, optimization, and it is quite challenging due to the complexity of the reaction pathway and products involved in this process. The aim of this thesis is to develop a comprehensive mathematical model with novel detailed kinetics of FT and water gas shift (WGS) reaction rates to accurately predict the results obtained from experimental study of cobalt-based FT synthesis process conducted in a fixed bed reactor.

A series of combined FT and WGS reaction mechanisms were developed in order to calibrate the model at twelve different operating conditions. The kinetics parameters were evaluated for each kinetics model developed herein, using an advanced optimization technique. In addition, physical and statistical consistencies of the kinetics parameters were evaluated by various statistical analyses. The results obtained from kinetic study were compared to the most recent findings that have been reported in literature. It was shown that the novel developed kinetic model based on a combination of alkyl/alkenyl mechanism for FT reactions (for production of n-paraffins and α-olefins) along with formate mechanism for WGS reaction can provide the most accurate predictions.

Model validation was carried out subsequent to completion of the model calibration and the estimation of proper kinetic parameters. The overall purpose of the validation study was to ensure that the model provides a robust and realistic assessment of all the parameters defined

by the mathematical model e.g. kinetic parameters, rate of reactants' consumption and products' formation. In order to ensure model is precise to an appropriate level, the model was assessed against experimental data at four different operating conditions.

The experimental data were taken and adapted from a mini-scale FT plant designed and operated by the co-worker in the School of Mechanical Engineering at the University of Birmingham. The experiments were conducted over an in-house 37% Co-based catalyst on a SiO_2 support over a broad range of operating conditions (i.e. temperature range of 503-543 *K*, pressure range of 10-25 *bar* and space velocity per mass of catalyst range of 1800-3600 $Nm\ell\ (STP)\ g_{cat}^{-1}\ h^{-1}$).

Parametric studies were performed to numerically investigate the effects of operating conditions on the catalytic performance of the fixed bed FT synthesis reactor over the supported cobalt catalyst with respect to product selectivities and conversion of feed compositions. Such parameters comprise the reaction temperature, total pressure, space velocity and H_2/CO molar ratio. Those parameters that have the most significant effects were then included in the multi-objective optimization process using Non-dominated Sorting Genetic Algorithm (NSGA–II) to optimize the selectivities and conversion. The Pareto-front solutions can be used as a dynamic database depending on the specific requirement. A different operating condition can be selected from such database which privileges the optimization of a particular output (e.g. conversion and selectivities).

TABLE OF CONTENTS

LIST OF FIGURES

LIST OF TABLES

LIST OF SYMBOLS

Symbols

a	Adsorption constant in rate equations	Various units
A	Pre-exponential factor	$\text{mol kg}^{-1}\ \text{s}^{-1}$
Al_2O_3	Alumina	
b	Adsorption constant in rate equations	Various units
c	Adsorption constant in rate equations	Various units
C	Carbon atom	
C_i	molar concentration of species *'i'*	
C_p	Specific heat capacity at constant pressure	$kJ\ kg^{-1}\ K^{-1}$
C_{5+}	Total liquid hydrocarbons	
CH	Methylidyne	
CH_2	Methylene	
CH_2O	Formaldehyde	
CH_3	Methyl	
CH_4	Methane	
C_nH_{2n}	Alkenes	
C_nH_{2n+1}	Alkyl group	
C_nH_{2n-1}	Alkenyl group	
C_nH_{2n+2}	Alkanes	
$C_{n-1}H_{2n-3}$	Vinyl group	
$C_nH_{2n+1}CHO$	Aldehydes group	
$C_nH_{2n+1}OH$	Alcohols group	
$C_nH_{2n-1}OOH$	Acid group	
CH(OH)	Hydroxyl carbenes	
Co	Cobalt	
CO	Carbon monoxide	
MgO	Magnesium oxide	
CO_2	Carbon dioxide	
CO_3	Carbonate species	
Cu	Copper	
CuO	Copper oxide	
D_{im}	Effective binary diffusivity for the diffusion of *'i'* in the multicomponent mixture	$m^2 s^{-1}$
d_p	Particle diameter	
E	Activation energy	$J\ mol^{-1}$
E_f	Forward activation energy	$J\ mol^{-1}$
f	Scalar function	
$f_{j,obj}$	Objective function	
F_c	*F*-critical	
Fe	Iron	
G	Mass velocity	$kg\ m^{-2}\ s^{-1}$

ΔG_f°	Standard Gibbs free energy of formation	$J\ mol^{-1}$
ΔG_R°	Standard Gibbs free energy due to reaction	$J\ mol^{-1}$
H	Hydrogen atom	
H_i	Partial molar enthalpy	$J\ mol^{-1}$
ΔH_{ads}°	Standard enthalpy change of adsorption	$J\ mol^{-1}$
ΔH_R°	Standard enthalpy change due to reaction	$J\ mol^{-1}$
H_2	Hydrogen molecule	
H_2O	Water	
HCO	Formyl	
HCOH	Hydroxycarbene	
HCOO	Formate	
H_2S	Hydrogen sulphide	
I	Unit matrix	
J_j	molar flux of species '*i*'	$mol\ s^{-1}$
k_i	Rate constant of species '*i*'	$mol\ kg_{cat}^{-1}\ s^{-1}$
k_v	Water gas shift equilibrium rate constant	$mol\ kg_{cat}^{-1}\ s^{-1}$
k_{WGS}	Water gas shift equilibrium rate constant	$mol\ kg_{cat}^{-1}\ s^{-1}$
k_0	Pre-exponential factor of rate constant	$\mathrm{mol\ kg^{-1}\ s^{-1}}$
K_P	Water gas shift equilibrium constant	
K_v	Water gas shift equilibrium constant	
K_W	Adsorption constant in water gas shift reaction rate equation	
L	Reactor Length	
La_2O_3	Lanthanum oxide	
m	Degree of freedom (number of kinetic parameters)	
m_{cat}	Mass of catalyst	kg_{cat}
M_i	Molecular weight of species '*i*'	$kg\ mol^{-1}$
M_m	Molecular weight of mixture	$kg\ mol^{-1}$
N	Total number of species	
N_2	Nitrogen	
N_{exp}	Total number of experimental runs	
N_{resp}	Number of responses (i.e. chemical species)	
Ni	Nickel	
NO_x	Nitrogen oxides	
O	Oxygen atom	
OH	Hydroxyl	
P	Total pressure	bar
P_i	Partial pressure of species '*i*'	bar
P_{CO}	Partial pressure of carbon monoxide	bar
P_{CO2}	Partial pressure of carbon dioxide	bar
P_{H2}	Partial pressure of hydrogen	bar
P_{H2O}	Partial pressure of water	bar
Q	Volumetric flow rate	m^3
r_{co}	Rate of consumption of carbon monoxide	$mol_{CO}\ kg_{cat}^{-1}\ s^{-1}$
r_{CO+H2}	Rate of consumption of syngas	$mol_{syngas}\ kg_{cat}^{-1}\ s^{-1}$
r_{WGS}	Rate of water gas shift reaction	$mol_{CO_2}\ kg_{cat}^{-1}\ s^{-1}$
R_g	Universal gas constant	$J\ mol^{-1}\ K^{-1}$

R_i	Rate of formation or consumption of species '*i*'	$mol_i\ kg_{cat}^{-1}\ s^{-1}$
Re	Reynolds number	
Ru	Ruthenium	
S_i	Selectivity of component '*i*'	
ΔS_{ads}°	Standard entropy change of adsorption	$J\ mol^{-1}\ K^{-1}$
SiC	Silicon carbide	
SiO_2	Silica	
SO_x	Sulphur oxides	
SS	Sum of the square difference	
SSE	Residual sum of squared deviations	
SST	Total sum of squared deviations	
t	time	s
t_c	Critical value of *t*-statistic	
T	Temperature	K
TiO_2	Titania	
u_s	Superficial velocity	$m\ s^{-1}$
V_l	Packed bed reactor volume	m^3
$w_{i,j}$	Mass fraction	
$\bar{X}$	Sample mean	
Y_i	Mole fraction	
z	z direction	
ZrO_2	Zirconia	
ZSM-x	Zeolites	

Greek symbols

α	Chain growth probability	
β	Volume fraction of active catalyst	
ε	Void fraction	
λ	Thermal conductivity of the mixture	$kJ\ m^{-1}\ s^{-1}\ K^{-1}$
λ_e	Effective thermal conductivity	$kJ\ m^{-1}\ s^{-1}\ K^{-1}$
μ	Molecular viscosity	$Pa\ s$
μ	Population mean	
v	Velocity vector	
v_{ij}	stoichiometric coefficient of component in '*i*' reaction '*j*'	
ρ_b^{cat}	Catalyst bulk density	
ρ_f	Density of the mixture	
σ	Total vacant surface coverage fraction of active site in WGS rate model	
ψ	Total vacant surface coverage fraction of active site in FT rate model	

Subscript

ads	Adsorption
des	Desorption
eth	Ethene
exp	Experiment

i	Species
j	Reactions
LB	Lower bound
m	Mixture
meth	Methane
n	Number of nodes in spatial dimension
olef	Olefins
org	Organic
par	Paraffins
pred	Prediction
r	Radial direction
rad	Radiation
resp	response
t	Termination step
UB	Upper bound
WGS	Water gas shift
z	Axial direction
θ	Angular direction

Superscript

cal	Calculated
exp	Experiment
m_j	Order of reaction '*j*' with respect to partial pressure of hydrogen
n_j	Order of reaction '*j*' with respect to partial pressure of carbon monoxide
T	Transpose

List of Abbreviation

ASF	Anderson-Schulz-Flory
BTL	Biomass-to-liquid
Co-LTFT	Cobalt-based low-temperature Fischer–Tropsch
CSTR	Continuous stirred tank reactor
CTL	Coal-to-liquid
DFT	Density functional theory
DRIFTS	Diffuse reflectance infrared Fourier transform spectroscopy
EIA	Energy information administration
Fe-HTFT	Iron-based high-temperature Fischer–Tropsch
FID	Flame ionisation detector
FT	Fischer–Tropsch
FTIR	Fourier transform infrared spectroscopy
GA	Genetic algorithm
GC-FID	Gas chromatography flame ionization detector
GC-MS	Gas chromatography-mass spectrometry
GHSV	Gas hourly space velocity
GTL	Gas-to-liquid
HTFT	High-temperature Fischer–Tropsch
IEO	International energy outlook
LH	Langmuir-Hinshelwood
LHHW	Langmuir-Hinshelwood-Hougen-Watson
LM	Levenberg-Marquardt
LNG	Liquefied natural gas
LTFT	Low-temperature Fischer–Tropsch
MAPD	Mean absolute percentage deviation
MFC	Mass flow controller
NLP	Nonlinear programming
NSGA–II	Non-dominated Sorting Genetic algorithm-II
ODE	Ordinary differential equation
OF	Objective function
PDE	Partial differential equation
PPF	Process path flow
RDS	Rate deterring step
RR	Relative residual
SASOL	South African synthetic oil limited
SEM	Standard error of the mean
SMDS	Shell middle distillate synthesis
WGS	Water gas shift
XPS	X-ray photoelectron spectroscopy

CHAPTER 1

INTRODUCTION

Nowadays there is a worldwide demand to develop energy-efficient and economical processes for sustainable production of alternative chemical compounds and fuels as a substitute for those emerging from petroleum. The excessive dependency of the world on conventional fossil fuels risks the future of the globe. The consistent existence of the present condition will result in an increase of the average temperature of ocean surfaces and global land by 5℃ in 2100; this will cause rising sea levels, which will be the next global crisis [1]. Climate change and global warming, due to the increase of carbon dioxide (CO_2) concentration in the atmosphere formed from the combustion of fossil fuel, and also air pollution, are major environmental concerns as a consequence of their direct influence on human breath and life. As a result, environmental agencies everywhere in the world have delivered more severe regulations to meet the current and forthcoming threats caused by emissions to the atmosphere e.g. the control of emission standards for particulates from diesel vehicles and residual sulphur in diesel fuel. All these facts have lately increased a renewed interest in Fischer–Tropsch (FT) synthesis. FT synthesis is an industrially important chemical process that typically uses syngas (a fuel gas mixture consisting mainly of carbon monoxide (CO) and hydrogen (H_2)) produced from methane, natural gas, coal or biomass through steam reforming, partial oxidation and/or

autothermal oxidation, as well as gasification processes, to convert synthesis gas into a wide spectrum of products containing mainly hydrocarbon compounds (i.e. olefins, paraffins and oxygenated products). The increased interest in FT synthesis is due to its ability to produce ultra-clean diesel oil fraction with a high cetane number (typically above 70) without any aromatic, sulphur and nitrogen compounds; with a very low particulate formation; and CO emissions [2-5]. The importance of FT synthesis processes will be discussed further in section 1.1.

The chemistry taking place in FT synthesis, as well as its kinetics, is very complex; however, the main reactions involved in this process can be described by the reactions listed in Table 1-1. Nonetheless, FT synthesis can be classified as a combination of the FT reactions and the water gas shift (WGS) reaction [6]. Based on this hypothesis, hydrocarbons (R. 1-1 to R. 1-6) are the main FT reaction products and carbon dioxide is only produced by the WGS reaction (R. 1-7), a reversible parallel-successive reaction with respect to CO [7]. Hydrocarbon R. 1-1 is related to the production of paraffins and R. 1-2 is associated with the production of olefins. Oxygenated products such as alcohols, acids and aldehyde products (R. 1-3 to R. 1-5, respectively) can also be formed either as the by-products or main products depending on the catalytic activity of the metal catalyst and the process conditions. The methanation reaction R. 1-6 is often assumed to be a separate reaction in this process. The kinetics details of FT synthesis as well as published FT synthesis reaction mechanisms in the literature will be discussed in section 2.6 to 2.7.

FT synthesis reactions occur in the presence of a catalyst in which the resulting product components are extremely influenced by the type of catalyst and the process operating conditions (reaction temperature, total pressure, space velocity, H_2/CO molar ratio) that are

employed in the process. The most common catalysts are the transition metals cobalt (Co), iron (Fe), ruthenium (Ru) and nickel (Ni) [8]. The details and differences between these catalysts will be discussed in section 2.4.

Table 1-1 Main reactions involved in FT synthesis

Production	Reaction Equations	Reaction Number
Paraffins' formation	$(n)CO + (2n+1)H_2 \rightarrow C_nH_{2n+2} + (n)H_2O;\ n \geq 2$	R. 1-1
Olefins' formation	$(n)CO + (2n)H_2 \rightarrow C_nH_{2n} + (n)H_2O;\ n \geq 2$	R. 1-2
Alcohols' formation	$(n)CO + (2n)H_2 \rightarrow C_nH_{2n+1}OH + (n-1)H_2O;\ n \geq 1$	R. 1-3
Acids' formation	$(n)CO + 2(n-1)H_2 \rightarrow C_nH_{2n-1}OOH + (n-2)H_2O;\ n \geq 3$	R. 1-4
Aldehydes' formation	$(n+1)CO + (2n+1)H_2 \rightarrow C_nH_{2n+1}CHO + (n)H_2O;\ n \geq 1$	R. 1-5
Methane formation	$CO + 3H_2 \rightarrow CH_4 + H_2O$	R. 1-6
WGS formation	$CO + H_2O \rightleftarrows CO_2 + H_2$	R. 1-7

1.1. Background

Interest in alternative fuels and renewable sources has grown significantly due to the concern regarding the requirement of CO_2 reduction, energy consumption, as well as the limitation of future oil reserves. Nowadays, the necessity of running engines with the new generation of liquid fuels is unavoidable. New diesel fuels are essential not only to improve the performance of an engine and its emissions, but also to ensure the fuel supplies' sustainability [4]. The U.S. Energy Information Administration (EIA) published the International Energy Outlook 2013 (IEO2013) schemes where the energy consumption of the world will escalate by

56% between 2010 and 2040, from 524×10^{15} British thermal units (*Btu*) to 820×10^{15} *Btu*. This indicates that renewable energy is one of the fast-growing energy resources in the world and its usage escalates 2.5%/year. Nevertheless, it is expected that fossil fuels will supply more or less 80% of the energy demand until 2040 [9].

In this context, the most abundant raw material existing on the earth i.e. lignocellulosic biomass, is a particularly interesting resource since it is the only renewable source of organic carbon compound that can be converted into liquid transportation fuels. The gasification of biomass produces syngas that can be converted into synthetic liquid hydrocarbon fuels by means of the FT synthesis process. This process has been widely considered as an attractive route for generating ultra-clean liquid hydrocarbon fuels from biomass that has been identified as a promising alternative to conventional fossil fuels, such as diesel and kerosene. From Figure 1-1 it is also apparent that the number of publications related to FT synthesis process fuels have increased substantially over the last decade. The raw material can either be natural gas (the final liquid fuel being GTL - gas-to-liquids), coal (CTL - coal-to-liquids) or residual biomass (BTL - biomass-to-liquids). GTL is already produced commercially and diesel fuels blended with GTL are available in several European countries [10]. A production of a significant volume (1 million barrels/day or more) of total GTL diesel fuel is being planned within the next decade due to a number of new large-scale GTL production plants that are currently under construction [11]. Lately, the performance of exhaust emissions of GTL diesel fuels has been the subject of an increasing number of technical publications [4]. Ultra-clean and high cetane number biofuels derived from an FT process enable lower combustion temperatures and pressures. These fuels can promote the decrease of engine-out emissions and increase the performance of the catalytic fuel reformers and after-treatments [12]. The following study is carried out based on the second generation of biofuels via FT synthesis.

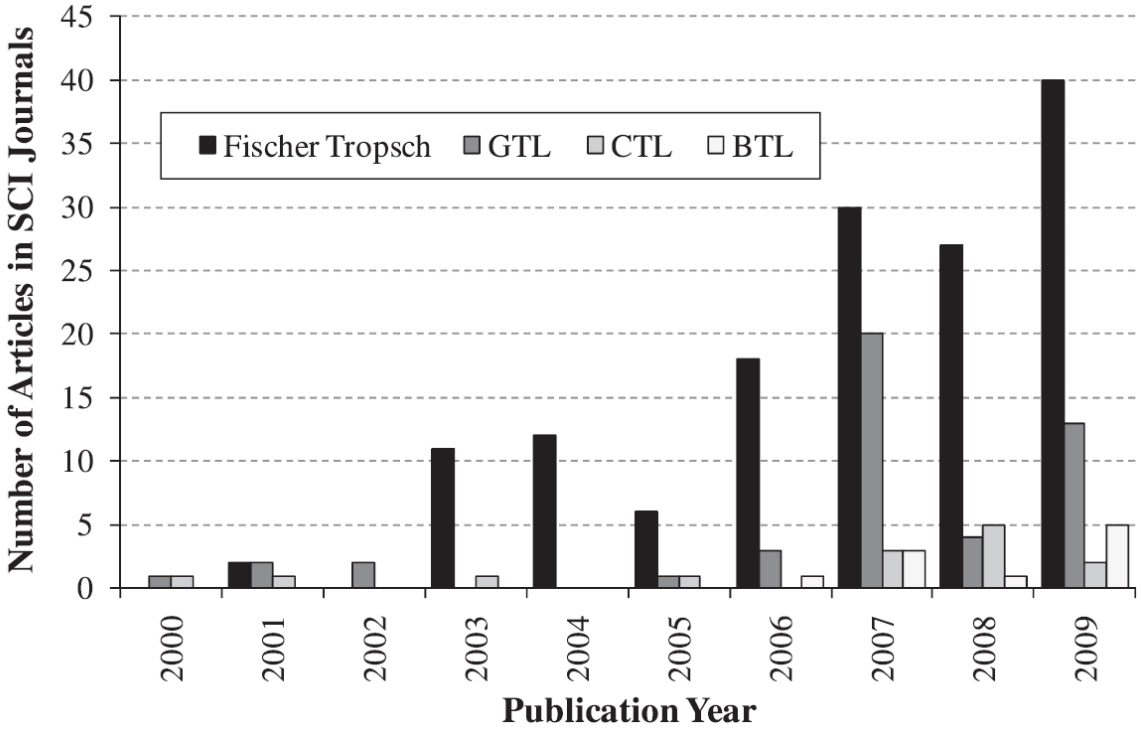

Figure 1-1 Number of publications related to FT synthesis compared to GTL, CTL and BTL processes (adopted from [4]).

FT synthesis is a well-known industrial process discovered by Professor Franz Fischer and Doctor Hans Tropsch (Figure 1-2) in Germany in 1923. It was used as a means to indirectly convert coal into a liquid fuel. During World War II, FT synthesis provided the required liquid hydrocarbon fuels for the German's war [13-15]. They obtained a liquid product that consisted mainly of hydrocarbons from the hydrogenation of CO over iron and cobalt catalysts, leading to their famous patent of the FT synthesis process in 1925. Their research greatly contributed to the later development of the synthesis process and its establishment. The process was first commercialized in 1936 by Ruhrchemie AG in Germany [16, 17] and the technology became valuable when Germany became isolated due to its war effort; which made it dependent on coal that was readily available in Germany [8, 18]. The technology implemented at the early stages

of development after the war, however, was too expensive to compete with crude oil [8]; the prices of which were extremely low in the post-war period, due to the discovery of the large oil reserves in the Middle East [8, 18, 19]. This led to minimal interest in FT synthesis during this time period and development of the process continued almost exclusively at South African Synthetic Oil Limited (SASOL) in South Africa, which was formed in 1950. This was attributed to the fact that South Africa faced an oil embargo sanctioned by the international community and relied on its vast coal deposits for the production of liquid fuels and higher value chemicals [20].

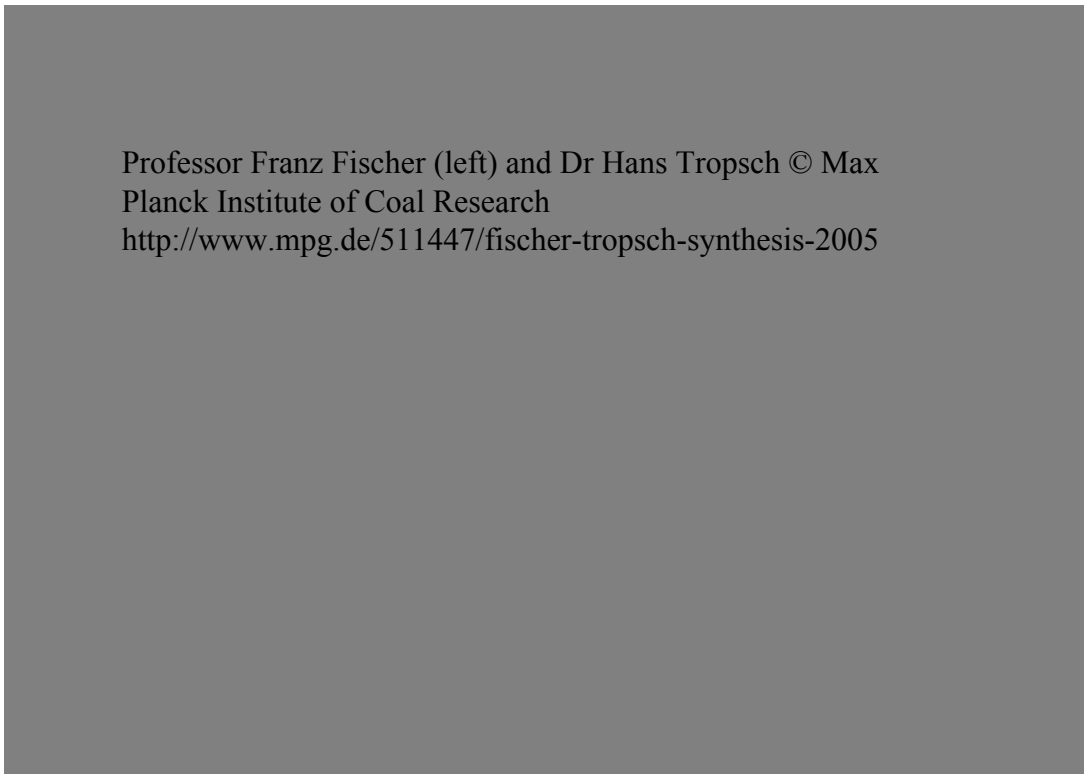

Figure 1-2 Inventors of Fischer-Tropsch synthesis, Professor Franz Fischer (on the left) and Doctor Hans Tropsch (on the right).

Interest in FT synthesis revived however in the 1970s and 1980s due to alarming forecasts at the time about depleting crude oil reserves, as well as international politics which included

oil embargoes by major oil producing nations [19]. The attention towards FT processing further increased in the 1990s when it was realised that the technology could be used to take advantage of remotely located sources of natural gas; which would be too expensive to transport in pipelines, but could either be liquefied and then transported as liquefied natural gas (LNG), or gasified and processed via FT synthesis to produce synthetic transport fuels [8].

1.2. Fischer-Tropsch Synthesis Process

In general, there are four main steps involved in the production of liquid fuels from feedstocks, produced from three main processes (see section 1.2.1**)**, via FT synthesis: (*i*) synthesis gas production; (*ii*) syngas cleaning and purification; (*iii*) FT synthesis; (*iv*) products' recovery and upgrading (see Figure 1-3). The falling supply of crude oil and growing demand for clean transportation fuels in recent years has led to intensive research and development worldwide for alternative sources of fuels through GTL, CTL and BTL, which comprise of both syngas and hydrogen as key components. Figure 1-3 depicts the flow diagram of alternative process paths to convert different feedstocks into synthetic fuels within an indirect liquefaction process.

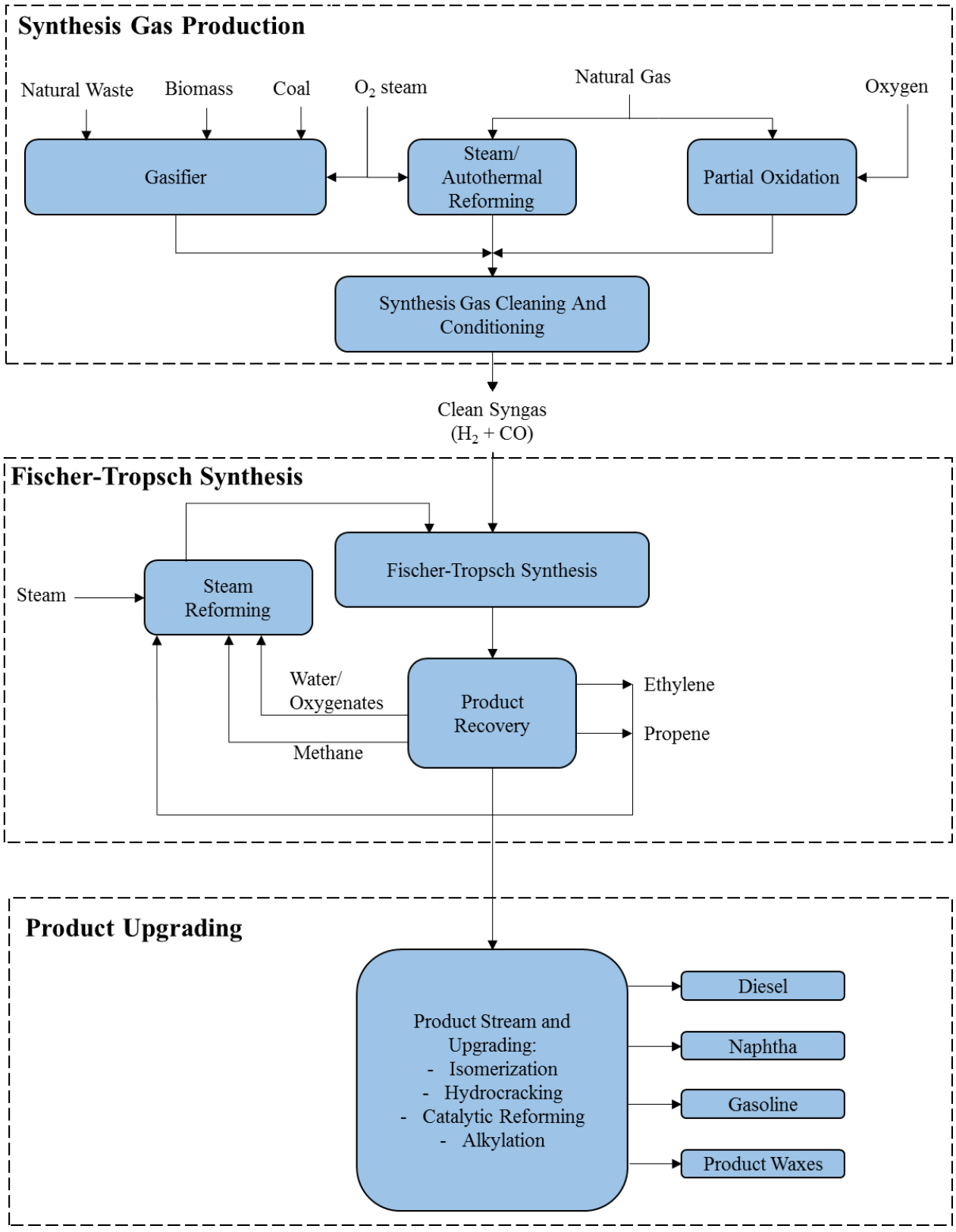

Figure 1-3 Flow diagram of the overall process of an FT plant, indirect liquefaction for GTL, CTL and BTL processes.

1.2.1. Synthesis Gas Production

In this framework the first step (i.e. syngas generation) is very important since the syngas can be produced from natural gas (GTL), coal (CTL) or biomass (BTL) [21]. Figure 1-4 illustrates the industrial options for syngas utilization, such as the fuels produced from syngas comprise methanol by methanol synthesis; hydrogen by the WGS reaction; alkanes and alkenes by FT synthesis; ethanol by fermentation; isobutene by isosynthesis; or with homogeneous catalysts and aldehydes or alcohols by oxosynthesis.

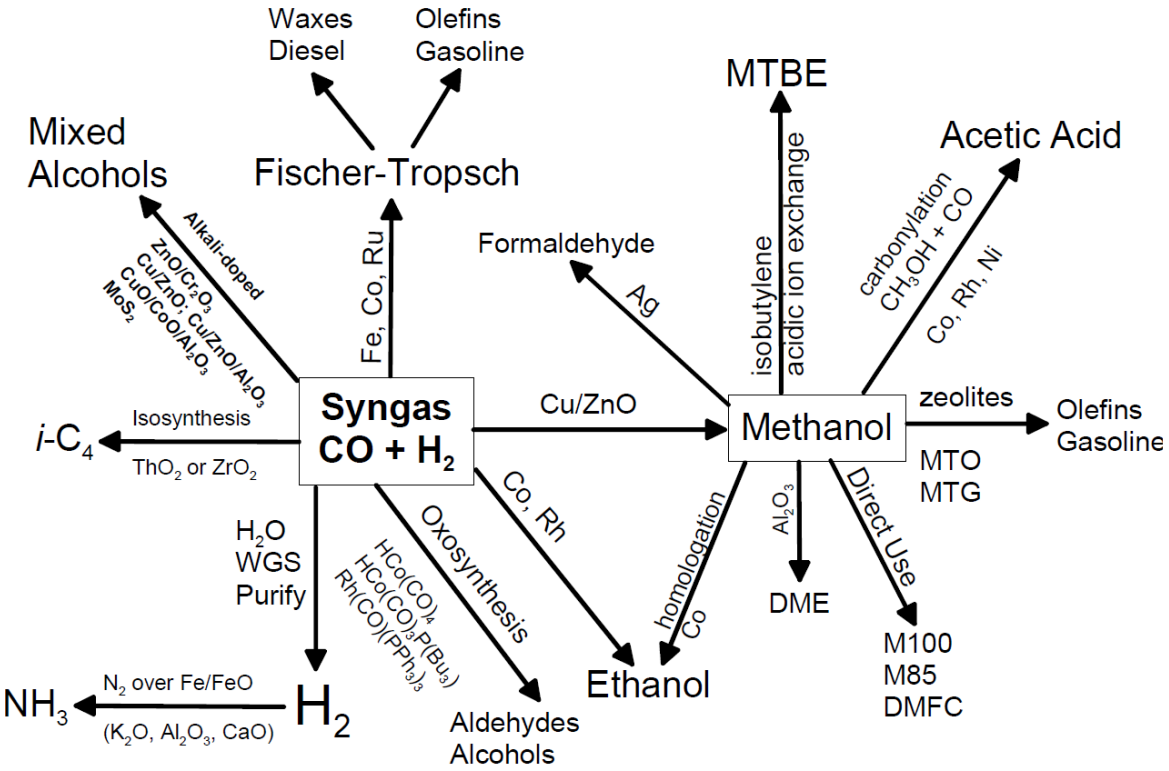

Figure 1-4 Flow diagram of syngas ($CO + H_2$) conversion (adopted from [22]).

The main difference between GTL, CTL and BTL lies in the synthesis gas production process where the syngas production requires the gasification of a solid feedstock. Today, with continuously depleting oil reserves and the added factors of environmental concerns, as well as

other limitations in the first generation biofuels and the recent improvements to the technology used in FT processing, research has turned towards second generation biofuels' technology for the production of clean and sustainable synthetic fuels [23, 24]. FT synthesis diesel derived from biomass (BTL) via gasification is an attractive carbon neutral and clean transportation fuel, directly functional in the current transport sector.

1.2.2. Syngas Cleaning and Purification

Besides a low H_2/CO molar ratio composition, the resulting syngas also contains many impurities; hence it is necessary to clean and condition it prior to its utilization in the FT reactor, as FT catalysts are significantly sensitive and can be easily deactivated or poisoned by syngas pollutants [25]. These contaminants are potentially capable of causing problems to other processes such as blockages and equipment fouling and corrosion, as well as environmental problems due to harmful emissions [26]. The acceptable levels of contaminants may vary for each plant and FT catalyst. Remarkably, it has been reported by Boerrigter *et al*. [27] that there are no syngas contaminants that are specific to biomass and consequently, conventional gas cleaning approaches can be adopted. This may or may not be true, however, as operational experience in biomass gasification applications is relatively small in comparison to that of coal and natural gas gasification, it is this uncertainty in the knowledge of the exact contents and contaminants of biosyngas that poses one of the greatest challenges in the commercialization of BTL-FT operations [26]. Some comprehensive details about syngas cleaning and purification can be found in the literature [28].

1.2.3. Fischer-Tropsch Synthesis

The next step after the syngas is cleaned and conditioned is to use it in the FT synthesis reaction that is carried out in the reactor vessel [29]. The choice of reactor has many concerns and the influence on refining is significant. The characteristics of the main reactor types used in FT synthesis are given in detail in the literature [30]. In general, there are three different main categories of reactor, i.e. fixed bed, fluidized bed and slurry bed used in FT synthesis technology. These will be discussed in section 2.5. The different types of catalyst used in FT synthesis, mode of operation (i.e. low-temperature FT (LTFT) and high temperature FT (HTFT)), and FT kinetics and reaction mechanism will be discussed in detail in sections 2.2, 2.4 and 2.6, respectively. The primary FT reactions were also given in Table 1-1.

1.2.4. Products' Recovery and Upgrading

The mixture of products leaving a standard FT synthesis reactor contains a wide range of paraffins (alkanes: C_nH_{2n+2}), olefins (alkenes: C_nH_{2n}), oxygenated products (i.e., alcohols: ($C_nH_{2n+1}OH$), acid: ($C_nH_{2n-1}OOH$) and aldehydes: ($C_nH_{2n+1}CHO$)) and aromatics, with water as a by-product. The product stream can also be defined as various fuel types which will be discussed in section 2.3. The products from FT synthesis are higher value as diesel fuel, jet fuel and gasoline are low in aromatics and free from sulphur. In addition, as discussed early in Chapter 1, the FT synthesis diesel fuel has a high cetane number (enabling lower combustion temperatures and pressures). The paraffins (in the range of C_9-C_{15}) are very suitable for the manufacturing of excellent lubricants; while the olefins make biodegradable detergents [31]. High selectivities towards fuels are obtained through hydrocracking, which is a selective

process converting heavy hydrocarbons into light hydrocarbons in the range of C_4-C_{12} with a small contents of C_1-C_3. This directly produces a high quality gas oil (low aromatics, low sulphur content, and high cetane index) and kerosene (high paraffin content), which are very suitable as blending components to upgrade lower quality stock [31]. The linearity of the FT naphtha is a drawback for gasoline production. The naphtha is therefore better used as feedstock for the petrochemical industry. Its high paraffin content makes the naphtha an ideal cracker feedstock for ethylene and propylene production. Product selectivity can be improved using multi-step processes to upgrade the FT synthesis products. Upgrading involves a combination of hydrotreating, hydrocracking and hydroisomerization, in addition to product separation. Hydrotreating involves adding hydrogen and a catalyst to remove impurities like nitrogen, sulphur and aromatic hydrocarbons. Hydrocracking is a catalytic cracking process assisted by an elevated partial pressure of hydrogen gas and hydroisomerization involves the addition of hydrogen and a catalyst to drive the isomerization processes. As mentioned previously, most upgrading units are considered to produce the desired hydrocarbons; however, the products from the FT synthesis will typically comprise hydrocarbons, waxes, alcohols, and undesired products such as unreacted synthesis gas and lighter hydrocarbons. These undesirable products can be recirculated to the reformer or to the FT reactor. This recycling process is one method of upgrading and it raises the yield of synthesis gas. Moreover, recirculated olefins and alcohols in the FT reactor feed will readsorb and form higher molecular weight hydrocarbons. This can also enhance overall conversions [32, 33]. The recycling process can be characterized by the feed location where the undesired compounds from C_1 to C_4 are recycled to either be used as co-feed to the FT reactor, or else be converted to synthesis gas [31].

1.3. Numerical Modelling and Detailed Kinetics

The kinetic description of the FT synthesis as well as mathematical modelling of the FT reactor is crucial to industrial practice, being a prerequisite for industrial process design, optimization and simulation. Large companies are now well aware of the importance of reliable kinetics data as a basis for design. Kinetics studies have benefited from more systematic methods for the design of experiments and improved methods for analysis of the data [34]. The principal governing factors for any FT kinetics mechanism are the reaction temperature, total pressure, space velocity and the H_2/CO molar ratio, which affect FT products' distribution and synthesis conversion. The main difficulty in precisely describing the kinetics of FT synthesis is the complex network of its reaction pathway and the existence of a high number of chemical product components in the process. The FT synthesis reaction is a highly complex system in which thousands of species take part in an extremely coupled mode. For this reason, it is unlikely a kinetics equation for every reaction species could be established with the conventional method used in reaction kinetics studies. Such a complex reaction system requires a simplified mathematical equation to elucidate the kinetic characteristics of syngas disappearance and products' distribution. In addition, mathematical modelling is significantly useful to assist in the development of the FT synthesis processes. In principle, a mathematical model should be tailored for its main purpose. It should be as simple as possible, but still include a sufficient representation of the essential mechanisms involved. Hence, several assumptions have to be considered to facilitate the computational procedure.

1.4. Thesis Aims and Objectives

Given the range of knowledge reported above, the objectives of the present thesis were: (*i*) to study different kinetics models from the available literature on a cobalt-based catalyst; (*ii*) develop comprehensive kinetics models including both Fischer-Tropsch and water gas shift reaction mechanisms; (*iii*) develop a mathematical model of a catalytic fixed bed reactor by deriving the governing conservation equations in order to assess the different kinetics models for the prediction of the experimental data; (*iv*) evaluate the kinetics parameters (kinetics constants and activation energies) for each model by employing an advanced global optimization technique (using a GlobalSearch algorithm); (*v*) calibrate and validate the developed mathematical model with the proposed kinetics mechanisms against the experimental results at a variety of operating conditions; (*vi*) investigate the effects of process conditions on products' selectivities as well as conversions of synthesis gases; and finally, (*vii*) to perform an optimization study of the process conditions to achieve an optimum in the performance of Fischer-Tropsch synthesis for liquid fuels' production as well as synthesis conversions.

1.5. Thesis Layout

The overview to the historical context of FT synthesis process, the importance of numerical modelling as well as kinetics study, and the aims and objectives of the present thesis were presented in this chapter up to section 1.5. However, the remainder of the thesis is systematically organised as follows:

Chapter 2: Literature Review

This chapter presents a comprehensive literature review, which introduces the FT synthesis process and its applications in the production of liquid hydrocarbons. This chapter also reviews the FT synthesis' different mode of operation, product distribution, characterization and various reactor types that are used in FT synthesis processes. Details of the FT kinetics and reaction mechanisms for the hydrocarbon productions in FT synthesis over a cobalt catalyst are discussed comprehensively.

Chapter 3: Kinetics of Fischer-Tropsch Synthesis

This chapter establishes the detailed development of a number of mechanistic kinetics models for the FT synthesis system over a Co/SiO_2 catalyst, while assessing extensive possibilities in mechanism combinations (i.e. FT synthesis and WGS reaction rate models), more than has been attempted at any time previously, compared to the published literature. In this chapter, eight different reaction pathways are proposed for FT reactions from the different kinetic mechanisms based on unassisted CO-dissociation, H-assisted CO dissociation as well as molecular H_2-assisted CO dissociation. The kinetics models are developed based on combined alkyl/alkenyl mechanisms to represent the production of paraffins and olefins compounds. Moreover, seven different reaction routes are postulated for water gas shift reaction from two general reaction mechanisms (i.e. formate mechanism and redox mechanism). Some elementary reactions in the presented reaction networks are hypothesised as rate-determining steps (slowest steps in reaction path) to elucidate the derivation of reaction rate equations.

Chapter 4: Mathematical Modelling

This chapter describes the detailed development of the mathematical model of a mini-scale fixed bed reactor for cobalt-based FT synthesis. The model's algorithm, as well as the solving technique, is described in detail. Moreover, the integration of the optimization technique (i.e. GlobalSearch algorithm) with the mathematical model and the implementation of the optimization constraints are explained thoroughly. In this chapter, various statistical methods (such as *F*-test and *t*-test) that have been used to evaluate the significance of the overall model predictions and to ensure the kinetic parameters (rate constants and activation energies) are acceptable from a statistical point of view, are highlighted.

Chapter 5: Experimental Setup, Model Calibration and Validation

This chapter outlines the overall experimental procedure that was carried out by a co-worker in the School of Mechanical Engineering at the University of Birmingham [1]. Such results are employed to assess the various kinetics mechanisms together with a mathematical model; these are developed in Chapter 3 and Chapter 4, respectively. The experimental data is used for calibration of the model and estimation of kinetic parameters. Then, the statistical analyses are performed to ensure model predictions and kinetic results are statistically relevant and physically meaningful. Furthermore, the results obtained from the proposed kinetic model for FT and WGS reaction mechanisms are compared to those of the literature and it indicates the significant improvement in model predictions. This chapter also provides the details of model validation which is carried out subsequent to completion of the model calibration and the estimation of proper kinetic parameters. The overall purpose of the validation study is to ensure that the model provides a robust and realistic calculation of all the parameters defined

by the mathematical model e.g. kinetic parameters, rate of reactants' consumption and products' formation. In order to ensure the model is relevant to an appropriate level, it is assessed against experimental data at four different operating conditions, which are available for validation.

Chapter 6: Parametric Studies and Optimization

This chapter utilizes the validated model from Chapter 5 in order to conduct comprehensive parametric studies to investigate the effects of various operating conditions on the critical performance parameters such as reactants' conversion, as well as various products' selectivity. Those parameters that have the most substantial effects on the reactor outcomes are then included in the optimization procedure. To do so, a NSGA–II (Non-dominated Sorting Genetic Algorithm-II) is employed to conduct the multi-objective optimization. Then such an optimization method is used to maximize the catalytic performance of the FT synthesis process with respect to conversions and selectivities.

Chapter 7: Conclusions

This chapter highlights the summary of the most remarkable results identified in the preceding chapters and recommendations for further developments of the current work.

CHAPTER 2

LITERATURE REVIEW

This chapter covers the importance of FT synthesis technology, different operating modes that FT synthesis can operate, as well as FT products' characterization and distribution. The specifications of various types of catalysts that can be activated for the FT reaction are highlighted. Different kinds of reactors that are used in FT processes such as a fixed bed reactor, slurry phase reactor and fluidized bed reactor are reviewed. In addition, this chapter encompasses the reaction kinetics mechanisms of the FT synthesis including the polymerization reaction mechanism and the significant and major contributions in the development of reaction mechanisms. The roles of the alkyl mechanism, alkenyl mechanism, enol mechanism, CO insertion mechanism and the WGS reaction mechanism are extensively discussed. Finally, the studies that have investigated the kinetics of FT synthesis over a cobalt-based catalyst, based on both empirical and mechanistic approaches, are broadly reviewed.

2.1. Fischer-Tropsch (FT) Synthesis Technology

FT synthesis can be defined as the means of indirect liquefaction, in which synthesis gas (a mixture of predominantly CO and H_2) obtained from either coal, peat, biomass or natural gas is catalytically converted to a multicomponent mixture of gaseous, liquid and solid hydrocarbons [35]. The FT synthesis is a surface polymerization reaction in which the reactants, CO and H_2, adsorb and dissociate at the surface of the solid catalyst and react to form methylene (CH_2) monomer, chain initiator i.e. methyl (CH_3) species and water. A wide product spectrum of hydrocarbons is formed by the successive addition of CH_2 units to growing chains on the surface of the catalyst and these will be discussed in section 2.6.

Currently, there are three main aspects for consideration regarding the FT synthesis processes. Firstly, there exists the FT synthesis reaction mechanism, the details of which are still not fully understood. Furthermore, from the outlook of chemical engineering, there is the design and scale-up of the commercial FT synthesis plant in which studies of the kinetics mechanisms as well as optimization study play significant roles. An optimal design of a commercial-scale reactor requires detailed information of the hydrodynamics and the reaction kinetics, as well as the mathematical model of the catalytic reactor. In fact, to reach the ideal performance of the FT process, a precise comprehensive kinetics model that can describe the product distribution of FT synthesis is essential.

2.2. Operating Modes

There are principally three main classifications of FT synthesis in commercial scale with respect to the operating mode. The three types of syntheses are iron-based high-temperature FT

(Fe-HTFT), iron-based low-temperature FT (Fe-LTFT) and cobalt-based low-temperature FT (Co-LTFT). It is apparent that the FT synthesis industry has come in a full loop, beginning with Co-LTFT with upgrading, moving to Fe-HTFT and Fe-LTFT with refining, and returning to Co-LTFT with upgrading [36, 37]. As an example, one can refer to the German Co-LTFT syncrude that was sufficiently upgraded so that it could be blended with coal liquids and crude-oil-derived fuels as final products without further refining. Similarly, there are the products from the Co-LTFT–based Shell Middle Distillate Synthesis (SMDS) process, where the distillate is blended with crude-oil-derived diesel fuel as a final product, while the rest of the products are refined to *n*-alkane (paraffin) solvents, waxes and lubricating oils [30]. Here, on the basis of temperature mode, FT synthesis processes are distinguished into two categories: HTFT and LTFT syntheses.

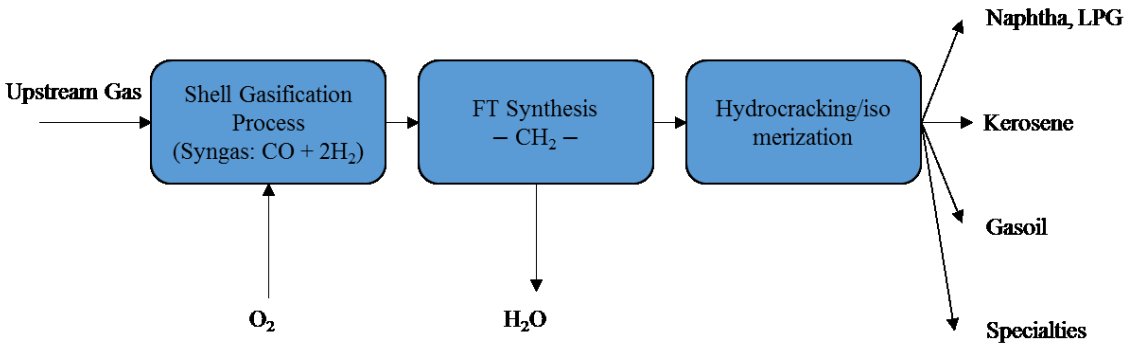

Figure 2-1 Shell Middle Distillate Synthesis (SMDS) process schematic.

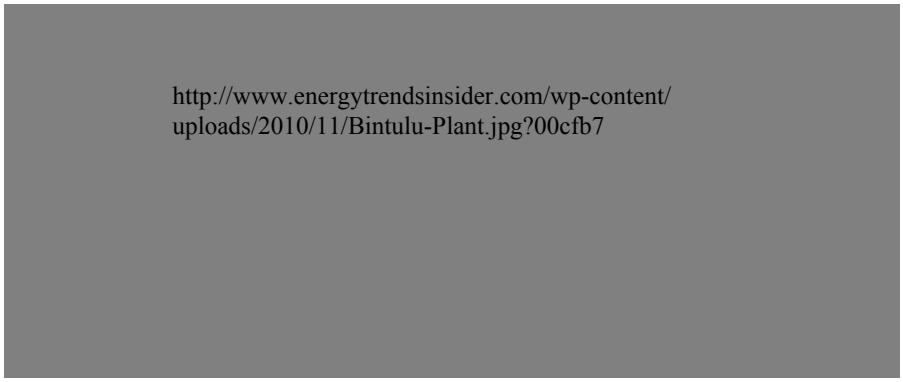

Figure 2-2 Shell's Bintulu GTL Plant [38].

2.2.1. High-Temperature Fischer-Tropsch (HTFT)

In HTFT, because of the process conditions and the catalysts involved, the syncrude produced includes a high percentages of short chain hydrocarbons (i.e., <10 carbon atoms) with significant amounts of propane and butane mixed with olefins (e.g. propylene and butylene). The Fe-HTFT process produces fuels including gasoline and diesel that are closer to those produced from conventional oil refining [39]. The HTFT processes operate in the temperature range of 573-623 *K* with pressures in the range of 25-60 *bar*; however, operation in a lower temperature (about 546 *K*) was also reported by another investigator and with pressures of approximately 25 *bar* [39]. Conversion in HTFT can be even more than 85% efficient [37], but not all the products are readily usable or capable of producing high-quality transport fuels. FT reactor operating temperatures do not normally exceed 623 *K*, since at higher temperatures the main product would be CH_4 [40]. HTFT processes tend to be conducted in either circulating fluidized bed reactors or fixed fluidized bed reactors [39, 41]. Different types of FT reactor exist in commercial scale, which will be discussed in section 2.5.

2.2.2. Low-Temperature Fischer-Tropsch (LTFT)

During World War II, Germany ran 12 high-pressure coal hydrogenation plants together with 9 LTFT plants to produce 4.5 million tons/annum of motor fuels; this was 90% of Germany's consumption at that time [17]. The FT diesel was obtained by distillation of the light hydrocarbons; however, it included oxygenates and olefins. Nevertheless, the FT process was at that time of secondary importance for the German fuel economy, producing 9.1% of the total German oil supply. In this context, the primary focus of most LTFT large-scale technologies in current market conditions is to produce high-quality low-emissions diesel, jet fuel, naphtha (for petrochemical feedstock or gasoline blending) and waxes (see Figure 2-3).

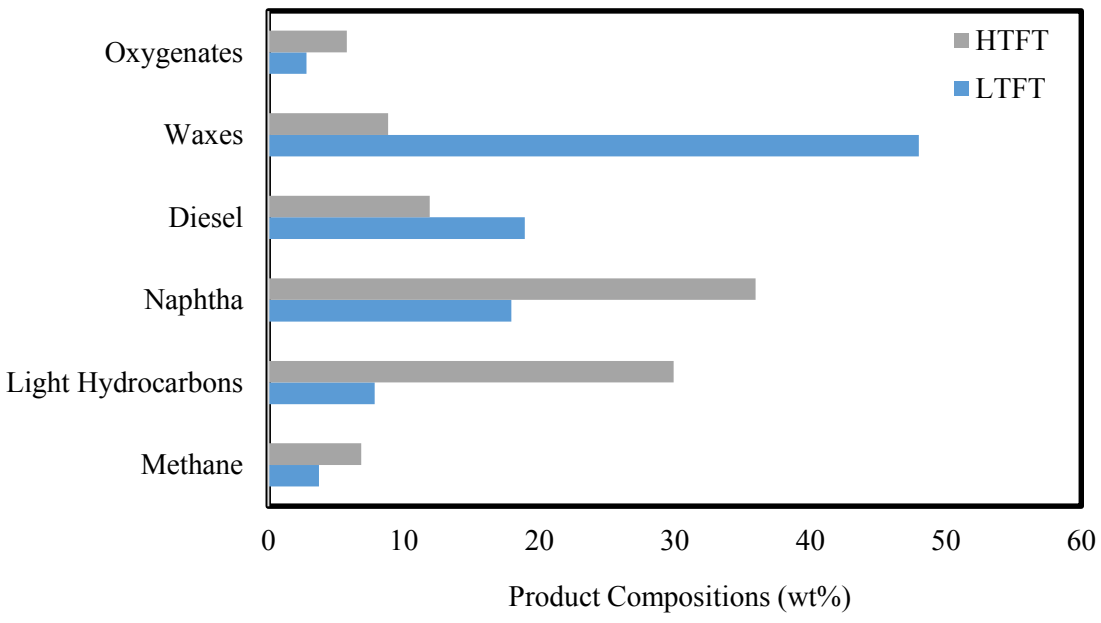

Figure 2-3 Typical product components of HTFT and LTFT (adopted from [17, 29]).

Co-LTFT processes are used either in multi-tubular fixed bed reactors (e.g. Shell) or in slurry-phase bubble-column reactors (e.g. Sasol). LTFT produces a synthetic fraction of diesel that is virtually free of sulphur and aromatics. Typical process operation conditions for LTFT are temperatures of about 493 *K* to 513 *K* and pressures of around 20 to 25 *bar*. LTFT synthesis conversion is usually around 60%, from the literature point of view, with recycling or the reactors operating in series to limit catalyst deactivation [37]. Another investigator depicted that LTFT processes typically operate in the temperature range of 473-523 *K* and pressures of 25-60 *bar* using cobalt or iron-based catalysts [42]. The FT synthesis operating mode affects significantly the nature and composition of the products obtained from the synthesis reaction. The main Fe-HTFT products contain naphtha (i.e. low-grade gasoline) and low molecular weight hydrocarbons. In contrast, the main Co-LTFT products are composed of diesel and waxes in which they are typically hydrocracked to maximize the diesel formation [35]. Figure 2-3 indicates the comparison of typical compositions of HTFT and LTFT products' weight fractions, arising from the different operating modes, obtained from a circulating fluidized bed reactor and a fixed bed reactor, respectively.

2.3. Product Distribution and Characterization

FT products are generally regarded as an alternative to crude oil for the production of synthetic liquid fuels (such as gasoline, diesel and kerosene) and higher-value chemicals. Synthetic fuel compositions that are representative of each type of FT synthesis with regard to temperature mode are listed in Table 2-1. Within each FT synthetic type, there is variation caused by the catalyst, catalyst deactivation, operation and reactor technology. The names derived for the fuels gained for the FT processes are obtained from crude oil refining

terminology, where the composition of a specific crude oil may vary not only between sources but also within a source between locations and with time [37, 43].

FT liquid fuels are considered to be environmentally superior to petroleum derived fuels, as they contain no nitrogen, sulphur, heavy metal contaminants, or aromatics [8, 42, 44, 45]. Consequently, the resulting emissions have considerably lower amounts of NO_x, SO_x and particulate matters. Table 2-2 shows the comparison of the properties of typical FT diesel with the specifications of standard diesel. A typical way to rate the quality of a diesel fuel is to assess its cetane number, which is a measure of its combustion quality during compression ignition so that the higher the cetane number, the easier the fuel ignites when it is injected into the engine [46].

Table 2-1 FT product compositions and their carbon chain lengths (adopted from [37])

Product element	Carbon number range			Compound class	Product composition (wt%)		
					Fe-HTFT	Fe-LTFT	Co-LTFT
Tail gas	C_1			Alkane	12.7	4.3	5.6
	C_2			Alkene	5.6	1	0.1
				Alkane	4.5	1	1
LPG	C_3–C_4			Alkene	21.2	6	3.4
				Alkane	3	1.8	1.8
Naphtha	C_5–C_{10}			Alkene	25.8	7.7	7.8
				Alkane	4.3	3.3	12
				Aromatic	1.7	0	0
				Oxygenate	1.6	1.3	0.2
Distillate	C_{11}–C_{22}	Kerosene:	$C_{11} - C_{13}$	Alkene	4.8	5.7	1.1
		Diesel:	$C_{11} - C_{18}$	Alkane	0.9	13.5	20.8
		Soft Wax:	$C_{19} - C_{23}$	Aromatic	0.8	0	0
				Oxygenate	0.5	0.3	0
Residue/ wax	C_{22+}	Medium Wax:	$C_{24} - C_{35}$	Alkene	1.6	0.7	0
		Hard Wax:	C_{35+}	Alkane	0.4	49.2	44.6
				Aromatic	0.7	0	0
				Oxygenate	0.2	0	0

Aqueous product	C_1–C_5	Alcohol	4.5	3.9	1.4
		Carbonyl	3.9	0	0
		Carboxylic acid	1.3	0.3	0.2

Table 2.2 indicates that the cetane number of diesel fraction produced from the FT process is significantly higher than that of conventional diesel (C_{11}-C_{18}) due to the significantly lower aromatics' value and the lower degree of branching of FT diesel fuels [30]. It is probable that FT diesel fuels are used for mixing with low cetane diesel from petroleum for upgrading purposes to meet the increasingly strict regulations of transportation fuel [40]. In fact, there is no need for extra modifications to be made in diesel engines or the existing fuel supply framework.

Table 2-2 Typical FT diesel specifications versus standard diesel (Adapted from [4, 29])

Property	US Diesel (ULSD) US07	FT Diesel
Cetane number	53.90	79.00
Sulphur (mg/m3)	46.00	0.05
Aromatics (wt %)	24.40	0.30
Density at 15ºC (kg/m3)	827.10	784.60
Viscosity at 40ºC (mm2/s)	2.47	3.50
Calorific Value (MJ/kg)	42.70	43.90

2.4. Fischer-Tropsch Catalysts

Research studies have shown that only four transition metals iron (Fe), cobalt (Co), nickel (Ni) and ruthenium (Ru) are activated in an FT reaction and have sufficiently high activity for synthesis processes [47-49]. Referring to [48], the relative cost of these metals can be expressed as Fe: 1, Ni: 250, Co: 1,000 and Ru: 48,000. In this respect, Ru is the most expensive but most active compared to other active catalysts used in the FT process. It is known that Ru does not oxidise or carburise under normal FT conditions and it gives high yields of oils and waxes [49]. However, because of its very high cost and low availability, large scale application of Ru as a catalyst is not viable for the production of low value chemicals and/or synthetic fuels, but could potentially be used in the production of higher value chemicals [43]. It is known that Ni forms volatile carbonyls during the FT reaction at 473-573 *K* (within the range used in typical FT conditions) [40]; this causes the continuous loss of the metal during the reaction [48]. In addition, Ni is considered more as a methanation catalyst as it produces mainly methane and gives the lowest yield of higher molecular weight compounds at typical FT conditions [49]. Under typical operating conditions for Fe-LTFT and Co-LTFT synthesis (473–523 *K* and 20–30 *bar*), the equilibrium carbonyl concentration is very low and unlikely to be a significant contributor to FT catalyst deactivation. In this respect, the risk of metal loss is higher with Ni- and Ru-based FT catalysts. Nickel-based catalysts have a higher equilibrium concentration of metal carbonyl species at low temperature; whereas the high pressures associated with ruthenium-based synthesis promote carbonyl formation [30, 50].

Consequently, only Co and Fe are the most common FT synthesis catalysts on a commercial scale [48, 51, 52]. Regarding the operating mode, iron-based catalysts are employed for both LTFT and HTFT processes; while Co-based on catalysts are suitable for LTFT processes [53]. In addition, the type of feedstock used and the kind of products desired (i.e. gasoline versus diesel and waxes) also play significant roles in the choice of catalyst.

Figure 2-4 indicates the differences in the compositions of typical Co- and Fe-based catalysts. The general composition for typical Co- and Fe-based catalysts in industrial application contains the metal (in its oxide form), a support or carrier material, and promoters (other metals and metal oxides) [54]. The oxide phases in the catalysts need to be reduced to the equivalent metallic phase prior to the FT reaction (usually using H_2). This is the phase that has the required activity for the FT reaction.

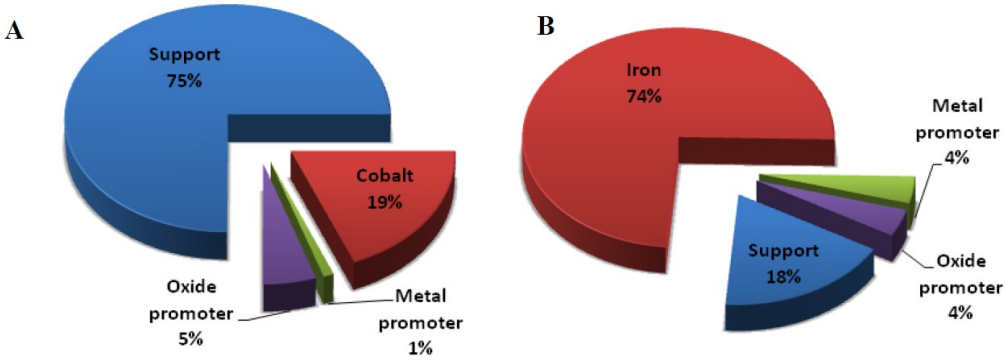

Figure 2-4 Typical composition of cobalt catalysts (A) and iron catalysts (B) [29].

Research on both cobalt and iron-based catalysts has focused on a number of aspects in an effort to improve catalyst reducibility and activity, tailor and enhance the selectivity to certain products and by the same token, decrease the selectivity to undesired products like

methane, as well as increasing their resistance to catalyst poisons, such as sulphur compounds. These aspects include the influence of physical and chemical properties, the support or carrier materials, promoters and other additives, the preparation techniques and the catalyst pre-treatment or activation procedures implemented.

2.4.1. Iron-based Catalysts

Compared to cobalt, iron is reported to be more responsive to promoters; the more alkaline the promoter is the higher the average carbon chain length of the hydrocarbon products [49]. This is because CO surface adsorption and subsequent decomposition into C and O atoms has been reported to be enhanced by surface alkalinity [53]. The main reported disadvantage of using Fe-based catalysts is that they deactivate faster due to oxidation and coke deposition and have a much shorter process life than cobalt-based catalysts (~2-3 months) [29, 55].

2.4.2. Cobalt-based Catalysts

Co-based catalysts are widely used in CO hydrogenation, especially when the desirable products are high molecular weight (long-chain hydrocarbons) paraffins, so that as cobalt has high selectivity to these types of products and such catalysts are favourable for diesel and wax products formation [53]. Co-based catalyst appears to be more suitable for FT synthesis because it has high FT synthesis activity; high resistance to deactivation by water; low oxygenates selectivity; low WGS activity and better catalyst stability in hydrogen-rich environments [56, 57]. In order to increase the catalyst activity, a Co-based catalyst is usually supported on a high surface area support to obtain a high metal dispersion. The commonly used supports include

silica (SiO_2), alumina (Al_2O_3), titania (TiO_2), zirconia (ZrO_2) and zeolites (ZSM-x). The productivity of Co-based catalysts at a high conversion level is currently greater than that of Fe-based catalysts. However, it is argued that Fe-based catalysts may be an interesting choice for BTL technology, since it is much cheaper, impacting on the cost of the process due to inevitable process set-ups in industrial operation. Nevertheless, due to the high catalytic activity of the Co-based catalyst and its long life, it is currently the catalyst of choice for the conversion of syngas to liquid fuels. Co-based catalysts are used in LTFT processes only, due to their high activity; it has been reported that they produce mainly methane at higher temperatures [53, 58]. At LTFT conditions, Co-based catalysts have been reported to be more stable than Fe-based catalysts, have a much higher resistance to deactivation by water and therefore have much longer process lives than Fe-based catalysts (~5 years in LTFT fixed bed reactors) [55, 59]. The differences in catalyst compositions illustrated in Figure 2-4 are mainly due to the relative cost of both metals, from the literature point of view [29]. The very high price of Co-based catalysts means that ideally, more of the metal needs to be exposed on the catalyst surface [53]. For this reason, Co-based catalysts are typically supported on carriers that are stable (during catalyst calcination, activation and reaction) and that have a high surface area such as Al_2O_3, SiO_2 and TiO_2 [60]. This is usually done by impregnation of these support materials with aqueous cobalt salt solutions. These support materials can also have an influence on the catalyst activity, catalytic performance (in terms of CO conversion versus time on stream), the product distribution and selectivity. Promoters like boron, ruthenium and rhenium are commonly used in order to improve the reducibility of the catalyst prior to the FT reaction, as well as enhancing the C_{5+} selectivity and catalyst activity, by keeping the metal surface clean from carbon deposition during the reaction [16, 61, 62]. This has been shown in different studies reported in the literature [59, 63, 64]. The cobalt oxide phase in the catalyst usually reduces at temperatures

above 573 *K*, which are higher than those used in LTFT conditions. Hence, the ease of catalyst reducibility is quite significant, as the catalyst has to be reduced before it is loaded into the reactor, adding extra costs and process stages.

2.5. Fischer-Tropsch Reactors

The next step after the syngas is cleaned and conditioned (see section 1.2.2), is to take part in the FT synthesis reaction that is carried out in the reactor vessel [29]. The choice of reactor creates many concerns and the influence on refining is substantial. The characteristics of the main reactor types used in FT synthesis are given in detail in the literature [30]. In general, three different main categories of reactor are used in FT synthesis technology. These are fixed bed, fluidized bed, and slurry bed. The essential parameters that need to be taken into account in reactor selection have been explained in detail in the literature [65]. The fundamentals and detailed development of FT reactors have also been reviewed in the literature [8, 18, 53, 66-70]. The highly exothermic nature of the synthesis reactions is the main consideration in the design of FT reactors. This necessitates the fast heat removal from the catalytic reactor bed by taking the reactor technology into account. It is very important to control the isothermal within the reactor or catalyst bed, since high temperature conditions in an FT reactor leads to high methane formation as well as low-chain hydrocarbons, which are not the favourable products in full conversion [29]. Moreover, a higher catalyst deactivation rate (due to sintering and other deactivation mechanisms) can be expected as a result of an overheated catalyst [53, 66]. High gas space velocities (and therefore turbulent gas flows) through narrow catalyst-packed tubes in fixed bed reactors can ensure high heat exchange rates [53]. On the other hand, fluidized bed

reactors are employed so that the catalyst is dispersed within the liquid phase leading to good isothermal temperature control due to very efficient heat transfer [53].

2.5.1. Fixed Bed Reactors

Typically, the plug flow reactor model is approximated in fixed bed reactors so that the reaction components and reaction conditions of the medium vary continuously along the axial length of the catalytic bed. The driving force for synthesis is maximized and, in the absence of heat and mass transfer limitations, fixed bed reactor technology is the most efficient reactor type for synthesis [30]. Compared to slurry and fluidized bed reactors, at the same level of conversion, the products from a fixed bed reactor can be expected to have higher hydrogenation activity (i.e. less olefins and oxygenates). For instance, considering Fe-LTFT synthesis at 521 *K*, 8 *bar* and 50–60% CO conversion, the C_2−C_4 olefin to paraffin ratio for fixed bed FT synthesis is typically 0.09, 0.9, and 1.2 respectively; whereas for slurry bed synthesis it is typically 3.7, 5.6, and 4.5 [30, 71]. Fixed bed reactors are employed in LTFT processes (see Figure 2-5) for mainly diesel and waxes production [17]. As discussed in section 2.4, the main types of catalysts used in LTFT reactors are Co-based catalysts, which have a high selectivity towards diesel and high molecular weight waxes. Fe-based catalysts can also be utilized in LTFT reactors; although, it has been reported that the operating temperature cannot exceed 533 *K*, as the reactor will be blocked with carbon deposition [66].

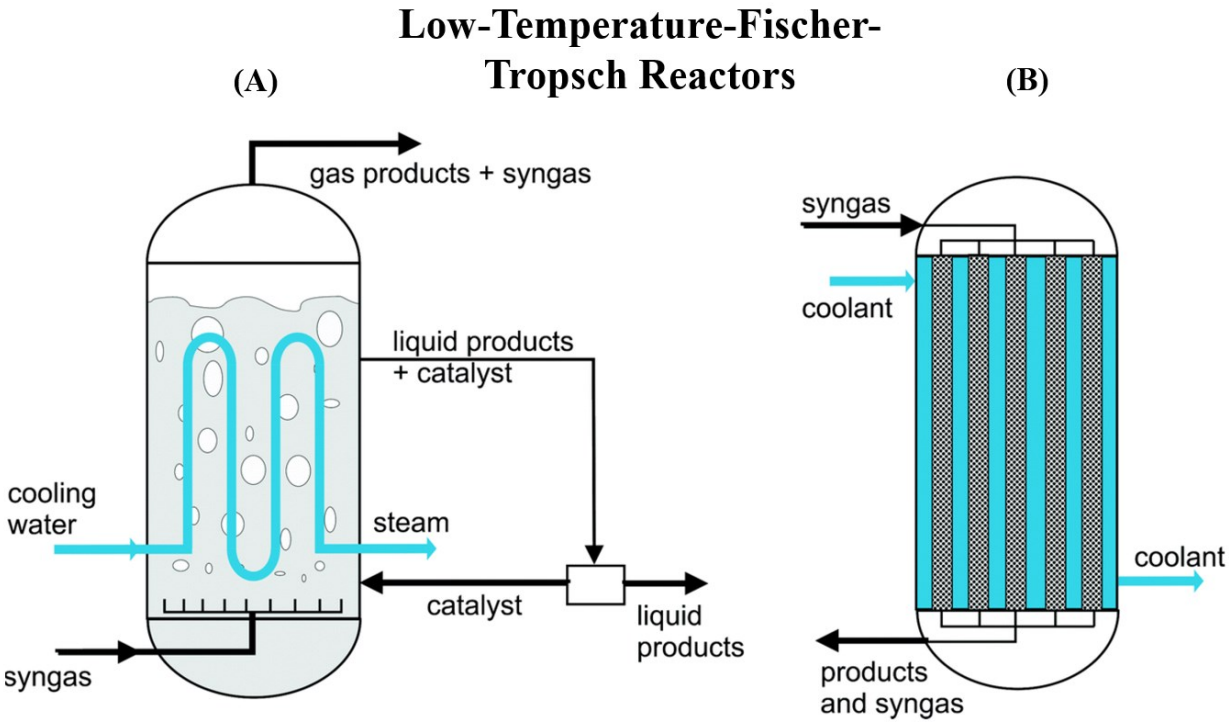

Figure 2-5 LTFT reactors: A) slurry phase reactor and B) multi-tubular fixed bed (adapted from [72]).

2.5.2. Slurry Phase Reactors

Similar to fixed bed reactors, a slurry phase reactor is typically utilized in LTFT processes (see Figure 2-5) for the production of diesel and waxes [17]. In this type of reactor, the syngas flows up the slurry bed, which contains mainly FT waxes and liquid products, as well as the suspended catalyst, making it a three-phase system [55]. This makes these reactors suitable for LTFT operation as the waxes produced also serve as the liquid phase within the reactor [66]. The pros of slurry beds are lower capital expense for the same capacity compared to a fixed bed reactor; lower pressure drop in the reactor vessel and hence lower gas compression costs; less catalyst loading and consumption; and longer reactor runs are possible, since the catalyst can be removed and replaced online. Regardless of the above merits of slurry bed reactors, they

have a few disadvantages. The wax produced from the slurry bed reactor requires to be separated from the bed as well as from the suspended catalyst. Such procedure needs an extra equipment to prevent losing any of the catalyst. If a contaminant such as H_2S enters the reactor, then unlike the poisoning of only the top layers that would occur in multi-tubular fixed-bed reactors, the entire amount of the catalyst used would be poisoned in the slurry phase reactor. For this reason, gas cleanliness requirements are stricter when operating slurry phase beds [29].

2.5.3. Two Phase Fluidized Bed Reactors

Circulating fluidized bed reactors and fixed fluidized bed reactors are usually used in HTFT processes (see Figure 2-6) for production of gasoline and higher-value chemicals. At HTFT conditions within the reactor, all the products are in the gas-phase and hence only two phases exist within the system (the catalyst being the solid phase) [65]. These reactors can only be used with two phases (gas/solid) as any liquid or wax deposits on the catalyst would lead to agglomeration of the catalyst and subsequent loss of the fluid phase [67]. Therefore, the heaviest hydrocarbons that are produced using these types of reactors are naphtha grade products [8]. As BTL-FT processes would usually aim for maximum yields of liquid fuels and diesel in particular, HTFT operations using fluidized beds have not been investigated for BTL-FT applications.

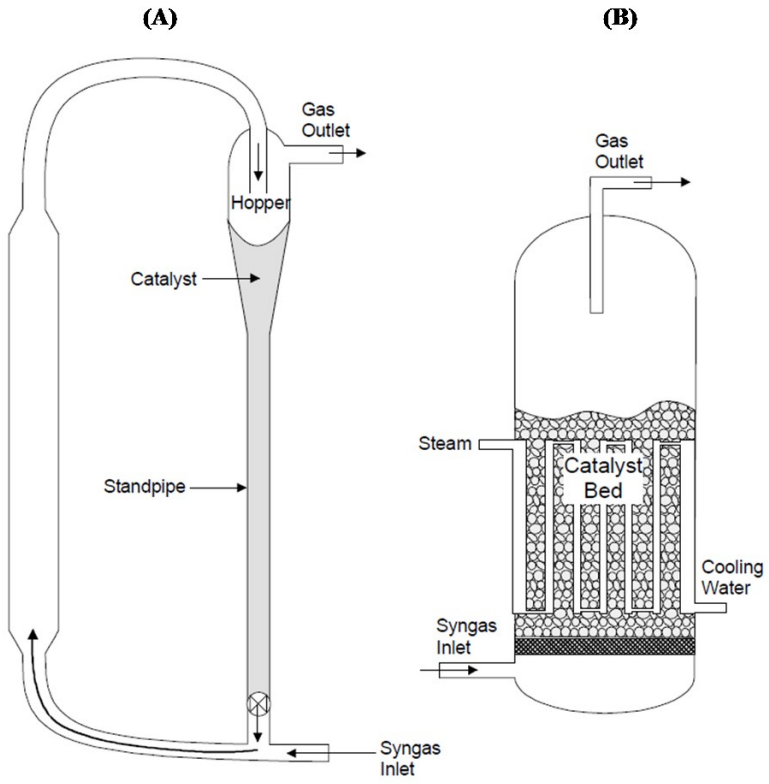

Figure 2-6 HTFT reactors: A) circulating fluidized bed and B) fixed fluidized bed (adapted from [22]).

2.6. Kinetics of Fischer-Tropsch Synthesis

The kinetics description of FT synthesis is crucial to industrial practice, being a prerequisite for industrial process design, optimization and simulation. The principal governing factors in any FT kinetics mechanism are the reaction temperature, total pressure, flow rate, catalyst loading and the H_2/CO molar ratio, which affect FT products' distribution. The FT synthesis reaction is a highly complex system in which thousands of species take part in an extremely coupled mode. For this reason, it is unlikely a kinetics equation could be established for every reaction species with the conventional method used in reaction kinetics studies. Such

a complex reaction system requires a simplified mathematical equation to elucidate the kinetics characteristics of syngas disappearance and products' distribution.

Many equations describing the intrinsic rate of FT synthesis have been proposed in the literature. They are categorized into two main types: the rate of FT synthesis reactions can be expressed either based on an empirical model, which will be discussed in section 2.6.1; or based on a proposed mechanism with a postulated rate deterring step (RDS) and this will be explained in section 2.6.2.

2.6.1. Fischer-Tropsch Kinetics Based on an Empirical Model and Power-Law Rate Expression

A number of kinetics studies have been reported based on an empirical power-law rate expression for Co- and Fe-based catalysts to fit the experimental data. A summary of these studies; the type of rector and catalyst used; operating conditions i.e. temperature, pressure and H_2/CO molar ratio; as well as the proposed rate equation; are given in Table 2-3 in the order of publication date [73-85]. With a glance at this table, one can deduce that unlike Fe-based catalysts reaction order for the CO partial pressure in the rate model is negative, proposing inhibition by adsorbed CO species. The FT reaction rates typically increase with the H_2 partial pressure and decrease (in some cases and depending on the nature of the mechanism and/or the developed rate model) with the H_2O partial pressure.

Equation 2-1 below is the general form of the rate expression for a proposed j^{th} reaction equation based on an empirical power-law rate expression. In this equation, P_{CO} and P_{H_2} stand

for partial pressure of CO and H_2, respectively; $k_{j,0}$ denotes the pre-exponential factor of rate constant and E_j denotes the activation energy; n_j and m_j indicate the order of reaction with respect to CO and H_2 partial pressures, respectively.

$$R_j = k_{j,0} exp\left(-\frac{E_j}{R_g T}\right) P_{CO}^{n_j} P_{H_2}^{m_j} \quad \text{Equation 2-1}$$

Anderson [75] found water inhibition in the rate expression, Equation 2-4, at higher conversion and stated that the first order rate equation, Equation 2-5, fits the data well when the syngas conversion is less than 60%. Mathematically, Equation 2-4 reduces to Equation 2-5 and the water partial pressure term can be neglected when water concentration is low ($P_{CO} \gg P_{H_2O}$). From the physical point of view, mathematical analysis seems to be true. In the beginning of the process, the mole fraction of water is zero so the water inhibition term will be zero. As the FT synthesis reaction takes place, water vapour concentration will be increased so that, depending on the nature of the catalyst and reaction process, it will be considered as the main product of the FT synthesis. Eventually, water decreases the reaction rate by competing with carbon monoxide for an available surface adsorption site. Dry *et al.* [76] studied the rate of FT synthesis over a triple promoted iron catalyst at the higher H_2/CO molar ratio given in Table 2-3. The reaction rate (Equation 2-5) was found to be of zero order with respect to the CO partial pressure and of first order with respect to the H_2 partial pressure; it is only applicable in the conditions used in that study. These findings were in agreement with the relative adsorption characteristics of H_2 and CO on reduced magnetite surfaces. It was concluded that the hydrogen concentration has stronger effect than the carbon monoxide and in fact, carbon monoxide merely has an influence on FT kinetics under certain conditions. Hence, the carbon monoxide partial pressure term could be eliminated from the kinetics rate expression; in this case the rate

expression becomes of the first order dependence as observed by Anderson [75] and Jess *et al.* [81]. Yang *et al.* [77] and Pannell *et al.* [79] obtained an empirical rate expression for their results based on Co supported catalysts using a fixed bed reactor via regression of a power-law rate expression of the general form of Equation 2-1. The reaction order for H_2 partial pressure was observed to be positive; while the reaction order for CO partial pressure was negative, suggesting inhibition by adsorbed CO. Bub and Baerns [78] predicted product distributions from kinetics measurements in a laboratory-scale recycled fixed bed reactor at high reaction temperature; but no information was given relating to the H_2/CO molar ratio. In this study, the species were CO, H_2, CO_2 and C_1-C_6 hydrocarbons as well as C_2-C_5 alcohols in the aqueous phase. The rates of formation of the individual hydrocarbons were described by power-law rate equations of the form of Equation 2-7. Wang *et al.* [80] studied catalytic behaviour of unsupported and alumina-supported borided cobalt catalysts for FT synthesis at a low temperature condition suitable for a Co-based catalyst. This study was carried out at low CO conversion rates (i.e. in the range of 2-5%); thereby assuring the absence of pore diffusional, mass transfer and heat transfer disguises. In this study, the statistical measures of significance were reported for the data and fitted parameters. Similar to other previous studies [77, 79], Wang obtained a positive order of reaction for H_2 and a negative order of reaction for CO. Zennaro *et al.* [82] obtained the rate data for CO hydrogenation on a 11.7% Co/TiO_2 catalyst in a differential fixed bed reactor at 453-513 *K*, space velocity of 5000 h^{-1} after 10-20 h of reaction with a CO conversion range lower than 18% over a range of reactant (CO and H_2) partial pressures with a relatively high H_2/CO ratio. Zhan *et al.* [83] studied the kinetics of FT synthesis over a Co/Al_2O_3 catalyst. This study was conducted in continuous stirred tank reactor (CSTR) reactor at 10%-60% CO conversion. All data were collected after at least 100 hours of time-on-stream to eliminate the ambiguity between initial catalyst activity and stable activity.

The kinetics expression in the simple power-law form of Equation 2-12 was adopted since the H_2/CO ratio in the feed gas, and thus in the reactor tail gas, was always approximately constant. In this expression, the exponent 'm' was, indeed, the sum of the reaction orders of hydrogen and carbon monoxide. They indicated that the simplified model significantly reduces the amount of experimental work and is appropriate when process design considerations are the primary motivation for developing the kinetics expression. They found that this empirical kinetics expression is adequate for both fresh and regenerated catalysts within a wide range of practical operating conditions. Marvast *et al.* [84] modelled a two-dimensional fixed bed FT reactor packed with an Fe-HZSM5 catalyst using the same approach. However, their results (for the rate of conversion and production) were not sufficiently accurate with a high relative error carried by the model. Das *et al.* [85] found empirical rate expressions for supported Co catalysts using a fixed bed reactor via regression of a power-law equation. The addition of H_2O in FT synthesis over a 12.4 wt% Co supported SiO_2 catalyst led to a significant increase in CO conversion. This positive reversible effect of water seems to be kinetics because the activity of the catalyst recovered when low levels of water addition were terminated. The rate expression for CO hydrogenation has been obtained at 10%-70% CO conversion. The data of this study were fitted by a simple power-law expression of the form of Equation 2-14. The negative value of 'm' shows that there is a positive water effect on the CO hydrogenation rate.

Table 2-3 FT synthesis overall reaction rate and/or consumption rate (in terms of either CO species or total syngas conversion) based on empirical power-law rate expression

Reactor Type	Catalyst	T (*K*)	P (*bar*)	H_2/CO molar ratio	Rate equation	Equation	Reference
Fixed bed	Co-MgO/ThO_2-Kieselguhr	458-473	1	2.0	$r_{C,org} = kP_{CO}P_{H_2}^2$	Equation 2-2	Brotz [73]
Fixed bed	Fe	523-593	20.2-40.2	2.0	$-r_{CO+H_2} = kP_{total}$	Equation 2-3	Hall *et al.* [74]
Fixed bed	Reduced and nitride Fe	498-528	20.2	0.25-2.0	$r_{FT} = \frac{kP_{CO}P_{H_2}}{P_{CO} + aP_{H_2O}}$	Equation 2-4	Anderson *et al.* [75]
Fixed bed	Promoted Fe	513	10-20	1.2-7.2	$-r_{CO+H_2} = kP_{H_2}$	Equation 2-5	Dry *et al.* [76]
Fixed bed	Co/CuO/Al_2O_3	458-473	17-55	1.0-3.0	$-r_{CO+H_2} = kP_{CO}^{-0.5}P_{H_2}$	Equation 2-6	Yang *et al.* [77]
Gradientless	100 Fe/5 Cu/4.2 K/25 SiO_2	522-562	3-20	N/A	$r_j = k_j P_{CO}^{m_j} P_{H_2}^{n_j}$	Equation 2-7	Bub and Baerns [78]

Berty	$Co/La_2O_3/Al_2O_3$	488	5.2-8.4	2.0	$-r_{CO+H_2} = kP_{CO}^{-0.33}P_{H_2}^{0.55}$	Equation 2-8	Pannell *et al.* [79]
Berty	$Co/B/Al_2O_3$	443-468	10-20	0.25-4.0	$-r_{CO} = kP_{CO}^{-0.5}P_{H_2}^{0.68}$	Equation 2-9	Wang [80]
Fixed bed	Fe	523	25	N/A	$-r_{CO} = kP_{H_2}$	Equation 2-10	Jess *et al.* [81]
Fixed bed	Co/TiO_2	453-513	8-16	1-4	$-r_{CO} = kP_{CO}^{-0.24}P_{H_2}^{0.74}$	Equation 2-11	Zennaro *et al.* [82]
CSTR	Co/Al_2O_3	483-503	20-30	2.1	$-r_{CO} = kP_{CO}^{m}$	Equation 2-12	Zhan *et al.* [83]
Fixed bed	Biofunctional Fe-HZSM5	573	17	0.96	$r_j = k_j P_{CO}^{m_j} P_{H_2}^{n_j}$	Equation 2-13	Marvast *et al.* [84]
CSTR	Co/SiO_2	483	22	1.0-2.4	$r_j = \frac{0.883\ P_{CO}^{-0.25}\ P_{H2}^{0.5}}{1-0.155(P_{H2O}/P_{H2})}$	Equation 2-14	Das *et al.*[85]

2.6.2. Reaction Pathways and Polymerization Reaction in the Fischer-Tropsch Synthesis

Different kinetic mechanisms proposed by the literature have involved the concept of the polymerization reaction, a stepwise chain growth process. The assumption was based on the fact that the distributions of hydrocarbon products are calculated only on chain growth probabilities that matched the experimentally measured data over widely varying process conditions, with different catalysts and in various reactor types and sizes. Nevertheless, these studies did not completely describe the FT synthesis reaction mechanism. Some of the major problems in describing the FT reaction kinetics are the complexity of its reaction mechanism, the large number of species involved; its dependency on operating conditions and the wide range of experimental conditions used; the choice of catalyst; and even the reactor type. Despite these complexities, there have been several attempts made to investigate the FT reaction mechanism; the earliest mechanism proposed by Fischer and later refined by Rideal [86], involved surface carbides. The progressive work of Fischer and Tropsch in the 1920s showed that hydrocarbon chain formation proceeds via the stepwise addition of one carbon atom at a time. Over the past 20 years a great deal more information has become available describing the application of various sophisticated surface analytical techniques and experiments. The general consensus from these experiments has been that carbene ($-CH_2$) species are involved in the chain growth mechanism with CO insertion accounting for the formation of oxygenates [87, 88]. There are many apparently different mechanisms reported [42, 49]. Since Anderson's research in 1956, most studies have assumed a simple polymerization reaction for the hydrocarbons yield. It is widely accepted that the FT reaction is based on polymerization of methylene units, which was originally proposed by Fischer and Tropsch [89]. Another widely

accepted theory maintains that the initiation of the FT reaction involves the adsorption and dissociation of CO on two vacant active sites. The adsorbed and dissociated CO on the catalyst surface reacts with hydrogen to form the surface carbyne (methylidyne, $CH-\Theta$) and surface carbene (methylene, $CH_2-\Theta$) which are the monomers of the overall polymerization reaction [90]. In spite of the differences, all the proposed mechanisms have the assumption which is related to the chain growth step in the polymerisation process**.** Figure 2-7 indicates the polymerisation steps involved in the FT reaction mechanism and illustrates the different reaction paths that these monomers can follow.

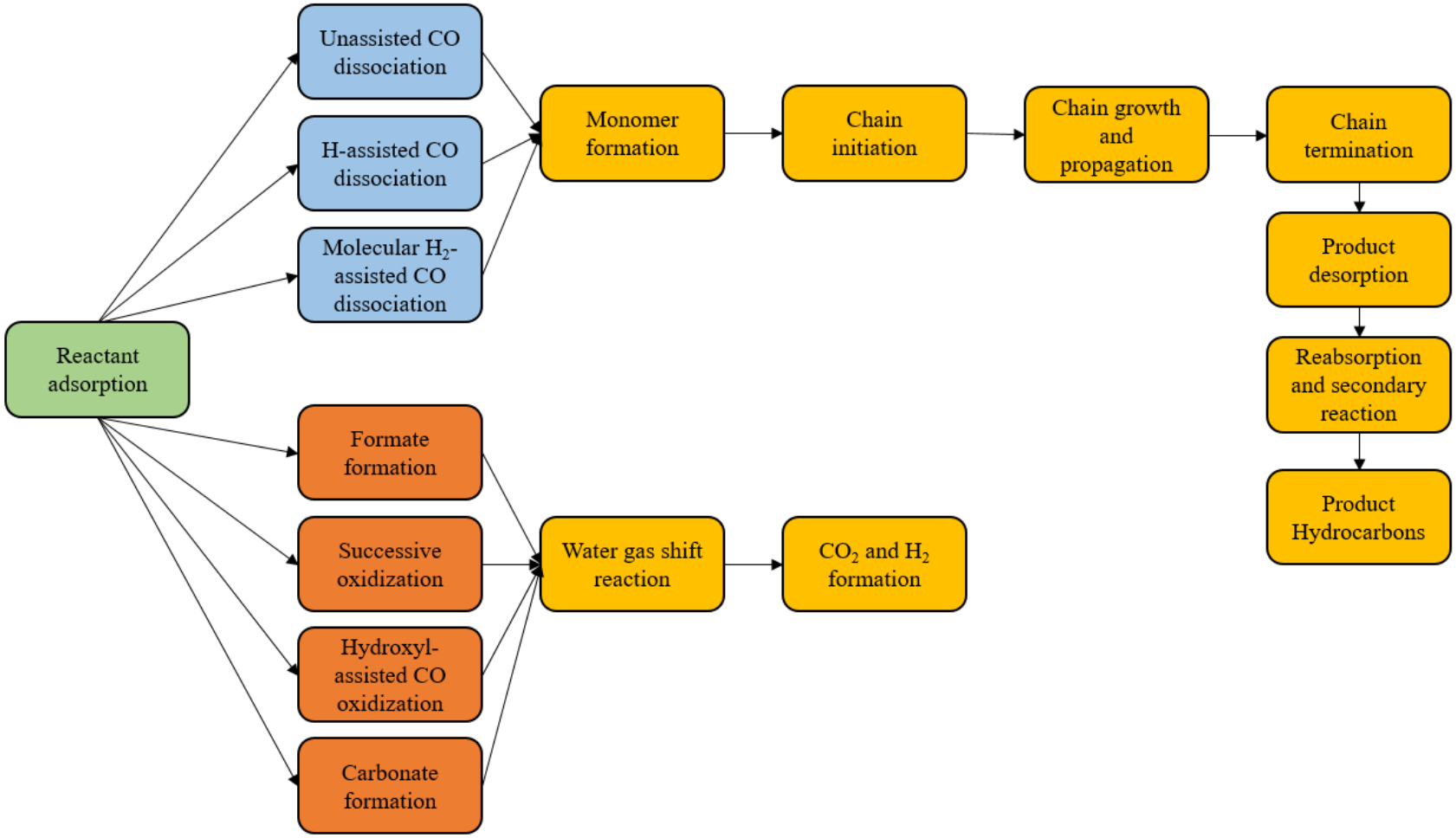

Figure 2-7 Flow diagram of FT synthesis reaction pathway considering different adsorption paths, polymerization steps, as well as water gas shift reaction.

Considering the surface polymerization reaction, the kinetic mechanism of FT synthesis consist of surface reaction steps in six categories: (1) adsorption of reactants (CO & H_2) on the catalytic surface; (2) chain initiation; (3) chain growth (propagation); (4) chain termination and desorption of products; (5) re-adsorption and secondary reaction (optional) as well as (6) WGS reaction. It is proposed that the FT synthesis reaction mechanism starts via adsorption of reactants (H_2 and CO) on the catalyst surface. The CO adsorbs on the catalyst surface either in a molecule or dissociated state. Wojciechowski [91] deduced that any FT kinetics mechanism must have the following characteristics:

I. Adsorption of all species on the catalyst surface onto one set of sites resulting in the decomposition of CO and H_2 to adsorbed C and O and hydrogen atoms, respectively. The interaction between these surface species leads to the formation of CH_x, OH, etc.

II. The monomeric species for oligomerisation is CH_2 and its formation from adsorbed C and H is the RDS for CO hydrogenation kinetics.

III. The growing radical on the surface is immobile except for C_1-C_4 species. Chain growth proceeds only with a monomer near the growing chain and can either be formed next to it or migrate via surface diffusion among an appropriate set of sites.

IV. Surface chain growth can produce spontaneous 1-2 shift attachments leading to branched hydrocarbons.

V. The termination event and hence product type is determined by the kind of occupant on the site adjacent to a growing radical. This occupant may be an appropriate termination function such as hydrogen atom, adsorbed OH, or even an empty site. However,

termination occurs after the growing chain has undergone one or more successive 1-2 shifts; internal functional groups will result yielding β-alkenes, 2-alcohols, etc.

VI. All classical distributions consist of product species that are primary; and each has its chain length distribution of the Anderson-Schulz-Flory (ASF) plot. This distribution is the property of a collocation grouping of growth, monomer and termination sites which constitute a 'growth location' for that molecular species. The locations are stable in composition and continue to produce only one type of molecule at a given set of reaction conditions.

VII. System temperature, total pressure and the H_2/CO ratio are fundamental governing factors that affect both kinetics and product distribution.

It is generally assumed that not a single reaction pathway exists for the FT synthesis process on the active site, but that a number of parallel operating pathways will exist. Several reaction mechanisms have been suggested depending on the creating steps I, II and III. Although the formation of the chain initiator and propagation steps are different from each other, all the mechanisms share hydrocarbon product desorption, hydrogenation for the paraffin and β-dehydrogenation for the olefin products. Most of the proposed mechanisms remain within four popular categories, which are: (i) alkyl mechanism; (ii) alkenyl mechanism; (iii) enol intermediate; (iv) CO-insertion; which will be discussed in sections 2.6.2.1 to 2.6.2.4.

2.6.2.1. *Alkyl Mechanism*

The earliest FT synthesis reaction mechanism proposed by Professor Franz Fischer and Hans Tropsch in 1926 and later refined by Craxford and Rideal [86] involved surface carbides [66]. The alkyl mechanism (also known as carbide mechanism) was first proposed by Brady and Pettit [92, 93]. Among different kinetics mechanisms, the alkyl mechanism is the most widely adopted mechanism for chain growth in FT synthesis. Figure 2-8 to Figure 2-10 illustrate the postulated reaction pathways for this mechanism including initiation, propagation and chain termination steps. In this mechanism, surface carbon and surface oxygen are generated via dissociative CO chemisorption. Surface oxygen is removed from the surface by reaction with adsorbed hydrogen yielding the most abundant product, a water molecule, or by reaction with adsorbed carbon monoxide yielding CO_2. Surface carbon is subsequently hydrogenated in sequential reactions yielding CH, CH_2 (methylene) and CH_3 (methyl) intermediate species. The surface methyl species is regarded as the chain initiator, and chain initiation in an alkyl mechanism takes place via this reaction pathway (see Figure 2-8). The surface methylene species is regarded as the monomer (building block) in this reaction scheme and chain growth is assumed to take place by successive insertion of methylene species into the metal-alkyl bond (see Figure 2-9). Termination of the chain growth (product formation) is generally thought as desorption of the surface complex species and takes place by either hydrogen addition or β-hydrogen elimination, yielding n-paraffins and α-olefins, respectively. Both have been identified as primary products in FT synthesis by a large number of previous studies. The schematic of the termination step of this mechanism is illustrated in Figure 2-10.

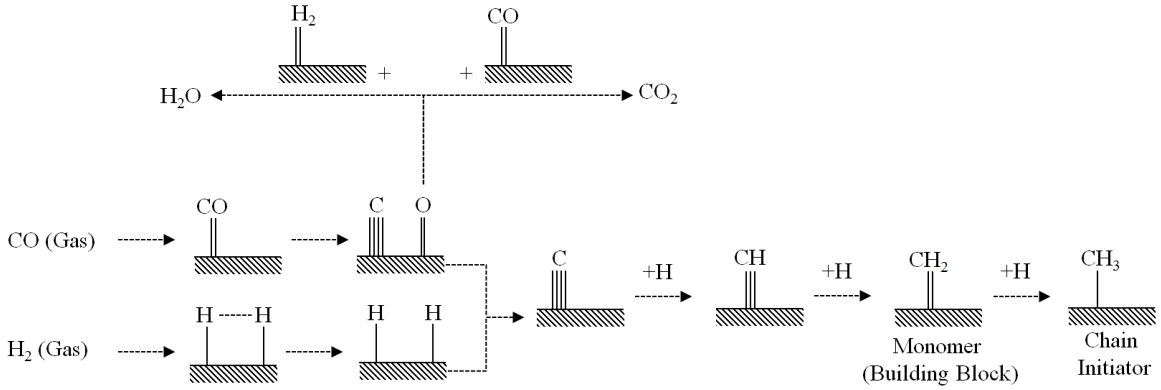

Figure 2-8 Schematic of FT synthesis reaction pathway based on alkyl mechanism ($R = C_nH_{2n+1}$) chain initiation step, alkyl (carbide) mechanism.

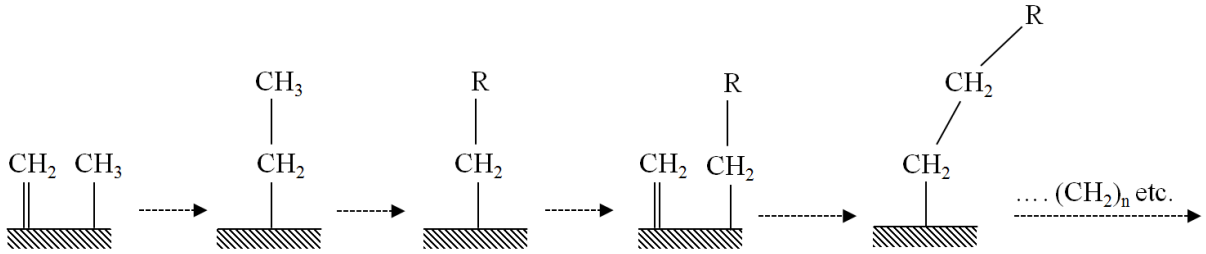

Figure 2-9 Propagation (chain growth) step, alkyl mechanism.

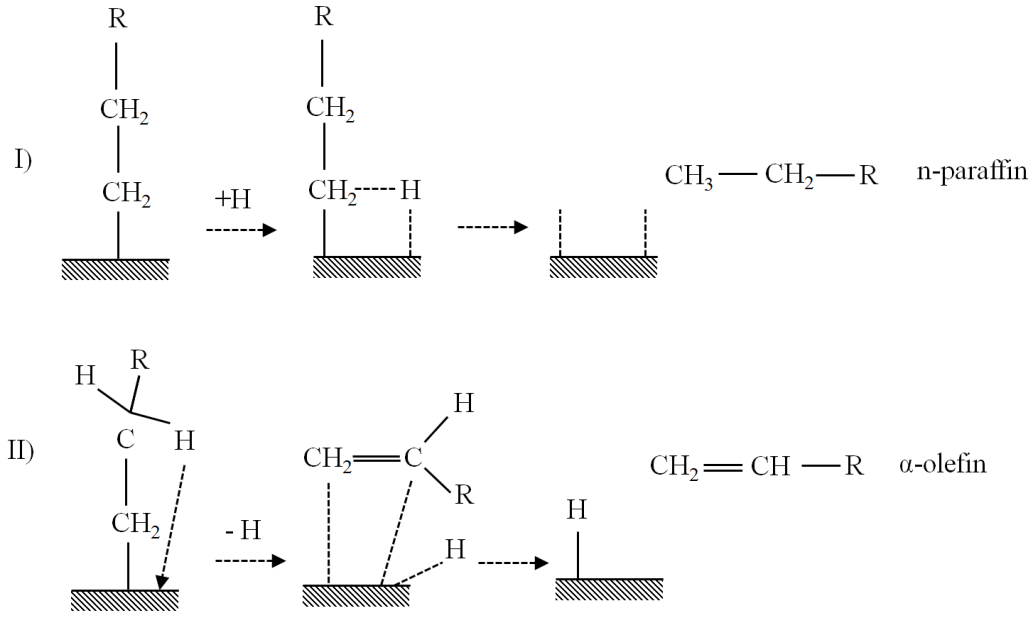

Figure 2-10 Termination (product desorption) step, alkyl mechanism.

2.6.2.2. *Alkenyl Mechanism*

An alternative reaction pathway has been proposed by Maitlis and co-workers [94, 95] (see Figure 2-11, Figure 2-12 and Figure 2-13) to predict the formation of olefins in the FT synthesis. From the alkenyl mechanism, it is postulated that the FT synthesis reaction is a surface polymerization of methylene intermediates formed by the synthesis gas dissociative chemisorption and is followed by carbide hydrogenation on the surface of the catalyst [96]. The initial carbon monoxide activation and its transformation into CH_x surface species are identical to the proposed alkyl mechanism [8]. In contrast to the alkyl mechanism, the reaction is initiated through the formation of the first C-C bond occurring through the coupling of methylidyne (CH) and methylene (CH_2) to form a vinyl surface species ($CH=CH_2$). The vinyl surface intermediate was regarded as the chain initiator.

The hydrocarbon chain growth takes place by the addition of a methylene species to a surface alkenyl species (vinyl species) yielding a surface allyl species ($–CH_2CH=CH_2$) and it is followed by an isomerization of allyl-vinyl, yielding an alkenyl (vinylic) species ($–CH=CHCH_3$), which may react further. Termination involves the addition of hydrogen to an alkenyl species forming α-olefins; however, this mechanism failed to explain the primary yielding of n-paraffins and the co-existence of an alternative chain growth pathway is required [8].

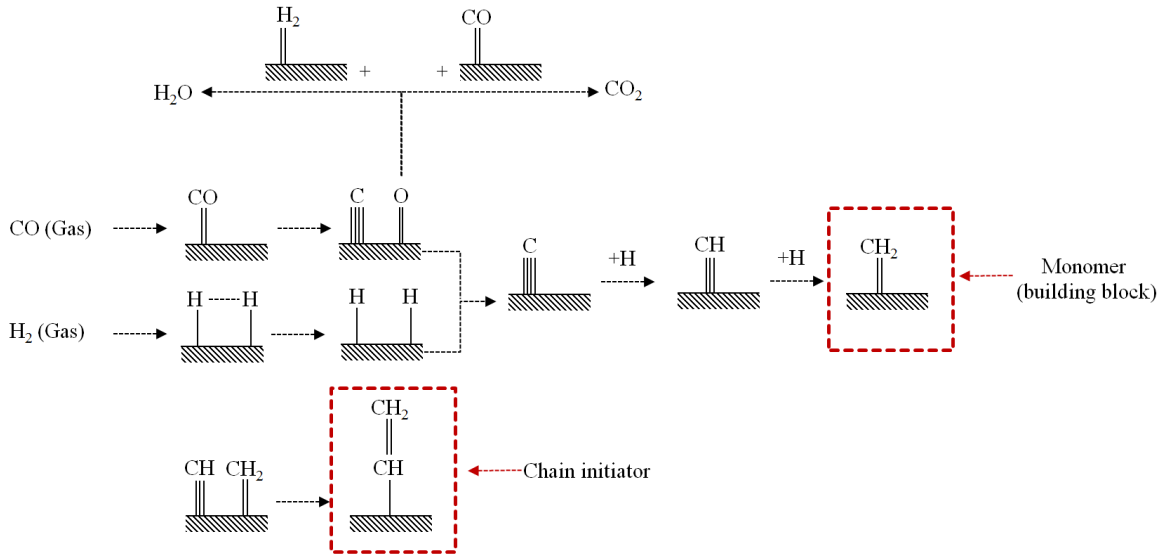

Figure 2-11 Schematic of FT synthesis reaction pathway based on alkenyl mechanism ($R = C_nH_{2n+1}$) chain initiation step.

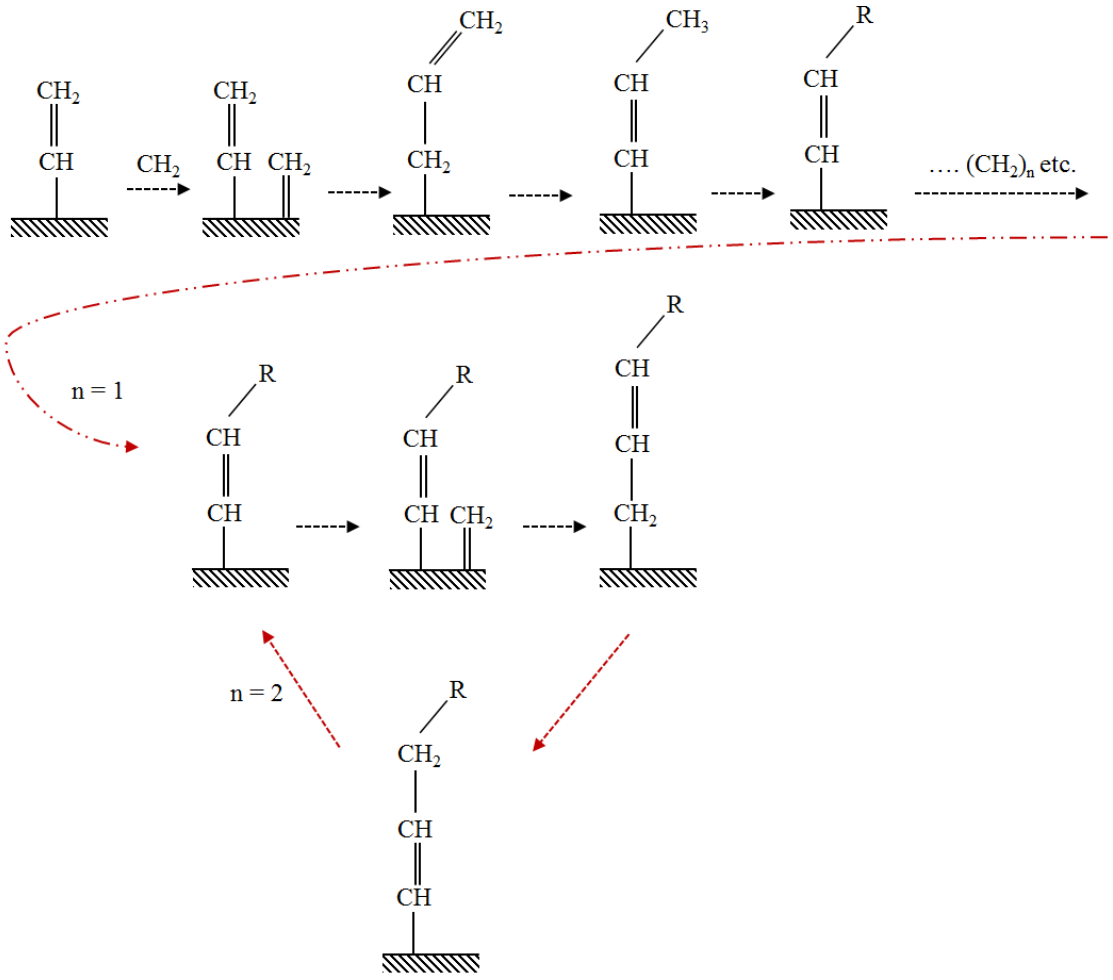

Figure 2-12 Propagation (chain growth) step, alkenyl mechanism.

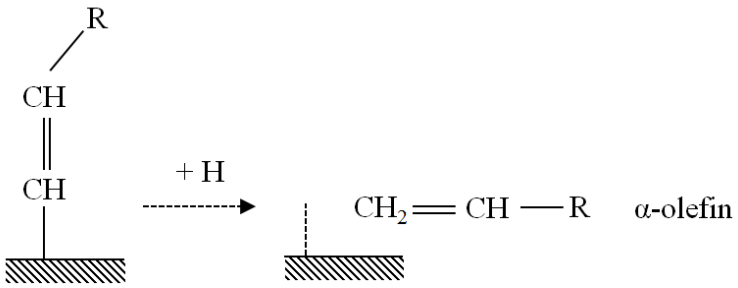

Figure 2-13 Termination (product desorption) step, alkenyl mechanism.

2.6.2.3. *Enol Mechanism*

The carbide mechanism is mostly aimed at the elucidation of production of α-olefins and n-paraffins. This mechanism is unable to describe the oxygenated products, such as alcohol. About 1951, Storch *et al.* [97] proposed an alternative reaction mechanism involving hydroxyl carbenes, =CH(OH). In the early 1950s, the oxygenate (enol) mechanism gained widespread acceptance [98]. This reaction mechanism involves the chemisorption of CO, which reacts with adsorbed hydrogen to form a hydroxyl (enol) species. In this mechanism, there is no distinct differentiation between chain initiator and monomer. Figure 2-14 shows formation of initiator and monomer intermediate species (($R = C_nH_{2n+1}$)). Chain growth occurs through a combination of condensation and water elimination steps between two enolic species (using adjacent groups) as depicted in Figure 2-15. Intermediate species are all enolic molecules so termination by a desorption process could only form oxygenated products; by which aldehydes and alcohol are produced by simple desorption and hydrogenation of the enolic species, respectively (see Figure 2-16). To account for the formation of the most abundant hydrocarbon (α-olefins and n-paraffins), another chain termination process is required in this mechanism. Alternative termination of the chain growth is supposed as the chain breaks into α-olefins and surface monomer itself. According to this reaction mechanism, n-paraffins are only formed secondarily by hydrogenation of primarily formed olefins [99].

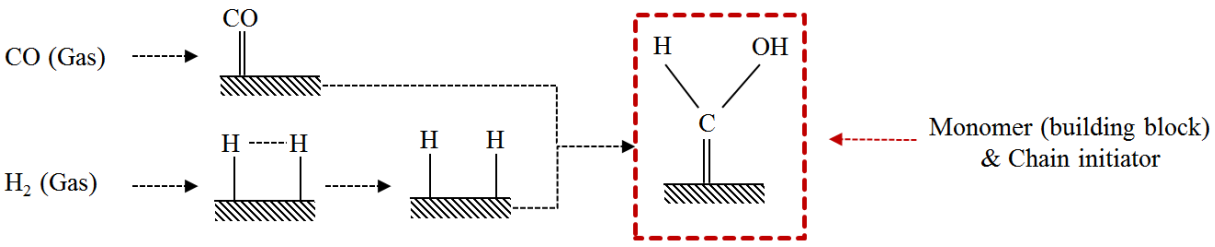

Figure 2-14 Schematic of FT synthesis reaction pathway based on enol mechanism, chain initiation step.

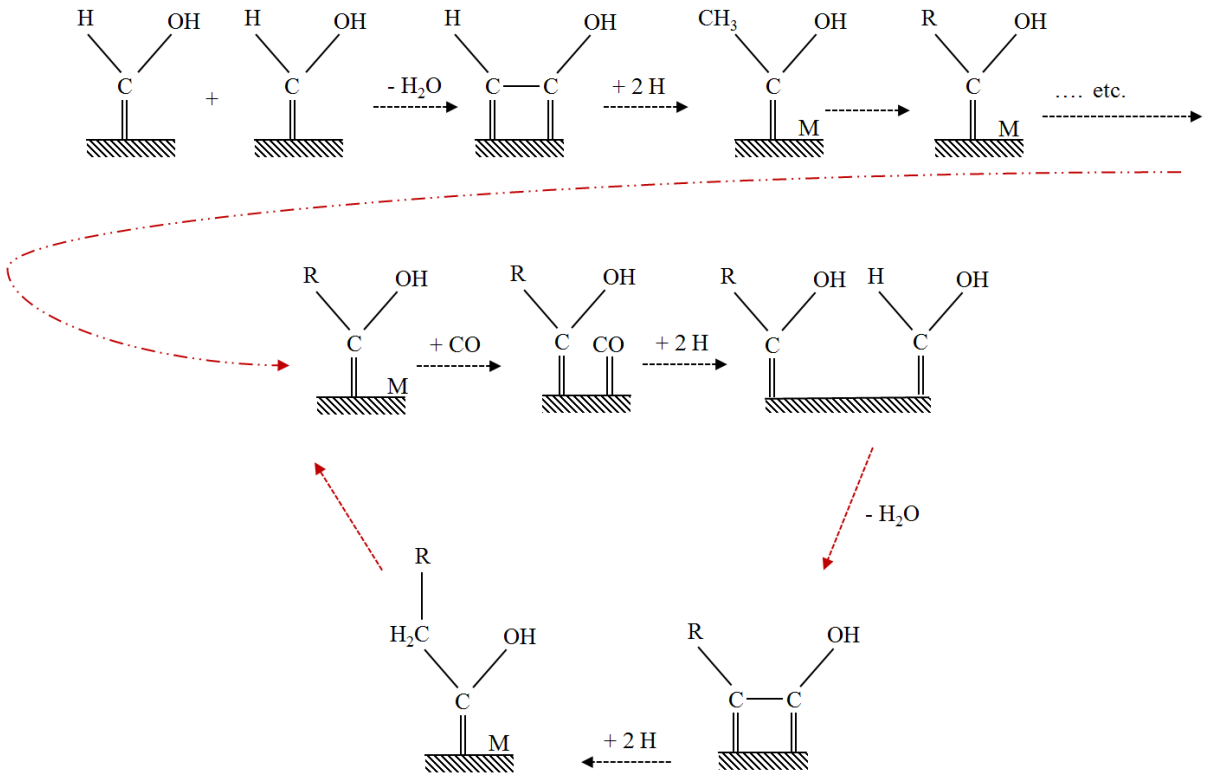

Figure 2-15 Propagation (chain growth) step, enol mechanism.

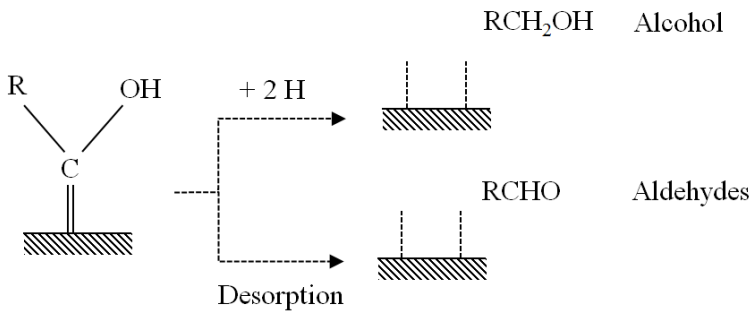

Figure 2-16 Termination (product desorption) step, enol mechanism.

2.6.2.4. *CO Insertion Mechanism*

The direct (CO) insertion mechanism, which was originally proposed by Sternberg and Wender [100] and Roginski [101], was fully developed by Pichler and Schulz (1970). This mechanism involves the insertion of carbon monoxide into a metal-methyl or metal-methylene carbon bond. As in the alkyl mechanism, the chain initiator in the CO insertion mechanism is adsorbed methyl (CH_3) species, but formation of the chain initiator differs from the former when the oxygen is eliminated from the surface species.

In this mechanism chemisorbed CO is the monomer (see Figure 2-17) and the chain growth occurs when CO is inserted directly into a metal-alkyl bond which leads to a formation of surface acyl species that is well known in homogeneous catalysis [102]. The removal of an oxygen atom from acyl leads to the chain growth process (see Figure 2-18). Several reaction pathways have been proposed for the termination step. This mechanism is capable of elucidating a termination process for both linear hydrocarbons (n-paraffins and/or α-olefins) and oxygenated. After a successful insertion of the CO species to the existing chain, the final surface intermediate is identical with that from the carbide (alkyl) mechanism. Therefore, the formation of n-paraffins and/or α-olefins is the same as in the alkyl mechanism (see Figure 2-19). In addition to this, during the progress of the elimination of oxygen, enolic intermediate could form n-alcohol and aldehydes (oxygenated products) by hydrogenation and β-hydrogen abstraction of the R−CHOH species, respectively (see Figure 2-20). This mechanism is also known as the alkyl migration. The CO insertion mechanism is considered by many researchers as the main reaction pathway leading to the oxygenated products formation [55, 103].

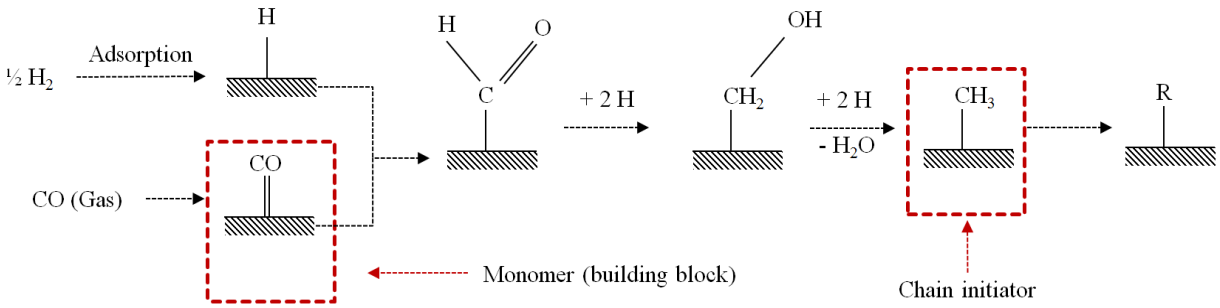

Figure 2-17 Schematic of FT synthesis reaction pathway based on CO insertion mechanism ($R = C_nH_{2n+1}$) chain initiation step.

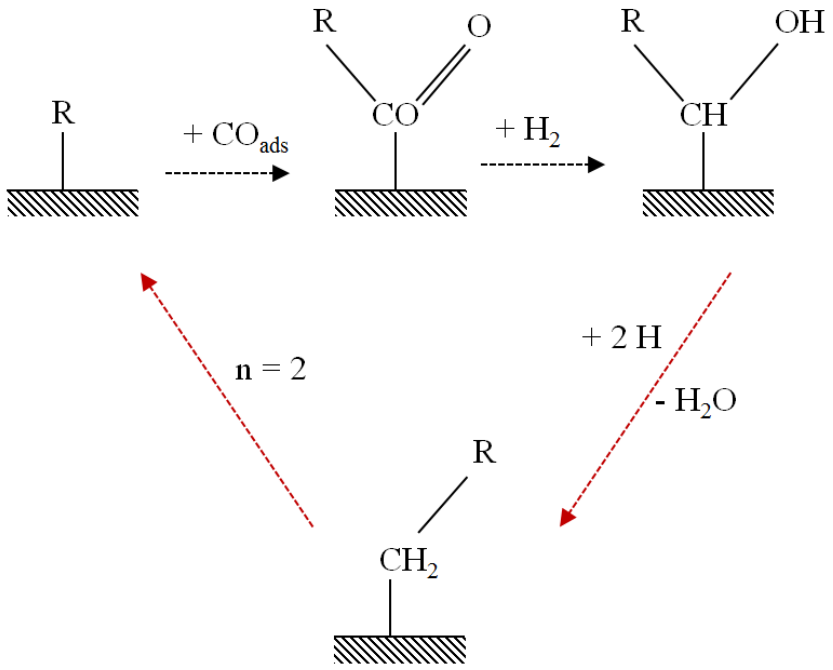

Figure 2-18 Propagation (chain growth) step, CO insertion mechanism.

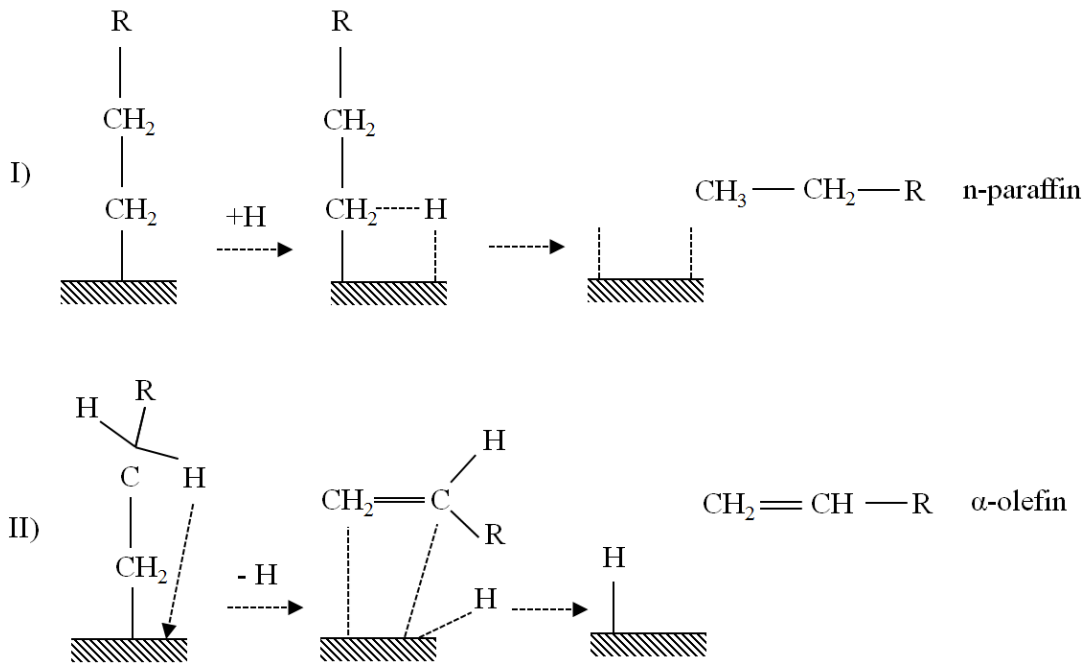

Figure 2-19 Termination (product desorption) step, CO insertion mechanism.

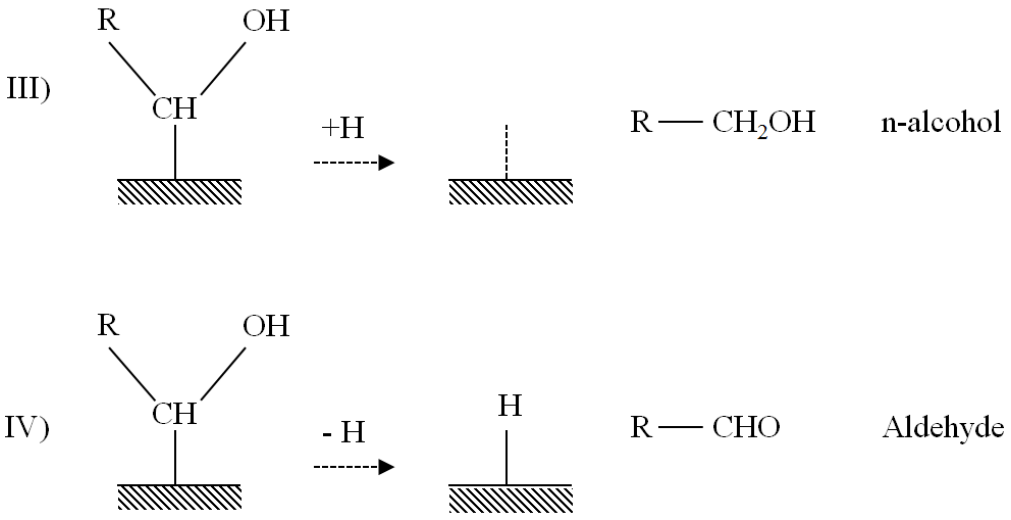

Figure 2-20 Termination (product desorption) step, CO insertion mechanism.

2.6.3. Published Literature on FT Reaction Mechanism

In the case of Co-based FT catalysts, the reaction rate expressions are very limited and have different from Fe-based catalysts. The rate-determining step is the most distinguished feature which results in a different order of the denominator in the rate equation. For Co-based catalyst, the rate-determining step usually involves a bimolecular surface reaction resulting in a quadratic denominator in the rate expression.

Rautavuoma and van der Baan [104] developed the rate equation (Equation 2-20) by assuming that the initiation proceeds via CO dissociation and formation of a CH_2 surface intermediate. It was assumed that CO dissociates on the catalyst surface, forming adsorbed carbon atoms that were the basis of at least the initiation step. The hydrogenation of surface carbon, R. 2-2, was the RDS; whereas the preceding dissociative carbon monoxide adsorption step, R. 2-1, was a fast equilibrium. The chain growth was supposed to proceed by the addition of the same CH_2 groups (i.e. CH_2 insertion mechanism) to the growing molecule. The FT products were then formed by desorption of surface species $C_j - \psi$ (i.e. which is formed by one initiation step and $j - 1$ insertion steps) with or without further hydrogenation from the catalyst surface. $C_j - \psi$ is the adsorbed surface species (C_j) on the vacant active site and ' ψ ' stands for the total vacant surface coverage fraction of the active site of the solid catalyst in the FT rate model.

$$CO + 2 - \psi \rightleftarrows C - \psi + O - \psi \quad \text{R. 2-1}$$

$$C - \psi + 2H - \psi \rightleftarrows CH_2 - \psi + 2 - \psi \quad \text{R. 2-2}$$

$$O - \psi + 2H - \psi \rightleftarrows H_2O - \psi + 3 - \psi \quad \text{R. 2-3}$$

This study aimed directly to investigate the production of small olefins by the FT process. Therefore, the reaction mechanisms as well as the factors that affect the molecular mass distribution and the olefin/paraffin ratio were the main concern. Although the iron is the most favourable catalyst for small olefin production, as it was indicated, the cobalt catalyst was used due to its higher stability which facilitated achieving reproducible measured data. They reported that it is possible that the kinetically equivalent R. 2-3 is the RDS. In this case, surface oxygen would be the most abundant surface species and not surface carbon. They found however that during FT synthesis, the amounts of hydrocarbons and water formed was almost stoichiometrically equivalent; whereas the amount of carbon dioxide formed was very small. Referring to the calculations made by Satterfield and Sherwood [105], it was assumed that no mass and heat transfer limitations existed under the studied operating conditions (see Table 2-5). In spite of the significant effort, the model fitted the experimental results at the constant temperature and pressure condition; therefore the model may not be valid at any other temperature and pressure conditions, since both parameters have significant influence on the rate of reaction.

Wojciechowski [91] and Sarup and Wojciechowski [106] developed six different rate expressions for the formation of the building block, methylene monomer ($-CH_2-$), based on both the enol/carbide and the carbide mechanism, by assuming various RDSs. Equation 2-15 is the generalized expression of the derived six rate equations. The results predicted by the six models were compared to the experimental results at the operating conditions tabulated in Table 2-5. Two models, one based on the H-assisted dissociation of carbon monoxide and the second based on the hydrogenation of surface carbon were developed, both of which provided a satisfactory fit to the experimental results. Equation 2-21 and Equation 2-22 were derived for conversion of CO species based on the postulated mechanism for the first and second model,

respectively. In the first model, the surface reactions R. 2-4 were assumed to be the RDSs which is the hydrogenation of adsorbed CO yielding adsorbed formyl ($HCO-\psi$). However, the RDS in the second model was assumed to be R. 2-5 and R. 2-6; where R. 2-5 is the first hydrogenation of the adsorbed carbon atom and R. 2-6 is the first hydrogenation of the adsorbed oxygen atom.

$$r_{FT} = \frac{kP_{CO}^{a}P_{H_2}^{b}}{\left(1+\sum_{i=1}^{n}K_i P_{CO}^{c}P_{H_2}^{d}\right)^2} \quad \text{Equation 2-15}$$

$$-r_{CO} = \frac{kP_{CO}^{0.5}P_{H_2}^{0.5}}{\left(1+K_1P_{H_2}^{0.5}+K_2P_{CO}^{0.5}+K_3P_{CO}\right)^2} \quad \text{Equation 2-16}$$

$$-r_{CO} = \frac{kP_{CO}P_{H_2}}{\left(1+K_1P_{H_2}^{0.5}+K_2P_{CO}+K_3P_{CO}P_{H_2}^{0.5}\right)^2} \quad \text{Equation 2-17}$$

Equation 2-22 was also reported from the above assumptions on the RDSs; however, this rate expression was not actually derived mechanistically, so it was a further simplified version of the very first two models. In fact, the P_{CO} term in the denominator of the original derived rate Equation 2-16 was dropped due to its comparatively small adsorption constant value – a difference in 4 orders of magnitude under the specified operating conditions (Table 2-5).

$$CO-\psi + H-\psi \rightleftarrows HCO-\psi+\psi \quad \text{R. 2-4}$$

$$C-\psi + H-\psi \rightleftarrows CH-\psi+\psi \quad \text{R. 2-5}$$

$$H-\psi + O-\psi \rightleftarrows OH-\psi+\psi \quad \text{R. 2-6}$$

All six developed models involved a bimolecular RDS (i.e. second order denominator) between the surface carbon and dissociated hydrogen species. Among these rate expressions,

Equation 2-21 and Equation 2-22 tabulated in Table 2-5 were not the best fit to the experimental results. After optimization of the kinetic parameters for the models Equation 2-21 and Equation 2-22, the relative variance of calculated and experimental rate results was over 40 %, signifying a large discrepancy between the results. Therefore, these two models could not accurately predict the measured data. Also, the best fit rate model (Equation 2-17) was rejected since one of the adsorption coefficients was negative, which represents physically unrealistic and meaningless results. In addition, the prediction was made at only constant temperature which is another important issue that will affect significantly the estimation of kinetic parameters.

The rate models developed by Sarup and Wojciechowski were further simplified by Yates and Satterfield [107], including the one that was rejected by original authors [106]. In order to have kinetically convenient and easy analysis, the model was simplified by assuming only two independent kinetic parameters (rate constant ('*k*') and adsorption constant, '*K*'). This simplification was accomplished by assuming that one absorbed intermediate is the predominant chemical species, which is justified by the non-reacting, single-component adsorption data on cobalt surfaces [108]. In the case of Equation 2-21 and Equation 2-17, it was assumed that the CO intermediate was the predominant absorbed species which was also assumed by Rautavuoma and van der Baan [104]. Hence, other surface intermediates such as C, H, O, OH, CH, CH_2, CH_3, CHOH, etc. were neglected. In contrast this, in the case of Equation 2-16 it was assumed that dissociated CO was a predominant species instead of un-dissociated CO and this was implicitly stated by the original authors, Sarup and Wojciechowski [106]. Yates and Satterfield [107] measured the kinetics of a cobalt catalyst in a slurry reactor and the detailed operating conditions were given in Table 2-5. A LH equation which included a bimolecular surface reaction, described the results. Equation 2-23 was derived by Yates and

Satterfield on the basis of the assumptions mentioned above and was found to be a satisfactory fit to the experimental results.

Iglesia *et al.* [109] indicated that the FT synthesis on Co and Ru involves stepwise incorporation of CH_2 species into growing chains and the removal of O atoms as water. Accordingly, CO hydrogenation and product formation rates were found to obey LH kinetics of the form:

$$r_i = \frac{k_i P_{CO}^a P_{H_2}^b}{1 + aP_{CO}} \qquad \text{Equation 2-18}$$

The kinetics constants (k_i) and the reaction orders (‘‘a’’ and ‘‘b’’) were obtained by measurements of synthesis rates and selectivity over a wide range of pressure (1 to 21 *bar*) and H_2/CO ratio (1 to 10). The resulting rate expression, Equation 2-24, is reported in Table 2-5. The results were very similar on Co and Ru catalysts, suggesting a mechanistic similarity in reaction pathways. Such rate expression was consistent with a catalytic sequence of steps involving stepwise hydrogenation of surface carbon formed by CO dissociation [110]. The CO reaction order was negative throughout the range of typical inlet pressure of CO, proposing that adsorbed CO and derived CH_x species were the most abundant reactive intermediates; however, at low CO pressure, the reaction order of ion CO became positive, indicating that the surface was no longer saturated with CO and CH_x species. Such low CO pressure can occur in FT synthesis when pellets or reactors become depleted of CO because transport restricts the arrival of CO molecules at catalytic sites.

As shown in section 2.6.1, Zennaro *et al.* [82] first derived the rate expression, Equation 2-11, on the basis of a empirical power-law rate model. In addition, a mechanistic rate model, Equation 2-25, was also developed for a titania-supported cobalt catalyst based on a simple LH rate form. The detailed FT process conditions are presented in Table 2-3 and Table 2-5. In fact, the second model was found to fit the experimental data better than the power-law rate model, Equation 2-11. This model was slightly similar to that proposed by Yates and Satterfield [107] which was explained above. This study was only investigated at a constant total pressure of 20 *bar* and space velocity of 5000 h^{-1}, which was one of the limitations of this study. Since the principal governing factors at any FT kinetics mechanism are the reaction temperature, total pressure, flow rate, catalyst loading and the H_2/CO molar ratio, the result may not be reliable for FT processes that operate at a different pressure and space velocity.

Elbashir [111] studied the FT synthesis reaction over a commercial 15% Co/Al_2O_3 catalyst in a high-pressure FT synthesis unit at three different operating conditions in the range that is tabulated in Table 2-5. A mechanistic-based equation was developed for the FT synthesis rate. The model was based on the molecular adsorption and dissociation of CO and H_2 that took place on the vacant active sites (ψ) of cobalt catalysts (first stage). The removal oxygen in the surfaces was represented by water and CO_2 formation as it took placed in the second stage; the hydrogenation of adsorbed carbon and the formation of oligomers occurred in the third stage. The postulation of oxygen removal was based on the modified surface reaction model originally developed by Kellner and Bell [112]. In addition, the monomer formation ($CH_2-\psi$) and the alkyl intermediate ($CH_3-\psi$) were both included in the third stage; whereas termination to methane occurred in the fourth stage. The rate equations for each of the reactions were derived using the Langmuir–Hinshelwood-Hougen-Watson (LHHW) approach. Equation 2-26 was the final rate equation for the rate of CO conversion. The study was performed at CO conversion

rate less than 50 %. The detailed experimental conditions were tabulated in Table 2-5. Since the model was investigated at a constant temperature and total pressure, one can deduce there is no guarantee that the model can be validated against experiments at different operating temperatures and pressures. Moreover, the rate model reported in this study appeared mechanistically identical to the one developed originally by Sarup and Wojciechowski [106] (see Equation 2-16).

Botes et al [113] derived a variety of two parameter rate equations based on assumed sets of elementary reaction steps. The only equation that could reasonably account for all the variations in the reaction rate was the semi-empirical rate expression, Equation 2-19. However, it was shown that this model was virtually indistinguishable from a mechanistically derived three-parameter rate model that assumes the following kinetically relevant steps in the cobalt-FT synthesis: CO dissociation is fast (i.e. is not a RDS) and occurs without involvement of hydrogen; the first hydrogenation step of surface carbon and the second hydrogenation step of surface oxygen are slow and determine the overall rate of CO conversion to hydrocarbons (i.e. they are RDSs). Testing all the kinetics expressions against the lumped set of data from three different runs confirmed that the Equation 2-27 was indeed the preferred model. One of the limitations of this study was that all measurements were performed at the same temperature for identifying the functional form of the kinetics model, so that this may not be applicable at different temperature values. This means that there is no guarantee that the semi-empirical rate model predicts well the experimental data at different operating temperatures.

$$r_i = \frac{k_i P_{CO}^{0.5} P_{H_2}^{0.75}}{\left(1 + K_{CO} {P_{CO}}^{0.5}\right)^2} \qquad \text{Equation 2-19}$$

Atashi et al [114] derived the rate equations based on the LHHW theory. Four mechanisms were reported based on the most important growth mechanism for the hydrocarbon formation (i.e. the surface carbide mechanism by CH_2 insertion). These mechanisms were different from each other with respect to their monomer formation and carbon chain distribution pathways. There were thirteen possible rate expressions were derived for CO disappearance rate by considering various RDSs. Among the thirteen kinetics equations, Equation 2-28 was the best fit to the experimental data with respect to CO conversion at sixteen different operating conditions in the range tabulated in Table 2-5. It was assumed that the surface reaction between adsorbed CO species and H_2 molecule (i.e. R. 2-8) is the slowest step and irreversible; whereas the steps R. 2-7, R. 2-9 and R. 2-10 were quick and at equilibrium.

$$CO + \psi \rightleftarrows CO - \psi \qquad \text{R. 2-7}$$

$$CO - \psi + H_2 \rightarrow H_2CO - \psi \qquad \text{R. 2-8}$$

$$H_2CO - \psi + H_2 \rightleftarrows CH_2 - \psi + H_2O \qquad \text{R. 2-9}$$

$$H_2O + \psi \rightleftarrows H_2O - \psi \qquad \text{R. 2-10}$$

Also, it was assumed that the CO is adsorbed more strongly than hydrogen which means that only CO occupies the majority of the total number of sites. Other species were assumed to be negligible in the stoichiometric balance. Overall each model presented above had some limitations and drawbacks which are summarized and given in Table 2-4.

Table 2-4 Limitation and weakness of different kinetic studies reported in the literature for FT synthesis over a Co-based catalyst

Model	Limitation & Weakness
Rautavuoma and van der Baan [104]	- Only investigated at constant temperature and total pressure (523 *K* and 1 *bar*). It may not be applicable at other temperatures and/or pressure conditions.
Wojciechowski [91]	- Only investigated at constant temperature (463 *K*). It may not be applicable at other temperature conditions.
Sarup and Wojciechowski [106]	- Only the CO consumption rate was investigated and no information related to the product distribution was reported. - Large discrepancy between the models and experimental data was reported, which was about 40% for two out of six models. - The best model was also rejected due to the physically unrealistic and meaningless value calculated for the adsorption coefficient.
Yates and Satterfield [107]	- Simplification towards the adsorbed intermediate and chemical species occupied the total active site, such that CO is the predominant adsorbed species and other surface intermediates were ignored.
Iglesia *et al.* [115]	- Narrow temperature range was investigated - Water gas shift reaction mechanism was not considered in the developed model
Zennaro *et al.* [82]	- Only investigated at constant pressure and space velocity (20 *bar* 5000 h^{-1}). It may not be applicable at other temperature conditions.
Elbashir [111]	- Only investigated at constant temperature and total pressure (503 *K* and 60 *bar*). It may not be applicable at other temperature and/or pressure conditions.

Botes *et al.* [113]	- The results were in good agreement with the measured data; however, the models were developed semi-empirically based on two and three rate parameters. - Only investigated at constant temperature (523 *K*). It may not be applicable at other temperature conditions.
Atashi *et al.* [114]	- Only the CO consumption rate was investigated and no information related to the product distribution was reported. - Only investigated at constant pressure (8 *bar*). It may not be applicable at other temperature conditions. - Simplification towards the adsorbed intermediate and chemical species occupied the total active site, such that CO is the predominant adsorbed species and other surface intermediates were ignored.

Table 2-5 FT kinetics rate models based on semi-empirical or mechanistic approach

Model	Name and Reference	Reactor Type	Catalyst	T (*K*)	P (*bar*)	H_2/CO Ratio	Intrinsic Kinetics Expression	Equation
L-FT–I	Rautavuoma and van der Baan [104]	Plug flow Fixed bed reactor (low conversion)	Co/Al_2O_3	523	1.0	0.2-4.0	$-r_{CO+H2} = \frac{k\ P_{CO}^{0.5}\ P_{H_2}}{(1\ +\ K_1 P_{CO}^{0.5}\ )^3}$	Equation 2-20
L-FT–II	Wojciechowski [91]	Berty	Co/Kieselguhr	463	2.0-15.0	0.5-8.3	$-r_{CO} = \frac{kP_{CO}P_{H_2}^{0.5}}{(1\ +\ K_1 P_{CO}\ +K_2 P_{H_2}^{0.5}\ )^2}$	Equation 2-21
L-FT–III	Sarup and Wojciechowski [106]	Internal recycle reactor (Berty)	Co/Kieselguhr	463	2.0-15.0	0.5-8.3	$-r_{CO} = \frac{kP_{CO}^{0.5}P_{H_2}^{0.5}}{(1\ +\ K_1 P_{CO}^{0.5}\ +K_2 P_{H_2}^{0.5}\ )^2}$	Equation 2-22
L-FT–IV	Yates and Satterfield [107]	Slurry	$Co/MgO/SiO_2$	493-513	5.0-15.0	1.5-3.5	$-r_{CO} = \frac{kP_{CO}P_{H_2}}{(1+KP_{CO})^2}$	Equation 2-23

L-FT–V	Iglesia *et al.* [115]	Fixed bed reactor	Co	473-483	1.0-21.0	1.0-10.0	$-r_{CO} = \frac{kP_{CO}^{0.65}P_{H_2}^{0.6}}{1 + aP_{CO}}$	Equation 2-24
L-FT–VI	Zennaro *et al.* [82]	Fixed bed reactor	Co/TiO_2	473-513	20	1.0-4.0	$-r_{CO} = \frac{kP_{CO}P_{H_2}^{0.74}}{(1 + KP_{CO})^2}$	Equation 2-25
L-FT–VII	Elbashir [111]	Fixed bed reactor	15% Co/Al_2O_3	523	60.0	0.5-2.0	$-r_{CO} = \frac{kP_{CO}^{0.5}P_{H_2}^{0.5}}{(1 + aP_{H_2}^{0.5} + bP_{CO}^{0.5} + cP_{CO})^2}$	Equation 2-26
L-FT–VIII	Botes *et al.* [113]	Slurry	$Co/Pt/Al_2O_3$	503	5.0-40.0	1.6-3.2	$-r_{CO} = \frac{kP_{CO}^{0.5}P_{H_2}^{0.75}}{(1 + aP_{CO}^{0.5}P_{H_2}^{0.25} + bP_{CO}^{0.5}P_{H_2}^{-0.25})^2}$	Equation 2-27
L-FT–IX	Atashi *et al.* [114]	Fixed bed micro reactor	$15\%Co/10\%K/Al_2O_3$	483-513	8.0	1.0-3.0	$-r_{CO} = \frac{kP_{CO}P_{H_2}}{1 + aP_{CO}}$	Equation 2-28

2.7. Water Gas Shift (WGS) Reaction Mechanism

The water gas shift (WGS) reaction, R. 1-7, is an old industrial process in which water in the form of steam is mixed with carbon monoxide to obtain hydrogen and carbon dioxide. The FT synthesis can be described as a combination of the FT reaction and the WGS reaction. FT reaction was discussed in detail in section 2.6. It is commonly believed that H_2O is the primary by-product of FT synthesis and carbon dioxide is only produced via the WGS reaction [76]; thus the rate of CO_2 production is generally given by:

$$R_{CO2} = R_{WGS} \qquad \text{Equation 2-29}$$

In fact, the WGS reaction is a reversible parallel-consecutive reaction with respect to carbon monoxide (see Figure 2-21). It is generally accepted that FT and WGS reactions take place on different active sites and the two reactions will only impact on each other via the gas phase.

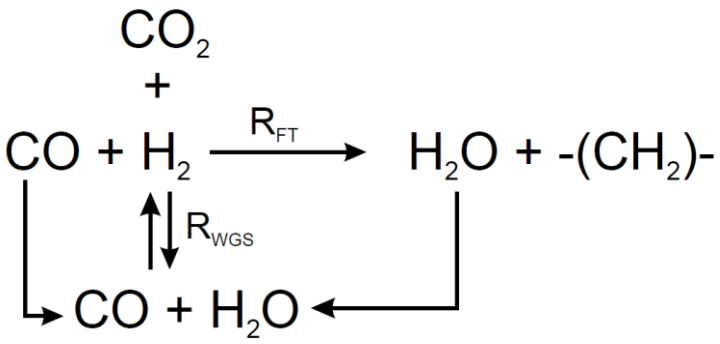

Figure 2-21 Scheme of the reaction of carbon monoxide and hydrogen [116].

There have only been a few studies of WGS kinetics in conjunction with FT synthesis reported in the literature. An excellent review for the WGS mechanism and kinetics over iron-based, copper-based and cobalt molybdenum-based catalysts was published by Newsome [117] in 1980. However, the kinetics study of WGS under FT synthesis reaction conditions receives relatively little attention [116, 118-124]; and only addressed Fe-based catalysis. This is partially due to the fact that the WGS kinetics in a FT synthesis process becomes difficult to address because of the additional FT synthesis reactions; which remarkably increases the complexity in the discrimination of WGS kinetics models as well as in the WGS kinetics parameter estimation. The rates of FT synthesis reactions can be increased or decreased by the rate of the WGS reaction. Due to the industrial importance of the WGS reaction, many researchers have studied the reaction mechanism and developed models to reflect the behaviour of the reaction over common industrial catalysts. A number of kinetics studies have been published for the WGS reaction mechanism over Fe-based catalysts under FT synthesis conditions. However, there is no WGS kinetics study for the case of a Co-based catalyst. Table 2-8 gives an overview. The results of different investigations suggest that the WGS reaction largely occurs via four specific mechanisms (*i*) the formate mechanism; (*ii*) the redox mechanism (*iii*); the associative

mechanism; as well as (*iv*) the carbonate mechanism. In the first mechanism, adsorbed water dissociates into an adsorbed hydroxyl (OH− σ) group and adsorbed atomic hydrogen (H − σ) (R. 2-14). 'σ' stands for the total vacant surface coverage fraction of the active site in WGS rate model. The hydroxyl group then combines with adsorbed carbon monoxide to form adsorbed formate (R. 2-16) which eventually decomposes into carbon dioxide and hydrogen via (R. 2-18, R. 2-21 and R. 2-24 or R. 2-20 and R. 2-21), yielding the WGS products. The second mechanism implies a successive oxidation by adsorbed oxygen from H_2O (R. 2-13, R. 2-19 and R. 2-22) and reduction of the reactive catalyst surface by CO occurs as CO is oxidized to CO_2 (R. 2-11, R. 2-24 and R. 2-28). In the associative mechanism (third mechanism) adsorbed water dissociates into an adsorbed OH and atomic hydrogen (R. 2-14). The adsorbed hydroxyl then oxidizes adsorbed CO resulting in adsorbed CO_2 and atomic hydrogen (R. 2-33). In addition to the formate, redox and associative mechanisms, researchers have also proposed that the WGS reaction may proceed via a carbonate mechanism. Finally, the fourth mechanism indicates the initial interaction of carbon dioxide with the catalyst active site is dissociative, producing carbon monoxide and a surface oxidized metal catalyst. Subsequent adsorption of carbon dioxide onto the surface produced carbonate species (R. 2-34 and R. 2-35). The existence of the surface carbonate species was found to have a reducing effect on the overall rate of the reaction. Due to its strong binding nature with the surface, the carbonate species blocks active surface sites, preventing other species from adsorbing to the surface and further reacting towards the generation of the products. This negative effect was also ascribed to the formate species resulting from dehydrogenation of the carbonate species.

Table 2-6 Four general plausible WGS mechanisms

Formate mechanism	**Redox mechanism**
$CO + \sigma \rightleftarrows CO - \sigma$	$H_2O + \sigma \rightleftarrows H_2O - \sigma$
$H_2O + \sigma \rightleftarrows H_2O - \sigma$	$H_2O - \sigma + \sigma \rightleftarrows OH - \sigma + H - \sigma$
$H_2O - \sigma + \sigma \rightleftarrows OH - \sigma + H - \sigma$	$OH - \sigma + \sigma \rightleftarrows O - \sigma + H - \sigma$
$CO - \sigma + OH - \sigma \rightleftarrows CHO_2 - \sigma + \sigma$	$2H - \sigma \rightleftarrows H_2 + 2\sigma$
$CHO_2 - \sigma \rightleftarrows CO_2 + H - \sigma$	$CO + \sigma \rightleftarrows CO - \sigma$
$2H - \sigma \rightleftarrows H_2 + 2\sigma$	$CO - \sigma + O - \sigma \rightleftarrows CO_2 - \sigma + \sigma$
	$CO_2 - \sigma \rightleftarrows CO_2 + \sigma$
Associative mechanism	**Carbonate mechanism**
$H_2O + \sigma \rightleftarrows H_2O - \sigma$	$CO + 2O - \sigma \rightleftarrows CO_3 - 2\sigma$
$H_2O - \sigma \rightleftarrows OH - \sigma + H - \sigma$	$CO_3 - 2\sigma \rightleftarrows CO_3 - \sigma + \sigma$
$OH - \sigma + CO - \sigma \rightleftarrows CO_2 - \sigma + H - \sigma$	$CO_3 - \sigma \rightleftarrows CO_2 + O - \sigma$
$CO_2 - \sigma \rightleftarrows CO_2 + \sigma$	$H_2O + \sigma \rightleftarrows H_2O - \sigma$
$2H - \sigma \rightleftarrows H_2 + 2\sigma$	$H_2O - \sigma + O - \sigma \rightleftarrows 2OH - \sigma$
	$2OH - \sigma \rightleftarrows 2O - \sigma + H_2$
	$H_2O - \sigma + \sigma \rightleftarrows OH - \sigma + H - \sigma$
	$2H - \sigma \rightleftarrows H_2 + 2\sigma$

Single studies of the WGS reaction over supported metals suggest the appearance of formate species [117, 121, 125, 126]. The formate species can be formed by the reaction between either a hydroxyl species or water and carbon monoxide, either in the gas phase or in the adsorbed state. The hydroxyl intermediate can be formed by the decomposition of water. The formate intermediate can be reduced to either adsorbed or gaseous carbon dioxide (see Table 2-7).

Table 2-7 The most plausible water gas shift elementary step reactions under FT synthesis reaction conditions

Reaction number	Elementary	Lox and Froment (1993)							Van der Laan (1999) WGS-I	Van der Laan (1999) WGS-II	Yang (2003) WGS	Wang (2003) WGS	Chang *et al.* (2007) WGS-I	Chang *et al.* (2007) WGS-II	Haghtalab (2012)
		WGSI	WGSII	WGSIII	WGIV	WGSV	WGSVI	WGSVII							
R. 2-11	$CO + \sigma \rightleftarrows CO - \sigma$	☒	☒	☒				☒	☒	☒	☒ (I)	☒ (I)	☒	☒	☒
R. 2-12	$CO_2 + \sigma \rightleftarrows CO_2 - \sigma$								☒	☒					☒
R. 2-13	$H_2O + \sigma \rightleftarrows H_2O - \sigma$							☒	☒	☒					☒
R. 2-14	$H_2O - \sigma + \sigma \rightleftarrows OH - \sigma + H - \sigma$									☒					☒
R. 2-15	$H_2 + 2\sigma \rightleftarrows 2H - \sigma$		☒ (5)	☒		☒	☒	☒	☒	☒					☒
R. 2-16	$CO - \sigma + OH - \sigma \rightleftarrows HCOO - \sigma + \sigma$		☒ (2)							☒ (6)	☒ (III)	☒ (III)	☒	☒	☒ (6)
R. 2-17	$CO - \sigma + H_2O - \sigma \rightleftarrows HCOO - \sigma + H - \sigma$							☒ (3)	☒ (5)						
R. 2-18	$HCOO - \sigma + \sigma \rightleftarrows CO_2 - \sigma + H - \sigma$							☒	☒	☒				☒	☒
R. 2-19	$H_2O + 2\sigma \rightleftarrows OH - \sigma + H - \sigma$		☒			☒	☒ (4)				☒	☒	☒	☒	
R. 2-20	$HCOO - \sigma \rightleftarrows CO_2 + H - \sigma$		☒	☒		☒	☒				☒ (IV)	☒ (IV)	☒ (II)		
R. 2-21	$2H - \sigma \rightleftarrows H_2 + 2\sigma$										☒	☒	☒	☒	
R. 2-22	$OH - \sigma + \sigma \rightleftarrows O - \sigma + H - \sigma$														

R. 2-23	$CO-\sigma+O-\sigma \rightleftarrows CO_2+2\sigma$														
R. 2-24	$CO_2-\sigma \rightleftarrows CO_2+\sigma$													⊠	
R. 2-25	$CO-\sigma+H_2O \rightleftarrows HCOOH-\sigma$	⊠	⊠												
R. 2-26	$HCOOH-\sigma \rightleftarrows CO_2+H_2+\sigma$	⊠	⊠												
R. 2-27	$CO-\sigma+H_2O+\sigma \rightleftarrows HCOO-\sigma+H-\sigma$			⊠ (2)											
R. 2-28	$CO-\sigma+O-\sigma \rightleftarrows CO_2-\sigma+\sigma$														
R. 2-29	$H_2O+\sigma \rightleftarrows H_2+O-\sigma$				⊠										
R. 2-30	$CO+H-\sigma \rightleftarrows CHO-\sigma$					⊠									
R. 2-31	$CHO-\sigma+OH-\sigma \rightleftarrows HCOO-\sigma+H-\sigma$					⊠ (2)									
R. 2-32	$CH+OH-\sigma \rightleftarrows HCOO-\sigma$						⊠								
R. 2-33	$CO-\sigma+OH-\sigma \rightleftarrows CO_2-\sigma+H-\sigma$														
R. 2-34	$CO+2O-\sigma \rightleftarrows CO_3-2\sigma$														
R. 2-35	$CO_3-2\sigma \rightleftarrows CO_3-\sigma+\sigma$														
R. 2-36	$CO_3-\sigma \rightleftarrows CO_2+O-\sigma$														

2.7.1. Published Literature on the Water-Gas-Shift Reaction Mechanism

The first WGS reaction rate model was reported by Dry [118] under FT synthesis conditions which were empirical rate expression and independent of the H_2O concentration (Equation 2-30). Feimer *et al.* [119] used the same equation on an Fe-based catalyst. Zimmerman and Bukur [120] used several existing kinetics equations for both FT and WGS reactions to determine which equations best described their experimental WGS and FT rates at a constant temperature of 523 *K* over an Fe-based catalyst. The details of their experiments are given in Table 2-8. Several kinetic models were examined to fit the experimental results with respect to WGS rate values. They studied the WGS reaction kinetics for their catalyst using the rate model from [127]. Their WGS rate equation, Equation 2-32, had a functionally similar denominator to that developed for the FT rate. Their second rate expression (Equation 2-33) was derived semi-empirically with an identical denominator term reported by Huff and Satterfield for the FT rate model [128]; it suggested the reaction occurred on the same active sites where the FT reaction took place. Actually, they eliminated the temperature dependency in the rate models; while this hypothesis may not be really applicable in a reaction rate study, as the temperature factor is one of the key elements that have significant influence on the rate of reactions. The estimations of the adsorption constants for the WGS rate were significantly different in comparison to the constants for the FT synthesis rate. In fact, the adsorption constant may not differ, if these reactions take place on the same catalytic sites. The authors indicated that the derived kinetic equations were not reliable for WGS kinetics under FT synthesis conditions and the results are mostly empirical. Their results, based on the best fit, also showed the relative residual of more than 20 % in some conditions in the case of WGS rate values;

which indicates that the predicted results did not fit the experimental values well. For the first time, Lox and Froment [121] mechanistically studied the FT reaction and WGS reaction on a commercial precipitated iron catalyst. Their models were based on a mechanistic approach in which the rate expression was based on elementary reactions involving a formate surface intermediate (adopting the formate mechanism). The two-site reaction (i.e. the formation of the formate intermediate) was proposed to be an RDS. The elementary reactions of the WGS were also chosen based on the literature data which proposed a formate species as reactive intermediate [129, 130]. For each set of elementary reactions, they assumed only one RDS, which was valid for the whole range of experimental conditions. They finally proposed seven elementary reaction paths and derived six WGS rate models all based on a formate mechanism, assuming each with a different RDS. The final kinetics expressions for these models were given in Table 2-8. Their results manifested that the CO_2 is formed through the WGS reaction involving a formate surface intermediate, by assuming the formation of the formate surface intermediate ($-\mathrm{HCOO}$) is an RDS, which involves two sites. Based on statistical analysis, the model WGS-II5 was rejected since none of the kinetics parameters were significantly different from zero and the mode WGS-VI4 was eliminated because the apparent adsorption enthalpy (K_v) had a significantly negative value. From the non-isothermal discrimination, modes WGS-III2, WGS-V2 and WGS$-$II3 were eliminated because of significantly negative estimates for the activation energy of the k_v constant. Discrimination between rival LHHW kinetics models resulted in the optimal form of Equation 2-34 when the equation was combined with their best developed FT rate model. Rethwisch and Dumesic [125] also indicated the WGS reaction proceeded on a different catalytic site than the FT synthesis reaction. They proposed that the WGS reaction over supported Fe catalysts was activated via a formate mechanism due to the inadequate change of the oxidation state of the Fe catalyst; whereas unsupported magnetite

proceeds via a direct oxidation mechanism [116]. They concluded the reaction between adsorbed hydroxyl species ($OH-\psi$), resulting from the dissociation of water molecule, and adsorbed CO were the slowest step. Van der Laan [116] studied the kinetics of the FT synthesis over a commercial Fe-based catalyst in a continuous spinning basket reactor. He derived two different rate equations based on a detailed set of reaction paths originating on the basis of the formate mechanism for the WGS reaction. It was indicated that the CO_2 formation rate (WGS) is determined by the formation of a formate intermediate species from adsorbed CO and dissociated hydrogen. They assumed that the active sites for the WGS are different from the sites for the hydrocarbon forming reactions and RDS is a dual-site elementary reaction between two adsorbed species. Two kinetic models for the WGS reaction rate models were fitted to the experimental reaction rates. The reaction sequences for both mechanisms are given in Table 2-7. It was assumed that the adsorption term for H_2 and CO_2 are negligible in comparison to CO and H_2O [120, 121, 131]. As a result, the mass balance of the catalytic sites consists of only adsorbed CO and H_2O. As discussed earlier, two RDSs were considered to be possible; one was the reaction between adsorbed water and carbon monoxide (R. 2-17) and the second is the reaction between adsorbed carbon monoxide and hydroxyl intermediate (R. 2-16). On the basis of the formate mechanism and the mentioned assumptions, Equation 2-40 and Equation 2-41 were developed for the kinetics of CO_2 formation.

Table 2-8 WGS reaction mechanisms based on literature studies

Model	Reference	Intrinsic Kinetics Expression	Equation	Reactor Type	Catalyst	T (K)	P (bar)	H_2/CO Ratio	Space Velocity NL kg_{cat}^{-1} s^{-1}
L-WGS-I	[118-120]	$r_{WGS} = k_{WGS}P_{CO}$	Equation 2-30	-	Iron catalyst	-	-	-	-
L-WGS-II	[120]	$r_{WGS} = k_{WGS}(P_{H2O}P_{CO} - P_{CO2}P_{H2}/K_P)$	Equation 2-31	Slurry tank reactor	Fe–Cu–K	493-523	7.9-29.6	0.67-1.06	1.0-4.0
L-WGS-III	[120, 122]	$r_{WGS} = k_{WGS}\frac{P_{H2O}P_{CO} - P_{CO2}P_{H2}/K_P}{P_{CO} + aP_{H2O} + bP_{CO2}}$	Equation 2-32	Slurry tank reactor	Fe–Cu–K	493-523	7.9-29.6	0.67-1.06	1.0-4.0
L-WGS-IV	[120, 122, 128]	$r_{WGS} = k_{WGS}\frac{P_{H2O}P_{CO} - P_{CO2}P_{H2}/K_P}{P_{CO}P_{H2} + aP_{H2O}}$	Equation 2-33	Slurry tank reactor	Fe–Cu–K	493-523	7.9-29.6	0.67-1.06	1.0-4.0
*L-WGS-V	[121] WGSII2	$r_{WGS} = k_v\frac{P_{H2O}P_{CO}/P_{H2}^{0.5} - P_{CO2}P_{H2}^{0.5}/K_P}{(1 + K_vP_{H2O}/P_{H2}^{0.5})^2}$	Equation 2-34	Fixed bed	Fe–Cu–K	523-623	6-21	3.0-6.0	0.36-2.43
L-WGS-VI	WGSII5	$r_{WGS} = k_v\frac{P_{H2O}P_{CO}/P_{CO2} - 1/P_{H2}K_P}{(1 + K_vP_{H2O}P_{CO}/P_{CO2})^2}$	Equation 2-35	Fixed bed	Fe–Cu–K	523-623	6-21	3.0-6.0	0.36-2.43
L-WGS-VII	WGSIII2	$r_{WGS} = k_v\frac{P_{H2O}P_{CO} - P_{CO2}P_{H2}/K_P}{(1 + K_vP_{CO})^2}$	Equation 2-36	Fixed bed	Fe–Cu–K	523-623	6-21	3.0-6.0	0.36-2.43

L-WGS-VIII	WGSV2	$r_{WGS} = k_v \frac{P_{H2O}P_{CO} - P_{CO2}P_{H2}/K_P}{(1 + K_v P_{H2O}/{P_{H2}}^{0.5})^2}$	Equation 2-37	Fixed bed	Fe–Cu–K	523-623	6-21	3.0-6.0	0.36-2.43
L-WGS-IX	WGSVI4	$r_{WGS} = k_v \frac{P_{H2O} - \frac{P_{CO2}P_{H2}}{P_{H2O}}K_P}{(1 + K_v P_{H2})^2}$	Equation 2-38	Fixed bed	Fe–Cu–K	523-623	6-21	3.0-6.0	0.36-2.43
L-WGS-X	WGSVII3	$r_{WGS} = k_v \frac{P_{H2O}P_{CO} - P_{CO2}P_{H2}/K_P}{(1 + K_v(P_{CO} + P_{H2O})^2}$	Equation 2-39	Fixed bed	Fe–Cu–K	523-623	6-21	3.0-6.0	0.36-2.43
*L-WGS-XI	[116] (WGS-I5)	$r_{WGS} = \frac{k_{WGS}(P_{H2O}P_{CO} - P_{CO2}P_{H2}/K_P)}{(1 + K_1 P_{CO} + K_3 P_{H2O})^2}$	Equation 2-40	Spinning basket reactor	Fe–Cu–K–SiO2	523	8.0-40	0.25-4.0	0.5-2.0
L-WGS-XII	[116, 124, 132] (WGS-II6)	$r_{WGS} = \frac{k_{WGS}(P_{H2O}P_{CO} - P_{CO2}P_{H2}/K_P)}{{P_{H2}}^{0.5}(1 + K_1 P_{CO} + K_3 P_{H2O})^2}$	Equation 2-41	Spinning basket reactor	Fe–Cu–K–SiO2	523	8.0-40	0.25-4.0	0.5-2.0
L-WGS-XIII	[133, 134] (RDS-I)	$r_{WGS} = k_v \frac{(P_{CO} - P_{CO2}P_{H2}{P_{H2O}}^{-1}/K_P)}{1 + K_v P_{CO2}P_{H2}/P_{H2O}}$	Equation 2-42	Spinning basket reactor	Fe–Cu–K–SiO2	523	8.0-40	0.25-4.0	0.5-2.0
L-WGS-XIV	[133, 134] (RDS-III)	$r_{WGS} = k_v \frac{P_{H2O}P_{CO}/{P_{H2}}^{0.5} - P_{CO2}{P_{H2}}^{0.5}/K_P}{\left(1 + K_v P_{H2O}/{P_{H2}}^{0.5}\right)^2}$	Equation 2-43	Spinning basket reactor	Fe–Cu–K–SiO2	523	8.0-40	0.25-4.0	0.5-2.0
L-WGS-XV	[133-135] (RDS-IV)	$r_{WGS} = k_v \frac{P_{H2O}P_{CO}/{P_{H2}}^{0.5} - P_{CO2}{P_{H2}}^{0.5}/K_P}{1 + K_v P_{CO}P_{H2O}/{P_{H2}}^{0.5}}$	Equation 2-44	Spinning basket reactor	Fe–Cu–K–SiO2	523	8.0-40	0.25-4.0	0.5-2.0

* Rate equations Equation 2-40 (L-WGS-XI) and Equation 2-43 (Model L-WGS-XIV) are identical with Equation 2-39 (Model L-WGS-X) and Equation 2-34 (Model L-WGS-V), respectively.

2.8. Summary and Conclusion

In this chapter, a comprehensive review of the FT synthesis kinetic was conducted including the FT reactions and the WGS reaction mechanism. Majority of the conducted studies employed an iron-based catalyst for the kinetic analysis; however, the kinetic study on a cobalt-based catalyst was less abundant. Among the reported studies that utilized the cobalt-based catalyst, most of them investigated the kinetics at either constant reaction temperature, total pressure or space velocity. Furthermore, majority of the reported studies only investigated either the kinetics mechanism of the FT reactions or the WGS reaction model; however, there is lack of published work considering the combined FT and WGS reaction mechanism due to the complex FT synthesis reaction network. In addition, the reported studies only estimated the kinetics parameters to calibrate their models with the experimental data; however, the model validation was not taken into account. Furthermore, the reactor operating conditions were selected iteratively and/or based on experience; however, such approach did not necessarily ensure that the optimum combination of input parameters (i.e. temperature, pressure, space velocity and H_2/CO molar ratio) was achieved for maximum performance of the catalytic FT synthesis. Such deficiency highlights the need for analytical optimization that can be integrated with the mathematical model to reliably find the optimum performance.

CHAPTER 3

KINETICS OF FISCHER–TROPSCH SYNTHESIS

3.1. Introduction

The kinetics studies of FT synthesis are distinguished into two categories. In the first category the aim is to focus on the rate of syngas (mixture of CO and H_2) disappearance only. In this category, no information is given related to product distribution, because FT synthesis products are very widespread and the description of the FT kinetics is quite challenging. In the second category however, information about the formation of product compositions are also considered. In both categories, the rate expressions can be derived either empirically (e.g. power-law rate expression), semi-empirically, or mechanistically. In the latter case, the detailed mechanistic of FT kinetics can be accomplished by considering appropriate sequential reaction pathways together with the assumptions about rate-determining steps. In Chapter 3, two different approaches are considered to develop a model for the FT synthesis reaction network. The first was based on an empirical approach; whereas the second approach explained the mechanistic details of FT kinetics in more depth. In the former, the rate equations were derived

by power-law rate expressions, while in the latter the rate equations were derived by the Langmuir–Hinshelwood-Hougen-Watson (LHHW) rate theory. It is worth mentioning that the power-law rate model has limited applications to catalytic reactions to some extent; that is to say, they usually predict rates well over a narrow range of experimental conditions; whereas the LHHW rate theory, due to its fundamental origin, predicts rates over a wider range of conditions. However, it is unclear which combination of a number of rate expressions and kinetics models of syngas conversion and product selectivity can provide the best representation of available data; this will be the main objective of Chapter 3. The goal was to employ the newly obtained experimental results to fit several plausible mechanism-derived FT kinetics models, which were likely to reflect the most significant facts of FT synthesis catalysis and chemistry.

3.2. Approach (i): Empirical Study of FT Synthesis Kinetics

3.2.1. Development of the Kinetics Model Based on Power-Law Rate Expression

Kinetics models of reduced complexity are attractive for reactor analysis and design purposes. These models are capable of capturing the essential features of the FT synthesis products' distribution without the need for a parameter such as chain growth probability (α). The reaction network can be classified as a number of lumped reactions by means of the kinetics characteristics of reaction molecules. For the first approach, the rate of reaction was derived based on a power-law rate expression. In this model, the rates of disappearance of reactants, as

well as the formation of products' species, were taken into account. Equation 3-1 below is the general form of the rate expression for a proposed j^{th} reaction. In this equation, P_{CO} and P_{H_2} stand for carbon monoxide and hydrogen partial pressures, respectively; A_j denotes the pre-exponential factor of rate constant and E_j denotes the activation energy of reaction 'j'; n_j and m_j indicate the order of reaction with respect to CO and H_2 partial pressures, respectively. The reaction network consisted of 11 reacting components (i.e. CO, H_2, CO_2, H_2O, CH_4, C_2H_4, C_2H_6, C_3H_8, i-C_4H_{10}, n-C_4H_{10}, and C_{5+}). From R. 3-1 to R. 3-8 the proposed reaction scheme in this work is shown. The representative single reaction equation is R. 3-7; it corresponds to the lumped rate of C_{5+} formation (which is the rate of formation of liquid hydrocarbon compositions) by setting $C_{6.05}H_{12.36}$ as the average molecular value of higher hydrocarbon compounds [136-138].

$$R_j = A_j exp\left(-\frac{E_j}{R_g T}\right) P_{CO}^{n_j} P_{H_2}^{m_j} \qquad \text{Equation 3-1}$$

Table 3-1 Proposed lumped FT synthesis kinetics approach (i) over Co/SiO_2 catalyst

Postulated reactions pathway	No.
$CO + 3H_2 \overset{R_1}{\rightarrow} CH_4 + H_2O$	R. 3-1
$2CO + 4H_2 \overset{R_2}{\rightarrow} C_2H_4 + 2H_2O$	R. 3-2
$2CO + 5H_2 \overset{R_3}{\rightarrow} C_2H_6 + 2H_2O$	R. 3-3
$3CO + 7H_2 \overset{R_4}{\rightarrow} C_3H_8 + 3H_2O$	R. 3-4
$4CO + 9H_2 \overset{R_5}{\rightarrow} i - C_4H_{10} + 4H_2O$	R. 3-5
$4CO + 9H_2 \overset{R_6}{\rightarrow} n - C_4H_{10} + 4H_2O$	R. 3-6

$$6.05CO + 12.23H_2 \overset{R_7}{\rightarrow} C_{6.05}H_{12.36}(C_{5+}) + 6.05H_2O \quad \text{R. 3-7}$$

$$CO + H_2O \overset{R_8}{\leftrightarrow} CO_2 + H_2 \quad \text{R. 3-8}$$

The rate of formation and disappearance of the species can be calculated by the sum of the products of the species' stoichiometric coefficient and the reaction rate of the corresponding reaction. Hence, the rates of the consumption of reactants as well as the formation of products' species mentioned above are as follows:

$$r_{CO} = \sum_{j=1}^{NR} v_j^{CO} R_j = -R_1 - 2R_2 - 2R_3 - 3R_4 - 4R_5 - 4R_6 - 6.05R_7 - R_8 \quad \text{Equation 3-2}$$

$$r_{H_2} = \sum_{j=1}^{NR} v_j^{H_2} R_j = -3R_1 - 4\,R_2 - 5R_3 - 7R_4 - 9R_5 - 9R_6 - 12.23R_7 + R_8 \quad \text{Equation 3-3}$$

$$r_{H_2O} = \sum_{j=1}^{NR} v_j^{H_2O} R_j = +R_1 + 2R_2 + 2R_3 + 3R_4 + 4R_5 + 4R_6 + 6.05R_7 - R_8 \quad \text{Equation 3-4}$$

$$r_{CO_2} = \sum_{j=1}^{NR} v_j^{CO_2} R_j = +R_8 \quad \text{Equation 3-5}$$

$$r_{CH_4} = \sum_{j=1}^{NR} v_j^{CH_4} R_j = +R_1 \quad \text{Equation 3-6}$$

$$r_{C_2H_4} = \sum_{j=1}^{NR} v_j^{C_2H_4} R_j = +R_2 \quad \text{Equation 3-7}$$

$$r_{C_2H_6} = \sum_{j=1}^{NR} v_j^{C_2H_6} R_j = +R_3 \quad \text{Equation 3-8}$$

$$r_{C_3H_8} = \sum_{j=1}^{NR} v_j^{C_3H_8} R_j = +R_4 \quad \text{Equation 3-9}$$

$$r_{i-C_4} = \sum_{j=1}^{NR} v_j^{i-C_4} R_j = +R_5 \quad \text{Equation 3-10}$$

$$r_{n-C_4} = \sum_{j=1}^{NR} v_j^{n-C_4} R_j = +R_6 \quad \text{Equation 3-11}$$

$$r_{C_{5+}} = \sum_{j=1}^{NR} v_j^{C_{5+}} R_j = +R_7 \quad \text{Equation 3-12}$$

3.3. Approach (ii): Mechanistic Study of FT Synthesis Kinetics

Unlike most of the kinetics studies in the literature, the combined kinetics of FT synthesis reactions and the WGS reaction were studied mechanistically and different mechanisms with postulated reaction pathways were proposed for both rate models (i.e. FT and WGS reactions). Section 3.3.1 below explains the development of the rate models for FT reactions; whereas the detailed WGS reaction rate models are presented in section 3.3.2. All rate equations were derived on the basis of various elementary step reaction routes and carbon chain distribution pathways (i.e. adsorption, initiation, propagation, and termination steps). The elementary step reactions proposed for each kinetic model are given in Table 3-2 and Table 3-11 respectively for FT reactions and WGS reaction. The proposed rate equations were used successfully to describe the kinetics of the reactants' consumption (i.e. carbon monoxide and hydrogen) for the formation of n-paraffins and α-olefins, as well as CO_2 and H_2O by-products, under the FT synthesis condition over a Co-based catalyst. The formation of oxygenates compounds were not taken into account due to the very small amount produced in the present study.

In order to derive the rate equation for each kinetic model, firstly a few elementary reactions were assumed to be rate-determining steps and the other remaining steps were considered at equilibrium state; these will be explained for both the FT rate equation and the WGS rate equation separately in sections 1.1.1.1 and 3.3.2.2, respectively. The combined FT

and WGS reaction models were then assessed separately against the experimental data to find the best kinetics model and rate expression for FT synthesis over a Co-based catalyst.

3.3.1. Fischer-Tropsch Reaction Rate Mechanism

3.3.1.1. *Kinetics models*

In the present study, the proposed kinetics models for FT reactions consisted of surface elementary reaction steps in four categories as follows:

i. Adsorption of the reactants (molecular CO and H_2 species) on the catalyst surface.

ii. Chain initiation step.

iii. Chain growth (propagation) step.

iv. Chain termination and desorption of the products step.

Herein, eight different sets of elementary reaction pathways were proposed for the FT synthesis reactions and they are listed in Table 3-2. In this table, for instance, '$C-\psi$' is the adsorbed carbon atom on the vacant active site and 'ψ' stands for the total vacant surface coverage fraction of the active site of the solid catalyst in the FT rate model. At the beginning, the molecular adsorption of CO and H_2 with their subsequent dissociation takes place on the free active sites (ψ) of the surface of the cobalt catalyst. Previously, the dissociative adsorption of CO was demonstrated by X-ray photoelectron spectroscopy (XPS) and pulse techniques on Ni, Co, Ru, and Fe [139]. As a consequence, CO first chemisorbed reversibly in the molecular state (step 1); H_2 chemisorbed reversibly on two adjacent free catalytic sites (2ψ) in the

dissociated state (step 2). The above assumptions were taken into account in all developed models from FT–I to FT–VIII listed in Table 3-2. These eight reaction paths were distinguished on the basis of different assumptions considered for adsorption of reactants and the remaining three polymerizations steps mentioned above. In all kinetics models, the combined alkyl and alkenyl mechanisms were adapted to describe the chain initiation, propagation and termination steps. The last seven steps of all developed FT models were written with the same assumptions so that the initiation, propagation and termination steps were proposed separately for olefins and paraffins' formation. In fact, the alkenyl mechanism represents the above three main steps exclusively for the formation of α-olefins; whereas the alkyl mechanism characterises these steps solely for n-paraffins. However, different hypotheses were made in proposing reaction steps of model FT–IV. Unlike the previous theory related to building blocks (i.e. methylene ($CH_2-\psi$) species), instead in these models methylidyne ($CH-\psi$) intermediate together with the addition of hydrogen atoms were assumed to be responsible for the growth mechanisms (see Table 3-2). In the present study, using a cobalt-based catalyst showed a higher tendency for the formation of paraffinic compounds compared to olefin products. The research studies also indicated that generally using Co and Ru transition metals as a catalyst present a higher tendency for the formation of paraffin compositions, in comparison with olefin formation [140]. Indeed, the alkyl mechanism favoured the formation of paraffins rather than olefins; hence it is a better choice for this case compared to other mechanisms e.g. alkenyl, CO insertion and/or enol mechanisms. However, using alkyl mechanism only, the olefins' selectivities were underestimated. To alleviate the prediction, the alkenyl mechanism which failed to explain the primary yielding of n-paraffins, can be incorporated for prediction of the formation of α–olefins without increasing the formation of n-paraffins. In addition, in these eight models, three main routes from reactants' adsorption towards building blocks and chain initiation were considered

i.e. unassisted CO dissociation (FT–I), H-assisted CO dissociation (FT–II to FT–V) and finally molecular H_2-assisted CO dissociation (FT–VI to FT–VIII). Models FT–I, FT–II and FT–VI were based on the assumption that the FT synthesis mechanism involved the hydrogenation of surface carbon formed by dissociation of chemisorbed CO, either directly (FT–I, step 3), leading to the oxygen atom formation, or by dissociation of $\mathrm{COH} - \psi$ isomers (FT–II, reaction step 4) leading to the hydroxyl species formation, or by interaction with molecular hydrogen (FT–VI, reaction step 3) which leads to the water formation. Very recently density functional theory (DFT) calculations seem to support the key role of H-assisted CO dissociation on both Fe and Co catalysts. A literature study provides both experimental (kinetics) and theoretical (DFT) evidence for the role of H-assisted CO activation as the exclusive kinetically relevant pathway on Co catalysts at conditions typical of FT synthesis practice [141]. Due to the above-mentioned facts, four different pathways, i.e. from FT–II to FT–V, were proposed on the basis of H-assisted chemisorbed CO dissociation to develop the FT reaction rates. Due to a higher formation of methane compared to other paraffinic values, the formation rate mechanism could not be the same as other n-paraffins. Hence, termination to methane was postulated by a different reaction step in which the methane was formed by H-addition of surface methyl intermediate. In addition, the selectivity of ethene was much lower than of other olefin species as indicated from the measured data. Hence, a different reaction step was proposed for the ethene formation so that two adjacent methylene intermediates were reacted at the surface of the catalyst to desorb the ethene molecule. From the outlook of the kinetic descriptions indicated above, eight different elementary reaction steps were proposed as follows:

Model FT–I: Model FT–I was based on unassisted CO dissociation. Considering the steps 1 and 2 explained above, this is followed by direct dissociation of adsorbed surface CO intermediate to form surface carbon and surface oxygen (step 3). Then, the reaction of surface

oxygen with adsorbed hydrogen yielded the formation of hydroxyl (step 4); that in turn reacted with adsorbed hydrogen yielding the most abundant product, water molecule (step 5). The sequential hydrogenation of surface carbon led to formation of surface methylidyne (step 6), surface methylene (step 7) and surface methyl (step 8) species. The surface methylene intermediate is regarded as the monomer (building block) in this reaction scheme. The surface methyl species ($-CH_3$) was assumed to be the chain initiator. The chain initiation step in the 'alkyl' mechanism takes place via this reaction pathway. Van Barneveld and Ponec [142] stated that the formation of CH_3 intermediate is essentially irreversible. This assumption was taken into account herein when the rate expressions were developed for each kinetic model.

Model FT–II: This model is described by dissociation of chemisorbed CO via the H-assisted mechanism. The first hydrogenation (H-assisted) of adsorbed CO led to the formation of surface $\mathrm{COH}-\psi$ isomers (step 3) followed by the formation of surface carbon atoms and hydroxyl intermediates from its dissociation (i.e. $\mathrm{COH}-\psi$ isomers) (step 4). Similar to FT–I, water formed by the addition of hydrogen atoms to hydroxyl (step 5) and the sequential hydrogenation of surface carbon led to the formation of surface methylidyne, methylene and methyl intermediates (steps 6-8).

Model FT–III: Similar to Model FT–II, this model is described by H-assisted chemisorbed CO, except that chemisorbed CO is hydrogenated two times giving the formyl intermediate $\mathrm{HCO}-\psi$ after the first H-addition (step 3, $\mathrm{H}-\psi$ addition to the C-atom in $\mathrm{CO}-\psi$) and the hydroxymethylene species $\mathrm{HCOH}-\psi$ after the second hydrogenation (step 4, $\mathrm{H}-\psi$ addition to the O-atom in $\mathrm{HCO}-\psi$). Hydroxymethylene dissociation then led to the formation of methylidyne and hydroxyl intermediates (step 5); that in turn reacted with adsorbed hydrogen

atoms forming the polymerization monomer CH_2 (step 7), the initiator required for the chain growth (methyl species, CH_3, step 8) and products H_2O (step 6).

Model FT–IV: This model was similar to model FT–III but the first H-addition of adsorbed CO (step 3) was then followed by dissociation of formed formyl species into methylidyne and surface oxygen atoms (step 4). This model was also different from other H-assisted models in order that the adsorbed reactive surface methylidyne could react with two adjacent hydrogen atoms producing surface methyl (step 7) i.e. the chain initiation for production of paraffinic compounds. Unlike the other FT models, the chain initiator ($C_2H_3 - \psi$) for the olefins' production was suggested to be formed by two-adjacent methylidyne species and successive interaction of two hydrogen atoms.

Model FT–V: The addition of $H-\psi$ to the C−atom in $HCO-\psi$ formed $CH_2O-\psi$ intermediates which was followed by dissociation to $CH_2-\psi$ and $O-\psi$ in which the oxygen atom was rejected through this step; possessing high activation barriers (see section 5.2.2.1). Water formed by the addition of hydrogen atoms to the hydroxyl (step 8) formed by hydrogenation of surface oxygen atoms and the hydrogenation of surface methylene led to the formation of methyl intermediates (step 6). The chain growth mechanism was similar to that reported for FT–III.

Model FT–VI: It is evident that an adsorbed reactive CO could also react with dihydrogen, which leads to the formation of dissociated carbon atoms and water molecules (step 3). This mechanism was regarded as molecular H_2-assisted CO dissociation. The dissociated carbon atoms hydrogenated sequentially (steps 4-6) to finally form the initiator required for the chain growth.

Model FT–VII: Similar to model FT–VI, this model is described by an H_2-assisted mechanism, but instead the reaction between adsorbed CO with dihydrogen formed hydroxymethylene species (step 3) which is then hydrogenated by H-addition forming surface methylidyne and surface water (step 4). Similar to model FT–VI, the adsorbed methylidyne hydrogenated in two successive steps (steps 6-7) to finally form the initiator required for the chain growth.

Model FT–VIII: Same as model FT–VII, the building block and chain initiator in model FT–VIII were respectively adsorbed methylene and methyl, but formation of the building block differs from the former when the hydroxymethylene species reacted with the hydrogen molecule at the surface instead forming the methylene intermediate and water molecule (step 4).

From the above eight kinetics mechanisms and elementary reaction paths tabulated in Table 3-2, twenty-four possible rate expressions were derived for overall conversion and FT reaction rates by considering different assumptions and various RDSs. The derivation of the rate equations for the FT reaction was explained in section 1.1.1.1.

Table 3-2 Sequence of elementary reaction steps of FT synthesis reaction in the present study

Model	No.	Elementary reaction steps	Model	No.	Elementary reaction steps
FT–I	1	$CO + \psi \rightleftarrows CO - \psi$	FT–III	1	$CO + \psi \rightleftarrows CO - \psi$
	2	$H_2 + 2\psi \rightleftarrows 2H - \psi$		2	$H_2 + 2\psi \rightleftarrows 2H - \psi$
	3	$CO - \psi + \psi \rightleftarrows C - \psi + O - \psi$		3	$CO - \psi + H - \psi \rightleftarrows HCO - \psi + \psi$
	4	$O - \psi + H - \psi \rightleftarrows OH - \psi + \psi$		4	$HCO - \psi + H - \psi \rightleftarrows HCOH - \psi + \psi$
	5	$OH - \psi + H - \psi \rightleftarrows H_2O + 2\psi$		5	$HCOH - \psi + \psi \rightleftarrows CH - \psi + OH - \psi$
	6	$C - \psi + H - \psi \rightleftarrows CH - \psi + \psi$		6	$OH - \psi + H - \psi \rightleftarrows H_2O + 2\psi$
	7	$CH - \psi + H - \psi \rightleftarrows CH_2 - \psi + \psi$		7	$CH - \psi + H - \psi \rightleftarrows CH_2 - \psi + \psi$
	8	$CH_2 - \psi + H - \psi \rightarrow CH_3 - \psi + \psi$		8	$CH_2 - \psi + H - \psi \rightarrow CH_3 - \psi + \psi$
	9	$CH_3 - \psi + H - \psi \rightarrow CH_4 + 2\psi$		9	$CH_3 - \psi + H - \psi \rightarrow CH_4 + 2\psi$
	10	$CH_2 - \psi + CH_2 - \psi \rightarrow C_2H_4 + 2\psi$		10	$CH_2 - \psi + CH_2 - \psi \rightarrow C_2H_4 + 2\psi$
	11	$CH_2 - \psi + CH - \psi \rightarrow C_2H_3 - \psi + \psi$		11	$CH_2 - \psi + CH - \psi \rightarrow C_2H_3 - \psi + \psi$
	12	$C_{n-1}H_{2n-1} - \psi + CH_2 - \psi \rightarrow C_nH_{2n+1} - \psi + \psi\ ;\ n \geq 2$		12	$C_{n-1}H_{2n-1} - \psi + CH_2 - \psi \rightarrow C_nH_{2n+1} - \psi + \psi\ ;\ n \geq 2$
	13	$C_nH_{2n+1} - \psi + H - \psi \rightarrow C_nH_{2n+2} + 2\psi$		13	$C_nH_{2n+1} - \psi + H - \psi \rightarrow C_nH_{2n+2} + 2\psi$
	14	$CH_2 - \psi + C_{n-1}H_{2n-3} - \psi \rightarrow C_nH_{2n-1} - \psi + \psi$		14	$CH_2 - \psi + C_{n-1}H_{2n-3} - \psi \rightarrow C_nH_{2n-1} - \psi + \psi$
	15	$C_nH_{2n-1} - \psi + H - \psi \rightarrow C_nH_{2n} + 2\psi$		15	$C_nH_{2n-1} - \psi + H - \psi \rightarrow C_nH_{2n} + 2\psi$
FT–II	1	$CO + \psi \rightleftarrows CO - \psi$	FT–IV	1	$CO + \psi \rightleftarrows CO - \psi$
	2	$H_2 + 2\psi \rightleftarrows 2H - \psi$		2	$H_2 + 2\psi \rightleftarrows 2H - \psi$
	3	$CO - \psi + H - \psi \rightleftarrows COH - \psi + \psi$		3	$CO - \psi + H - \psi \rightleftarrows HCO - \psi + \psi$
	4	$COH - \psi + \psi \rightleftarrows C - \psi + OH - \psi$		4	$HCO - \psi + \psi \rightleftarrows CH - \psi + O - \psi$
	5	$OH - \psi + H - \psi \rightleftarrows H_2O + 2\psi$		5	$O - \psi + H - \psi \rightleftarrows OH - \psi + \psi$
	6	$C - \psi + H - \psi \rightleftarrows CH - \psi + \psi$		6	$OH - \psi + H - \psi \rightleftarrows H_2O + 2\psi$
	7	$CH - \psi + H - \psi \rightleftarrows CH_2 - \psi + \psi$		7	$CH - \psi + H_2 \rightarrow CH_3 - \psi$
	8	$CH_2 - \psi + H - \psi \rightarrow CH_3 - \psi + \psi$		8	$CH_3 - \psi + H - \psi \rightarrow CH_4 + 2\psi$
	9	$CH_3 - \psi + H - \psi \rightarrow CH_4 + 2\psi$		9	$CH - \psi + CH - \psi + 2H - \psi \rightarrow C_2H_4 + 4\psi$
	10	$CH_2 - \psi + CH_2 - \psi \rightarrow C_2H_4 + 2\psi$		10	$CH - \psi + CH - \psi + H - \psi \rightarrow C_2H_3 - \psi + 2\psi$
	11	$CH_2 - \psi + CH - \psi \rightarrow C_2H_3 - \psi + \psi$		11	$C_{n-1}H_{2n-1} - \psi + CH - \psi + H - \psi \rightarrow C_nH_{2n+1} - \psi + 2\psi\ ;\ n \geq 2$
	12	$C_{n-1}H_{2n-1} - \psi + CH_2 - \psi \rightarrow C_nH_{2n+1} - \psi + \psi\ ;\ n \geq 2$		12	$C_nH_{2n+1} - \psi + H - \psi \rightarrow C_nH_{2n+2} + 2\psi$
	13	$C_nH_{2n+1} - \psi + H - \psi \rightarrow C_nH_{2n+2} + 2\psi$		13	$CH - \psi + C_{n-1}H_{2n-3} - \psi + H - \psi \rightarrow C_nH_{2n-1} - \psi + 2\psi$
	14	$CH_2 - \psi + C_{n-1}H_{2n-3} - \psi \rightarrow C_nH_{2n-1} - \psi + \psi$		14	$C_nH_{2n-1} - \psi + H - \psi \rightarrow C_nH_{2n} + 2\psi$

Model	No.	Elementary reaction steps
	15	$C_nH_{2n-1} - \psi + H - \psi \rightarrow C_nH_{2n} + 2\psi$
FT–V	1	$CO + \psi \rightleftarrows CO - \psi$
	2	$H_2 + 2\psi \rightleftarrows 2H - \psi$
	3	$CO - \psi + H - \psi \rightleftarrows HCO - \psi + \psi$
	4	$HCO - \psi + H - \psi \rightleftarrows CH_2O - \psi + \psi$
	5	$CH_2O - \psi + \psi \rightleftarrows CH_2 - \psi + O - \psi$
	6	$CH_2 - \psi + H - \psi \rightleftarrows CH_3 - \psi$
	7	$O - \psi + H - \psi \rightleftarrows OH - \psi + \psi$
	8	$OH - \psi + H - \psi \rightleftarrows H_2O + 2\psi$
	9	$CH_3 - \psi + H - \psi \rightarrow CH_4 + 2\psi$
	10	$CH_2 - \psi + CH_2 - \psi \rightarrow C_2H_4 + 2\psi$
	11	$CH_2 - \psi + CH - \psi \rightarrow C_2H_3 - \psi + \psi$
	12	$C_{n-1}H_{2n-1} - \psi + CH_2 - \psi \rightarrow C_nH_{2n+1} - \psi + \psi\ ;\ n \geq 2$
	13	$C_nH_{2n+1} - \psi + H - \psi \rightarrow C_nH_{2n+2} + 2\psi$
	14	$CH_2 - \psi + C_{n-1}H_{2n-3} - \psi \rightarrow C_nH_{2n-1} - \psi + \psi$
	15	$C_nH_{2n-1} + H - \psi \rightarrow C_nH_{2n} + 2\psi$
FT–VI	1	$CO + \psi \rightleftarrows CO - \psi$
	2	$H_2 + 2\psi \rightleftarrows 2H - \psi$
	3	$CO - \psi + H_2 \rightleftarrows C - \psi + H_2O$
	4	$C - \psi + H - \psi \rightleftarrows CH - \psi + \psi$
	5	$CH - \psi + H - \psi \rightleftarrows CH_2 - \psi + \psi$
	6	$CH_2 - \psi + H - \psi \rightarrow CH_3 - \psi + \psi$
	7	$CH_3 - \psi + H - \psi \rightarrow CH_4 + 2\psi$
	8	$CH_2 - \psi + CH_2 - \psi \rightarrow C_2H_4 + 2\psi$
	9	$CH_2 - \psi + CH - \psi \rightarrow C_2H_3 - \psi + \psi$
	10	$C_{n-1}H_{2n-1} - \psi + CH_2 - \psi \rightarrow C_nH_{2n+1} - \psi + \psi\ ;\ n \geq 2$
	11	$C_nH_{2n+1} - \psi + H - \psi \rightarrow C_nH_{2n+2} + 2\psi$
	12	$CH_2 - \psi + C_{n-1}H_{2n-3} - \psi \rightarrow C_nH_{2n-1} - \psi + \psi$
	13	$C_nH_{2n-1} + H - \psi \rightarrow C_nH_{2n} + 2\psi$
FT–VII	1	$CO + \psi \rightleftarrows CO - \psi$
	2	$H_2 + 2\psi \rightleftarrows 2H - \psi$
	3	$CO - \psi + H_2 \rightleftarrows HCOH - \psi$
	4	$HCOH - \psi + H - \psi \rightleftarrows CH - \psi + H_2O - \psi$
	5	$H_2O - \psi \rightleftarrows H_2O + \psi$
	6	$CH - \psi + H - \psi \rightleftarrows CH_2 - \psi + \psi$
	7	$CH_2 - \psi + H - \psi \rightarrow CH_3 - \psi + \psi$
	8	$CH_3 - \psi + H - \psi \rightarrow CH_4 + 2\psi$
	9	$CH_2 - \psi + CH_2 - \psi \rightarrow C_2H_4 + 2\psi$
	10	$CH_2 - \psi + CH - \psi \rightarrow C_2H_3 - \psi + \psi$
	11	$C_{n-1}H_{2n-1} - \psi + CH_2 - \psi \rightarrow C_nH_{2n+1} - \psi + \psi\ ;\ n \geq 2$
	12	$C_nH_{2n+1} - \psi + H - \psi \rightarrow C_nH_{2n+2} + 2\psi$
	13	$CH_2 - \psi + C_{n-1}H_{2n-3} - \psi \rightarrow C_nH_{2n-1} - \psi + \psi$
	14	$C_nH_{2n-1} + H - \psi \rightarrow C_nH_{2n} + 2\psi$
FT–VIII	1	$CO + \psi \rightleftarrows CO - \psi$
	2	$H_2 + 2\psi \rightleftarrows 2H - \psi$
	3	$CO - \psi + H_2 \rightleftarrows HCOH - \psi$
	4	$HCOH - \psi + H_2 \rightleftarrows CH_2 - \psi + H_2O$
	5	$CH_2 - \psi + H - \psi \rightarrow CH_3 - \psi + \psi$
	6	$CH_3 - \psi + H - \psi \rightarrow CH_4 + 2\psi$
	7	$CH_2 - \psi + CH_2 - \psi \rightarrow C_2H_4 + 2\psi$
	8	$CH_2 - \psi + CH_2 - \psi \rightarrow C_2H_3 - \psi + H - \psi$
	9	$C_{n-1}H_{2n-1} - \psi + CH_2 - \psi \rightarrow C_nH_{2n+1} - \psi + \psi\ ;\ n \geq 2$
	10	$C_nH_{2n+1} - \psi + H - \psi \rightarrow C_nH_{2n+2} + 2\psi$
	11	$CH_2 - \psi + C_{n-1}H_{2n-3} - \psi \rightarrow C_nH_{2n-1} - \psi + \psi\ ;\ n \geq 3$
	12	$C_nH_{2n-1} + H - \psi \rightarrow C_nH_{2n} + 2\psi$

3.3.1.2. *Derivation of Rate Equation*

In order to derive the rate equations from the detailed mechanistic kinetics models developed in section 3.3.1.1, the LHHW rate theory was used and the possible RDSs were identified; while all other steps were assumed to be at quasi-equilibrium. In order to derive the rate expressions, the FT synthesis (hydrocarbon formation) and WGS reaction were assumed to proceed on different active sites. Hence, there were two types of uniformly distributed active sites for FT synthesis and WGS reactions on the catalyst's surface. On the basis of the detailed sequence of elementary reaction steps for FT synthesis tabulated in Table 3-2, the rates of the n-paraffins and α-olefins' formation were derived for each kinetic model. Initially, it was assumed that the steady-state conditions were reached for both the surface composition of the catalyst and the concentration of all the intermediate species involved. Then, it was assumed that the rate constant parameter of the reaction steps for the hydrocarbon formation is independent of the carbon number of the intermediate species involved in the elementary steps. However, different rate constants were considered for methane and ethene in order to avoid the plausible deviation of the results; as from the experimental results (see section 5.1), it is clear that the amount of methane produced is much higher than other paraffins and this can cause the deviation. For the same reason, the rate constant of ethene was defined solely due to its low production rate value. The estimated values for rate constants are given in section 5.2.

In order to derive the rate expressions, the kinetics model FT–III with RDS-1 in Table 3-2 was selected to be demonstrated as an example of the derivation of the rate equations. In

fact not all of the kinetics parameters are kinetically significant; that is to say not all of them are controlling the overall rate. The rate determining step in a series of elementary steps is that step which has the maximum effect on the overall rate of reaction. Herein, steps 6 and 8 to 15 (model FT–III with RDS-1) were assumed to be RDSs. The remaining steps were assumed to be rapid and at an equilibrium condition. According to the literature [91, 143], the CH_3 intermediate has a high potential to be hydrogenated to form methane. This leads to the correspondingly low opportunity for the methanol and formic acid formation. From the elementary steps 9, 10, 13 and 15, respectively the rate of formation of methane, ethene, n-paraffins and α-olefins were written as follows:

$$R_{CH_4} = k_{meth}\psi_{CH_3}\psi_H \qquad \text{Equation 3-13}$$

$$R_{C_2H_4} = k_{eth}{\psi_{CH_2}}^2 \qquad \text{Equation 3-14}$$

$$R_{olefins} = k_{t,olef}\psi_{C_nH_{2n-1}}\psi_H \qquad \text{Equation 3-15}$$

$$R_{parffins} = k_{t,par}\psi_{C_nH_{2n+1}}\psi_H \qquad \text{Equation 3-16}$$

The elementary steps 1-5 and 7 were assumed to proceed at quasi-equilibrium so the net rate of these steps would be zero. From the kinetics model FT–III, the area coverage fraction of species (concentration of surface intermediate) i.e. ψ_{CO}, ψ_H, ψ_{HCO}, ψ_{HCOH}, ψ_{CH}, ψ_{CH_2}, ψ_{OH} were expressed as a function of the partial pressure of CO, H_2, and H_2O.

From the LHHW rate theory [144], the equilibrium mechanism of adsorption and desorption of reactants and products at the catalyst surface, was used to develop the rate

expressions. Therefore, the following equations were written for the adsorption and desorption at the catalyst surface of the absorbent as:

$$\left(\frac{dn_i}{dt}\right)_{ads.} = R_{i,ads.} = k_{i,ads.}(1-\psi_i)P_i \quad \text{Equation 3-17}$$

$$\left(\frac{dn_i}{dt}\right)_{des.} = R_{i,des.} = k_{i,des.}\psi_i \quad \text{Equation 3-18}$$

Where P_i is the partial pressure of species 'i' and ψ stands for the total vacant surface coverage fraction of active site in the FT rate model. By applying the pseudo-equilibrium assumption for any elementary reaction step, the rate of adsorption equals to the rate of desorption, which can be expressed as Equation 3-19 and the equilibrium constant can be described by Equation 3-20. Hence, by extending these relations one can obtain the Langmuir isotherm as the adsorption by Equation 3-21.

$$R_{i,ads.} = k_{i,ads.}(1-\psi_i)P_i = R_{i,des.} = k_{i,des.}\psi_i \quad \text{Equation 3-19}$$

$$K_1 = \frac{k_{i,ads.}}{k_{i,des.}} = \frac{\psi_i}{P_i(1-S_i)} \quad \text{Equation 3-20}$$

$$\psi_i = \frac{k_{i,ads.}(1-\psi_i)P_i}{k_{i,des.}} \quad \text{Equation 3-21}$$

$R_{i,ads.}$ and $R_{i,des.}$ are respectively the rates of adsorption and desorption of adsorbent on the catalyst surface. The other adsorbed intermediates' surface coverages were found by the same way in the following forms:

$$\psi_{CO} = K_1 P_{CO} \psi \quad \text{Equation 3-22}$$

$$\psi_H = \sqrt{K_2} P_{H2}^{0.5} \psi \quad \text{Equation 3-23}$$

$$\psi_{HCO} = \frac{K_3 \psi_{CO} \psi_H}{\psi} = K_1 \sqrt{K_2} K_3 P_{CO} P_{H2}^{0.5} \psi \quad \text{Equation 3-24}$$

$$\psi_{HCOH} = \frac{K_4 \psi_{HCO} \psi_H}{\psi} = K_1 K_2 K_3 K_4 P_{CO} P_{H2} \psi \quad \text{Equation 3-25}$$

$$\psi_{CH} = \frac{K_5 \psi_{HCOH} \psi}{\psi_{OH}} = K_1 K_2^{1.5} K_3 K_4 K_5 k_6 \frac{P_{CO} P_{H2}^{1.5}}{R_{FT}} \psi^3 \quad \text{Equation 3-26}$$

$$\psi_{CH_2} = \frac{K_7 \psi_{CH} \psi_H}{\psi} = K_1 K_2^2 K_3 K_4 K_5 k_6 K_7 \frac{P_{CO} P_{H2}^2}{R_{FT}} \psi^3 \quad \text{Equation 3-27}$$

Since the rate of hydrogenation of the surface hydroxyl was the RDS, therefore the rate of FT synthesis was expressed by Equation 3-28. The rate of the initiation step (formation of methyl from hydrogenation of methylene) in model FT–III was also assumed to be an RDS as well, hence one can be written as Equation 3-29.

$$R_{FT} = k_6 \psi_{OH} \psi_H \quad \text{Equation 3-28}$$

$$R_{FT} = k_8 \psi_{CH_2} \psi_H = K_1 K_2^{2.5} K_3 K_4 K_5 k_6 K_7 k_8 \frac{P_{CO} P_{H2}^{2.5}}{R_{FT}} \psi^4 \quad \text{Equation 3-29}$$

Therefore, one can obtain the second expression for the rate of FT synthesis as below:

$$R_{FT} = \sqrt{K_1 K_2^{2.5} K_3 K_4 K_5 k_6 K_7 k_8} P_{CO}^{0.5} P_{H2}^{1.25} \psi^2 \quad \text{Equation 3-30}$$

So by substituting Equation 3-30 into the Equation 3-26 and Equation 3-27, the area coverage fraction of CH and CH_2 intermediates can be expressed in terms of partial pressures as follows:

$$\psi_{CH} = \frac{K_1 K_2^{1.5} K_3 K_4 K_5 k_6}{\sqrt{K_1 K_2^{2.5} K_3 K_4 K_5 k_6 K_7 k_8}} P_{CO}^{0.5} P_{H2}^{0.25} \psi \quad \text{Equation 3-31}$$

$$\psi_{CH_2} = \frac{K_1 K_2^2 K_3 K_4 K_5 k_6 K_7 \frac{P_{CO} P_{H2}^2}{R_{FT}} \psi^3}{\sqrt{K_1 K_2^{2.5} K_3 K_4 K_5 k_6 K_7 k_8} P_{CO}^{0.5} P_{H2}^{1.25} \psi^2} \quad \text{Equation 3-32}$$

$$= \sqrt{\frac{K_1 K_2^{1.5} K_3 K_4 K_5 k_6 K_7}{k_8}} P_{CO}^{0.5} P_{H2}^{0.75} \psi$$

From the Langmuir adsorption theory in a multicomponent system with a single site type, the area coverage fraction of species was written as stoichiometric balance concentrations. Normalization of the concentration of all intermediates on the catalyst surface leads to the following form of the total area coverage fractions:

$$\psi + \psi_{CO} + \psi_H + \psi_{HCO} + \psi_{HCOH} + \psi_{CH} + \psi_{CH_2} = 1 \quad \text{Equation 3-33}$$

Combining all the above equations and substitution of Equation 3-22-Equation 3-25 into Equation 3-33, the concentration of the total vacant active site ψ can be expressed in terms of partial pressure of different species and the equilibrium constant parameters as follows:

$$\psi = \frac{1}{\left(1 + K_1 P_{CO} + \sqrt{K_2} P_{H2}^{0.5} + K_1\sqrt{K_2} K_3 P_{CO} P_{H2}^{0.5} + K_1 K_2 K_3 K_4 P_{CO} P_{H2} + \cdots \right.} \quad \text{Equation 3-34}$$
$$\left. \frac{K_1 K_2^{1.5} K_3 K_4 K_5 k_6}{\sqrt{K_1 K_2^{2.5} K_3 K_4 K_5 k_6 K_7 k_8}} P_{CO}^{0.5} P_{H2}^{0.25} + \sqrt{\frac{K_1 K_2^{1.5} K_3 K_4 K_5 k_6 K_7}{k_8}} P_{CO}^{0.5} P_{H2}^{0.75} \right)^2$$

Substituting the above formula for the total free active site into the rate expression obtained from hydrogenation of methylene (Equation 3-29) gave the following equation with respect to the partial pressure of species and kinetic parameters:

$$R_{FT} = \frac{\sqrt{k_8 K_7 k_6 K_5 K_1 K_2^{2.5} K_3 K_4} P_{CO}^{0.5} P_{H2}^{1.25}}{\left(1 + K_1 P_{CO} + \sqrt{K_2} P_{H2}^{0.5} + K_1\sqrt{K_2} K_3 P_{CO} P_{H2}^{0.5} + K_1 K_2 K_3 K_4 P_{CO} P_{H2} + \cdots \right.} \quad \text{Equation 3-35}$$
$$\left. \frac{K_1 K_2^{1.5} K_3 K_4 K_5 k_6}{\sqrt{K_1 K_2^{2.5} K_3 K_4 K_5 k_6 K_7 k_8}} P_{CO}^{0.5} P_{H2}^{0.25} + \sqrt{\frac{K_1 K_2^{1.5} K_3 K_4 K_5 k_6 K_7}{k_8}} P_{CO}^{0.5} P_{H2}^{0.75} \right)^2$$

The surface coverages of methyl and vinyl radical were obtained by considering the quasi-steady state assumption for the surface intermediate. From the model FT–III, the balance equations were obtained from reaction steps 8, 9 and 12 for methyl and steps 11 and 14 for

vinyl. Rearranging Equation 3-36 and Equation 3-37 gave the expression of the intermediate ψ_{CH3} and ψ_{C2H3} (Equation 3-38 and Equation 3-39), respectively.

$$\frac{dS_{CH_3}}{dt} = 0 \Longrightarrow +R_8 - R_9 - R_{12} = 0$$

$$\Longrightarrow + k_{i,par}\psi_{CH_2}\psi_H - k_{meth}\psi_{CH_3}\psi_H - k_{p,par}\psi_{CH_3}\psi_{CH_2} = 0 \quad \text{Equation 3-36}$$

$$\frac{dS_{C_2H_3}}{dt} = 0 \Longrightarrow +R_{11} - R_{14} = 0$$

$$\Longrightarrow + k_{i,olef}\psi_{CH_2}\psi_{CH} - k_{p,olef}\psi_{CH_2}\psi_{C_2H_3} = 0 \quad \text{Equation 3-37}$$

$$\psi_{CH_3} = \frac{k_{i,par}\psi_{CH_2}\psi_H}{k_{p,par}\psi_{CH_2} + k_{meth}\psi_H} \quad \text{Equation 3-38}$$

$$\psi_{C_2H_3} = \frac{k_{i,olef}\psi_{CH}}{k_{p,olef}} \quad \text{Equation 3-39}$$

Similarly, applying the quasi-steady state assumption for the surface intermediates $\psi_{C_nH_{2n-1}}$ and $\psi_{C_nH_{2n+1}}$ were as follows:

$$\frac{d\psi_{C_nH_{2n-1}}}{dt} = 0 \Longrightarrow +R_{12} - R'_{12} - R_{13} = 0$$

$$\Longrightarrow + k_{p,olef}\psi_{C_{n-1}H_{2n-3}}\psi_{CH_2} - k_{p,olef}\psi_{C_nH_{2n-1}}\psi_{CH_2}$$

$$- k_{t,olef}\psi_{C_nH_{2n-1}}\psi_H = 0 \quad \text{Equation 3-40}$$

$$\frac{d\psi_{C_nH_{2n+1}}}{dt} = 0 \Longrightarrow +R_{12} - R'_{12} - R_{13} = 0$$

$$\Longrightarrow + k_{p,par}\psi_{C_{n-1}H_{2n-1}}\psi_{CH_2} - k_{p,par}\psi_{C_nH_{2n+1}}\psi_{CH_2}$$

$$- k_{t,par}\psi_{C_nH_{2n+1}}\psi_H = 0$$

Equation 3-41

Rearranging the above equations leads to the final expression for $\psi_{C_nH_{2n-1}}$ and $\psi_{C_nH_{2n+1}}$ intermdiates.

$$\psi_{C_nH_{2n-1}} = \frac{k_{p,olef}\psi_{C_{n-1}H_{2n-3}}\psi_{CH2}}{k_{p,olef}\psi_{CH2} + k_{t,olef}\psi_H}$$

Equation 3-42

$$\psi_{C_nH_{2n+1}} = \frac{k_{p,par}\psi_{C_{n-1}H_{2n-1}}\psi_{CH_2}}{k_{p,par}\psi_{CH_2} + k_{t,par}\psi_H}$$

Equation 3-43

The dependence of the reaction rate and adsorption constants on temperature were expressed by the Arrhenius equation as follows:

$$k_j = k_{j,0}exp\left(-\frac{E_j}{RT}\right)$$

Equation 3-44

$$K_i = K_{i,0}exp\left(-\frac{\Delta H_{ads,i}}{RT}\right)$$

Equation 3-45

Where k_j is the rate constant of reaction 'j' and K_i is adsorption constant of component 'i'. It was shown that a different kinetics approach, which accounted for the polymerisation character of the FT synthesis, led to a rate formula which was identical to those derived

previously in many aspects. As a consequence, repeating and reporting similar rate expressions developed by a different FT kinetics model is avoided. Hence, the mechanistically developed FT rate equations with three plausible RDS assumptions for each FT model are summarized in Table 3-3 to Table 3-10. The full mathematical procedure in developing of each rate expression for FT reaction models is given in Appendix (Table A. 1 to Table A. 32). These RDS assumptions are explained below for each FT model. For each derived rate equation in each FT model, there is different kinetically relevant RDSs. Three different rate equations were derived for each FT kinetic model; hence the FT rate expressions totalled twenty-four equations. In models FT–I to FT–VIII, the elementary steps for chain initiation, growth and termination reactions including formation of methane, ethene, as well as higher paraffins and olefins, were assumed as the RDSs. However, additional RDSs were considered for each model; where each one was different for each FT model (see Table 3-3 to Table 3-10).

Table 3-3 Reaction rate expressions derived on the basis of kinetics model FT–I

RDS/No.	Rate equation
5,8-15 Equation 3-46	$$R_{FT} = \frac{\left(k_{i,par}k_5K_1K_2^{2.5}K_3K_4K_6K_7\right)^{0.5}P_{H_2}^{1.25}P_{CO}^{0.5}}{\left(\begin{array}{c} 1+K_1P_{CO}+\sqrt{K_2}P_{H2}^{0.5}+\frac{(k_5K_4K_3K_1)^{0.5}}{K_2^{0.25}\left(k_{i,par}K_6K_7\right)^{0.5}}P_{H_2}^{-0.25}P_{CO}^{0.5}+\cdots \\ \frac{K_2^{0.25}\left(k_{i,par}K_1K_3K_6K_7\right)^{0.5}}{(k_5K_4)^{0.5}}P_{H_2}^{0.25}P_{CO}^{0.5}+.\frac{K_2^{0.75}\left(k_{i,par}K_1K_3K_4K_6K_7\right)^{0.5}}{k_5^{0.5}}P_{H_2}^{0.75}P_{CO}^{0.5}+\cdots \\ \frac{K_2^{0.25}(k_5K_1K_3K_4K_6)^{0.5}}{\left(k_{i,par}K_7\right)^{0.5}}P_{H_2}^{0.25}P_{CO}^{0.5}+\frac{K_2^{0.75}(k_5K_7K_6K_4K_3K_1)^{0.5}}{k_{i,par}^{0.5}}P_{H_2}^{0.75}P_{CO}^{0.5} \end{array}\right)^2}$$

3, 8-15 Equation 3-47	$$R_{FT} = \frac{k_3 K_1 P_{CO}}{\left(\begin{array}{c} 1 + K_1 P_{CO} + \sqrt{K_2 P_{H_2}} + \frac{1}{K_5 K_4 K_2}\frac{P_{H_2O}}{P_{H_2}} + \cdots \\ \frac{1}{K_5\sqrt{K_2}}\frac{P_{H_2O}}{P_{H2}^{0.5}} + \frac{k_3 K_1}{k_{i,par} K_7 K_6 K_2^{1.5}}\frac{P_{CO}}{P_{H_2}^{1.5}} + \frac{k_3 K_1}{k_{i,par} K_7 K_2}\frac{P_{CO}}{P_{H_2}} + \frac{k_3 K_1}{k_{i,par}\sqrt{K_2}}\frac{P_{CO}}{P_{H2}^{0.5}} \end{array}\right)^2}$$
8-15 Equation 3-48	$$R_{FT} = \frac{k_{i,par} K_7 K_6 K_5 K_4 K_3 K_2^{2.5} K_1 \frac{P_{CO}}{P_{H_2O}} P_{H2}^{2.5}}{\left(\begin{array}{c} 1 + K_1 P_{CO} + \sqrt{K_2 P_{H_2}} + \frac{P_{H_2O}}{K_5 K_4 K_2 P_{H_2}} + \frac{P_{H_2O}}{K_5\sqrt{K_2} P_{H2}^{0.5}} + \cdots \\ \frac{K_5 K_4 K_3 K_2 K_1 P_{CO} P_{H_2}}{P_{H_2O}} + K_6 K_5 K_4 K_3 K_2^{1.5} K_1 \frac{P_{CO}}{P_{H_2O}} P_{H_2}^{1.5} + K_7 K_6 K_5 K_4 K_3 K_2^2 K_1 \frac{P_{CO}}{P_{H_2O}} P_{H_2}^2 \end{array}\right)^2}$$

Table 3-4 Reaction rate expressions derived on the basis of kinetics model FT–II

RDS/No.	Rate equation
4,7-14 Equation 3-49	$$R_{FT} = \frac{\sqrt{k_{i,par} k_5 K_1 K_2^{2.5} K_3 K_4 K_6 K_7} P_{CO}^{0.5} P_{H_2}^{1.25}}{\left(\begin{array}{c} 1 + K_1 P_{CO} + \sqrt{K_2 P_{H_2}} + K_3 K_1 \sqrt{K_2} P_{CO} P_{H2}^{0.5} \psi + \cdots \\ \sqrt{K_2} K_3 K_4 K_6 k_5 \frac{\psi_{CO} \psi_H^2}{R_{FT}} \sqrt{P_{H_2}} + K_1 K_2^2 K_3 K_4 K_6 K_7 k_5 \frac{P_{CO} P_{H_2}^2}{R_{FT}} + \cdots \\ \sqrt{k_{i,par} K_1 K_2^2 K_3 K_4 K_6 K_7} \frac{P_{CO}^{0.5} P_{H_2}^{0.75}}{k_5^{0.5}} + \frac{k_5^{0.5} K_4 K_3 K_1 P_{CO}^{0.5}}{\sqrt{k_{i,par} K_1 K_2^{1.5} K_3 K_4 K_6 K_7} P_{H_2}^{0.25}} \end{array}\right)^2}$$
3, 7-14 Equation 3-50	$$R_{FT} = \frac{k_4 K_3 K_1 \sqrt{K_2} P_{CO} P_{H2}^{0.5}}{\left(\begin{array}{c} 1 + K_1 P_{CO} + \sqrt{K_2 P_{H_2}} + K_3 K_1 \sqrt{K_2} P_{CO} P_{H2}^{0.5} + \frac{P_{H_2O}}{K_5\sqrt{K_2 P_{H_2}}} + \cdots \\ \frac{P_{H_2O}}{K_6\sqrt{K_2 P_{H_2}}} + \frac{k_4 K_1 K_3}{K_2^{0.5} k_{i,par} K_7}\frac{P_{CO}}{P_{H2}^{0.5}} + \frac{k_4 K_1 K_3}{k_{i,par}} P_{CO} \end{array}\right)^2}$$

7-14 Equation 3-51	$$R_{FT}=\frac{k_{i,par}\frac{K_1K_2^{2.5}K_3K_4K_5K_7}{K_6}\frac{P_{CO}P_{H_2}^{2.5}}{P_{H_2O}}}{\left(\begin{array}{c}1+K_1P_{CO}+\sqrt{K_2P_{H_2}}+\frac{P_{H_2O}}{K_6\sqrt{K_2P_{H_2}}}+K_3K_1\sqrt{K_2}P_{CO}P_{H2}^{0.5}+\cdots\\ K_4\left(K_5K_3K_1K_2\frac{P_{CO}P_{H_2}}{P_{H_2O}}\right)+\frac{P_{H_2O}}{K_5\sqrt{K_2P_{H_2}}}+\cdots\\ \frac{K_1K_2^{1.5}K_3K_4K_5}{K_6}\frac{P_{CO}P_{H_2}^{1.5}}{P_{H_2O}}+\frac{K_1K_2^2K_3K_4K_5K_7}{K_6}\frac{P_{CO}P_{H_2}^2}{P_{H_2O}}\end{array}\right)^2}$$

Table 3-5 Reaction rate expressions derived on the basis of kinetics model FT–III

RDS/No.	Rate equation
6,8-15 Equation 3-52	$$R_{FT}=\frac{\sqrt{k_{i,par}K_7k_6K_5K_1K_2^{2.5}K_3K_4}P_{CO}^{0.5}P_{H2}^{1.25}}{\left(\begin{array}{c}1+K_1P_{CO}+\sqrt{K_2P_{H_2}}+K_2^{0.75}\sqrt{\frac{k_{i,par}K_7K_5K_1K_3K_4}{k_6}}P_{CO}^{0.5}P_{H2}^{0.75}+\\ K_3K_1\sqrt{K_2}P_{CO}P_{H2}^{0.5}+K_1K_2K_3K_4P_{CO}P_{H2}+\\ K_2^{0.25}\sqrt{\frac{k_6K_1K_3K_4K_5}{k_{i,par}K_7}}P_{CO}^{0.5}P_{H2}^{0.25}+\sqrt{\frac{K_7k_6K_5K_1K_2^{1.5}K_3K_4}{k_{i,par}}}P_{CO}^{0.5}P_{H2}^{0.75}\end{array}\right)^2}$$
4, 8-15 Equation 3-53	$$R_{FT}=\frac{k_4K_1K_2K_3P_{CO}P_{H_2}}{\left(\begin{array}{c}1+K_1P_{CO}+\sqrt{K_2P_{H_2}}+\frac{P_{H_2O}}{K_6\sqrt{K_2P_{H_2}}}+K_3K_1\sqrt{K_2}P_{CO}P_{H2}^{0.5}+\\ \frac{k_4K_1K_3}{k_{i,par}K_5K_6K_7}P_{H_2O}P_{CO}+\frac{k_4K_1K_2^{0.5}K_3}{k_{i,par}K_7}P_{CO}P_{H_2}^{0.5}+\frac{k_4K_1K_2^{0.5}K_3}{k_{i,par}}P_{CO}P_{H_2}^{0.5}\end{array}\right)^2}$$
8-15 Equation 3-54	$$R_{FT}=\frac{k_{i,par}K_7K_5K_1K_2^{2.5}K_3K_4K_6\frac{P_{CO}P_{H_2}^{2.5}}{P_{H_2O}}}{\left(\begin{array}{c}1+K_1P_{CO}+\sqrt{K_2P_{H_2}}+\frac{P_{H_2O}}{K_6\sqrt{K_2P_{H_2}}}+K_3K_1\sqrt{K_2}P_{CO}P_{H2}^{0.5}+\\ K_1K_2K_3K_4P_{CO}P_{H_2}+K_5K_1K_2^{1.5}K_3K_4K_6\frac{P_{CO}P_{H_2}^{1.5}}{P_{H_2O}}+\\ K_7K_5K_1K_2^2K_3K_4K_6\frac{P_{CO}P_{H_2}^2}{P_{H_2O}}\end{array}\right)^2}$$

Table 3-6 Reaction rate expressions derived on the basis of kinetics model FT–IV

RDS/No.	Rate equation
4,6-13 Equation 3-55	$R_{FT} = \frac{\sqrt{k_{i,par} k_6^2 K_4 K_3 K_1 K_2^2 K_5 P_{CO}^{0.5}} P_{H2}^{1.25}}{\left(1 + K_1 P_{CO} + \sqrt{K_2 P_{H_2}} + K_3 K_1 \sqrt{K_2} P_{CO} P_{H2}^{0.5} + K_1 K_2 K_3 K_4 P_{CO} P_{H_2}\right)^{0.5}}$
3, 6-13 Equation 3-56	$R_{FT} = \frac{k_4 K_3 K_1 \sqrt{K_2} P_{CO} P_{H2}^{0.5}}{\left(1 + K_1 P_{CO} + \sqrt{K_2 P_{H_2}} + K_3 K_1 \sqrt{K_2} P_{CO} P_{H2}^{0.5} + \frac{P_{H_2O}}{K_7 K_2 K_5 P_{H_2}} + \frac{P_{H_2O}}{K_6 \sqrt{K_2 P_{H_2}}}\right)^2}$
6-13 Equation 3-57	$R_{FT} = \frac{k_{i,par} K_6 K_2^{1.5} K_5 K_4 K_3 K_1 \frac{P_{CO} P_{H2}^{2.5}}{P_{H_2O}}}{\left(\begin{array}{c} 1 + K_1 P_{CO} + \sqrt{K_2 P_{H_2}} + K_3 K_1 \sqrt{K_2} P_{CO} P_{H2}^{0.5} + K_6 K_2^{1.5} K_5 K_4 K_3 K_1 \frac{P_{CO} P_{H2}^{1.5}}{P_{H_2O}} \\ \frac{P_{H_2O}}{K_6 K_2 K_5 P_{H_2}} + \frac{P_{H_2O}}{K_6 \sqrt{K_2 P_{H_2}}} \end{array}\right)^2}$

Table 3-7 Reaction rate expressions derived on the basis of kinetics model FT–V

RDS/No.	Rate equation
4,5-12 Equation 3-58	$R_{FT} = \frac{\sqrt{k_{i,par} \frac{\left(k_7 K_6 K_1 K_2^{2.5} K_3 K_4\right)}{K_5}} P_{CO} P_{H_2}^{1.25}}{\left(\begin{array}{c} 1 + K_1 P_{CO} + \sqrt{K_2 P_{H_2}} + K_3 K_1 \sqrt{K_2} P_{CO} P_{H2}^{0.5} + K_1 K_2 K_3 K_4 P_{CO} P_{H_2} \\ \frac{\left(\sqrt{k_7 K_6 K_1 K_3 K_4} K_2^{0.75}\right)}{\sqrt{K_5}} \frac{P_{CO} P_{H_2}^{0.75}}{\sqrt{k_{i,par}}} + \cdots \\ \frac{\sqrt{k_{i,par}\left(K_1 K_2^{0.25} K_3 K_4\right)} P_{CO} P_{H_2}^{0.25}}{K_5 \sqrt{k_7 K_6}} + \sqrt{k_{i,par} \frac{\left(K_6 K_1 K_2^2 K_3 K_4\right)}{K_5}} \frac{P_{CO} P_{H_2}^{0.5}}{k_7^{0.5}} \end{array}\right)^2}$

3, 5-12 Equation 3-59	$$R_{FT} = \frac{k_4 K_3 K_1 K_2 P_{CO} P_{H_2}}{\left(\begin{array}{c} 1 + K_1 P_{CO} + \sqrt{K_2 P_{H_2}} + K_3 K_1 \sqrt{K_2} P_{CO} P_{H2}^{0.5} + K_1 K_2 K_3 K_4 P_{CO} P_{H_2} \\ \frac{k_4 K_3 K_1 K_2^{0.5}}{k_{i,par} K_7 K_2 K_5 K_5} P_{CO} \frac{P_{H_2O}}{P_{H_2}^{0.5}} + \frac{P_{H_2O}}{K_7 K_2 K_5 P_{H_2}} + \frac{P_{H_2O}}{K_7 \sqrt{K_2 P_{H_2}}} + \frac{k_4 K_3 K_1 K_2^{0.5} P_{CO} P_{H_2}^{0.5}}{k_{i,par}} \end{array}\right)^2}$$
5-12 Equation 3-60	$$R_{FT} = \frac{k_{i,par} K_1 K_2^{2.5} K_3 K_4 K_7 K_5 \frac{P_{CO} P_{H_2}^{2.5}}{P_{H_2O}}}{\left(\begin{array}{c} 1 + K_1 P_{CO} + \sqrt{K_2 P_{H_2}} + K_3 K_1 \sqrt{K_2} P_{CO} P_{H2}^{0.5} + K_1 K_2 K_3 K_4 P_{CO} P_{H_2} \\ \frac{k_4 K_3 K_1 K_2^{0.5}}{k_{i,par} K_7 K_2 K_5 K_5} P_{CO} \frac{P_{H_2O}}{P_{H_2}^{0.5}} + \frac{P_{H_2O}}{K_7 K_2 K_5 P_{H_2}} + \frac{P_{H_2O}}{K_7 \sqrt{K_2 P_{H_2}}} + \frac{k_4 K_3 K_1 K_2^{0.5} P_{CO} P_{H_2}^{0.5}}{k_{i,par}} \end{array}\right)^2}$$

Table 3-8 Reaction rate expressions derived on the basis of kinetics model FT–VI

RDS/No.	Rate equation
3,6-13 Equation 3-61	$$R_{FT} = \frac{k_3 K_1 P_{CO} P_{H_2}}{\left(1 + K_1 P_{CO} + \sqrt{K_2 P_{H_2}}\right)}$$
4, 6-13 Equation 3-62	$$R_{FT} = \frac{k_4 K_3 K_1 \sqrt{K_2} \frac{P_{CO} P_{H_2}^{1.5}}{P_{H_2O}}}{\left(1 + K_1 P_{CO} + \sqrt{K_2 P_{H_2}} + K_3 K_1 \frac{P_{CO} P_{H_2}}{P_{H_2O}} + \frac{k_4 K_3 K_1}{k_{i,par} K_5 \sqrt{K_2}} \frac{P_{CO} P_{H_2}^{0.5}}{P_{H_2O}} + \frac{k_4 K_3 K_1}{k_{i,par}} \frac{P_{CO} P_{H_2}}{P_{H_2O}}\right)^2}$$
6-13 Equation 3-63	$$R_{FT} = \frac{k_{i,par} K_1 K_2^{1.5} K_3 K_4 K_5 \frac{P_{CO} P_{H_2}^{2.5}}{P_{H_2O}}}{\left(+K_1 P_{CO} + \sqrt{K_2 P_{H_2}} + K_3 K_1 \frac{P_{CO} P_{H_2}}{P_{H_2O}} + K_1 \sqrt{K_2} K_3 K_4 \frac{P_{CO} P_{H_2}^{1.5}}{P_{H_2O}} + K_1 K_2 K_3 K_4 K_5 \frac{P_{CO} P_{H_2}^2}{P_{H_2O}}\right)^2}$$

Table 3-9 Reaction rate expressions derived on the basis of kinetics model FT–VII

RDS/No.	Rate equation
5,7-14 Equation 3-64	$$R_{FT}=\frac{\frac{\sqrt{k_5K_1K_2^{0.5}K_3K_4K_6}}{k_{i,par}^{0.5}}\sqrt{P_{CO}}P_{H_2}^{0.75}}{\left(1+K_1P_{CO}+\sqrt{K_2P_{H_2}}+K_1K_3P_{CO}P_{H_2}+\frac{\sqrt{\frac{k_5K_1K_2^{1.5}K_3K_4}{k_{i,par}K_6}}}{K_2^{0.25}}P_{CO}^{0.5}P_{H_2}^{0.25}+\sqrt{\frac{k_{i,par}K_1K_2^{1.5}K_3K_4K_6}{k_5}}P_{CO}^{0.5}P_{H_2}^{1.25}+\frac{\sqrt{k_5K_1K_2^{0.5}K_3K_4K_6}}{k_{i,par}^{0.5}}\sqrt{P_{CO}}P_{H_2}^{0.75}\right)^2}$$
3, 7-14 Equation 3-65	$$R_{FT}=\frac{k_3K_1P_{CO}P_{H_2}}{\left(1+K_1P_{CO}+\sqrt{K_2P_{H_2}}+\frac{P_{H_2O}}{K_5}\right)}$$
7-14 Equation 3-66	$$R_{FT}=\frac{k_{i,par}K_7K_5K_1K_2^{2.5}K_3K_4K_6\frac{P_{CO}P_{H_2}^{2.5}}{P_{H_2O}}}{\left(1+K_1P_{CO}+\sqrt{K_2P_{H_2}}+\frac{P_{H_2O}}{K_6\sqrt{K_2P_{H_2}}}+K_3K_1\sqrt{K_2}P_{CO}P_{H2}^{0.5}+K_1K_2K_3K_4P_{CO}P_{H_2}+K_5K_1K_2^{1.5}K_3K_4K_6\frac{P_{CO}P_{H_2}^{1.5}}{P_{H_2O}}+K_7K_5K_1K_2^2K_3K_4K_6\frac{P_{CO}P_{H_2}^2}{P_{H_2O}}\right)^2}$$

Table 3-10 Reaction rate expressions derived on the basis of kinetics model FT–VIII

RDS	Rate equation	No.
4,5-12	$$R_{FT}=\frac{K_1K_3k_4P_{CO}P_{H_2}^2}{\left(1+K_1P_{CO}+\sqrt{K_2P_{H_2}}+K_1K_3P_{CO}P_{H_2}\right)}$$	Equation 3-67

3, 5-12	$R_{FT} = \frac{K_1 k_3 P_{CO} P_{H_2}}{\left(1 + K_1 P_{CO} + \sqrt{K_2 P_{H_2}}\right)}$	Equation 3-68
5-12	$R_{FT} = \frac{k_{i,par} K_1 K_3 K_4 \sqrt{K_2} \frac{P_{CO} P_{H_2}^{2.5}}{P_{H_2O}}}{\left(1 + K_1 P_{CO} + \sqrt{K_2 P_{H_2}} + K_1 K_3 P_{CO} P_{H_2} + \frac{K_1 K_3 K_4 P_{CO} P_{H_2}^2}{P_{H_2O}}\right)^2}$	Equation 3-69

3.3.2. Water-Gas-Shift Reaction Rate Mechanism

3.3.2.1. *Kinetics model*

In the present study, the kinetics models were discriminated on the basis of seven sets of WGS elementary reaction steps in which they were considered for a WGS reaction under FT synthesis conditions. These models are WGS-I to WGS-VII. The sequence of elementary reaction pathways are tabulated in Table 3-11. These kinetics models were proposed based on two different mechanisms. The kinetics models from WGS-I to WGS-V were written based on a direct oxidation mechanism (redox mechanism). According to a literature study [123], the CO_2 can be formed either in an adsorbed or desorbed state via direct oxidation of surface CO intermediate as illustrated below:

$$CO - \sigma + O - \sigma \rightleftarrows CO_2 - \sigma + \sigma \quad \text{R. 3-9}$$

$$CO - \sigma + O - \sigma \rightleftarrows CO_2 + 2\sigma \quad \text{R. 3-10}$$

Both paths were considered for the kinetics analysis in the present study. As a consequence, models WGS-II and WGS-III and WGS-V were considered for direct oxidation via the formation of adsorbed CO_2; while another two kinetics models, i.e. WGS-I, WGS-IV, were considered to proceed via CO_2 desorbed state. The oxide ion $(O - \sigma)$ is formed either through the direct hydroxyl intermediate dissociation, viz. R. 3-11 or the direct dissociation of the water molecule in the vicinity of either one or two active sites (R. 3-12 and R. 3-13, respectively).

$$OH - \sigma + \sigma \rightleftarrows H - \sigma + O - \sigma \quad \text{R. 3-11}$$

$$H_2O + 2\sigma \rightleftarrows H_2 - \sigma + O - \sigma \quad \text{R. 3-12}$$

$$H_2O + \sigma \rightleftarrows H_2 + O - \sigma \quad \text{R. 3-13}$$

Apart from direct oxidation, the formate mechanism was also investigated in the development of the WGS reaction under FT synthesis conditions in the present study. Models WGS-VI and WGS-VII are both based on the formate mechanism in which the formate species is formed through the reaction between adsorbed CO intermediate and a hydroxyl surface species $(-OH)$ viz. R. 3-14; that surface hydroxyl intermediate is formed via the decomposition of water by R. 3-15.

$$CO - \sigma + OH - \sigma \rightleftarrows CHO_2 - \sigma + \sigma \quad \text{R. 3-14}$$

$$H_2O + 2\sigma \rightleftarrows H - \sigma + OH - \sigma \quad \text{R. 3-15}$$

From the quantum calculations on transition metals [145], it was concluded that the hydroxyl dissociation in which the adsorbed hydrogen and oxygen are formed has an unfavourably high activation barrier under FT synthesis conditions. There is also evidence that the formate species is more favourable than the direct oxidation mechanism, as in situ, the existence of formate species was confirmed by infrared spectroscopy under an FT reaction condition; however, the conclusion was made on the Fe-based catalyst [146]. In addition, in situ formate species over some transition metals was detected by Fourier transform infrared spectroscopy (FTIR) in the diffuse reflectance mode (DRIFTS) [147]. Corresponding to models WGS-VI and WGS-VII, the kinetics analysis also showed that it is not possible to distinguish whether water reacts as an associative state ($-H_2O$, considering reactions R. 3-16 and R. 3-17), or a dissociative form (R. 3-15), in the surface reaction if the RDS is the dissociation of formate intermediate to CO_2 (R. 3-18); since the outcomes of these two kinetics forms were nearly theoretically identical. This conclusion was also supported by Dry [66].

$$H_2O + \sigma \rightleftarrows H_2O - \sigma \quad \text{R. 3-16}$$

$$H_2O - \sigma + \sigma \rightleftarrows H - \sigma + OH - \sigma \quad \text{R. 3-17}$$

$$CHO_2 - \sigma \rightleftarrows H - \sigma + CO_2 \quad \text{R. 3-18}$$

It was pointed out that different surface chemical reactions and pathways may lead to the same kinetics and rates expression and kinetics studies cannot definitely ‘prove’ a proposed mechanism. Characterization over the catalyst and also quantum chemical calculation [148] are

the ways to discriminate whether water reacts associatively or dissociatively. In addition, microkinetic analysis of every elementary reaction step [149] is necessary. However, these types of works are out of the scope of the present study.

Table 3-11 Elementary reaction steps for WGS reaction

Model	No.	Elementary reaction steps	Model	No.	Elementary reaction steps
WGS-I	1	$CO + \sigma \rightleftarrows CO - \sigma$	WGS-V	1	$CO + \sigma \rightleftarrows CO - \sigma$
	2	$H_2O + 2\sigma \rightleftarrows H - \sigma + OH - \sigma$		2	$H_2O + \sigma \rightleftarrows H_2 + O - \sigma$
	3	$OH - \sigma + \sigma \rightleftarrows H - \sigma + O - \sigma$		3	$CO - \sigma + O - \sigma \rightleftarrows CO_2 - \sigma + \sigma$
	4	$CO - \sigma + O - \sigma \rightleftarrows CO_2 + 2\sigma$		4	$CO_2 - \sigma \rightleftarrows CO_2 + \sigma$
	5	$2H - \sigma \rightleftarrows H_2 + 2\sigma$			
WGS-II	1	$CO + \sigma \rightleftarrows CO - \sigma$	WGS-VI	1	$CO + \sigma \rightleftarrows CO - \sigma$
	2	$H_2O + 2\sigma \rightleftarrows H - \sigma + OH - \sigma$		2	$H_2O + \sigma \rightleftarrows H_2O - \sigma$
	3	$OH - \sigma + \sigma \rightleftarrows H - \sigma + O - \sigma$		3	$CO - \sigma + H_2O - \sigma \rightleftarrows CHO_2 - \sigma + H - \sigma$
	4	$CO - \sigma + O - \sigma \rightleftarrows CO_2 - \sigma + \sigma$		4	$CHO_2 - \sigma \rightleftarrows CO_2 + H - \sigma$
	5	$CO_2 - \sigma \rightleftarrows CO_2 + \sigma$		5	$2H - \sigma \rightleftarrows H_2 + 2\sigma$
	6	$2H - \sigma \rightleftarrows H_2 + 2\sigma$			
WGS-III	1	$CO + \sigma \rightleftarrows CO - \sigma$	WGS-VII	1	$CO + \sigma \rightleftarrows CO - \sigma$
	2	$H_2O + 2\sigma \rightleftarrows H_2 - \sigma + O - \sigma$		2	$H_2O + 2\sigma \rightleftarrows H - \sigma + OH - \sigma$
	3	$CO - \sigma + O - \sigma \rightleftarrows CO_2 - \sigma + \sigma$		3	$CO - \sigma + OH - \sigma \rightleftarrows CHO_2 - \sigma + \sigma$
	4	$CO_2 - \sigma \rightleftarrows CO_2 + \sigma$		4	$CHO_2 - \sigma \rightleftarrows H - \sigma + CO_2$
	5	$H_2 - \sigma \rightleftarrows H_2 + \sigma$		5	$2H - \sigma \rightleftarrows H_2 + 2\sigma$
WGS-IV	1	$CO + \sigma \rightleftarrows CO - \sigma$			
	2	$H_2O + 2\sigma \rightleftarrows H_2 - \sigma + O - \sigma$			

3	$CO - \sigma + O - \sigma \rightleftarrows CO_2 + 2\sigma$
4	$H_2 - \sigma \rightleftarrows H_2 + \sigma$

3.3.2.2. *Derivation of Rate Equation*

As explained, in order to derive the rate expressions, the FT reactions (hydrocarbon formation) and WGS reaction were assumed to proceed on different active sites. One rate-determining step (RDS) was considered in the sequence of the WGS elementary reaction steps; while the remaining elementary reaction steps were assumed to be at quasi-equilibrium. Corresponding to the reaction mechanisms listed in Table 3-11 and reaction rate expression in Table 3-12 to Table 3-18, WGS-II RDS-4 means that the reaction mechanism is WGS-II, and the RDS-4 means that step-4 of the elementary reaction steps is the slowest step (RDS) and other reactions are at quasi-equilibrium condition. From the WGS-II RDS-4, the rate of formation of CO_2 (i.e. rate of WGS reaction) was written as:

$$R_{WGS} = k_{WGS_4}\sigma_{CO}\sigma_O - k_{WGS_{-4}}\sigma_{CO_2}\sigma \qquad \text{Equation 3-70}$$

Considering the elementary reaction steps 1-3 and 5-6 in model WGS-II that proceed at quasi-equilibrium, the net rate of the above-mentioned reactions will be zero. As a result, the intermediate species e.g. σ_{CO}, σ_{OH}, σ_O, σ_{CO_2}, and σ_H were equated from elementary reaction steps 1, 2, 3, 5, and 6, respectively as follows:

$$\sigma_{CO} = K_{W_1} P_{CO}\, \sigma \qquad \text{Equation 3-71}$$

$$\sigma_{OH} = \frac{K_{W_2} P_{H_2O} \sigma^2}{\sigma_H} = \frac{K_{W_2} P_{H_2O} \sigma^2}{\sqrt{\frac{P_{H_2}}{K_{W_6}}} \sigma} = K_{W_2} K_{W_6}^{0.5} \frac{P_{H_2O}}{\sqrt{P_{H_2}}} \sigma$$ Equation 3-72

$$\sigma_O = \frac{K_{W_3} \sigma_{OH} \sigma}{\sigma_H} = \frac{K_{W_3} \left(K_{W_2} K_{W_6}^{0.5} \frac{P_{H_2O}}{\sqrt{P_{H_2}}} \sigma \right) \sigma}{\sqrt{\frac{P_{H_2}}{K_{W_6}}} \sigma} = K_{W_2} K_{W_3} K_{W_6} \frac{P_{H_2O}}{P_{H_2}} \sigma$$ Equation 3-73

$$\sigma_{CO_2} = \frac{P_{CO_2}}{K_{W_5}} \sigma$$ Equation 3-74

$$\sigma_H = \sqrt{\frac{P_{H_2}}{K_{W_6}}} \sigma$$ Equation 3-75

From the Langmuir adsorption theory in a multicomponent system of a single site type, the area coverage fraction of species was written as in the stoichiometric balance of the following form:

$$\sigma + \sigma_{CO} + \sigma_O + \sigma_{OH} + \sigma_{CO_2} + \sigma_H = 1$$ Equation 3-76

Substitution of Equation 3-71-Equation 3-75 into Equation 3-76 gave the final form of σ in terms of partial pressure of different species and the equilibrium constant parameters as follows:

$$\sigma = \frac{1}{\left(1 + K_{W_1}P_{CO} + \sqrt{\frac{P_{H_2}}{K_{W_6}}} + K_{W_2}K_{W_3}K_{W_6}\frac{P_{H_2O}}{P_{H_2}} + K_{W_2}K_{W_6}^{0.5}\frac{P_{H_2O}}{\sqrt{P_{H_2}}} + \frac{P_{CO_2}}{K_{W_5}}\right)} \quad \text{Equation 3-77}$$

Substituting the surface intermediates (Equation 3-71, Equation 3-73 and Equation 3-75) into the early WGS rate expression (Equation 3-70) gave the following equation with respect to the total active site:

$$R_{WGS} = k_{WGS_4}\left(K_{W_1}P_{CO}\sigma\right)\left(K_{W_2}K_{W_3}K_{W_6}\frac{P_{H_2O}}{P_{H_2}}\sigma\right) - k_{WGS_{-4}}\frac{P_{CO_2}}{K_{W_5}}\sigma\sigma \quad \text{Equation 3-78}$$

Therefore the final form of the WGS reaction rate expression (Equation 3-78) for the model WGS-II with RDS-4 was derived by substituting Equation 3-77 into Equation 3-78.

$$R_{WGS} = \frac{\left(k_{WGS_4}K_{W_1}K_{W_2}K_{W_3}K_{W_6}\frac{P_{CO}P_{H_2O}}{P_{H_2}} - k_{WGS_{-4}}\frac{P_{CO_2}}{K_{W_5}}\right)}{\left(1 + K_{W_1}P_{CO} + \sqrt{\frac{P_{H_2}}{K_{W_6}}} + K_{W_2}K_{W_3}K_{W_6}\frac{P_{H_2O}}{P_{H_2}} + K_{W_2}K_{W_6}^{0.5}\frac{P_{H_2O}}{\sqrt{P_{H_2}}} + \frac{P_{CO_2}}{K_{W_5}}\right)^2} \quad \text{Equation 3-79}$$

Table 3-12 Reaction rate expressions derived on the basis of kinetics model WGS-I

RDS	Rate equation	No.
1	$R_{WGS} = \frac{\left(k_{WGS_1}P_{CO} - k_{WGS_{-1}}\frac{1}{K_{W_2}K_{W_3}K_{W_4}K_{W_5}}\frac{P_{CO_2}P_{H_2}}{P_{H_2O}}\right)}{\left(1 + \frac{1}{K_{W_2}K_{W_3}K_{W_4}K_{W_5}}\frac{P_{H_2}P_{CO_2}}{P_{H_2O}} + K_{W_2}K_{W_3}K_{W_5}\frac{P_{H_2O}}{P_{H_2}} + K_{W_2}K_{W_5}^{0.5}\frac{P_{H_2O}}{P_{H2}^{0.5}} + \sqrt{\frac{P_{H_2}}{K_{W_5}}}\right)}$	Equation 3-80

2	$$R_{WGS}=\frac{\left(k_{WGS_2}P_{H_2O}-k_{WGS_{-2}}\frac{1}{K_{W_1}^2K_{W_3}K_{W_4}^2K_{W_5}^{0.5}}\frac{P_{H_2}^{0.5}P_{CO_2}^2}{P_{CO}^2}\right)}{\left(1+K_{W_1}P_{CO}+\sqrt{\frac{P_{H_2}}{K_{W_5}}}+\frac{P_{CO_2}}{K_{W_4}K_{W_1}P_{CO}}+\frac{1}{K_{W_1}K_{W_3}K_{W_4}K_{W_5}^{0.5}}\frac{P_{CO_2}P_{H_2}^{0.5}}{P_{CO}}\right)^2}$$	Equation 3-81
3	$$R_{WGS}=\frac{\left(k_{WGS_3}K_{W_5}K_{W_2}\frac{P_{H_2O}}{P_{H_2}}-k_{WGS_{-3}}\frac{P_{CO_2}P_{H_2}^{0.5}}{K_{W_4}K_{W_1}K_{W_5}^{0.5}P_{CO}}\right)}{\left(1+K_{W_1}P_{CO}+\sqrt{\frac{P_{H_2}}{K_{W_5}}}+\frac{P_{CO_2}}{K_{W_4}K_{W_1}P_{CO}}+K_{W_5}^{0.5}K_{W_2}\frac{P_{H_2O}}{P_{H_2}^{0.5}}\right)^2}$$	Equation 3-82
4	$$R_{WGS}=\frac{\left(k_{WGS_4}K_{W_1}K_{W_2}K_{W_3}K_{W_5}\frac{P_{CO}P_{H_2O}}{P_{H_2}}-k_{WGS_{-4}}P_{CO_2}\right)}{\left(1+K_{W_1}P_{CO}+K_{W_5}K_{W_2}\frac{P_{H_2O}}{P_{H_2}}+K_{W_1}K_{W_2}K_{W_3}K_{W_5}\frac{P_{CO}P_{H_2O}}{P_{H_2}}+\frac{P_{H_2}}{K_{W_5}}\right)}$$	Equation 3-83
5	$$R_{WGS}=\frac{\left(k_{WGS_5}K_{W_1}K_{W_2}K_{W_3}K_{W_4}\frac{P_{CO}P_{H_2O}}{P_{CO_2}}-k_{WGS_{-5}}P_{H_2}\right)}{\left(1+K_{W_1}P_{CO}+\frac{1}{K_{W_1}K_{W_3}K_{W_4}}\frac{P_{CO_2}}{P_{CO}}+K_{W_1}K_{W_2}K_{W_3}K_{W_4}\frac{P_{CO}P_{H_2O}}{P_{CO_2}}+\frac{P_{CO_2}}{K_{W_4}}\right)}$$	Equation 3-84

Table 3-13 Reaction rate expressions derived on the basis of kinetics model WGS-II

RDS	Rate equation	No.
1	$$R_{WGS}=\frac{\left(k_{WGS_1}P_{CO}-k_{WGS_{-1}}\frac{1}{K_{W_2}K_{W_3}K_{W_4}K_{W_5}K_{W_6}}\frac{P_{H_2}P_{CO_2}}{P_{H_2O}}\right)}{\left(1+\frac{1}{K_{W_2}K_{W_3}K_{W_4}K_{W_5}K_{W_6}}\frac{P_{H_2}P_{CO_2}}{P_{H_2O}}+\sqrt{\frac{P_{H_2}}{K_{W_6}}}+\cdots\right.}$$ $$\left.K_{W_3}K_{W_2}K_{W_6}\frac{P_{H_2O}}{P_{H_2}}+K_{W_2}K_{W_6}^{0.5}\frac{P_{H_2O}}{P_{H_2}^{0.5}}+\frac{P_{CO_2}}{K_{W_5}}\right)$$	Equation 3-85

2	$$R_{WGS} = \frac{\left(k_{WGS_2} P_{H_2O} - k_{WGS_{-2}} \frac{1}{K_{W_1} K_{W_3} K_{W_5} K_{W_6}} \frac{P_{CO_2} P_{H_2}}{P_{CO}}\right)}{\left(1 + K_{W_1} P_{CO} + \sqrt{\frac{P_{H_2}}{K_{W_6}}} + \frac{1}{K_{W_1} K_{W_5}} \frac{P_{CO_2}}{P_{CO}} + \frac{1}{K_{W_1} K_{W_3} K_{W_5} K_{W_6}^{0.5}} \frac{P_{CO_2} P_{H_2}^{0.5}}{P_{CO}} + \frac{P_{CO_2}}{K_{W_5}}\right)^2}$$	Equation 3-86
3	$$R_{WGS} = \frac{\left(k_{WGS_3} K_{W_2} K_{W_6}^{0.5} \frac{P_{H_2O}}{\sqrt{P_{H_2}}} - k_{WGS_{-3}} \frac{1}{K_{W_1} K_{W_5} K_{W_6}^{0.5}} \frac{P_{CO_2} P_{H_2}^{0.5}}{P_{CO}}\right)}{\left(1 + K_{W_1} P_{CO} + \sqrt{\frac{P_{H_2}}{K_{W_6}}} + \frac{1}{K_{W_1} K_{W_5}} \frac{P_{CO_2}}{P_{CO}} + K_{W_2} K_{W_6}^{0.5} \frac{P_{H_2O}}{\sqrt{P_{H_2}}} + \frac{P_{CO_2}}{K_{W_5}}\right)^2}$$	Equation 3-87
4	$$R_{WGS} = \frac{\left(k_{WGS_4} K_{W_1} K_{W_2} K_{W_3} K_{W_6} \frac{P_{CO} P_{H_2O}}{P_{H_2}} - k_{WGS_{-4}} \frac{P_{CO_2}}{K_{W_5}}\right)}{\left(1 + K_{W_1} P_{CO} + \sqrt{\frac{P_{H_2}}{K_{W_6}}} + K_{W_2} K_{W_3} K_{W_6} \frac{P_{H_2O}}{P_{H_2}} + K_{W_2} K_{W_6}^{0.5} \frac{P_{H_2O}}{\sqrt{P_{H_2}}} + \frac{P_{CO_2}}{K_{W_5}}\right)^2}$$	Equation 3-88
5	$$R_{WGS} = \frac{\left(k_{WGS_5} K_{W_1} K_{W_2} K_{W_3} K_{W_4} K_{W_6} \frac{P_{CO} P_{H_2O}}{P_{H_2}} - k_{WGS_{-5}} P_{CO_2}\right)}{\left(1 + K_{W_1} P_{CO} + \sqrt{\frac{P_{H_2}}{K_{W_6}}} + K_{W_2} K_{W_3} K_{W_6} \frac{P_{H_2O}}{P_{H_2}} + \cdots\right)\left(K_{W_2} K_{W_6}^{0.5} \frac{P_{H_2O}}{\sqrt{P_{H_2}}} + K_{W_1} K_{W_2} K_{W_3} K_{W_4} K_{W_6} \frac{P_{CO} P_{H_2O}}{P_{H_2}}\right)}$$	Equation 3-89
6	$$R_{WGS} = \frac{\left(k_{WGS_6} K_{W_2} K_{W_1} K_{W_3} K_{W_5} \frac{P_{CO} P_{H_2O}}{P_{CO_2}} - k_{WGS_{-6}} P_{H_2}\right)}{\left(1 + K_{W_1} P_{CO} + \sqrt{K_{W_2} K_{W_1} K_{W_3} K_{W_5}} \sqrt{\frac{P_{CO} P_{H_2O}}{P_{CO_2}}} + \cdots\right)^2 \left(\frac{1}{K_{W_1} K_{W_5}} \frac{P_{CO_2}}{P_{CO}} + \sqrt{\frac{K_{W_2}}{K_{W_1} K_{W_3} K_{W_5}} \frac{P_{CO_2} P_{H_2O}}{P_{CO}}} + \frac{P_{CO_2}}{K_{W_5}}\right)}$$	Equation 3-90

Table 3-14 Reaction rate expressions derived on the basis of kinetics model WGS-III

RDS	Rate equation	No.

1	$R_{WGS}=\frac{\left(k_{WGS_1}P_{CO}-k_{WGS_{-1}}\frac{1}{K_{W_2}K_{W_3}K_{W_4}K_{W_5}}\frac{P_{H2}P_{CO2}}{P_{H2O}}\right)}{\left(1+\frac{1}{K_{W_2}K_{W_3}K_{W_4}K_{W_5}}\frac{P_{H2}P_{CO2}}{P_{H2O}}+K_{W_5}K_{W_2}\frac{P_{H2O}}{P_{H2}}+\frac{P_{CO2}}{K_{W_4}}+\frac{P_{H2}}{K_{W_5}}\right)}$	Equation 3-91
2	$R_{WGS}=\frac{\left(k_{WGS_2}P_{H2O}-k_{WGS_{-2}}\frac{1}{K_{W_1}K_{W_3}K_{W_4}K_{W_5}}\frac{P_{H2}P_{CO2}}{P_{CO}}\right)}{\left(1+K_{W_1}P_{CO}+\frac{1}{K_{W_1}K_{W_3}K_{W_4}}\frac{P_{CO2}}{P_{CO}}+\frac{P_{CO2}}{K_{W_4}}+\frac{P_{H2}}{K_{W_5}}\right)^2}$	Equation 3-92
3	$R_{WGS}=\frac{\left(k_{WGS_3}K_{W_1}K_{W_5}K_{W_2}\frac{P_{CO}P_{H2O}}{P_{H2}}-k_{WGS_{-3}}\frac{P_{CO2}}{K_{W_4}}\right)}{\left(1+K_{W_1}P_{CO}+K_{W_5}K_{W_2}\frac{P_{H2O}}{P_{H2}}+\frac{P_{CO2}}{K_{W_4}}+\frac{P_{H2}}{K_{W_5}}\right)^2}$	Equation 3-93
4	$R_{WGS}=\frac{\left(k_{WGS_4}K_{W_1}K_{W_2}K_{W_3}K_{W_5}\frac{P_{CO}P_{H2O}}{P_{H2}}-k_{WGS_{-4}}P_{CO2}\right)}{\left(1+K_{W_1}P_{CO}+K_{W_5}K_{W_2}\frac{P_{H2O}}{P_{H2}}+K_{W_1}K_{W_2}K_{W_3}K_{W_5}\frac{P_{CO}P_{H2O}}{P_{H2}}+\frac{P_{H2}}{K_{W_5}}\right)}$	Equation 3-94
5	$R_{WGS}=\frac{\left(k_{WGS_5}K_{W_1}K_{W_3}K_{W_4}K_{W_2}\frac{P_{CO}P_{H2O}}{P_{CO2}}-k_{WGS_{-5}}P_{H2}\right)}{\left(1+K_{W_1}P_{CO}+\frac{1}{K_{W_1}K_{W_3}K_{W4}}\frac{P_{CO2}}{P_{CO}}+K_{W_1}K_{W_3}K_{W_4}K_{W_2}\frac{P_{CO}P_{H2O}}{P_{CO2}}+\frac{P_{CO2}}{K_{W_4}}\right)}$	Equation 3-95

Table 3-15 Reaction rate expressions derived on the basis of kinetics model WGS-IV

RDS	Rate equation	No.
1	$R_{WGS}=\frac{\left(k_{WGS_1}P_{CO}-k_{WGS_{-1}}\frac{1}{K_{W_2}K_{W_3}K_{W_4}}\frac{P_{H2}P_{CO2}}{P_{H2O}}\right)}{\left(1+\frac{1}{K_{W_2}K_{W_3}K_{W_4}}\frac{P_{H2}P_{CO2}}{P_{H2O}}+K_{W_2}K_{W_4}\frac{P_{H2O}}{P_{H2}}+\frac{P_{H2}}{K_{W_4}}\right)}$	Equation 3-96
2	$R_{WGS}=\frac{\left(k_{WGS_2}P_{H2O}-k_{WGS_{-2}}\frac{1}{K_{W_3}K_{W_1}K_{W_4}}\frac{P_{CO2}P_{H2}}{P_{CO}}\right)}{\left(1+K_{W_1}P_{CO}+\frac{1}{K_{W_3}K_{W_1}}\frac{P_{CO2}}{P_{CO}}+\frac{P_{H2}}{K_{W_4}}\right)^2}$	Equation 3-97
3	$R_{WGS}=\frac{\left(k_{WGS_3}K_{W_1}K_{W_4}K_{W_2}\frac{P_{CO}P_{H2O}}{P_{H2}}-k_{WGS_{-3}}P_{CO2}\right)}{\left(1+K_{W_1}P_{CO}+\frac{K_{W_4}K_{W_2}P_{H2O}}{P_{H2}}+\frac{P_{H2}}{K_{W_4}}\right)^2}$	Equation 3-98

4	$R_{WGS}=\frac{\left(k_{WGS_4}K_{W_1}K_{W_3}K_{W_4}K_{W_2}\frac{P_{CO}P_{H_2O}}{P_{CO_2}}-k_{WGS_{-4}}P_{H_2}\right)}{\left(1+K_{W_1}P_{CO}+\frac{1}{K_{W_3}K_{W_1}}\frac{P_{CO_2}}{P_{CO}}+\frac{K_{W_1}K_{W_2}K_{W_3}P_{H_2O}P_{CO}}{P_{CO_2}}\right)}$	Equation 3-99

Table 3-16 Reaction rate expressions derived on the basis of kinetics model WGS-V

RDS	Rate equation	No.
1	$R_{WGS}=\frac{\left(k_{WGS_1}P_{CO}-k_{WGS_{-1}}\frac{1}{K_{W_2}K_{W_3}K_{W_4}}\frac{P_{H_2}P_{CO_2}}{P_{H_2O}}\right)}{\left(1+\frac{1}{K_{W_2}K_{W_3}K_{W_4}}\frac{P_{H2}P_{CO2}}{P_{H2O}}+\frac{K_{W_2}P_{H2O}}{P_{H2}}+\frac{P_{CO_2}}{K_{W_4}}\right)}$	Equation 3-100
2	$R_{WGS}=\frac{\left(k_{WGS_2}P_{H2O}-k_{WGS_{-2}}\frac{1}{K_{W_1}K_{W3}K_{W4}}\frac{P_{H2}P_{CO2}}{P_{CO}}\right)}{\left(1+K_{W_1}P_{CO}+\frac{1}{K_{W_1}K_{W3}K_{W4}}\frac{P_{CO2}}{P_{CO}}+\frac{P_{CO2}}{K_{W_4}}\right)}$	Equation 3-101
3	$R_{WGS}=\frac{\left(k_{WGS_3}K_{W_1}K_{W_2}\frac{P_{CO}P_{H2O}}{P_{H2}}-k_{WGS_{-3}}\frac{P_{CO2}}{K_{W_4}}\right)}{\left(1+K_{W_1}P_{CO}+\frac{K_{W_2}P_{H2O}}{P_{H2}}+\frac{P_{CO2}}{K_{W_4}}\right)^2}$	Equation 3-102
4	$R_{WGS}=\frac{\left(k_{WGS_4}K_{W_3}K_{W_1}K_{W_2}\frac{P_{CO}P_{H2O}}{P_{H2}}-k_{WGS_{-4}}P_{CO2}\right)}{\left(1+K_{W_1}P_{CO}+\frac{K_{W_2}P_{H2O}}{P_{H2}}+K_{W_3}K_{W_1}K_{W_2}\frac{P_{CO}P_{H2O}}{P_{H2}}\right)}$	Equation 3-103

Table 3-17 Reaction rate expressions derived on the basis of kinetics model WGS-VI

RDS	Rate equation	No.
1	$R_{WGS}=\frac{\left(k_{WGS_1}P_{CO}-k_{WGS_{-1}}\frac{1}{K_{W_4}K_{W_5}K_{W_3}K_{W_2}}\frac{P_{CO2}P_{H2}}{P_{H2O}}\right)}{\left(1+\frac{1}{K_{W_4}K_{W_5}K_{W_3}K_{W_2}}\frac{P_{CO2}P_{H2}}{P_{H2O}}+\sqrt{\frac{P_{H2}}{K_{W_5}}}+\frac{P_{CO2}\sqrt{P_{H2}}}{K_{W_4}K_{W_5}^{0.5}}+K_{W_2}P_{H2O}\right)}$	Equation 3-104

2	$$R_{WGS} = \frac{\left(k_{WGS_2} P_{H2O} - k_{WGS_{-2}} \frac{1}{K_{W_4} K_{W_5} K_{W_3} K_{W_1}} \frac{P_{CO2} P_{H2}}{P_{CO}}\right)}{\left(1 + K_{W_1} P_{CO} + \sqrt{\frac{P_{H2}}{K_{W_5}}} + \frac{P_{CO2}\sqrt{P_{H2}}}{K_{W_4} K_{W_5}^{0.5}} + \frac{1}{K_{W_4} K_{W_5} K_{W_3} K_{W_1}} \frac{P_{CO2} P_{H2}}{P_{CO}}\right)}$$	Equation 3-105
3	$$R_{WGS} = \frac{\left(k_{WGS_3} K_{W_1} K_{W_2} P_{CO} P_{H2O} - k_{WGS_{-3}} \frac{P_{CO2} P_{H2}}{K_{W_4} K_{W_5}}\right)}{\left(1 + K_{W_1} P_{CO} + \sqrt{\frac{P_{H2}}{K_{W_5}}} + K_{W_2} P_{H2O} + \frac{P_{CO2}\sqrt{P_{H2}}}{K_{W_4} K_{W_5}^{0.5}}\right)^2}$$	Equation 3-106
4	$$R_{WGS} = \frac{\left(k_{WGS_4} K_{W_3} K_{W_1} K_{W_2} K_{W_5}^{0.5} \frac{P_{CO} P_{H2O}}{\sqrt{P_{H2}}} - k_{WGS_{-4}} \frac{P_{CO2}\sqrt{P_{H2}}}{\sqrt{K_{W_5}}}\right)}{\left(1 + K_{W_1} P_{CO} + \sqrt{\frac{P_{H2}}{K_{W_5}}} + K_{W_2} P_{H2O} + K_{W_3} K_{W_1} K_{W_2} K_{W_5}^{0.5} \frac{P_{CO} P_{H2O}}{\sqrt{P_{H2}}}\right)}$$	Equation 3-107
5	$$R_{WGS} = \frac{\left(k_{WGS_5} K_{W_4} K_{W_3} K_{W_1} K_{W_2} \frac{P_{CO} P_{H2O}}{P_{CO_2}} - k_{WGS_{-5}} P_{H_2}\right)}{\left(1 + K_{W_1} P_{CO} + \sqrt{K_{W_4} K_{W_3} K_{W_1} K_{W_2}} \sqrt{\frac{P_{CO} P_{H2O}}{P_{CO_2}}} + \cdots \sqrt{\frac{K_{W_3} K_{W_1} K_{W_2} P_{CO} P_{H2O} P_{CO_2}}{K_{W_4}}} + K_{W_2} P_{H2O}\right)^2}$$	Equation 3-108

Table 3-18 Reaction rate expressions derived on the basis of kinetics model WGS-VII

RDS	Rate equation	No.
1	$$R_{WGS} = \frac{\left(k_{WGS_1} P_{CO} - \frac{k_{WGS_{-1}}}{K_{W_2} K_{W_3} K_{W_4} K_{W_5}} \frac{P_{CO_2} P_{H_2}}{P_{H_2O}}\right)}{\left(1 + \frac{1}{K_{W_2} K_{W_3} K_{W_4} K_{W_5}} \frac{P_{CO_2} P_{H_2}}{P_{H_2O}} + \sqrt{\frac{P_{H_2}}{K_{W_5}}} + \frac{P_{CO_2}\sqrt{P_{H_2}}}{K_{W_4} K_{W_5}^{0.5}} + K_{W_2} P_{H_2O} \sqrt{\frac{P_{H_2}}{K_{W_5}}}\right)}$$	Equation 3-109

2 $$R_{WGS} = \frac{\left(k_{WGS_2} P_{H_2O} - \frac{k_{WGS_{-2}}}{K_{W_1} K_{W_3} K_{W_4} K_{W_5}} \frac{P_{CO_2} P_{H_2}}{P_{CO}}\right)}{\left(1 + K_{W_1} P_{CO} + \sqrt{\frac{P_{H_2}}{K_{W_5}}} + \frac{P_{CO_2}\sqrt{P_{H_2}}}{K_{W_4} K_{W_5}^{0.5}} + \frac{P_{CO_2}\sqrt{P_{H_2}}}{K_{W_1} K_{W_3} K_{W_4} K_{W_5}^{0.5} P_{CO}}\right)^2}$$ Equation 3-110

3 $$R_{WGS} = \frac{\left(k_{WGS_3} K_{W_1} K_{W_2} K_{W_5}^{0.5} \frac{P_{CO} P_{H2O}}{P_{H2}^{0.5}} - k_{WGS_{-3}} \frac{P_{CO2}\sqrt{P_{H2}}}{K_{W_4} K_{W_5}^{0.5}}\right)}{\left(1 + K_{W_1} P_{CO} + \sqrt{\frac{P_{H2}}{K_{W_5}}} + \frac{P_{CO2}\sqrt{P_{H2}}}{K_{W_4} K_{W_5}^{0.5}} + K_{W_2} K_{W_5}^{0.5} \frac{P_{H2O}}{P_{H2}^{0.5}}\right)^2}$$ Equation 3-111

4 $$R_{WGS} = \frac{\left(k_{WGS_4} K_{W_3} K_{W_1} K_{W_2} K_{W_5}^{0.5} \frac{P_{H_2O}\, P_{CO}}{P_{H_2}^{0.5}} - k_{WGS_{-4}} P_{CO_2} \sqrt{\frac{P_{H_2}}{K_{W_5}}}\right)}{\left(1 + K_{W_1} P_{CO} + \sqrt{\frac{P_{H_2}}{K_{W_5}}} + K_{W_3} K_{W_1} K_{W_2} K_{W_5}^{0.5} \frac{P_{H_2O}\, P_{CO}}{P_{H_2}^{0.5}} + K_{W_2} K_{W_5}^{0.5} \frac{P_{H_2O}}{P_{H_2}^{0.5}}\right)}$$ Equation 3-112

5 $$R_{WGS} = \frac{\left(k_{WGS_5} K_{W_1} K_{W_2} K_{W_3} K_{W_4} \frac{P_{CO} P_{H_2O}}{P_{CO_2}} - k_{WGS_{-5}} P_{H_2}\right)}{\left(1 + K_{W_1} P_{CO} + \sqrt{K_{W_1} K_{W_2} K_{W_3} K_{W_4} \frac{P_{CO} P_{H_2O}}{P_{CO_2}}} + \sqrt{\frac{K_{W_2} P_{H_2O} P_{CO_2}}{K_{W_1} K_{W_3} K_{W_4} P_{CO}}} + \sqrt{\frac{K_{W_1} K_{W_2} K_{W_3}}{K_{W_4}} P_{CO_2} P_{CO} P_{H_2O}}\right)^2}$$ Equation 3-113

All the above-mentioned WGS rate expressions developed from the proposed kinetics models were initially coupled with the FT synthesis rate expressions developed in section 3.3.1 and then they were each evaluated against the experimental data at a variety of operating conditions. The results and discussion obtained from the overall kinetics models are explained in section 5.2. The full mathematical procedure in developing of each rate expression for WGS reaction models is given in Appendix (Table A. 33 to Table A. 46).

3.3.2.3. *Formulation (equating) of the Reverse Rate Constant*

The rate constant for the reverse reaction ($k_{WGS_{-1}}$) in the above rate equation can be represented by the equilibrium constant, K_p, of the WGS reaction. Generally, K_p in the WGS reaction can be expressed by the equilibrium partial pressure of CO, H_2, CO_2 and H_2O species as follows:

$$K_p = \frac{P_{CO_2} P_{H_2}}{P_{CO} P_{H_2O}} \qquad \text{Equation 3-114}$$

The partial pressures of CO, H_2, CO_2 and H_2O were obtained by rearranging Equation 3-71, Equation 3-75, Equation 3-74 and Equation 3-71 respectively. This gave the following expression for K_p:

$$K_p = \frac{\left(\frac{\sigma_{CO_2} K_{W_5}}{\sigma}\right)\left(\frac{\sigma_{H_2} K_{W_6}}{\sigma}\right)}{\left(\frac{\sigma_{CO}}{K_{W_1}\sigma}\right)\left(\frac{\sigma_O \sigma_{H_2}}{K_{W_2}\sigma^2}\right)} \qquad \text{Equation 3-115}$$

In Equation 3-115, the term $(\frac{\sigma_{CO_2}\sigma}{\sigma_{CO}\sigma_O})$ should be also defined with respect to equilibrium constants. Considering elementary step 4 and assuming that step 3 reached the equilibrium state, one can obtain:

$$\frac{\sigma_{CO_2}\sigma}{\sigma_{CO}\sigma_O} = K_{W_3} K_{W_4} \qquad \text{Equation 3-116}$$

The K_p term was eventually expressed by substituting Equation 3-116 into Equation 3-115 in the following form:

$$K_p = K_{W_1} K_{W_2} K_{W_3} K_{W_4} K_{W_5} K_{w_6}$$ Equation 3-117

According to the above-mentioned details of the chemical reaction equilibrium and since the equilibrium constant is the ratio of the rate constant for the forward reaction to the rate constant for the reverse reaction, therefore the term $k_{WG\psi_{-1}}$ was obtained as follows:

$$k_{WGS_{-1}} = K_{W_2} K_{W_3} K_{W_4} K_{W_5} K_{w_6} k_{WGS_1} / K_p$$ Equation 3-118

3.3.2.4. *Development of the WGS Reaction Equilibrium Constant (temperature dependence correlation)*

Generally the value of equilibrium constant K_P depends on the value of the standard free energy change of reaction, which is the free energy of formation difference between the products and the reactants, with both in their standard states (1 atm and the temperature of the system). Thus the equilibrium constant is a function of temperature and its dependency on temperature is given by Equation 3-119 [144].

$$lnK_p = -\frac{\Delta G_R^\circ}{R_g T}$$ Equation 3-119

The value of ΔG_R° was computed from the available literature standard free energy of formation data at a temperature of 298.15 *K*. These values were substituted into Equation 3-120 to compute the standard free energy of formation at 298.15 *K*, so that the K_P value at the reference temperature (298.15 *K*) was computed from Equation 3-119.

$$\Delta G^{\circ}_{R,298.15} = \frac{1}{\alpha_k}\left(\sum_{i}^{Products} \alpha_i \, \Delta G^{\circ}_{f,298.15} - \sum_{i}^{Reactants} \alpha_i \, \Delta G^{\circ}_{f,298.15} \right) \quad \text{Equation 3-120}$$

Here, α_i and α_k stand for a stoichiometric coefficient of 'i' and 'k' species, respectively. In addition, the K_P value at other temperatures can be calculated from the classic van't Hoff equation via Equation 3-121. By integrating this equation, one can compute for equilibrium constant K_P, at any temperature (Equation 3-122).

$$\frac{lnK_P}{dT} = -\frac{\Delta H^{\circ}_R}{R_g T^2} \quad \text{Equation 3-121}$$

$$ln\left(\frac{K_P}{K}\right) = -\frac{\Delta H^{\circ}_R}{R_g}\left(\frac{1}{T} - \frac{1}{T_r}\right) \quad \text{Equation 3-122}$$

The enthalpy changes that accompany the temperature changes were calculated by the heat capacities of the respective mixtures. The heat of reaction at temperature *T* was the sum of enthalpy changes for: i) the temperature of the reactants from *T* to 298.15 *K*. ii) carrying out the reaction at 298.15 *K*. and iii) the temperature of the products to the (same) temperature *T*. The heat of reaction can therefore be computed from Equation 3-123 and normalized to species *k*, to Equation 3-124.

$$\Delta H^{\circ}_{R,T} = \frac{1}{\alpha_k}\left[\sum_{i}^{Reactants} \int_{T}^{298.15} \alpha_i C_P dT \right] + \Delta H^{\circ}_{R,298.15} + \frac{1}{\alpha_k}\left[\sum_{i}^{Products} \int_{298.15}^{T} \alpha_i C_P dT \right] \quad \text{Equation 3-123}$$

$$\Delta H^{\circ}_{R,T} = \Delta H^{\circ}_{R,298.15} + \frac{1}{\alpha_k}\left[\int_{298.15}^{T}\left(\sum_{i}^{Products} \alpha_i C_P - \sum_{i}^{Reactants} \alpha_i C_P\right) dT\right] \quad \text{Equation 3-124}$$

The difference in heat capacity between products and reactants was determined from Equation 3-125. The polynomial temperature dependency of the heat capacity and the coefficients' changes (i.e. Δa, Δb, Δc and Δd) are determined by Equation 3-126 and Equation 3-127 to Equation 3-130, respectively.

$$\Delta C_P = \left(\sum_{i}^{Products} \alpha_i C_P - \sum_{i}^{Reactants} \alpha_i C_P\right) \quad \text{Equation 3-125}$$

$$\Delta C_P = \Delta a + \Delta b + \Delta c + \Delta d \quad \text{Equation 3-126}$$

$$\Delta a = \left(\sum_{i}^{Products} \alpha_i a_i - \sum_{i}^{Reactants} \alpha_i a_i\right) \quad \text{Equation 3-127}$$

$$\Delta b = \left(\sum_{i}^{Products} \alpha_i b_i - \sum_{i}^{Reactants} \alpha_i b_i\right) \quad \text{Equation 3-128}$$

$$\Delta c = \left(\sum_{i}^{Products} \alpha_i c_i - \sum_{i}^{Reactants} \alpha_i c_i\right) \quad \text{Equation 3-129}$$

$$\Delta d = \left(\sum_{i}^{Products} \alpha_i d_i - \sum_{i}^{Reactants} \alpha_i d_i\right) \quad \text{Equation 3-130}$$

The coefficients were obtained from the literature [144] and they are tabulated in Table 3-19.

Table 3-19 Enthalpy and free energy of formation at 298.15 K and constant coefficients of heat capacity polynomial, Cp in unit J mol^{-1} K^{-1} [144]

Species	Molar mass	ΔH_f°	ΔG_f°	a	b	c	d
CO	28.01	-110.6	-137.4	28.11	$0.1672 \cdot 10^{-2}$	$0.5363 \cdot 10^{-5}$	$-2.218 \cdot 10^{-9}$
H_2O	18.02	-242.0	-228.7	32.19	$0.1920 \cdot 10^{-2}$	$1.054 \cdot 10^{-5}$	$-3.589 \cdot 10^{-9}$
CO_2	44.01	-393.8	-394.6	22.22	$5.9711 \cdot 10^{-2}$	$-3.495 \cdot 10^{-5}$	$7.457 \cdot 10^{-9}$
H_2	2.02	0	0	29.06	$-0.1913 \cdot 10^{-2}$	$-0.8690 \cdot 10^{-5}$	$-0.8690 \cdot 10^{-9}$

From the above computation, an expression was derived for the equilibrium constant as a function of temperature (Equation 3-131). This equation was used in the present study to calculate the WGS equilibrium constant at different experimental temperature conditions.

$$ln(K_P) = -3.72 + \frac{4861.49}{T} - 6.90 \cdot 10^{-3} \cdot T + 1.33 \cdot 10^{-5} \cdot T^2 - 8.38 \cdot 10^{-9} \cdot T^3 + 1.25 \cdot 10^{-12} \cdot T^4 \quad \text{Equation 3-131}$$

3.4. Summary

In this chapter, two different approaches were used to develop a model for the FT synthesis reaction network. The first was based on an empirical approach; whereas the second approach explained the novel mechanistic details of FT kinetics. In the former, the rate

equations were derived by power-law rate expressions, while in the latter the rate equations were derived by the Langmuir–Hinshelwood-Hougen-Watson (LHHW) rate theory. The limitations of power-law rate model were highlighted for the applications that wider range of operating conditions has to be selected. In contrast the advantages of LHHW for predicting a wider range of operating conditions were underlined. A comprehensive plausible mechanism-derived FT kinetics models with eight novel elementary reaction pathways along with seven novel WGS kinetics models were developed. Such reaction networks were investigated to fit and validate against the newly obtained experimental results which can be used as a key tool to emphasise the most significant facts of FT synthesis catalysis and chemistry.

CHAPTER 4

MATHEMATICAL MODELLING

4.1. Introduction

In addition to experimental studies, numerical analysis and mathematical modelling can be used as an effective tool to provide knowledge about a catalytic reaction. Experimental studies are typically very expensive; whereas theoretical modelling studies require only a suitable model formulation and adequate physicochemical data. The information such as temperature, reactant composition and products' distributions obtained from the modelling is significantly helpful in reactor design, scale-up, the understanding of its behaviour in operation and predicting the effect of changing operating conditions. Modelling studies have been considered in many pieces of research to assist in the development of the FT synthesis processes. In this chapter, the procedures in developing the mathematical model of a fixed bed FT synthesis reactor that is used in the evaluation of the kinetic parameters, parametric studies and optimization of the reactor operations, are discussed in detail. In addition, the general selection criteria and the governing equations used in the modelling of a fixed bed reactor are

explained. In principle, a model should be tailored for its main purpose. It should be as simple as possible, but still include a sufficient representation of the essential mechanisms involved. Hence, several assumptions were taken into account in order to facilitate the computational procedure and the model equations; such as species balance, continuity equation and pressure drop. An algorithm was developed to solve the system of equations which includes the mathematical description of the reactor model, reaction kinetics, and steps towards estimating kinetic parameters.

4.2. Principles in the Modelling of a Catalytic Reactor

In general, procedures for obtaining the kinetics parameters involved several steps; such as (*i*) selection and construction of experimental equipment; (*ii*) planning of experiments; (*iii*) conducting them; (*iv*) checking the consistency of the experimental data; (*v*) developing kinetics models; (*vi*) developing a mathematical model of a catalytic reactor by derivation of governing conservation equations; and (*vii*) evaluation of the kinetics parameters. The latter tasks can be carried out by classical methods, which are mostly on the basis of graphical procedures; or by modern approaches, which rely on statistical methods as will be explained in section 4.8.2. The evaluation of kinetics parameters based on statistical methods necessitates the implementation of a particular kinetics model on a computer and subsequent parameter estimation; then, the physical and statistical consistency of the kinetics parameters has be to evaluated. If the values of the parameters are for some reason unacceptable, then the estimation of the parameters should be repeated, sometimes with additional experiments or by reducing the number of system parameters by simplifying the reactor model and/or kinetics model. Corresponding to

the procedures mentioned above, one can say that the following steps are the next sequences for the whole theoretical investigation of the model: (*viii*) validation of the mathematical model using the evaluated kinetics parameters in the latter task; (*ix*) parametric studies of effective independent variables to investigate the performance of the fixed bed FT synthesis reactor over a Co/SiO_2 catalyst for conversion and selectivities; (*x*) numerical optimization of the operating conditions to maximize the FT synthesis conversion, selectivities and productions of favourable compositions. A block diagram of the complete process is illustrated in Figure 4-1.

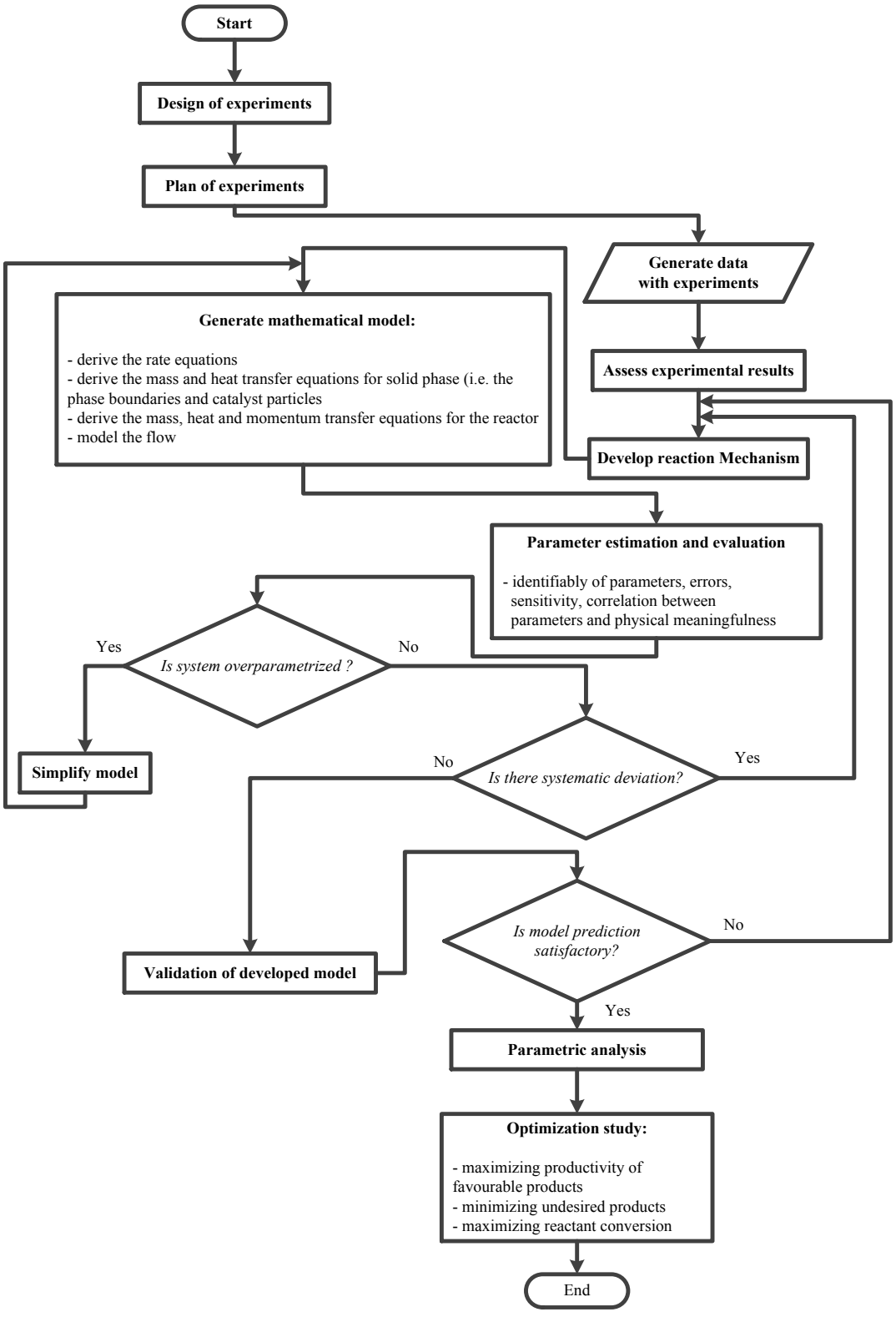

Figure 4-1 The whole process involved in the development of kinetics modelling of the FT synthesis process.

4.3. Governing Equations in a Fixed Bed Reactor

In a one-dimensional model (also known as a plug flow model), fluid properties (e.g. temperature, concentration and velocity) are assumed to be uniform over the tube cross-section. Hence, the gradients of these properties (i.e. the resistance to heat and mass transfer) in the radial and angular directions are neglected; the properties are varied only in the axial direction (e.g. along the reactor bed length).

Focusing on the phenomena occurring in the reactor reduces the apparent diversity into a small number of models or basic reactor types. The phenomena taking place in the reactor can be broken down into transfer of mass, heat and momentum as well as chemical reactions. The chemical reaction and kinetics of FT synthesis were comprehensively studied in Chapter 3. The design and modelling of the reactor is on the basis of equations that describe the above-mentioned phenomena i.e. the continuity, energy and momentum equations, as well as the reaction rate equation. The first step towards the calculation of the conversion of reactant components or formation of products (e.g. '*A'*) in the reactor involves the law of mass conservation on a volume portion of the reactor that is fixed in space. Equation 4-1 is principally the continuity equation for species '*A'*.

$$\begin{bmatrix} amount\ of\ A \\ introduced\ into \\ the\ system\ per\ unit\ time \end{bmatrix} - \begin{bmatrix} amount\ of\ A \\ leaving\ the\ system \\ per\ unit\ time \end{bmatrix}$$

$$- \begin{bmatrix} amount\ of\ A \\ Disappeared\ (or\ formed)\ from \\ the\ system\ per\ unit\ time \end{bmatrix} = \begin{bmatrix} amount\ of\ A \\ accumulated\ in \\ the\ system\ per\ unit\ time \end{bmatrix}$$

Equation 4-1

The mechanisms by which '*A*' can enter or leave the volume element are flow and/or molecular diffusion (where the concentration is not uniform in the reactor). The motion of a fluid, even through empty pipes, is not really ordered and is difficult to describe. Even if the true detailed flow pattern were known, the continuity equation would be so complicated that its integration would be extremely complex and tedious, if not impossible. The crossing of different streamlines and mixing of fluid elements with different characteristics that result from this crossing, are difficult points in the design of chemical reactors. It is therefore natural to consider two extreme conceptual cases: first, where there is no mixing of the streamlines; and second, where the mixing is complete. These two extremes can be formulated with sufficient approximation by the plug flow reactor and the continuous flow stirred tank with complete mixing; however, the latter case is not in the scope of the present study.

As pointed out, in a plug flow reactor all fluid elements move with equal velocity along parallel streamlines. The plug flow is the only mechanism for mass transport and there is no mixing between fluid elements. The reaction, therefore, leads to a concentration gradient in the axial flow direction. For steady-state conditions, for which the last term in Equation 4-1 is zero, the continuity equation is a first-order ordinary differential equation (ODE) with the axial coordinate as variable. For non-steady-state conditions (transient condition), the continuity equation is a partial differential equation (PDE) with the axial coordinate and time as variables. Narrow and long tubular reactors closely satisfy the conditions for plug flow when the viscosity of the fluid is low [34].

In an energy balance over a volume element of a chemical reactor, kinetics, potential, and work terms may usually be neglected relative to the heat of reaction and other heat transfer terms, so that the balance reduces to the following expression:

$$\begin{bmatrix} amount\ of\ heat \\ entered\ into \\ system\ per\ unit\ time \end{bmatrix} - \begin{bmatrix} amount\ of\ heat \\ removed\ from\ system \\ per\ unit\ time \end{bmatrix} - \begin{bmatrix} amount\ of\ heat \\ generated\ from\ catalytic \\ exothermic\ reaction \\ per\ unit\ time \end{bmatrix}$$

$$= \begin{bmatrix} amount\ of\ heat \\ accumulated\ in \\ system\ per\ unit\ time \end{bmatrix}$$

Equation 4-2

The mathematical expression for Equation 4-2 is the energy equation and its integrated form is the heat balance (see Equation 4-10). The form of these equations results from considerations closely related to those for the different types of continuity equations. When the mixing is so intense that the concentration is uniform over the reactor, it is possible to consider that the temperature is also uniform. When plug flow is postulated, it is natural to accept that heat is also only transferred by that mechanism. When molecular diffusion is neglected, the same is typically assumed for heat conduction. When the concentration in a section perpendicular to the flow is assumed to be uniform, then it is usual to consider the temperature to be uniform in this section as well. It follows that when heat is exchanged with the surroundings, the temperature gradient has to be situated entirely in a thin "film" along the wall. This also implies that the resistance to heat transfer in the central core is zero in a direction perpendicular to the flow.

In addition, the momentum balance can be obtained by application of Newton's second law on a moving fluid element. Over a volume element of a chemical reactor, the balance of momentum in direction *i* can be written as:

$$\begin{bmatrix} amount\ of\ momentum\ in\ direction\ 'i' \\ entered\ into \\ system\ per\ unit\ time \end{bmatrix} - \begin{bmatrix} amount\ of\ momentum\ in\ direction\ 'i' \\ removed\ from\ system \\ per\ unit\ time \end{bmatrix}$$

$$- \begin{bmatrix} amount\ of\ momentum\ in\ direction \\ 'i'\ generated\ from\ pressure\ and \\ shear\ stress\ forces\ per\ unit\ time \end{bmatrix} = \begin{bmatrix} amount\ of\ momentum\ in \\ direction\ 'i'\ accumulated \\ in\ system\ per\ unit\ time \end{bmatrix}$$

Equation 4-3

4.3.1. The Species Continuity Equations

The derivation of differential mass balances or continuity equations for the components of an element of fluid flowing in a reactor is considered in detail in texts on transport processes, for example, by Bird *et al.* [150]. These authors showed that a fairly general form of the continuity equation for a chemical species *'i'* reacting in a flowing fluid with varying density, temperature, and composition is:

$$\frac{\partial C_i}{\partial t} + \nabla \cdot (C_i u) + \nabla \cdot J_i = R_i$$

Equation 4-4

If species *'i'* occurs in more than one phase, such a continuity equation has to be written for each phase. These equations are linked by the boundary conditions and generally also by a term expressing the transfer of *'i'* between the phases. Such a term is not included by (Equation 4-4), since the following discussion is focussed on the various forms that the continuity equations can take in single-phase, or in pseudo-homogeneous reactors, as a consequence of the flow pattern. The terms and symbols used in this equation have the following meaning: C_i is the molar concentration of species *'i'* (mol/m³ fluid); so that $\partial C_i/\partial t$ is the non-steady-state term expressing accumulation or depletion. In a cylindrical coordinate system, r, z, θ with unit

vectors δr, δz, and $\delta\theta$; the gradient of a scalar function f is represented by ∇f and the divergence of a vector function v by $\nabla \cdot v$; more explicitly:

$$\nabla f = \frac{1}{r}\frac{\partial f}{\partial r}\delta r + \frac{1}{r}\frac{\partial f}{\partial \theta}\delta\theta + \frac{\partial f}{\partial z}\delta z \qquad \text{Equation 4-5}$$

$$\nabla \cdot v = \frac{\partial v_r}{\partial r} + \frac{1}{r}\frac{\partial v_\theta}{\partial \theta} + \frac{\partial v_z}{\partial z} \qquad \text{Equation 4-6}$$

In Equation 4-4, u is the three-dimensional mass-average velocity vector in ($m\ s^{-1}$) and defined by Equation 4-7, where ρ_f is the density of the mixture; and u_i represents the velocity of molecules of species *'i'*.

$$u = \sum_{i=1}^{N} \frac{M_i C_i}{\rho_f} u_i \qquad \text{Equation 4-7}$$

The term $\nabla \cdot (C_i u)$ in Equation 4-4 above therefore accounts for the transport of mass by convective flow. The J_i term is the molar flux vector for species *'i'* with respect to the mass average velocity (mol/m² s). When the flow is laminar or perfectly ordered, the term $\nabla \cdot J_i$ results from molecular diffusion only. It can be written more explicitly as an extension of Fick's law for diffusion in binary systems, as in Equation 4-8 below, where D_{im} is the effective binary diffusivity for the diffusion of *'i'* in the multicomponent mixture [34].

$$J_i = -\rho_f D_{im} \nabla\left(\frac{C_i}{\rho_f}\right) \qquad \text{Equation 4-8}$$

Multicomponent diffusion laws were also used for ideal gases; as in the Stefan-Maxwell equation. In (Equation 4-5) the driving force was taken as moles of *'i'* per total mass of fluid [150]. The term $\nabla \cdot J_i$ can also stand for the flux resulting from deviations of perfectly ordered

flow, as encountered with turbulent flow or with flow through a bed of solid particles. The term R_i is the total rate of change of amount of *'i'* because of reaction; that is, $\sum_{j=1}^{NR} \alpha_{ij} R_i$ for multiple reactions. The α_{ij} are negative for reactants and positive for reaction products. The units of R_i depend on the nature of the reaction. For a reaction catalysed by a solid, preference would be given to ($mol\ kg_{cat}^{-1}\ s^{-1}$), multiplied by the catalyst bulk density (ρ_b^{cat}) in the reactor. From the definitions given it is clear that $\sum_i M_i J_i = \sum_i M_i C_i (u_i - u) = 0$, while $\sum_i M_i R_i = 0$, due to the conservation of mass in a reacting system. If each term of (Equation 4-4) is multiplied by the molecular weight M_i and the equation is then summed over the total number of species *N*, accounting for the relation $\rho_f = \sum_i M_i C_i$, the total continuity equation is obtained:

$$\frac{\partial \rho_f}{\partial t} + \nabla \cdot (\rho_f u) = 0 \qquad \text{Equation 4-9}$$

Generally, when the reactor contains a solid catalyst, the flow pattern is strongly determined by the presence of the solid, and the flux of *'i'* resulting from the mixing effect is expressed in the form of Fick's law.

4.3.2. The Energy Equation

Moreover, the derivation of energy equation of an element of fluid flowing in a reactor is considered in detail in [150]. Equation 4-10 is the energy balance equation that contains the phenomena that are of importance in a fixed bed reactor; where C_{pi} is the specific heat of species *'i'* ($kJ\ kg^{-1}\ K^{-1}$); λ is the thermal conductivity of the mixture ($kJ\ m^{-1}\ s^{-1}\ K^{-1}$); and the H_i *is* partial molar enthalpy ($kJ\ kmol^{-1}$). The respective terms arise from: (*i*) change of heat content with time; (*ii*) convective flow; (*iii*) heat effect of the chemical reactions; (*iv*) heat transport by conduction; (*v*) energy flux by molecular diffusion; and (*vi*) radiation heat flux.

$$\sum_i M_i C_i C_{pi} \left(\frac{\partial T}{\partial t} + u \cdot \nabla T\right) = \sum_i (-\Delta H_i) r_i + \nabla \cdot (\lambda \nabla T) - \sum_i J_i \nabla H_i + Q_{rad} \qquad \text{Equation 4-10}$$

(*i*) (*ii*) (*iii*) (*iv*) (*v*) (*vi*)

Heat radiation in the reactor is often neglected, except in the case of fixed bed catalytic reactors operating at high temperatures, but then it is generally lumped with the heat conduction and a few more heat transport mechanisms into an "effective" heat conduction, having the form of term (*iv*) in (Equation 4-10). When this is done in (Equation 4-10) and the diffusion term (*v*) is neglected, the result is Equation 4-11, where λ_e is an effective thermal conductivity. When there is more than one phase, more than one energy equation has to be written and a transfer term has to be introduced.

$$\sum_i M_i C_i C_{pi} \left(\frac{\partial T}{\partial t} + u \cdot \nabla T\right) = \sum_i (-\Delta H_i) r_i + \lambda_{ez} \left(\frac{\partial^2 T}{\partial z^2}\right) + \lambda_{er} \left(\frac{1}{r}\frac{\partial T}{\partial r} + \frac{\partial^2 T}{\partial r^2}\right) + \lambda_{e\theta} \left(\frac{1}{r^2}\frac{\partial^2 T}{\partial \theta^2}\right) \qquad \text{Equation 4-11}$$

4.3.3. The Momentum Equation

The balance of momentum in directions z_i (i = 1, 2, 3) is described by the Navier-Stokes equations in Equation 4-12, with μ the molecular viscosity in ($Pa\ s$) and uu, s, I, and ∇u second-order tensors; I is the unit tensor and superscript T indicates transpose of ∇u. In (7.3.3-1), the respective terms result from: (1) change of momentum with time; (2) convection; (3) the pressure gradient; (4) the shear stress; and (5) gravity.

$$\frac{\partial}{\partial t}(\rho_f u) + \nabla \cdot (\rho_f uu) + \nabla P + \nabla \cdot s - \rho_f g = 0 \quad \text{Equation 4-12}$$

$$s = -\left(-\frac{2}{3}\mu(\nabla \cdot u)I + \mu\left((\nabla u) + (\nabla u)^T\right)\right) \quad \text{Equation 4-13}$$

The pressure field, required for the solution of Equation 4-12, can be determined from the total continuity equation (Equation 4-9) and a relation between pressure, density, temperature and composition; for example the ideal gas law for gas flows. Appropriate boundary conditions have to be used. At walls, the no-slip condition is applied, that is, a zero velocity is imposed. At inlets, a given velocity or velocity profile can be imposed. The solutions of Equation 4-12 and Equation 4-13 are not straightforward. Therefore, a given type of velocity field can be applied and the corresponding pressure field is calculated from a specific pressure drop equation as will be explained in section 4.5.

4.4. Model Assumptions

The FT synthesis process was carried out in a stainless steel mini-scale fixed bed reactor with an inner diameter of 15.7 mm and a reactor length of 52.83 cm. A mathematical model of the reactor was developed based on the following assumptions. A series of eggshell cobalt catalysts supported with silica powder were used. The detail of the catalyst and support materials will be discussed in section 5.1.1. The utilization of the eggshell catalyst in a mini-scale fixed bed reactor is an advanced technique, which can overcome the mass transfer limitation due to diffusion limitations in catalyst pellets in the fixed bed reactor system [1, 151]. In the present work, the catalyst was loaded in the reactor in powder form (2 g catalyst with particle size of 75-150 μm) in order to prevent internal mass transfer limitations. The above

assumption was also taken into account by other investigators utilizing a catalyst in the form of powder to prevent the internal mass transfer limitations [152]. Based on the above justifications, the effects of the internal and external mass transfer resistances (interphase and intraparticle mass transport) were neglected; hence only the rate of surface reaction in the reactor was the controller.

In order to describe the kinetics of the experimental conditions the reactor model was assumed to be a plug-flow pseudo-homogeneous state. Therefore, transportation in the catalyst's pores (transport phenomena in solid phase) was not considered, to avoid the unsolvable difficulties in the integration of the reactor model embedded in a parameter optimization procedure [133].

Also, in order to improve the temperature distribution along the catalytic beds, minimize the formation of heat spots and prevent the temperature gradients caused by the strongly exothermic FT synthesis reaction, 2 g of the pre-calcined catalyst was weighted for each experiment and then diluted with 12 g of inert silicon carbide (mesh particle size 200-450). The dilution of the catalyst avoids local hot-spots [1]. Dilution of a solid catalyst (in powder form) with inert diluent (i.e. silicon carbide) is a common practice in the laboratory scale FT synthesis process to have better heat removal as well as an effective use of a catalyst bed [153]. In addition, to provide a uniform wall temperature along the reactor bed length, a metal jacket was installed between the furnace and the fixed bed reactor and it surrounded the reactor. A steady-state condition was assumed so that there was no change over time including catalytic activity, selectivity and stability. Based on the above assumptions, a one-dimensional steady-state pseudo-homogeneous mathematical model was developed to describe the hydrodynamic of the

fixed bed reactor for FT synthesis. The reactor model equations will be presented in the following section.

4.5. Model Equations

Equations 4-14 and 4-15 describe the conservation equations of i^{th} species with respect to concentration and partial pressure, respectively. The mole balance equations were first order ordinary differential equations (ODEs). For homogeneous system $\alpha^* = 1$, whereas for heterogeneous catalytic reactions α^* equals to the bulk density of the catalyst (ρ_B) which is determined by the ratio of mass of the catalyst (m_{cat}) over the packed bed reactor volume (V_l). Gas velocity was calculated from the continuity equation (Equation 4-16).

$$u_s \frac{\partial C_i}{\partial z} = \alpha^* \beta \sum_{j=1}^{NR} v_{ij} R_j - C_i \frac{\partial u_s}{\partial z} \quad \text{Equation 4-14}$$

$$\frac{u_s}{R_g T} \frac{\partial p_i}{\partial z} = \alpha^* \beta \sum_{j=1}^{NR} v_{ij} R_j - \left(\frac{P_T}{R_g T} \frac{\partial u_s}{\partial z} \right) \quad \text{Equation 4-15}$$

$$\rho_f \frac{\partial u_s}{\partial z} = -u_s \frac{\partial \rho_f}{\partial z} \quad \text{Equation 4-16}$$

Density of the fluid mixtures was computed by applying the chain rule to the ideal gas law (Equation 4-17). In this equation, the average molar weight of the fluid mixture was simply determined by the molar mass of each species and its mole fraction in the mixture (Equation 4-18).

$$\frac{\partial \rho_f}{\partial z} = \frac{\partial \left(\frac{P_T M_m}{R_g T}\right)}{\partial z} = \frac{M_m}{R_g}\frac{1}{T}\frac{\partial P_T}{\partial z} - \frac{M_m P_T}{T^2 R_g}\frac{\partial T}{\partial z} \quad \text{Equation 4-17}$$

$$M_m = \sum_{i=1}^{NS} Y_i M_i \quad \text{Equation 4-18}$$

The classic Ergun equation is the most popular equation used to calculate overall pressure drop through catalytic packed bed reactors. Equation 3-23is the general form of this equation. The first term on the right side of this equation corresponds to the Blake-Kozeny equation for laminar flow, while the second term corresponds to the Bruke-Plummer equation for turbulent flow. The Hagen-Poiseuille equation, expressing the pressure drop for laminar flow in an empty conduit, when written in the form of (Equation 4-24), leads to a friction factor in the form of Equation 4-19.

$$f = \frac{(1-\varepsilon)^2}{\varepsilon^3}\frac{36}{G d_p/\mu_m} \quad \text{Equation 4-19}$$

Since the channels in a packed bed are not straight, a correlation factor of 25/6 had to be introduced by Ergun to fit the experimental data, so that (Equation 4-19) becomes:

$$f = \frac{(1-\varepsilon)^2}{\varepsilon^3}\frac{150}{G d_p/\mu_m} \quad \text{Equation 4-20}$$

The Burke and Plummer equation for highly turbulent flow in a channel, written in the form of (11.5.1-3), leads to a friction factor:

$$f = 1.75\frac{1-\varepsilon}{\varepsilon^3} \quad \text{Equation 4-21}$$

Adding both contributions Ergun proposed,

$$f = \frac{1-\varepsilon}{\varepsilon^3}\left[a + \frac{b(1-\varepsilon)}{Re}\right] \quad \text{Equation 4-22}$$

With a=1.75 and b=150. Handley and Heggs [1968] derived a value of 1.24 for *a* and 368 for *b*. McDonald *et al.* [1979] proposed *a* = 1.8 for smooth particles and 4.0 for rough particles and *b* = 180.

Consequently, the Ergun law was applied to calculate the overall pressure drop along the reactor bed length and among different parametrization for the friction factor, Equation 4-25 was assumed to be the proper form of the friction factor for the flow in the fixed bed reactor [34].

$$\frac{dP_T}{L} = \frac{150G\mu_m}{{d_p}^2\rho_f}\frac{(1-\varepsilon)^2}{\varepsilon^3} + 1.75\frac{G^2}{\rho_f d_p}\frac{(1-\varepsilon)}{\varepsilon^3} \quad \text{Equation 4-23}$$

$$\frac{dP_T}{dz} = -f\frac{u_s^2\rho_f}{d_p} \quad \text{Equation 4-24}$$

$$f = \frac{(1-\varepsilon)^2}{\varepsilon^3}\frac{36(25/6)\mu_m}{\rho_f u_s d_p} \quad \text{Equation 4-25}$$

The model aimed at predicting the axial profiles of radially averaged concentrations, partial pressure, feed conversion and selectivity of different compositions at different operating conditions (which were available for calibration and validation), with respect to reaction temperature, total pressure and space velocity in a wide range of 503-543 *K*, 10-25 bar and 1.8-3.6 L g_{cat}^{-1} h^{-1}, respectively.

4.5.1. Reactor Performance Criteria

In this section, some intensive dimensionless quantities are expressed to characterize the operation of an FT reactor and present the methods used for reactor performance measurement and analysis. The conversion of reactant '*i*' in a plug flow reactor operating at steady state is defined by Equation 4-26 [154].

$$f_{i_{out}} = \frac{Rate\ of\ reactant\ 'i'\ disappeared\ from\ the\ system}{Rate\ of\ reactant\ 'i'\ entered\ into\ the\ system} = \frac{F_{i_{in}} - F_{i_{out}}}{F_{i_{in}}} \quad \text{Equation 4-26}$$

The conversion is related to the composition of the reactant and was defined only for carbon monoxide, which by definition, its value is between 0 and 1. Therefore, Equation 4-27 was employed to quantify the fraction of carbon monoxide that has been consumed in the FT reactor. The conversion only depends on the boundaries of the system, "in" and "out" [155]. It should be mentioned that the conversion was not defined on the basis of any particular FT reaction in which multiple co/main reactions take place. Note that none of the reactions in the FT synthesis process produce carbon monoxide.

$$Conversion = x_i\ (\%, i: CO, H_2) = \frac{C_{in,i} - C_{out,i}}{C_{in,i}} \times 100 \quad \text{Equation 4-27}$$

Equation 4-28 to Equation 4-30 were used to measure the portion of reactant converted to desired and undesired products in the FT process. Since the carbon dioxide is the only co-product which consumed the carbonaceous reactant to be produced, Equation 4-28 was used to compute the selectivity of CO_2 species which is the ratio of concertation of CO_2 produced to that of CO consumed.

$$Carbon\ dioxide\ selectivity\ =$$

$$S_{CO_2}(\%) = \frac{C_{out,CO_2}}{C_{in,CO} - C_{out,CO}} \times 100$$ Equation 4-28

$$Lighter\ hydrocarbon\ selectivity =$$

$$S_{x\,(C_1-C_4)}\,(\%) = \frac{C_{in,C_n}}{C_{in,CO} - C_{in,CO} - C_{out,CO_2}} \times 100$$ Equation 4-29

$$Total\ liquid\ selectivity =$$

$$S_{C_{5+}}(\%) = 100 - \left(S_{HC_1} + S_{HC_2} + S_{HC_3} + S_{HC_4}\right)$$ Equation 4-30

In Equation 4-30, the desired products' selectivity was determined relative to the amount of carbon monoxide reactant converted to hydrocarbon products; hence, in the denominator, the moles of carbon monoxide converted to carbon dioxide, was subtracted. The numerical values of products' selectivity are between 0 to 100% based on their definitions. The summation of all products' selectivity must be equal to 100%.

Equation 4-30 describes how to determine the selectivity of the heavy hydrocarbons (carbon number ≥ 5). As some of the compounds in a standard gas bottle used for quantitative analysis of gaseous products by GC-FID (gas chromatography flame ionization detector) were not available, the measurement of the quantities of particular constituents presented in the gaseous products downstream of a reactor was not possible; therefore the product selectivity of detailed hydrocarbons was measured up to hydrocarbons with a carbon number ≤ 7.

4.6. Development of the Algorithm

Regardless of the technique (e.g. finite difference or finite element method) that is used to solve the system of differential equations (e.g. ODE or PDE), it is necessary to build the solution method into an algorithm which will be turned into a computer program. The intention was to provide recipes for solving the final problem in which experimental data is predicted satisfactorily by a mathematical model. Here, the developed algorithm was found useful in solving the reactor problem not only in a fixed bed reactor but also in a different reactor type. A solution algorithm was presented that is effective in solving the single tube reactor model. Such a solution methodology can be applied to a wide variety of problems which require the solution of sets of coupled non-linear partial differential equations. The algorithm was applied after the decision was made about which numerical scheme to employ and the equations were reformulated in the appropriate manner. The algorithm illustrated in Figure 4-2 and Figure 4-3 referred to a steady-state one-dimensional model; however, the methodology is easily extended to two- or three-dimensional models or shifted to an unsteady-state condition.

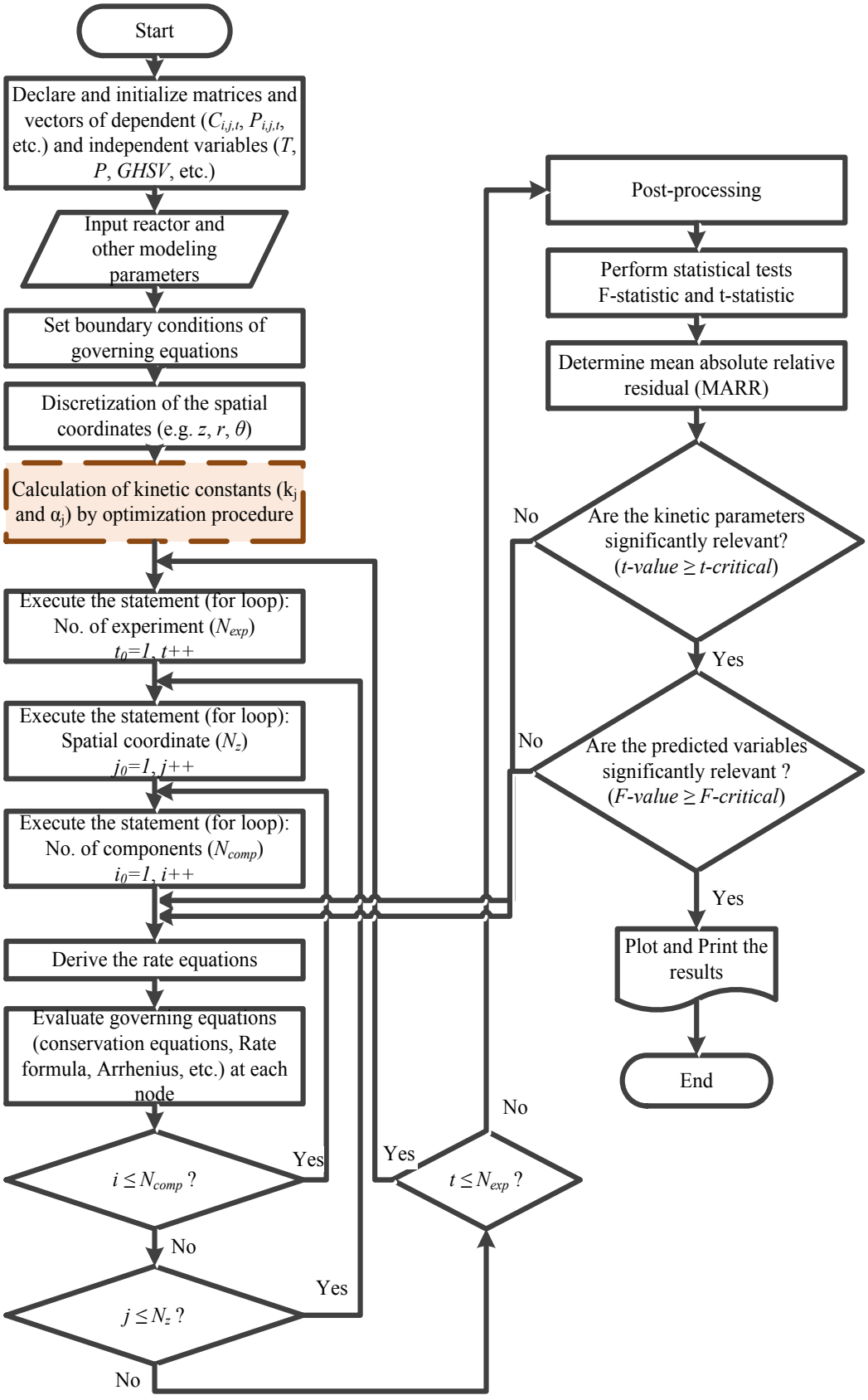

Figure 4-2 Flow-chart diagram of mathematical and kinetics modelling procedure.

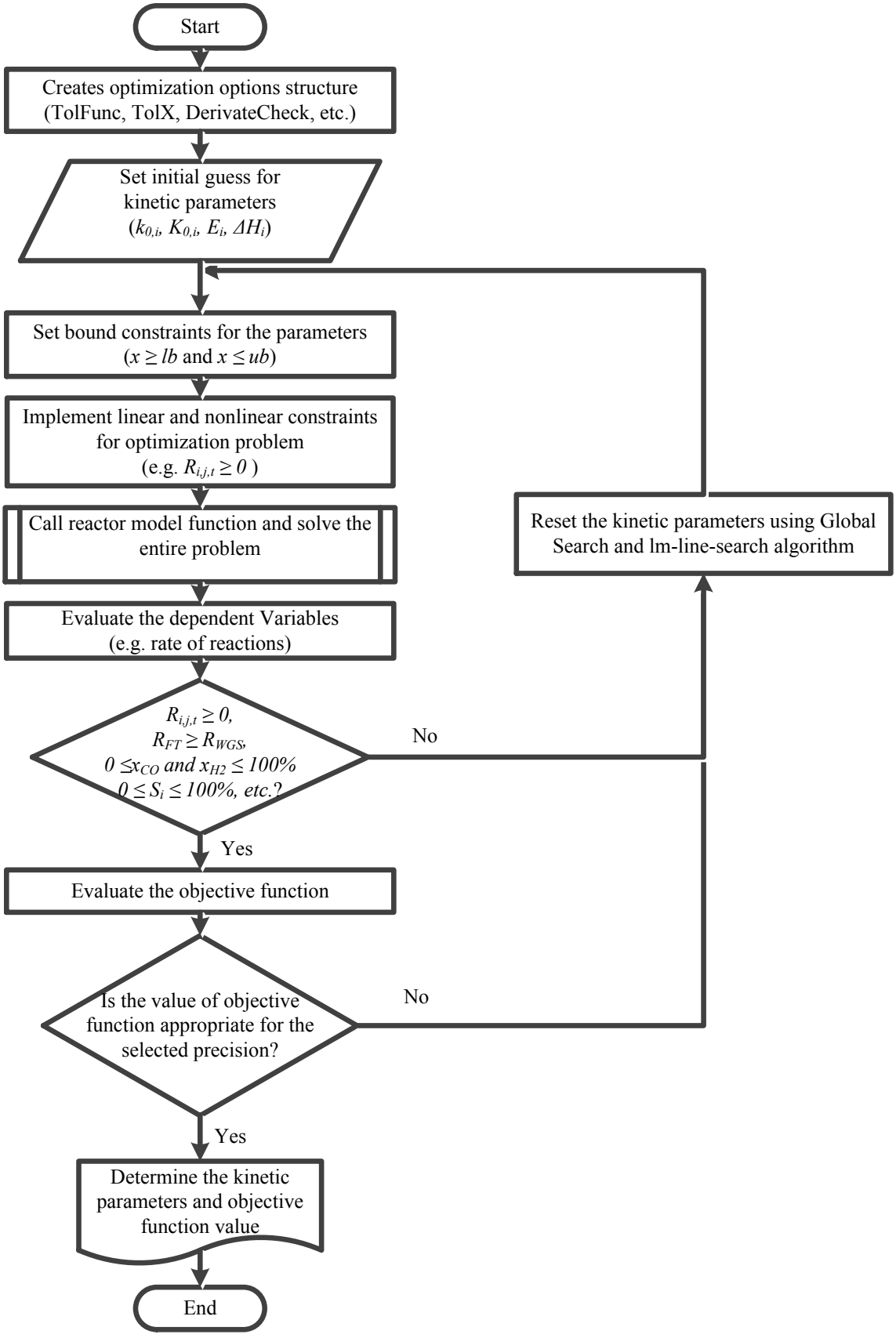

Figure 4-3 Flowchart diagram of optimization procedure in estimation of kinetics parameters.

The mole balance equation is, in fact, the most difficult to solve because it is highly nonlinear due to the nature and order of reaction rates in terms of concentration of different species such as CO,CO_2, H_2 and H_2O. The unknown dependent variables in the reactor were the concentration, mole fraction and partial pressure of the species in the flow direction; the rate equation for the multiple reactions; as well as the fluid velocity and total pressure of the system. The approach was to solve each differential equation in turn, cycling through the equations one after another, repeating the process until a final converged solution was gained at the reactor outlet. It was assumed that the domain was discretized and that the solution was calculated at a number of fixed points (locations) along the length of the packed bed. The steps were as follows:

i. The physical and chemical parameters involved in the reactor model were initialized. These parameters were either fixed values or functions of temperature, concentration, pressure and/or velocity. Some of these values were stored in a data file and some others were built into library of functions to be called by the main MATLAB program.

ii. The temperature was assumed to be constant. Therefore, the species partial pressure, concentration, and mole fraction, as well as the total pressure and velocity of the fluid flow were initialized.

iii. The total pressure of the fluid flow i.e. Equation 4-23, was solved using the most recent values for concentration and partial pressure. The value of the pressure was then updated to be used to solve the density of the fluid mixture i.e. Equation 4-17.

iv. The fluid velocity field i.e. Equation 4-16, was then determined by using the updated (the most recent) value of pressure and fluid velocity which was stored as an input to the next steps.

v. Then, the last stored data were used to calculate the partial pressure (Equation 4-15), concentration (Equation 4-14), mole fraction and weight fraction of each chemical compound defined in the reactor problem.

vi. Steps (*ii*) to (*v*) were repeated using several nested loops until all the unknown dependent variables were solved at each specified fixed node (location) in the spatial coordinate and for different experimental cases (conditions).

vii. The results were then stored in the library and data file to be used in the post processing section that was used to perform statistical analysis, such as *F*-test and *t*-test to ensure that the model and the parameters were statistically significant. Also, the relative residual between the calculated and measured data was determined to check the accuracy of the prediction.

viii. A statement was made so that if the accuracy of the prediction and/or statistical analysis failed, then the model must be rejected and steps (*iii*) to (*vii*) must be repeated.

ix. Finally, the results were printed and plotted for further analysis and investigation.

4.7. Numerical Method

In order to solve the dependent variables (e.g. concentrations, partial pressures, reactants' conversions and products' selectivity) a numerical method was used. Euler's and finite

difference approximation were employed to solve Equation 4-14 to Equation 4-18 at each point (z_1, z_2, z_3, …, z_{n-1}, and z_n) from an initial value of z_0. The backward finite difference for the first order ODEs was programmed in the space increments. Therefore, the node z_n is directly calculated from the z_{n-1} by computing the derivative at z_n. The exact solution was converged by reducing the step size which leads to a decrease of the error. The variables were calculated along the axial dimension in multi-nested loops. The advantage of this combined method was that the percentage error produced by the program code was negligible.

The model was discretized in the dimension needed by the code (i.e. ''z'', ''i''and ''t'' which are length, number of species and number of experimental conditions, respectively) as follows:

$$Size\ of\ the\ mesh = [Number\ of\ nodes\ in\ z\ direction] \times [Number\ of\ species] \times [Number\ of\ experimental\ conditions] \quad \text{Equation 4-31}$$

Eqs. 4-32-4-36 are the boundary conditions applied to the balance equations for the reactor model.

$$C(z,i,t) = C(0,i,t) \quad \text{Equation 4-32}$$

$$p(z,i,t) = p(0,i,t) \quad \text{Equation 4-33}$$

$$p_T(z,t) = p_T(0,t) \quad \text{Equation 4-34}$$

$$u_s(z,t) = u_s(0,t) \quad \text{Equation 4-35}$$

$$\rho_f(z,t) = \rho_f(0,t) \quad \text{Equation 4-36}$$

4.8. Optimization Study in Kinetics Parameter Estimation

4.8.1. Optimization Method

Parameter estimation problems were stated as minimizing the objective function that measured the correctness of the fit of individual models with respect to a given experimental data set. Each presented model contained a number of unknown independent parameters so that the values should be estimated by an advanced optimization technique to obtain a model fitting the experimental results. The procedures were as follows: the value of the dependent variables (i.e. reaction rates, conversion and selectivity of different components) were predicted by the model; a function 'f', contained independent variables (i.e. temperature (T), pressure (P_T) and gas hourly space velocity (GHSV)) and parameters (i.e. kinetics parameters such as kinetic rate constants (k_i), adsorption equilibrium constants (K_i) and activation energies (E_j). The choice of optimization technique depends on the level of sophistication of the problem. In the case of a reactor problem, the reactor model along with the chemical reaction networks was stated as a nonlinear programming (NLP) problem, especially when a high order of reaction rates builds the network. There is evidence that traditional (gradient-based), local, optimization methods fail to arrive at satisfactory solutions and are not suitable for nonlinear problems. As a consequence, the values of the parameters were estimated by an advanced global optimization technique, which is a powerful and objective tool for this purpose. Among different global

optimization methods, the GlobalSearch algorithm together with the Levenberg-Marquardt (LM) algorithm were delivered as an alternative to surmount the difficulties mentioned above. This method is capable of avoiding convergence to the local minima (sub-optimal solutions) during the search process. In the optimization procedure, the independent parameters (e.g. kinetics parameters) were subject to upper and lower bounds acting as inequality constraints $(p_{LB} \leq p \leq p_{UB})$. The optimization problem aimed at estimating the kinetics parameters in such a way that the objective function was not just minimized, but also the global minimum value of the objective function was achieved. The optimization problem contained the estimation of kinetics parameters for each kinetics model developed in the present thesis. Each problem consisted of $N_{exp} \times (N_{resp} + N_v + N_\rho)$ Partial Differential Equations (PDEs) that described the changes of concentration of reactants and products, as well as fluid velocity and density along the reactor bed length and one Ordinary Differential Equation (ODE) for that of total pressure (P_T). The term N_{exp} denotes the total number of experimental runs; N_{resp} is the number of responses (i.e. chemical species); N_v is the equation related to the velocity field and N_ρ is related to that of fluid density. The goal was to find such numerical values of the parameters that the model gives the best possible agreement with the experimental data. From the governing balance equations in the model, it is clear that the model was non-linear with respect to the parameters and variables. For estimation of the kinetic models, the dependent variable (i.e. model responses in the regression procedure) were the outlet conversion of CO, the selectivities of CO_2, CH_4, C_2H_4, C_2H_6, C_3H_6, C_3H_8, C_4H_{10}, C_5H_{12}, C_6H_{12}, C_7H_{16} and overall selectivity of C_{5+} that represents the overall formation of liquid products. The objective function is defined by Equation 4-37.

$$f_{j,obj} = \left(\frac{y_j^{exp} - y_j^{cal}}{y_j^{exp}}\right)^2 \quad j = 1, 2, 3, \ldots, N_{exp} \qquad \text{Equation 4-37}$$

Where y_j^{exp} and y_j^{cal} are the measured and predicted values of conversions of reactants or the selectivities of products, respectively. Due to the complexity of the models, a multi-response objective function was introduced, in the following form:

$$OF = \sum_{i=1}^{N_{resp}} \sum_{j=1}^{N_{exp}} \left(w_{i,j} \left(\frac{y_{i,j}^{exp} - f(x_{i,j}, p)}{y_{i,j}^{exp}} \right)^2 \right) \qquad \text{Equation 4-38}$$

Where 'i' denotes each component in the reaction mixture; $w_{i,j}$ represents the weighting factor of the response 'i' in experimental run 'j', which was used as the experimental scattering varying between different data. Those responses with the most accurate measurement and/or with special significance in the regression were provided with greater weights. In fact, the weighting factor expressed the relative importance of the response 'i' in experimental run 'j'; $f(x_{i,j}, p)$ is the value of model prediction.

4.8.2. Data Analysis

As explained in section 4.8.1, to avoid getting trapped in local minima, the globally kinetic parameters of the various rival models in this thesis were estimated using the combined GlobalSearch algorithm and Levenberg-Marquardt (LM) algorithm. Then, the statistical tests as well as physicochemical constraints were employed to evaluate the significance of the models and kinetic parameters. The optimisation procedure was designed to find the optimal minimum value of the objective function defined in section 4.8.1, which delivered: (i) a

reasonable fit to the measured values; (ii) physically meaningful values of the kinetic model parameters; (iii) acceptable values of statistical parameters, e.g. F_{value} for the predicted model as well as t_{value} for the estimated kinetic parameters and these criteria were studied in the following sections (4.8.2.1-4.8.2.4).

4.8.2.1. *Physicochemical Constraints*

For scanning the models by parameter optimization, several physicochemical criteria were applied, such as those defined for rate constants (k_j), adsorption equilibrium constants (K_i) and activation energies (E_j). Kinetic rate constants and adsorption equilibrium constants should be positive. Also, the values of activation energies should be positive and for different components e.g. methane, ethene, WGS, higher paraffin and olefins' formation should be in the range of values reported in the literature. These will be discussed in section 5.2.

4.8.2.2. *Mean Absolute Percentage Deviation (MAPD)*

Equation 4-39 indicates the relative residual (RR) percentage error between predicted values and experimental data of individual response $'i'$. This equation was used to indicate the deviation between the model and experiment for each individual response. The RR (%) values for the responses of each model were presented in section 5.2.

$$RR_i(\%) = \frac{m_i^{exp} - m_i^{cal}}{m_i^{exp}} \times 100 \qquad \text{Equation 4-39}$$

In order to measure the accuracy of the fit of the models relative to the experimental data, the results were analysed quantitatively by the mean absolute percentage deviation (MAPD) using Equation 4-40. The MAPD (%) values were determined for developed mechanistic

models as well as for power-law rate expression and presented and compared with those from literature models in section 5.2.2.

$$MAPD(\%) = \frac{1}{N_{exp}N_{resp}} \sum_{i=1}^{N_{resp}} \left[\sum_{j=1}^{N_{exp}} \left(\left| \frac{y_{i,j}^{exp} - f(x_{i,j}, p)}{y_{i,j}^{exp}} \right| \times 100 \right) \right] \quad \text{Equation 4-40}$$

4.8.2.3. *F-Test Analysis*

In addition to providing an excellent fit to the experiments, all the models should be significantly relevant and physically meaningful. One way to assure the significance of the predicted model results is the statistical analysis called the *F*-test, where the significances of the overall regression were statistically determined. The *F*-test was used to see if the fit has any significance at all. The test was performed by taking two factors into account:

I. SST term that is the total sum of squared deviations of the experimental data with respect to their mean value.

II. SSE term that is the residual sum of squared deviations of the experimental results with respect to the predicted values by the model.

Finally, the F_{ratio} for each individual response and the total responses were calculated by Equation 4-41. The F_{ratio} determined for the models are presented in section 5.2 (see Table 5-1 and Table 5-7).

$$F_{ratio} = \frac{(SST - SSE)\ /(m-1)}{SSE/(n-m)}$$

$$= \frac{\left(\sum_{j=1}^{Nexp}(y_{j,exp} - \bar{y})^2 - \sum_{j=1}^{Nexp}(y_{j,exp} - y_{j,pred})^2\right)/(m-1)}{\sum_{j=1}^{Nexp}(y_{j,exp} - y_{j,pred})^2\ /(n-m)} \quad \text{Equation 4-41}$$

In this equation, n is a degree of freedom of a number of data points ($N_{exp} \times N_{resp}$) and m is corresponding to the number of kinetics parameters. It is possible to reject the null hypothesis and hence accept the model. This happens when the F_{ratio} determined for the responses are higher than the value of $F_{critical}$ which is the corresponding tabulated value [156-158] ($F_{ratio} > F_{critical}(m-1, n-m; 1-\alpha)$); $F_{critical}$ is the tabulated α-percentage point of the *F*-distribution with $m-1$ and $n-m$ degrees of freedom. If the calculated value is larger than the tabulated value, there is a probability of $1-\alpha$ (e.g., 99%) that the model is adequate and the regression is considered to be meaningful, therefore the model is accepted. Among a set of rival models, the one with the highest F_{ratio} would be considered the ‘‘best’’ and that it would be statistically adequate.

4.8.2.4. *t-Test Analysis*

The *t*-test was performed to ensure that the kinetics parameters obtained by the optimization, optimization, were significantly relevant. The estimated kinetics parameters were tested for their significance based on their individual t_{value} calculated by the procedure below (see Table 4-1). The parameter with the lowest t_{value} is the least significant parameter and here a parameter is evaluated as insignificant if its t_{value} is less than the $t_{critical}$ from the tabulated values that can be obtained from the literature [156, 157, 159]. For the optimum kinetics model, the calculated t_{value} of the kinetic parameters was determined for the models

and presented in section 5.2 (see Table 5-1 and Table 5-7). The steps for calculating the t_{value} of the kinetic parameters are as follows:

I. Determination of the hypothesized or population mean (μ). When the errors are normally distributed with zero mean and constant variance, the random variables are distributed like the normal (Gaussian) distribution. At the given probability level (e.g. 99%), the calculated n values have to exceed tabulated t_{value} for the parameter to be significantly different from a reference value, which is zero (μ=0). This property is used in a two-sided *t*-test to verify if the estimated parameters differ from a reference value (zero), when other parameters are kept constant at their optimal estimated value.

II. Computation of the sample mean ($\bar{X}$) (see Equation 4-42).

III. Computation of the sum of the squares of the individual parameters obtained from each experimental run (see Equation 4-43).

IV. Computation of the sum of the square difference as expressed (see Equation 4-44).

V. Computation of the estimated variance of the sample data (see Equation 4-45).

VI. Computation of the standard error of the mean (SEM) (see Equation 4-46).

VII. Calculation of the t_{value} from (see Equation 4-47).

VIII. Computation of the degree of freedom (see Equation 4-48).

IX. Computation of the critical value for *t* (called t_{score} or $t_{critical}$) with that degree of freedom and probability value using a provided table in the literature [156, 157, 159].

X. Comparison of the calculated t_{value} of individual kinetic parameters to the tabulated $t_{critical}$.

When $t_{value} > t_{critical}(n-m; 1-\alpha)$ the hypothesis that the parameter would be zero can be rejected. The quantity $t_{critical}(n-m; 1-\alpha)$ is the tabulated α percentage point of the *t*-distribution with $n-m$ degrees of freedom. There are limits on the complete collection of reference values which are not significantly different from the optimal estimates, a_j at the selected probability level 1– α, provided that the other estimates are kept constant upon their optimal estimate. They are symmetrical with respect to the optimal point estimate a_j. Hence, the confidence intervals of individual kinetic parameters a_j are defined by: $a_j - CF < a_j < a_j + CF$.

Table 4-1 Steps through the computation of t_{value} to test the level of significance of obtained kinetic parameters

Step (II)	Step (III)	Step (IV)	
Equation 4-42	Equation 4-43	Equation 4-44	
$\bar{X} = \frac{\sum_{j=1}^{N_{exp}} X}{n}$	$\sum_{j=1}^{N_{exp}} X^2$	$SS = \sum_{j=1}^{N_{exp}} X^2 - \frac{\left(\sum_{j=1}^{N_{exp}} X\right)^2}{n}$	
Step (V)	Step (VI)	Step (VII)	Step (VIII)
Equation 4-45	Equation 4-46	Equation 4-47	Equation 4-48

$$s^2 = \frac{SS}{n-1} \qquad SEM = \sqrt{s^2/n} \qquad t_{value} = \frac{\bar{X}}{SEM} \qquad df = n - 1$$

4.9. Summary

In this chapter, the advantages of numerical modelling compare to experimental studies, were highlighted. This chapter detailed the hydrodynamic of the rector model as well as the developed algorithm for solving the system of equations and the procedure of estimating kinetics parameters. Integration of the GlobalSearch optimization algorithm with the developed model was explained for estimation of kinetics parameters in the preceding chapter. The capability of the developed mathematical model for calculating the trend of changes of reactant and products' concentrations, partial pressures, mole fractions as well as conversion and selectivities was highlighted. Such outcomes are profoundly beneficial in reactor design, scale-up, the understanding of its behaviour in operation and predicting the effect of changing operating conditions which highlights the effectiveness of the develop mathematical tool.

CHAPTER 5

EXPERIMENTAL SETUP, MODEL CALIBRATION AND VALIDATION

5.1. Experimental Setup

The experimental studies of the FT synthesis process at the University of Birmingham were started in 2010 and the setup was designed and operated by a co-worker [1] in the School of Mechanical Engineering. A mini-scale FT plant with fixed bed reactor was designed and built to study the production of liquid hydrocarbons over Co-based FT catalysts. According to this study, a series of eggshell Co catalysts on powder SiO_2 support with dissimilar structure were investigated in the FT synthesis process. The detailed experimental set-up, catalyst preparation procedures and different characterization experiments including methods and tools can be found in the literature [1]. In sections 5.1.1 to 5.1.2, the aim is to highlight and represent the overall information about the experiments which were employed for the kinetics study and mathematical modelling in the present study.

5.1.1. Experimental Apparatus and Catalysts

The experimental work [1] aimed at the development of a miniaturised version of the FT plant that could accomplish a preliminary investigation of the synthesis process before being scaled-up to a pilot plant. The FT synthesis was conducted in a fixed bed reactor packed with a cobalt catalyst supported with silica powder. Figure 5-1 shows the schematic illustration of the apparatus as well as the Process Path Flow (PPF) that implements the path of the syngas conversion into the liquid hydrocarbon products. In this process, a simulated N_2-rich syngas bottle (containing: 33% H_2, 17% CO and 50% N_2) was used to feed into the reactor inlet for the production of synthetic fuels. The catalytic reactor bed was purged by the N_2 bottle and the bed was activated by employing the H_2 gas bottle. Both bottles comprised of a highly precise compressed gas pressure regulator to decrease the gaseous pressure in the cylinders to a value necessitated for the next steps, Figure 5-2 (d). Flashback arrestors were setup one for the gas supply lines and one for the flammable syngas and hydrogen bottles to prevent a flame generated by the gas flow. The one-way valves were setup to avoid backward flow of gases to the gas sources, Figure 5-3 (e). A calibrated smart Mass Flow Controller (MFC), shown in Figure 5-2 (c), was used to regulate the volumetric flow rate of the feedstock (Bronkhorst Ltd). As illustrated in the figure, a bypass line let the gases bypass the mass flow controller and release the pressure right after the experimental procedure was over [1].

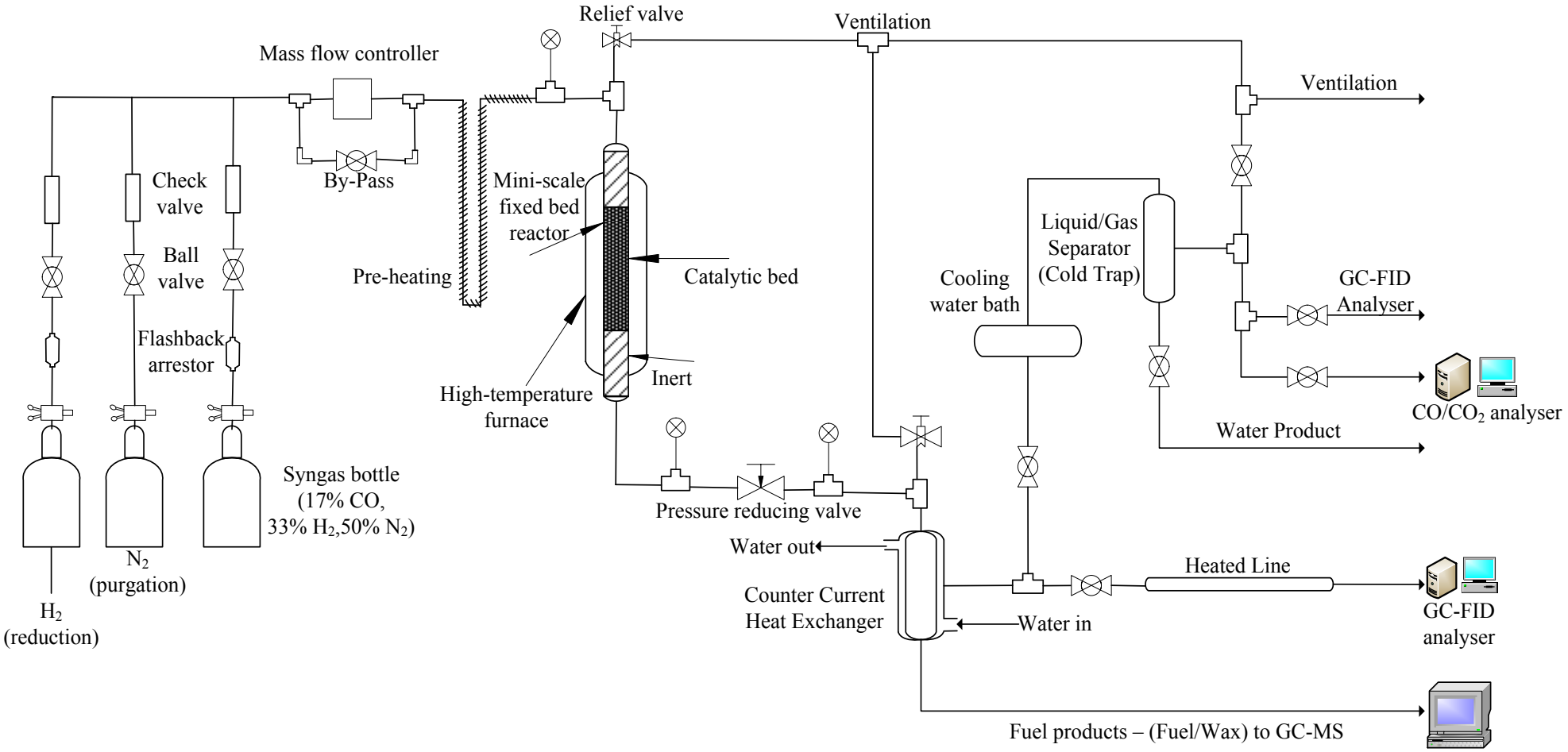

Figure 5-1 Schematic diagram of experimental setup designed for FT synthesis process.

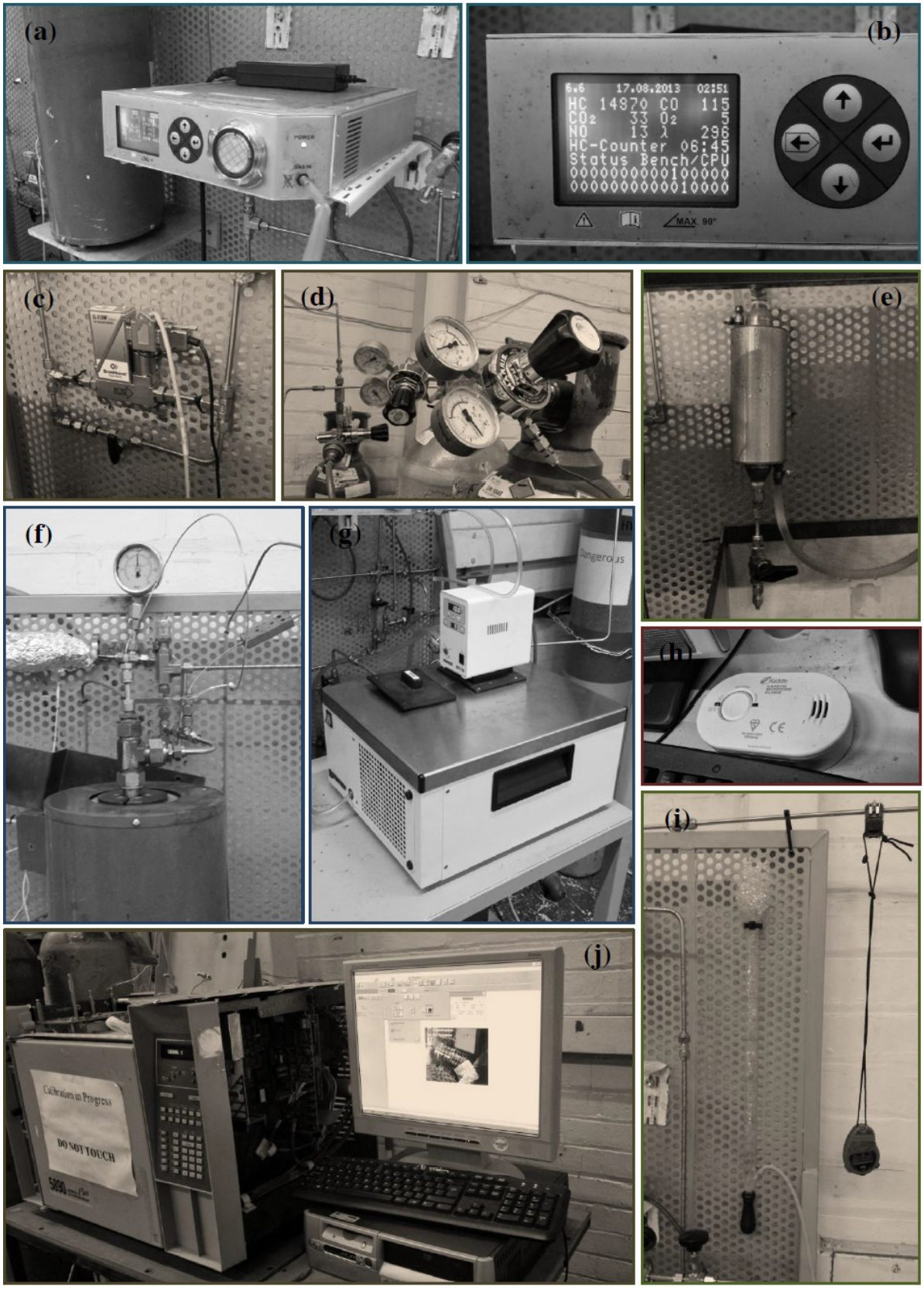

Figure 5-2 Mini-scale FT synthesis apparatus and the experimental components (adopted from [1]).

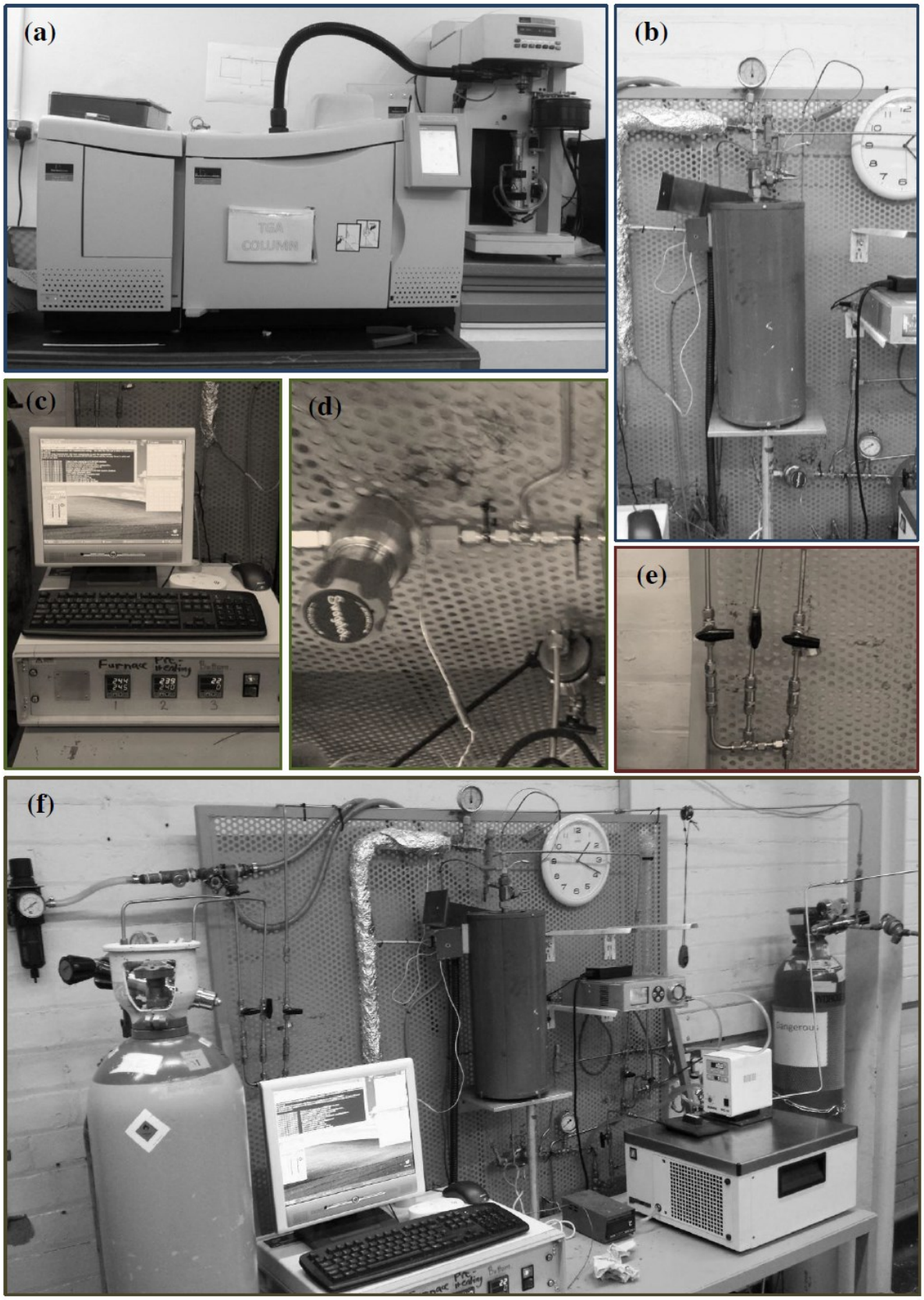

Figure 5-3 Mini-scale FT synthesis apparatus and the experimental components (adopted from [1]).

A heater tape (which has an electrical heating element) was used to increase the inlet gas temperature before reaching the rector. The heater tape was completely in physical contact with the pipe and the flow that entered into the reactor to preserve the temperature of the flow continuously. In order to avoid the heat losses from the pipe, the heater tape was covered with thermal isolation (see Figure 5-3 (f)). The pressure of the system was monitored using a pressure gauge right before and after the reactor (see Figure 5-3 (b)). Moreover, a proportional relief valve was set at 40 *bar* and setup just before the reactor so that when the system failed, it would discharge the pressure. The syngas conversion was carried out in the FT unit with a seamless stainless steel single mini-structured downdraft fixed bed reactor with a tube length of 52.83 cm, outer diameter of 19.05 mm and wall thickness of 1.651 mm (see Figure 5-3 (b)). The reactor was mounted in a tube furnace (with the temperature ranging from 50 to 1100 °C). The tube furnace was used to provide the heat zone and it was controlled by a thermocouple that was placed along the centreline of the reactor located roughly 60-80 mm inside the catalytic bed. Additionally, a metal jacket was installed between the furnace and the reactor and it surrounded the reactor to deliver a uniform wall temperature along the reactor bed length. Following the reactor outlet, the lines were covered with heater tape to avoid the liquid products condensing before the separation step. Prior to this, a discharge valve was used to release the pressure of the system to prevent any blockage (see Figure 5-3 (b)). The streams of product mixtures were distinguished into liquid products and unreacted gaseous flow using the vapour-liquid separator so that the condensed liquid products flowed down and collected; whereas the gases left from the column at the upper side (see Figure 5-2 (e)). A counter current heat exchanger was utilized to decease the temperature of the column. A refrigerated laboratory water bath (see Figure 5-2 (g)) was used to keep the coolant fluid at a constant temperature. The temperature was set at 10 °C during all the experiments.

The Co catalyst in the form of powder was diluted by inert diluent i.e. silicon carbide (SiC) to have better heat removal as well as an effective use of the catalytic bed. In fact, the reactant conversions are highly impacted by the nature of the diluters in exothermic heterogeneous catalytic reactions; so that the diluent will aid the heat transfer, minimize the formation of the heat spot, and improve the temperature distribution along the reactor bed. This is a common practice in laboratory-scale FT synthesis processes, which is also reported by the literature [160]. The catalyst's particles were stabilized by employing a commercial sphere silica support (provided by Fuji Silysia^{TM} Chemical Ltd) because it has significant characteristics such as: stability under reaction condition, high mechanical strength (due to its high purity), inertness, its remarkable high porosity degree and surface roughness and having low manufacturing costs [161]. The supports were stable chemically and mechanically due to their high purity. The catalyst beds were packed with the glass wool and the glass beads with diameter of 3 mm. To load the catalyst into the reactor, the reactor tube was placed in upside down. First of all, glass beads were inserted at the top of the reactor in the pre-heating zone; thereafter insulating glass wool was loaded in to avoid movement of the glass beads. The reactor was loaded with the pre-mixed catalyst with diluent materials. Before loading the catalyst, a thick layer of glass wool was placed at the bottom of the catalytic bed to keep the catalyst at the specified position. Then, the glass beads were added to fill the remaining space of the reactor.

5.1.2. Analysis of Gas and Products

After the catalytic bed was purged by the N_2 bottle and the bed was activated by employing the H_2 gas bottle, the synthesis gas then entered into the reactor from the inlet and the system was pressurized to the desired pressure for the FT process to begin. After the inlet flow rate was regulated to the desired reaction space velocity the FT activity was started. The catalytic performances were considered as a function of time on stream for 12 h. The changes in the CO_2 and CO concentration were monitored on-line by using a modified CO analyser (AVL Digas™ 440). An HP® 5890 gas chromatograph (see Figure 5-2 (j)), equipped with a Flame Ionisation Detector (FID) and Pora-Plot Q column, was utilized to analyse the effluent gas products. The concentration of different compounds in a sample gas was measured quantitatively. The liquid hydrocarbon products were analysed off-line using a DB1 column combined with a gas chromatography-mass spectrometry (GC-MS) PerkinElmer™ as illustrated in Figure 5-3 (a). For liquid samples, the qualitative analysis was performed to identify the components. The experiments were carried out at sixteen different operating conditions (i.e. reaction temperature range of 503-543 *K*, pressure range of 10-25 *bar* and gas hourly space velocity per mass of catalyst range of 1800-3600 $Nm\ell\ (STP)\ g_{cat}^{-1}\ h^{-1}$). The values of the operating conditions are listed in Table 5-1.

Table 5-1 Experimental results at sixteen different operating conditions with respect to reaction temperature, total inlet pressure and GHSV.

No.	T (K)	P_{tot} (bar)	GHSV ($Nm\ell$ (STP) g_{cat}^{-1} h^{-1})	P_{H_2} (bar)	P_{CO} (bar)	X_{CO} (%)	S_{CO_2} (%)	S_{CH_4} (%)	$S_{C_{5+}}$ (%)
1	503	10	1800	3.30	1.70	78.04	4.52	7.06	90.45
2	503	15	2400	4.95	2.55	79.34	4.46	16.59	76.23
3	503	20	3000	6.60	3.4	66.55	2.63	11.17	81.88
4	503	25	3600	8.25	4.25	54.34	1.72	12.60	81.43
5	518	10	2400	3.30	1.70	93.03	14.10	23.27	68.57
6	518	15	1800	4.95	2.55	99.15	14.68	10.96	85.29
7	518	20	3600	6.60	3.40	92.52	10.25	24.38	66.52
8	518	25	3000	8.25	4.25	98.22	11.45	16.25	77.79
9	528	10	3000	3.30	1.70	90.78	16.38	28.72	57.46
10	528	15	3600	4.95	2.55	96.81	17.05	38.25	48.93
11	528	20	1800	6.60	3.40	99.96	20.70	21.55	71.72
12	528	25	2400	8.25	4.25	99.74	18.34	28.25	62.41
13	543	10	3600	3.30	1.70	93.95	21.01	39.66	48.38
14	543	15	3000	4.95	2.55	99.74	24.75	35.89	54.03
15	543	20	2400	6.60	3.40	99.59	25.36	55.82	23.61
16	543	25	1800	8.25	4.25	99.88	24.93	49.72	37.98

Table 5-2 Experimental results at different operating conditions, selectivity of available olefins and paraffins' components with carbon number less than seven (C_2-C_7)

No.	$S_{C_2H_4}$ (%)	$S_{C_2H_6}$ (%)	$S_{C_3H_6}$ (%)	$S_{C_3H_8}$ (%)	$S_{C_4H_{10}}$ (%)	$S_{C_5H_{12}}$ (%)	$S_{C_6H_{14}}$ (%)	$S_{C_7H_{16}}$ (%)
1	0.03	0.55	0.65	0.35	0.17	0.10	0.09	0.05
2	0.07	1.39	1.89	0.89	0.34	0.26	0.15	0.13
3	0.10	1.42	2.09	0.82	1.58	0.12	0.08	0.01
4	0.08	0.97	1.56	0.56	1.22	0.76	0.48	0.23
5	0.04	2.24	1.28	1.86	0.87	0.44	0.19	0.08
6	0.01	1.04	0.55	0.93	0.33	0.15	0.07	0.02
7	0.06	2.32	1.58	1.90	1.17	0.41	0.27	0.12
8	0.04	1.54	1.28	1.13	0.78	0.47	0.13	0.06
9	0.10	3.76	2.52	2.85	1.65	1.65	1.03	0.64
10	0.08	3.81	1.39	3.27	1.17	0.47	0.35	0.17
11	0.01	2.04	0.48	2.05	0.38	0.08	0.07	0.04
12	0.01	2.77	0.86	2.66	0.65	0.28	0.18	0.10
13	0.08	3.66	1.75	2.85	1.03	0.35	0.22	0.15
14	0.02	3.43	0.45	3.19	0.55	0.32	0.13	0.03
15	5.28	5.40	0.45	5.07	0.70	0.43	0.07	0.02
16	0.01	4.54	0.08	4.24	0.41	0.19	0.07	0.02

5.2. Results and Discussion

5.2.1. Kinetics Results Using Power-Law Rate Model

Using the empirical power-law rate expression developed in section 3.2.1, the model aimed at predicting the conversion of syngas species (CO and H_2) as well as selectivity of carbon dioxide and hydrocarbon products by estimating the kinetic parameters which consisted of: order of reaction with respect to CO and H_2 partial pressures; pre-exponential factor; and activation energy for each proposed chemical reaction listed in Table 3-1. A total of 84 responses were incorporated in estimation of the parameters. These responses encompassed seven species: CO conversion; CO_2; methane (CH_4); light hydrocarbons (i.e. C_2, C_3, and C_4) and total FT liquid hydrocarbons' (C_{5+}) selectivities which were calculated at twelve different experimental conditions (listed in Table 5-3); availability for calibration, with respect to reaction temperature, total pressure and gas hourly space velocity (GHSV) in the range of 503-543 *K*, 10-25 *bar* and 1800-3600 $Nm\ell\ (STP)\ g_{cat}^{-1}\ h^{-1}$, respectively. Table 5-4 shows the kinetic parameters estimated by the empirical power-law rate expression (see Equation 3-1 and Equation 3-2 to Equation 3-12) that was developed in section 3.2.1. The predicted results were compared to those of the experiments with respect to the above components. The goodness of fit was examined by employing the *F*-test and the MAPD values were computed based on the formula provided in section 4.8.2 (see Equation 4-39 to Equation 4-41). From Table 5-4, since the F_{ratio} with value of 55.34 exceeded the critical value ($F_{critical}$), with a significance level of 0.01 (i.e. the cumulative probability of 0.99), hence one can be confident that the model is significant. In addition, the MAPD value of 13.23% that were obtained indicated that the model can fit the experimental results with reasonable accuracy. In fact, the calculated value of MAPD

was in the range of the available literature, and kinetic parameters were all physically meaningful. Nevertheless, part of the scope of the present study was to achieve a model prediction much better than that obtained by the literature and predicted by power-law empirically. It will be shown that the results were not satisfactorily predicted by the power-law model for some species at some specific operating conditions those which significantly affected the model predictions. It will be explained that this model may not be able to predict well at a wide range of process conditions; however, this model is suitable when a narrower range is selected.

Table 5-3 Values of experimental data employed in the present study considered for the power-law model

	T	P_0	$GHSV$	Conversion	Selectivities					
				CO	CO_2	CH_4	C_2	C_3	C_4	C_{5+}
	(K)	(bar)	$Nm\ell\ (STP)\ g_{cat}^{-1}\ h^{-1}$	(%)	(%)	(%)	(%)	(%)	(%)	(%)
Test-01	503	10	1800	78.04	4.52	7.06	0.58	1.00	0.90	90.45
Test-02	503	15	2400	79.34	4.46	16.59	1.47	2.79	2.93	76.23
Test-03	503	20	3000	66.55	2.63	11.17	1.52	2.90	2.53	81.88
Test-05	518	10	2400	93.03	14.1	23.27	2.28	3.14	2.74	68.57
Test-06	518	15	1800	99.15	14.68	10.96	1.05	1.48	1.22	85.29
Test-07	518	20	3600	92.52	10.25	24.38	2.38	3.48	3.24	66.52
Test-10	528	15	3600	96.81	17.05	38.25	3.89	4.66	4.27	48.93
Test-11	528	20	1800	99.96	20.7	21.55	2.05	2.53	2.14	71.72
Test-12	528	25	2400	99.74	18.34	28.25	2.78	3.52	3.04	62.41

Test-13	543	10	3600	93.95	21.01	39.66	3.74	4.61	3.62	48.38
Test-14	543	15	3000	99.74	24.75	35.89	3.45	3.64	3.00	54.03
Test-15	543	20	2400	99.59	25.36	55.82	10.69	5.55	4.34	23.61

In addition, the significance of individual kinetic parameters was statistically examined by the *t*-test analysis in order to ensure that the kinetic model and parameters were relevant. The detail of computation of t_{value} was explained in section 4.8.2.4. The *t*-test results (e.g. t_{value} and $t_{critical}$) are shown in Table 5-4. Absolute t_{value} of all parameters fell within the range of 7.14−100.34, which were greater than the $t_{critical}$ with the value of 2.4 at a 0.99% confidence interval, indicating that all parameters in the power-law kinetic model contributed relevantly.

Table 5-4 Values of kinetic parameters estimated in the present study considering power-law kinetic model presented in section 3.2.1 as well as F_{ratio} and t_{value} calculated from the statistical analyses

Reaction	n_j*	t_{value}	m_j*	t_{value}	E_j*	t_{value}	A_j*	t_{value}
	$(-)$		$(-)$		$(kJ\ mol^{-1})$		$\left(mol\ g_{cat}^{-1}\ s^{-1}Pa^{(n_j+m_j)}\right)$	
R. 3-1	-0.39	53.34	1.02	97.25	101.15	69.25	5.45E+01	68.44
R. 3-2	-0.24	60.14	0.15	7.14	78.79	30.05	1.20E-03	64.59
R. 3-3	-0.26	15.71	0.18	7.25	59.95	51.82	1.45E-03	52.98

R. 3-4	-0.55	93.36	0.25	94.23	33.73	64.99	2.32E-06	16.80
R. 3-5	-0.82	34.23	0.35	55.94	23.04	100.34	2.81E-09	32.70
R. 3-6	-0.76	17.34	0.32	70.30	17.83	93.86	6.57E-10	15.85
R. 3-7	-0.15	88.67	1.25	26.19	21.25	63.83	3.24E-08	62.38
R. 3-8	-1.10	51.44	1.26	100.08	50.24	80.59	5.99E-05	34.95

*Results of statistical analysis:
(i) F-test: $F_{\text{ratio}} = 55.34 > F_{critical}\,(n-m, m-1; 1-\alpha) = F_{critical}\,(84-32, 32-1; 1-0.01) = 2.07$
(ii) t-test: lowest t-value $= 7.14 > t_{critical}\,(n-m; 1-\alpha) = t_{critical}\,(84-32; 1-0.01) = 2.4$

Furthermore, the parity diagram as well as relative residual percentage plots were illustrated in Figure 5-4 and Figure 5-5 (a-g) respectively, representing the overall adequacy of the prediction with respect to the individual variables (i.e. CO, CO_2, CH_4, C_2, C_3, C_4 and C_{5+}) and total response. It was seen that around 60% of the results were predicted with a relative error of less than 15% and all the data points were predicted below 32% error, indicating that the rate model did not effectively predict the rate of reactions at all operating conditions. From the predicted results, it was found that at high temperature conditions, especially when $T \geq 528$ *K*, the predicted results were not in good agreement with the measured data in which the predicted values presented a higher relative residual than those obtained at a lower temperature. However, the results presented in the past studies [136, 138, 162] revealed that with the narrower temperature range, for instance when *T* changes between 500-528 *K*, the power-law

model provided satisfactory prediction with the MAPD less than 7% in which about 89% of the data points were obtained with an error below 10%. Considering a wider range for the process conditions, the selectivities of CO_2 and CH_4 were overestimated, while those of C_2-C_3 and C_4 were underestimated. This implies that the temperature can significantly impact on the estimation of the parameters and the mathematical modelling predictions. Indeed, this was due to the temperature dependency of the activation energies and the Arrhenius equation (Equation 3-44) in the rate formula: at a high temperature condition; predicting a lower value of activation energy would increment the rate constant as well as rate of products' formation; while at a lower temperature condition this would be vice versa. For instance, Figure 5-5 (b) shows the relative residual between the calculated and experimental values in terms of CO_2 selectivity, indicating the overestimation of the results at higher temperature conditions since some of data points were predicted below -15%. Referring to Table 5-4, R. 3-8 was the reaction responsible for the production of CO_2 and its activation value was 50.24 $kJ\ mol^{-1}$, which was considerably lower than the expectation. It will be discussed in details that the order of reaction (i.e. 'm' and 'n' in Equation 3-44) of H_2 and CO partial pressures would have significant effects on the products rate of formation concurrently and can significantly control the estimation. Hence, the temperature would not be the only reason for the overestimation and/or underestimation of the modelling results. Figure 5-5 (d) to (f), represent the relative error in terms of C_2, C_3, and C_4 selectivities. In contrast to CO_2 and CH_4, these components were underestimated. From Table 5-4, the order of reaction with respect to H_2 partial pressure ('m') for R. 3.6 to R. 3.10 was lower than 0.35. Since 'm' is a positive value for each of these reactions then it has direct influence on the rate of formation: decreasing 'm' would decrease the value of $P_{H_2}^m$ and as $P_{H_2}^m \propto R_i$, hence the rate of formation would gradually decrease.

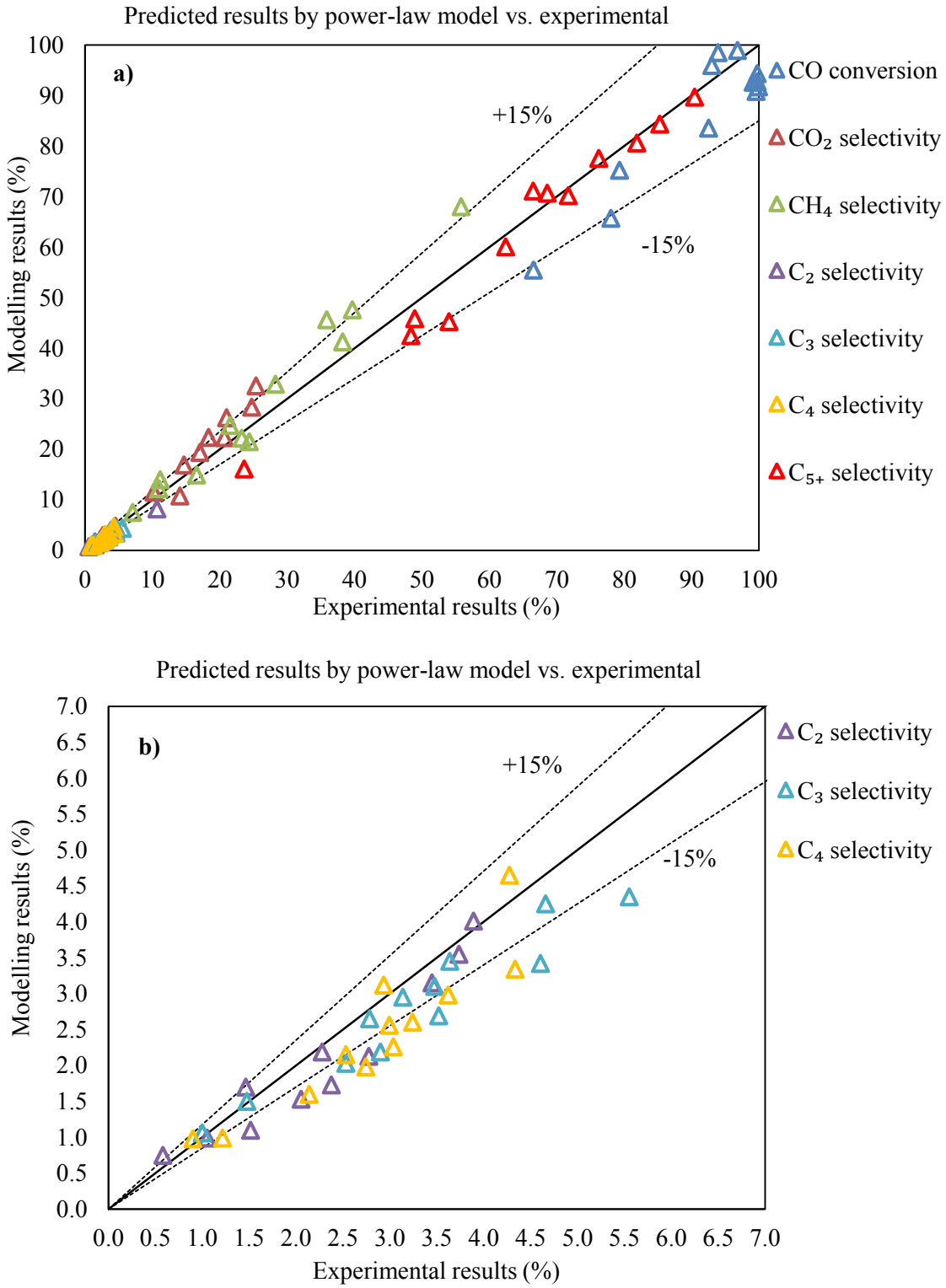

Figure 5-4 Parity plot and comparison of experimental data and predicted results obtained from power-law rate model, a) all existing components used for prediction such as CO

conversion, CO_2, CH_4, C_2, C_3, C_4, and C_{5+} selectivities, b) products with a very low range selectivities e.g. C_2, C_3, and C_4.

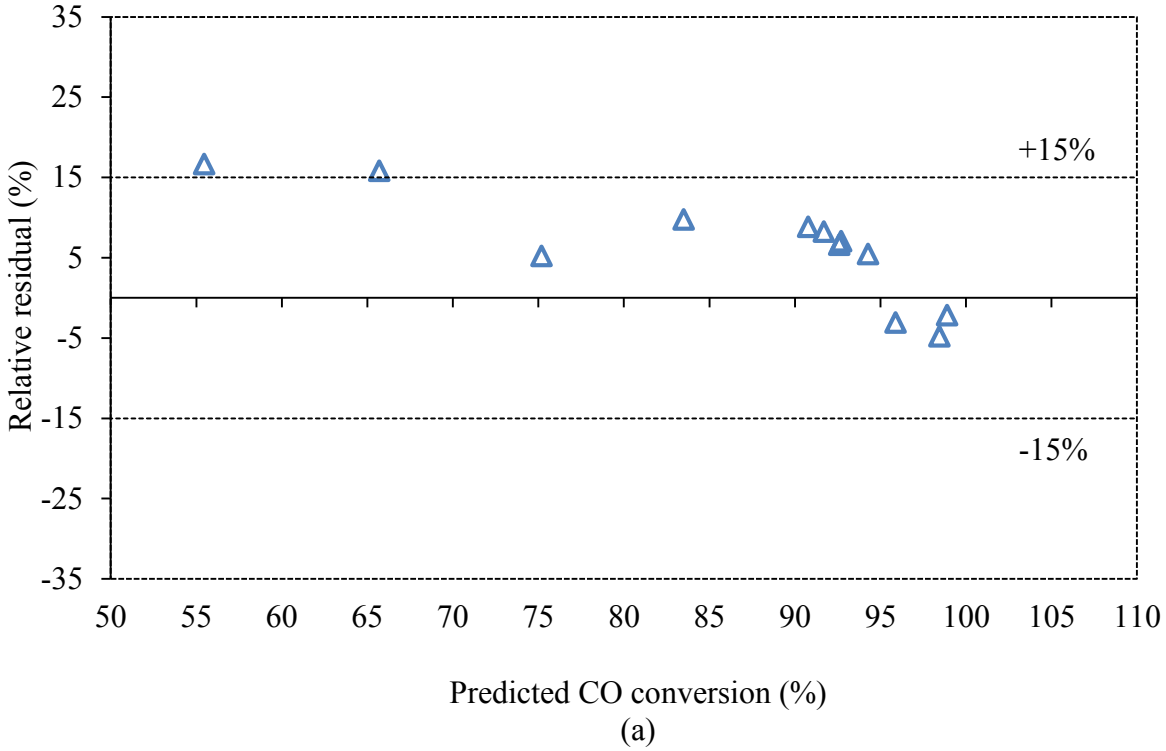

(a)

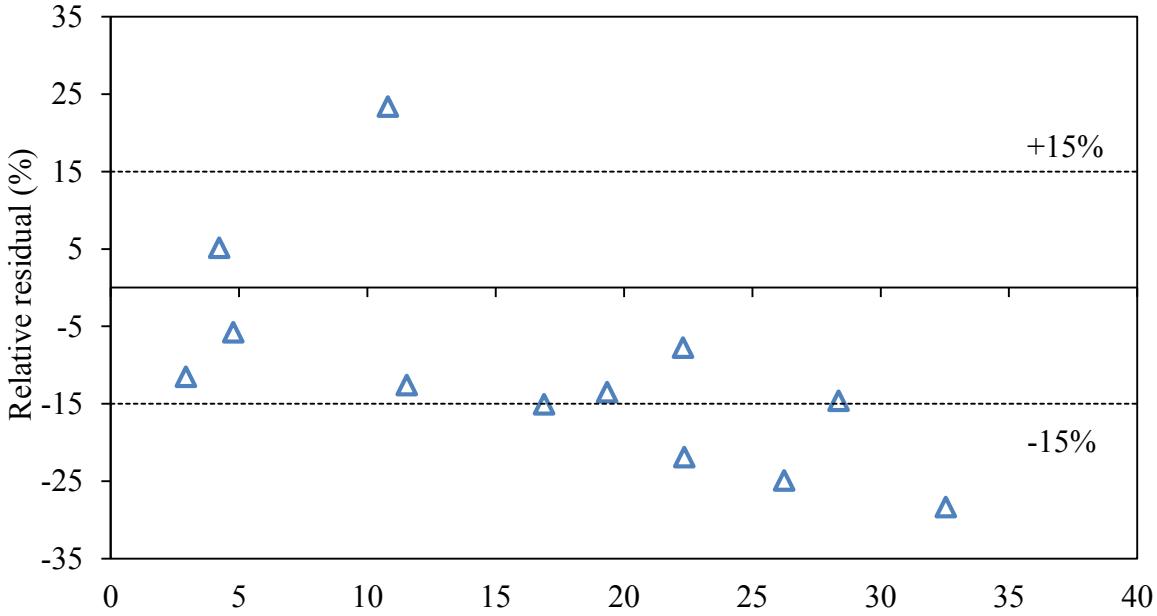

(b)

Figure 5-5 (*continued*).

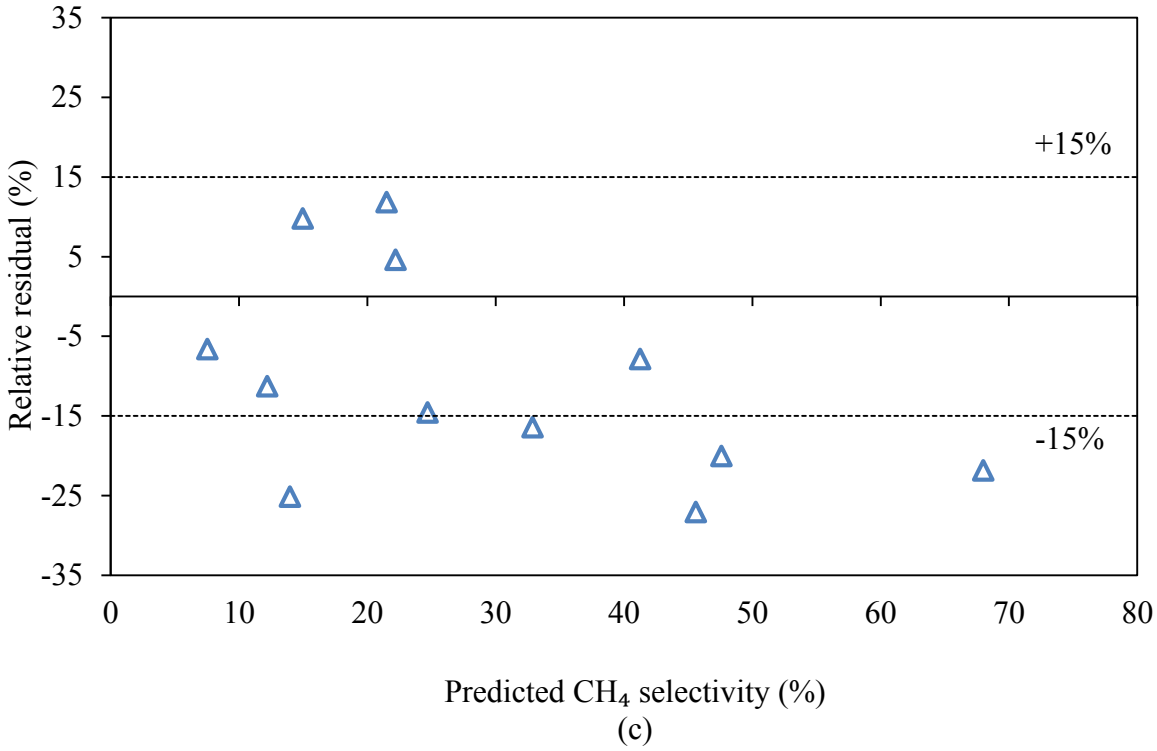

(c)

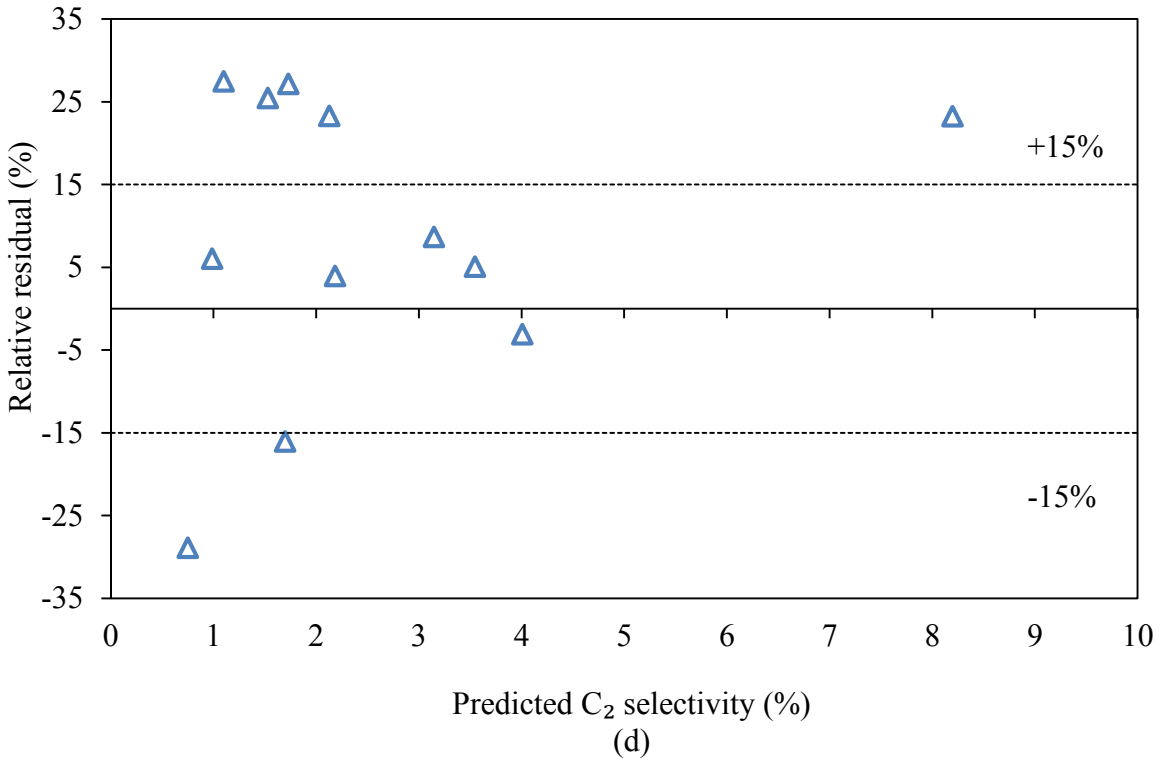

(d)

Figure 5-5 (*continued*).

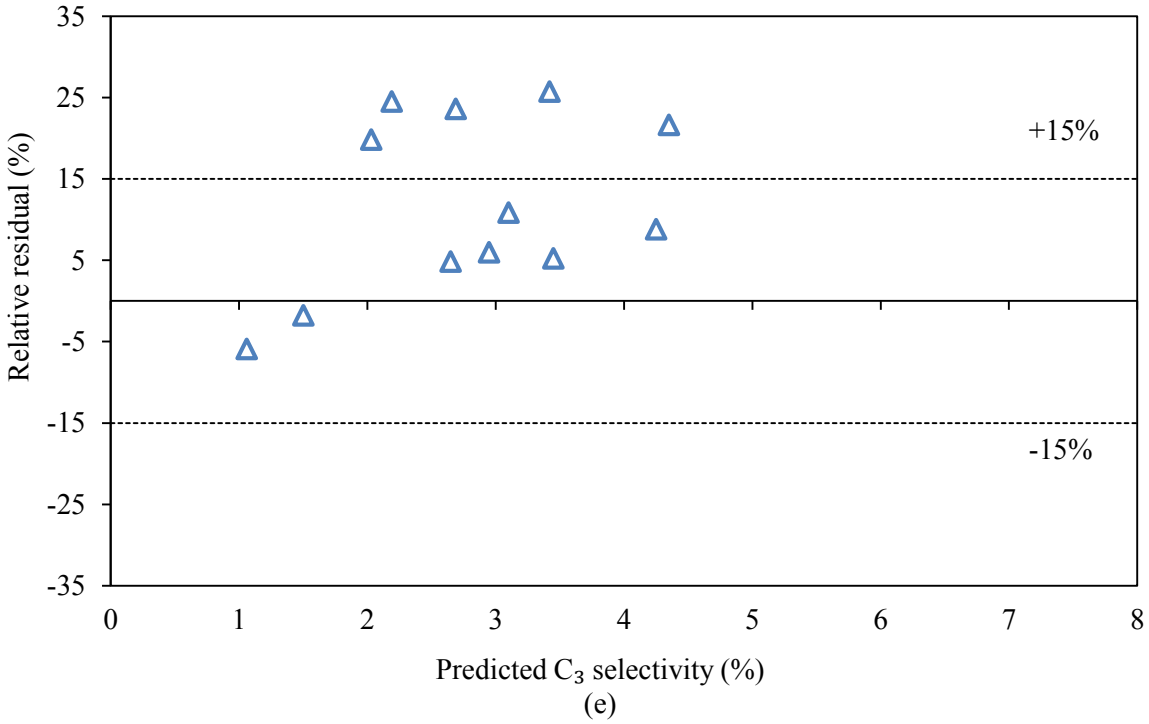

(e)

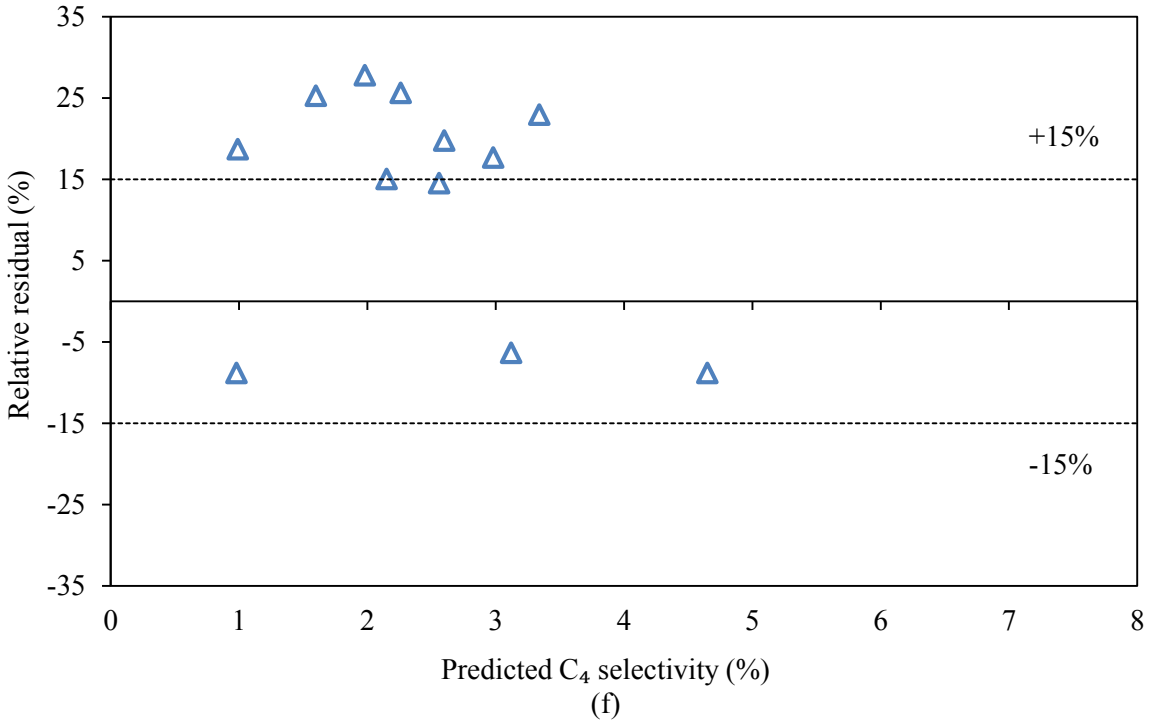

(f)

Figure 5-5 (*continued*).

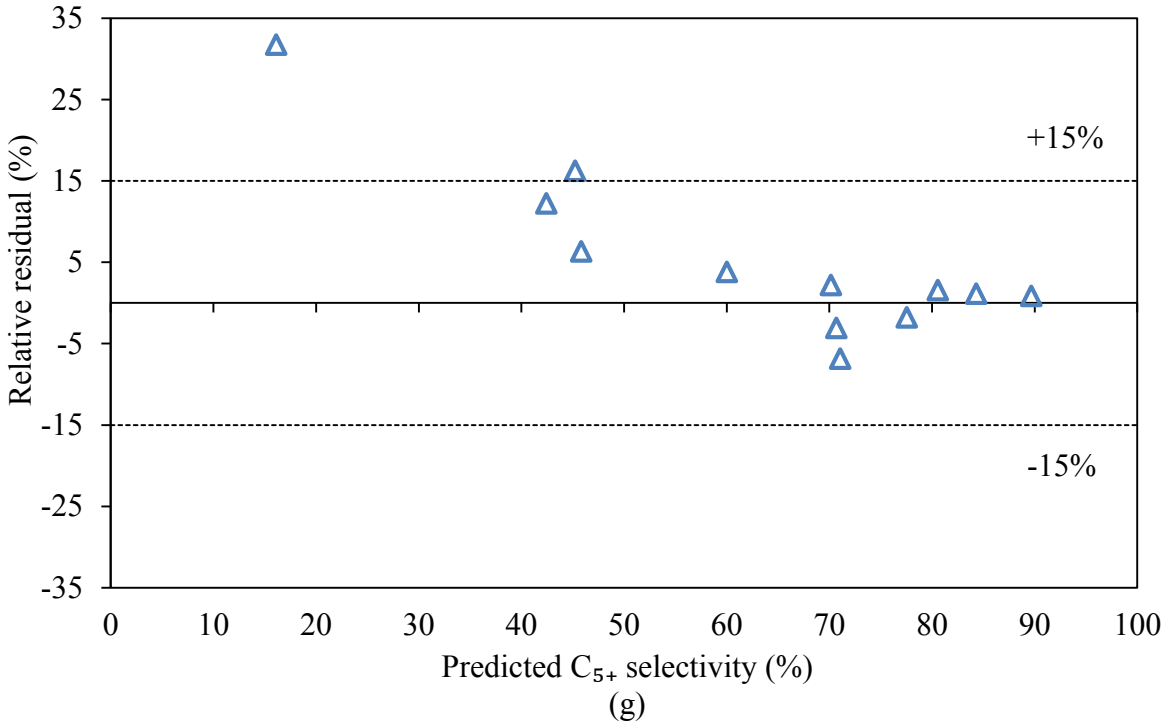

Figure 5-5 Relative residual percentages of experimental data and modelling values for each component; (a) CO conversion, (b) CO_2 selectivity, (c) CH_4 selectivity, (d) C_2 selectivity, (e) C_3 selectivity, (f) C_4 selectivity, (g) C_{5+} selectivity.

From the optimization of the kinetic parameters, the CH_4 activation energy, corresponding to the Co/SiO_2 catalyst, was calculated to be 101.15 $kJ\ mol^{-1}$. This result was consistent with the literature values of 100−145 $kJ\ mol^{-1}$ on Co, Fe, and Ni catalysts [163-167] and also fell within the range estimated by van Santen *et al.* [168] using the DFT technique (100−170 $kJ\ mol^{-1}$). In contrast, this value was significantly higher than the value of 63−65 $kJ\ mol^{-1}$ for a Re−Co/ Al_2O_3 catalyst reported by Todic *et al.* [169] and much lower than the value of 177.4 $kJ\ mol^{-1}$ for a Co/Al_2O_3 catalyst estimated by Visconti *et al.* [170]. Nevertheless, further investigation revealed the fact that the CH_4 formation was overestimated by the model, as can be seen in Figure 5-5 (c). However, the activation energy value (101 $kJ\ mol^{-1}$) was higher than expected; which can be explained by its relatively higher estimated

pre-exponential factor, being at least four orders of magnitude greater than the same parameter for other reactions, and the order of reaction of CO partial pressure, being of a lower negative value than expected.

From Table 3-1, R. 3-1 is responsible for predicting the rate of CH_4 formation. The reaction orders obtained for the partial pressures of CO and H_2 were determined to be −0.39 and 1.02, respectively (see Table 5-4). The negative order of reaction for CO partial pressure suggested a CO inhibition effect, by its adsorption on Co/SiO_2 catalyst, and a significant influence of partial pressure of H_2 on CH_4 formation. This implied that the CH_4 formation rate is controlled by the hydrogenation of either unassisted or H-assisted carbon species dissociation; but the CO adsorption on Co/SiO_2, as indicated by a negative number (−0.39), obstructs the steps of the hydrogenation process. These values were in line with the reported values for Co, Fe, Ru, and Ni catalysts; the reaction order for P_{CO} and P_{H_2} was in the range of −1.3 to −0.2 and 0.8 to 1.6 respectively, from the literature studies [165-167].

As pointed out, the P_{CO} has an inhibiting effect which means that the lower negative value of order of reaction would result in having less inhibition effects and therefore would estimate higher CH_4 formation and selectivity than is expected. From the CH_4 kinetic model and results, this was expected since a smaller negative and positive order for the P_{CO} and P_{H_2}, like −0.04 and 0.02 respectively, results in differential changes in the CH_4 formation rate with respect to partial pressures (see Figure 5-6 (a)).

It will be shown later that the prediction of CH_4 selectivities were improved considerably by using a mechanistic kinetic model (i.e. FT−III (RDS−2)), indicating that the discrepancy (overestimation) of CH_4 selectivity from the power-law kinetic was due to the estimated low value for the P_{CO} reaction order. Numerical analyses were continued to see the changes of CH_4,

C_2, C_3, C_4, and C_{5+} rates of formation with respect to partial pressures of CO or H_2. Assuming the power-law kinetic model, the results were illustrated in Figure 5-6 (a-e). At a constant CO or H_2 partial pressure, increasing the partial pressure of H_2 or CO significantly raised or reduced the CH_4 rate, respectively (see Figure 5-6 (a)). Indeed, the changes in CO partial pressure shows a weaker influence on the CH_4 formation rate and its selectivity than that of H_2 partial pressure as it can be seen from the ratios of the CH_4 rate changes to the variation of CO and H_2 partial pressure: $\Delta R_{CH_4}/\Delta P_{CO} = 2.96$ and $\Delta R_{CH_4}/\Delta P_{H_2} = 6.57$. This was not in agreement with a recent kinetic study of Re-promoted Co/CNT catalysts by Yang *et al.* [171] and Ma *et al.* [172] who reported that CO partial pressure has a greater impact on CH_4 formation rate and selectivity than H_2 partial pressure. This confirmed the above conclusion related to the reaction order of P_{CO} which was expected to be a higher negative value than the estimated value (i.e. -0.39), so that CO partial pressure would have more inhibiting effects on the CH_4 reaction rate.

It can be concluded that the power-law rate models have some limitations in the representation of catalytic reactions; that is to say, they could predict the rates almost well enough but only over a narrow range of experimental conditions; whereas, as it will be shown, Langmuir–Hinshelwood (LH) rate expressions, due to their fundamental origin, predict the rates over wider range of conditions. It was unclear which combination of a number of rate expressions and kinetics models proposed for syngas conversion and product selectivity, as well as the water gas shift reaction on cobalt, can provide the best representation of the available data. Nevertheless, section 3.3 contributed to this uncertainty mentioned above and provided adequate and comprehensive details regarding the kinetics of the FT reaction together with the WGS reaction. The results obtained from the numerical studies will be explained in section 5.2.2.

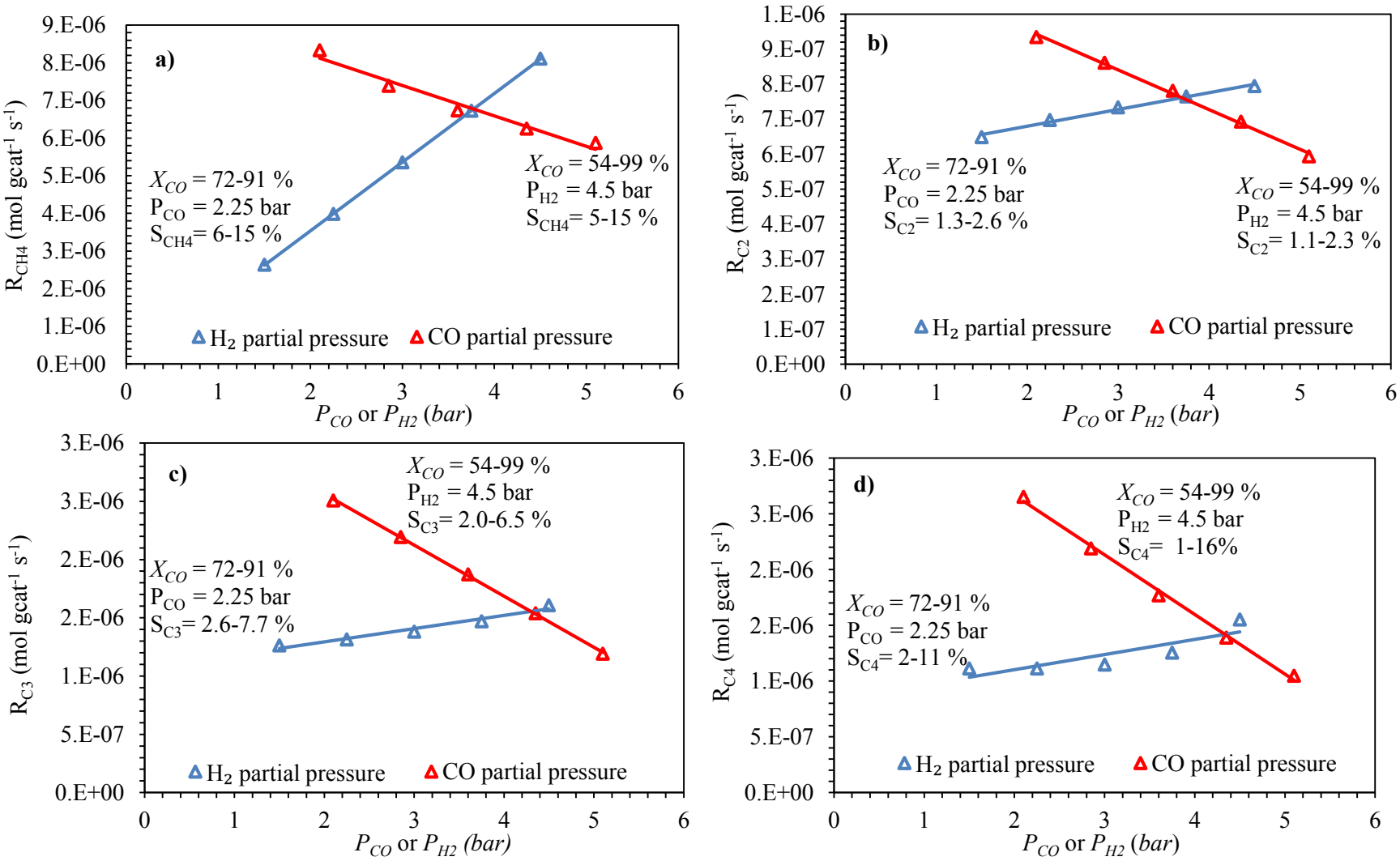

Figure 5-6 (*continued*).

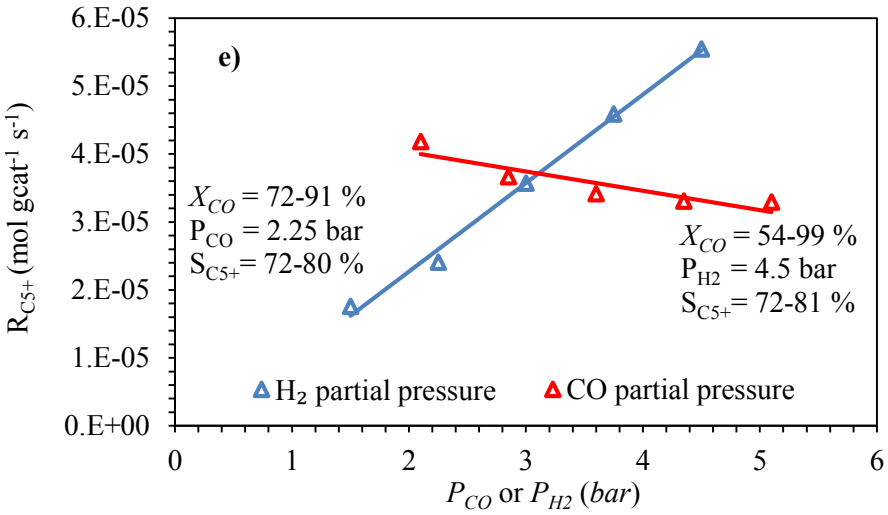

Figure 5-6 The influence of partial pressure of CO and H_2 on CH_4 formation rate over Co/SiO_2 catalyst. Constant reaction condition: *T*=503 (*K*), P=15 (*bar*) H_2/CO= 0.5-2, and GHSV=2400 ($Nm\ell$ *(STP)* g_{cat}^{-1} h^{-1}).

5.2.2. Kinetic Results Using Mechanistic Developed Rate Models

5.2.2.1. *Comparison of Results Obtained Based on Different Kinetic Models*

All the rate models developed in Chapter 3, were employed to fit the experimental results collected in a mini-scale fixed bed reactor at a steady-state condition in the wide range of total pressure of 10-25 *bar*, temperature of 503-543 *K* and GHSV of 1800-3600 $Nm\ell$ *(STP)* g_{cat}^{-1} h^{-1}. The kinetic parameters involved in each model were estimated and the models were examined against the experiments to find the best mechanistic model that predicted the FT synthesis experimental data satisfactorily, as well as satisfying the consistency of the physicochemical properties and statistical analyses. Such information can provide guidelines for the design of more active and selective catalyst materials. The adequacy of the best developed kinetic model to describe the experimental data with respect to CO conversion as well as CO_2, CH_4, C_2H_4,

C_2H_6, C_3H_6, C_3H_8, C_4H_{10}, C_5H_{12}, C_6H_{14}, C_7H_{16}, and C_{5+} (total liquid products) selectivities at all investigated operating conditions was demonstrated by the parity plot and relative residuals which will be discussed in the following section.

The results obtained from a total of 336 combined FT/WGS rate models (twenty-four FT rate model along with fourteen WGS rate model) indicated the errors between the experimental data and predicted data for the total of 144 data points ($N_{exp} \times N_{resp}$), consisted of twelve different chemical components mentioned above at twelve experimental conditions, falling in the range of 5.93−53.73%. The rival models were discriminated by determining RR, MAPD and statistical analysis performed by an *F*-test. These criteria (explained in section 4.8.2) were essential procedures that should be accomplished to identify a model that has the best fit to the experimental data and has the most significant physically meaningful kinetic parameters.

Four out of eight proposed kinetic models, from FT−II to FT−V, were based on an H−assisted CO dissociation mechanism (see Table 3-2). Considering the model fit obtained from FT−II to FT−V, the results (see values of MAPD listed in Table 5-5) indicated the important role of H−assisted pathways as the kinetically-relevant CO dissociation steps on a cobalt catalyst at reaction conditions essential for significant chain initiation and propagation. As can be seen from the elementary reaction steps in Table 3-2, these pathways (Model FT−II to FT−V) instead of directly dissociating CO−ψ into O-atoms and carbon atoms (as in model FT−I), gave precedence to the rejection of the O-atoms in CO as H_2O either via direct cleavage of species such as HCO−ψ and CH_2O−ψ (see model FT–IV and FT–V respectively), or via the direct formation of OH−ψ precursors through either the COH−ψ species (see model FT–II) formed through interaction between CO−ψ and H−ψ or the HCOH−ψ species (see model FT–III) formed through interactions between chemisorbed H−ψ and HCO−ψ. Based on the

adequacy of the results, these assisted pathways signified the exclusive CO activation paths on the surfaces of cobalt catalysts at the reaction conditions.

The results obtained from H−assisted pathways indicated more accurate results than those obtained from FT−I reaction paths which requires quasi-equilibrated CO−ψ dissociation via unassisted routes. This may imply that the latter pathways may have higher energy barriers compared to the former. In fact, this was in agreement with a recent study [141] that employed Density Functional Theory (DFT) calculations which indicated high CO dissociation activation barriers with a value of 367 $kJ\ mol^{-1}$ on a CO-saturated cobalt surface, proposing that alternate paths for CO activation must be kinetically-accessible during FT synthesis catalysis i.e. H-assisted routes.

In addition, direct CO dissociation was unfavourable compared with H-assisted dissociation, because of the higher MAPD value of the former (i.e. ranging from 12.72% to 39.25%) compared to the latter (i.e. ranging from 5.93% to 53.73%). Also, the best FT kinetic model was found to be model FT−III (i.e. H-assisted CO dissociation through formation of hydroxymethylene) with MAPD in a range of 5.9% to 31.38% for various WGS rate models. Also, there is evidence that an H-assisted pathway, which includes the initial addition of H−ψ to CO−ψ to form formyls (HCO−ψ), has a relatively much lower barrier (E_f = 138 $kJ\ mol^{-1}$) than direct CO−ψ dissociation on Co-saturated catalyst (E_f = 367 $kJ\ mol^{-1}$). Also the addition of another H−ψ to HCO−ψ gives HCOH−ψ with a relatively low activation energy barrier (E_f = 90 $kJ\ mol^{-1}$), followed by dissociation to CH-ψ and OH-ψ (E_f = 106 $kJ\ mol^{-1}$), in which both have relatively lower activation barriers, favourable pathways for monomer formation. Furthermore, the results indicate that the first H-addition to CO−ψ is equilibrated and the second H-addition is the kinetically-relevant step on Co catalysts.

Comparing the predicted results by model FT−II to FT−I, the former model was closer to the experimental data that can be described by its lower forward energy barrier of 125 $kJ\ mol^{-1}$; compared to that of FT−I with CO dissociation activation barriers with a value of 367 $kJ\ mol^{-1}$, when COH−ψ intermediate was formed via the addition of another H−ψ to CO−ψ, signifying that the former route was more favourable for FT synthesis at typical process conditions. Nevertheless, this path was followed by dissociation to C−ψ and OH−ψ with a very high activation energy (i.e. E_f = 315 $kJ\ mol^{-1}$), indicating that it was an unfavourable pathway for monomer formation compared to model FT−III with lower energy barriers as explained above. Considering the FT−IV, the addition of H−ψ to CO−ψ produced formyl which dissociated to yield CH−ψ + O−ψ. In this path, CH−ψ species formed CH_3−ψ via the addition of molecular hydrogen without forming the chain growth monomers (CH_2−ψ), causing the predicted result to deviate from the experiments and was kinetically unfavourable and unproductive in hydrocarbon synthesis.

Considering FT−V, the addition of H−ψ to the C−atom in HCO−ψ formed CH_2O−ψ with a 58 $kJ\ mol^{-1}$ barrier; CH_2O−ψ species can be followed by dissociation to CH_2−ψ and O−ψ in which the oxygen atom was rejected through this step possessing high activation barriers (E_f = 157 $kJ\ mol^{-1}$). A relatively higher error obtained by this model suggested that this route did not satisfactorily contribute as much as model FT−III to the FT growth mechanism.

Alternate molecular H_2 assisted CO dissociation via direct reactions of H_2 (g) with CO−ψ, forming either C−ψ + H_2O or HCOH−ψ comprising very high activation barriers, suggested that these steps do not contribute to hydrogenation or CO activation pathways. Hence, the last three kinetic models (i.e. FT−VI, FT−VII and FT−VIII) generally did not

contribute to the FT growth mechanism compare to that of FT−III as was shown by their higher MAPD values.

The results listed in Table 5-5 indicated that the formate mechanism generally provided a better fit to the experimental data than the direct oxidation mechanism (see MAPD of model WGS-VI and WGS-VII). The results showed that the best WGS kinetics model achieved from the formate ($CHO_2-\psi$) mechanism (i.e. WGS-VII (RDS-4)) with MAPD of 5.93% is better in fitting to the experimental data than the best model from the direct oxidation mechanism (WGS-II (RDS-4)) with MAPD of 11.68%. Presumably, this can be explained by the fact that the dissociation of hydroxyl intermediate to adsorbed $O-\psi$ and $H-\psi$ species (which was step 3 in this reaction scheme) is not energetically favourable under FT synthesis reaction conditions. This conclusion was also supported by quantum calculation on transition metals that the hydroxyl dissociation is energetically unfavourable with a relatively high activation barrier [145]. In addition, in situ infrared spectroscopy confirmed the existence of formate ($CHO_2-\psi$) species on different surface catalysts [146, 147, 173]. Furthermore, the formate species was detected in situ by Fourier transform infrared spectroscopy (FTIR) in the diffuse reflectance mode (DRIFTS) over some transition metals. From the tabulated values (in Table 5-5) obtained for $CHO_2-\psi$ routes (WGS-VII) with different RDSs (RDS-4 and RDS-3), it can be seen that MAPD value was below 10% indicating satisfactory prediction of experimental results. The elementary steps CO adsorption, H_2O dissociation and H_2 formation (for instance steps 1, 2 and 5 in model WGS-I respectively, Table 3-11) are not the RDSs in the WGS reaction under the FT synthesis reaction conditions because of the large deviations of these models from the experimental data, hence their errors were not listed in Table 5-5. Considering the redox mechanism, the MAPD obtained for rate models of WGS-I with RDS-4 and RDS-5 were identical to that of WGS-III with RDS-4 and RDS-5, respectively. From the derived rate

equations (Table 3-12 and Table 3-14), it was seen that the two kinetics models had the same rate expression formula despite having different reaction kinetic routes. This suggested that the kinetic models cannot discriminate whether surface oxygen intermediate formed directly from the dissociation of water molecule (step 2 in model WGS-III, Table 3-11) or via dissociation of hydroxyl species decomposed from water (steps 2 and 3 in model WGS-I, Table 3-11) if the RDS is the formation of CO_2 from either by adsorbed $O-\sigma$ into $CO-\sigma$ or decomposition of $CO_2-\sigma$ from the catalyst surface.

The errors calculated from the combined FT/WGS models are tabulated in Table 5-5. The minimum error (i.e. 5.93%) was achieved when the adsorbed CO molecule on a catalyst surface dissociated via the H-assisted route. In this reaction pathway, the formyl and hydroxymethylene intermediates ($HCO-\psi$ and $HCOH-\psi$) formed via two successive hydrogenation of the chemisorbed CO and the produced $HCO-\psi$ in which the second hydrogenation was assumed to be the slowest step and kinetically considered to be more relevant compare to other elementary steps in this route (RDS-2). Considering the WGS reaction kinetics, the formate mechanism in which the formate species was formed through the reaction between adsorbed CO intermediate and a hydroxyl surface species ($-OH$), was considered as the most kinetically relevant route. The above-mentioned novel reaction mechanisms for the formation of paraffins and olefins' products as well as carbon dioxide are illustrated in Figure 5-7.

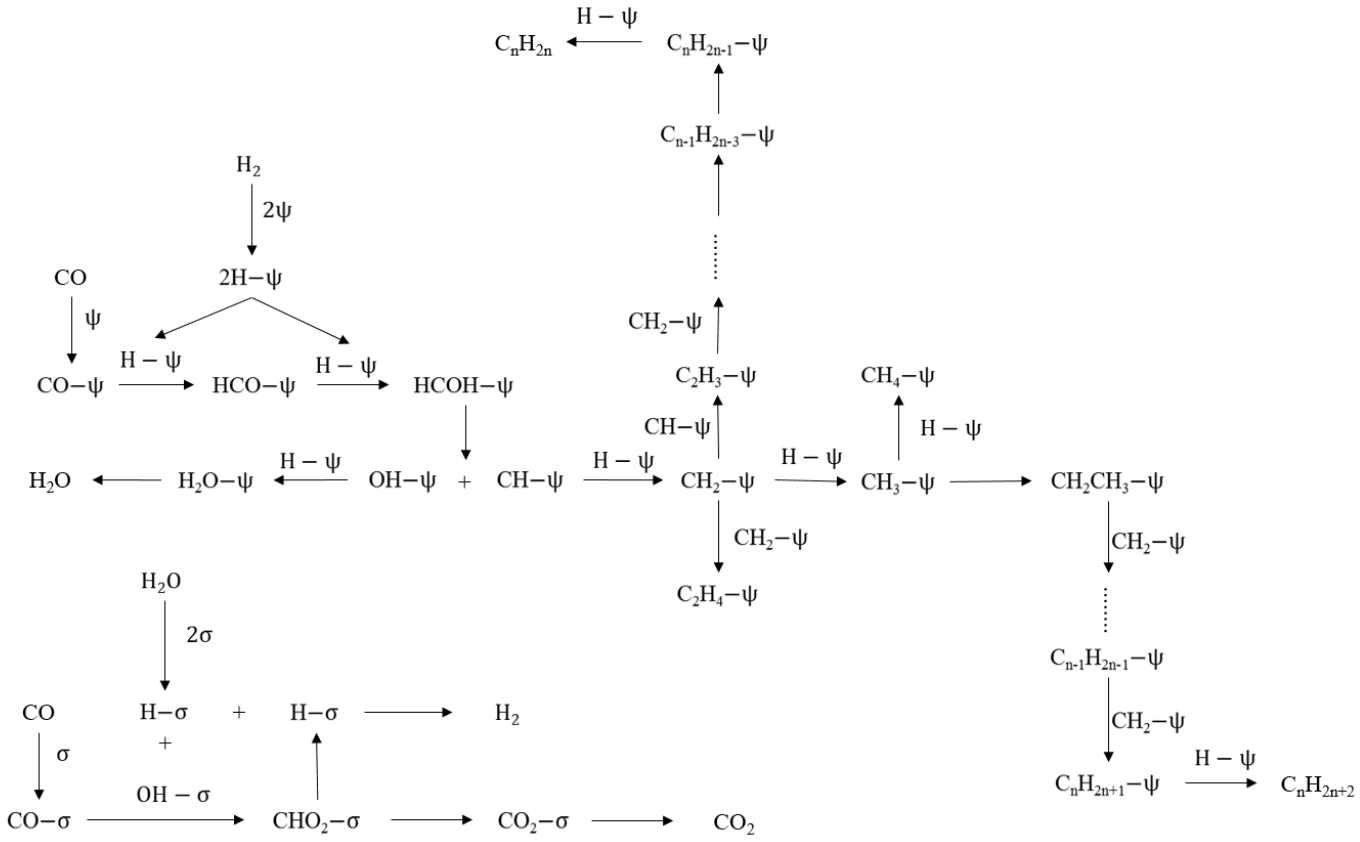

Figure 5-7 Reaction mechanism for the formation of paraffinic hydrocarbons (C_nH_{2n+2}) via alkyl species, olefins' products (C_nH_{2n}) via vinyl intermediates and WGS reaction via formation of formate intermediates (developed combined FT/WGS mechanism).

Table 5-5 Values of MAPD obtained from optimization of each proposed FT/WGS combination rate model: twenty-four FT reaction rate models with fourteen WGS reaction rate models in total were considered in the present thesis (to be continued on the next page)

No.	Reaction model	1 FT−I (RDS-1)	2 FT−I (RDS-2)	3 FT−I (RDS-3)	4 FT−II (RDS-1)	5 FT−II (RDS-2)	6 FT−II (RDS-3)	7 FT−III (RDS-1)	8 FT−III (RDS-2)	9 FT−III (RDS-3)	10 FT−IV (RDS-1)
1	WGS-I (RDS-3)	23.85	29.69	23.83	32.44	30.15	28.18	20.30	14.21	22.62	38.30
2	WGS-I (RDS-4)	25.43	31.15	25.15	34.31	31.62	30.06	20.95	14.95	24.42	40.89
3	WGS-II (RDS-3)	22.67	28.42	22.49	30.65	28.71	27.01	18.32	13.95	21.17	36.33
4	WGS-II (RDS-4)	19.15	25.56	19.80	27.12	26.65	23.95	15.32	11.68	18.16	32.86
5	WGS-II (RDS-5)	21.12	27.01	21.05	28.66	27.70	25.03	17.12	12.65	19.82	35.06
6	WGS-III (RDS-3)	27.36	32.77	26.75	35.62	32.98	31.26	21.65	16.95	26.22	43.86
7	WGS-III (RDS-4)	25.43	31.15	25.15	34.31	31.62	30.06	20.95	14.95	24.42	40.89
8	WGS-IV (RDS-3)	30.21	35.72	30.25	38.28	36.25	33.72	22.63	18.35	29.04	46.38
9	WGS-V (RDS-3)	31.36	37.62	31.99	39.86	37.26	35.33	22.93	20.16	30.33	49.29
10	WGS-V (RDS-4)	33.21	39.25	33.02	40.90	38.53	36.56	24.50	21.60	31.38	51.46
11	WGS-VI (RDS-3)	17.33	23.85	17.96	25.84	24.66	22.83	13.95	11.25	16.67	31.19
12	WGS-VI (RDS-4)	15.95	22.15	15.96	24.25	23.57	21.08	13.60	10.12	14.67	28.75
13	WGS-VII (RDS-3)	14.68	20.33	14.29	22.29	21.58	19.64	11.88	8.93	12.98	26.37
14	WGS-VII (RDS-4)	12.72	19.33	13.27	20.63	19.81	18.58	9.50	5.93	11.25	24.36

No.		11	12	13	14	15	16	17	18	19	20	21	22	23	24
	Reaction model	FT−IV (RDS-2)	FT−IV (RDS-3)	FT−V (RDS-1)	FT−V (RDS-2)	FT−V (RDS-3)	FT−VI (RDS-1)	FT−VI (RDS-2)	FT−VI (RDS-3)	FT−VII (RDS-1)	FT−VII (RDS-2)	FT−VII (RDS-3)	FT−VIII (RDS-1)	FT−VIII (RDS-2)	FT−VIII (RDS-3)
1	WGS-I (RDS-3)	36.02	39.87	25.07	21.41	25.57	29.24	26.54	30.74	36.57	32.31	40.75	36.16	32.09	36.02
2	WGS-I (RDS-4)	37.43	42.79	26.76	22.49	27.55	31.48	27.78	31.97	38.89	34.09	42.48	38.12	33.27	37.43
3	WGS-II (RDS-3)	33.11	37.18	23.11	19.96	23.99	28.16	24.59	29.42	34.65	29.52	39.74	34.78	29.55	33.11
4	WGS-II (RDS-4)	29.83	33.68	19.96	16.18	21.37	23.55	21.59	25.96	31.65	26.71	34.92	30.35	24.87	29.83
5	WGS-II (RDS-5)	31.48	35.84	21.42	18.02	22.42	25.89	22.73	28.37	32.87	28.34	37.31	32.68	26.64	31.48
6	WGS-III (RDS-3)	38.93	44.86	28.27	24.18	28.62	32.82	29.41	33.17	40.09	35.61	43.53	40.64	35.45	38.93
7	WGS-III (RDS-4)	40.31	47.83	29.36	26.05	30.41	35.07	30.86	35.16	41.31	37.59	45.67	41.81	36.91	40.31
8	WGS-IV (RDS-3)	42.47	50.54	30.56	27.63	32.26	36.37	32.67	37.92	43.35	40.47	47.55	43.96	38.79	42.47
9	WGS-V (RDS-3)	43.97	52.63	31.89	28.90	33.30	38.28	33.69	40.63	44.43	43.04	49.47	45.46	40.94	43.97
10	WGS-V (RDS-4)	46.37	53.73	33.19	30.53	34.66	40.34	35.09	42.47	45.69	45.12	51.15	46.47	43.43	46.37
11	WGS-VI (RDS-3)	27.09	32.14	18.46	14.97	19.75	22.40	20.22	24.18	30.21	25.51	32.45	27.78	23.29	27.09
12	WGS-VI (RDS-4)	25.29	30.82	17.13	13.46	18.15	20.84	18.93	23.13	28.79	23.70	29.63	26.63	20.73	25.29
13	WGS-VII (RDS-3)	22.67	29.79	15.63	12.12	16.85	19.31	17.32	21.17	25.82	21.44	27.57	24.01	18.96	22.67
14	WGS-VII (RDS-4)	20.65	27.65	13.69	10.50	15.27	16.58	15.58	19.52	23.58	20.14	26.50	21.52	17.65	20.65

5.2.2.2. *Goodness of Model Prediction Compared to Available Literature*

The best mechanistically developed model for complete FT synthesis (i.e. model FT−III with RDS-2/WGS-VII with RDS-4) was compared to the experimental values with respect to CO conversion, as well as the selectivity of CO_2, CH_4, C_2H_4, C_2H_6, C_3H_6, C_3H_8, C_4H_{10}, C_5H_{12}, C_6H_{14}, C_7H_{16}, and C_{5+} species. The parity plot that compares experiments against modelling prediction is presented in Figure 5-8 (a) and (b). These figures show that the relative error percentage between the model and experimental data of almost all data points was within $\pm$10%.

The best mechanistically developed model for complete FT synthesis was compared to the most recent findings in detailed kinetics of FT synthesis with respect to CO conversion and CO_2 selectivity, as well as the total experimental responses including both conversion and selectivities. The best complete model estimated the CO conversion at all process conditions with a mean relative error percentage of 3.3%. This value was lower than the lowest error reported by Yang et al (see Figure 5-9 (b)) and Teng et al (see Figure 5-9 (a)), Atashi *et al.* [114] with 9.2%, Mirzaei *et al.* [174] with 9.7%, Visconti *et al.* [152, 170] with 14.5% and 7.3% all accounted for CO conversion and were also better than that estimated for the power-law kinetic model developed in section 3.2, with 7.8% error. In addition, the best model predicted an average relative error of 10.3%, in terms of CO_2 selectivity, which was comparable with that obtained by Yang *et al.* [133] with the error of 10.04% and Teng *et al.* [123, 175] with errors of 7.53% and 11.93% respectively. In fact, the study conducted by Teng *et al.* [123] was solely based on the WGS reaction mechanism and as a result twelve WGS rate models were derived with an error in a range of 7.85-23.44%.

In addition, the best model estimated all experimental responses (including the conversion and selectivities) at all process conditions with a MAPD value of 5.93%, whereas Yang *et al.* [133] reported the value of 18.6% and 19.2% for their two best models considering combined FT and WGS mechanisms. Even the values of 33.99% and 35.52% reported by Wang *et al.* [134] and Teng *et al.* [175] respectively, was based on the total syngas consumption rate and product selectivity. The error obtained by the proposed mechanistic model was even better than that obtained by the power-law kinetic model developed in section 3.2, with a value of 13.23%. Another significant point was the ability of the model to predict the CO conversion, lighter product formation and CO_2 selectivity as a function of pressure and temperature. The model indicates a significant improvement compare to the previously developed rate model by the power-law kinetic rate expression (in section 3.2), that underestimated the CO_2, C_3, C_4, selectivity at a high temperature range ($T > 528$) and overestimated CO conversion and CH_4 selectivity at a low temperature range ($T < 528$).

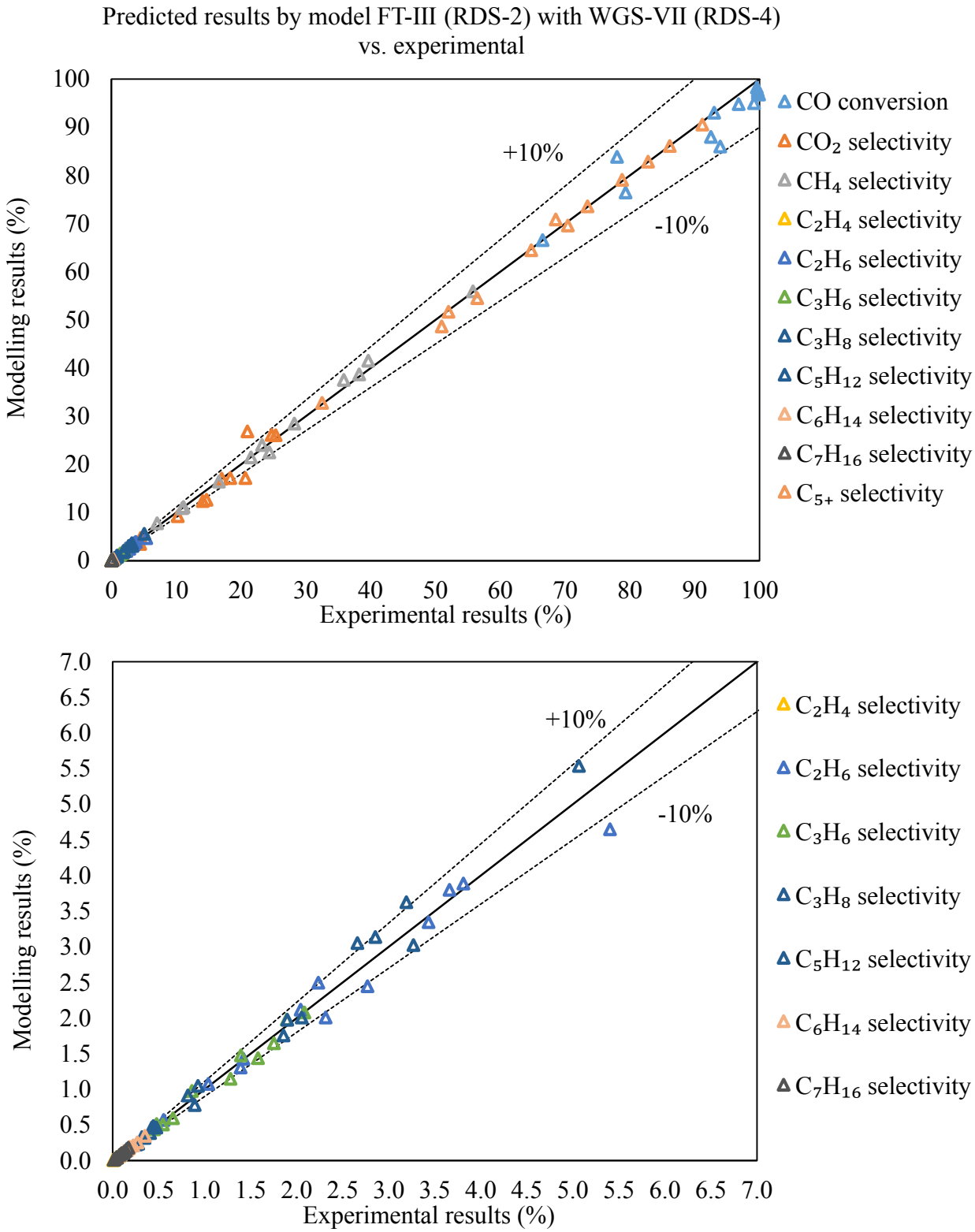

Figure 5-8 Parity plot: modelling prediction against experiments using best kinetic model (i.e. FT−III (RDS-2) with WGS-VII (RDS-4)).

Table 5-6 Model calibration against experimental data using kinetic model FT−III (RDS-2) with WGS-VII (RDS-4)

Experimental Run	Experiments vs. predictions	x_{CO}	S_{CO_2}	S_{CH_4}	$S_{C_2H_4}$	$S_{C_2H_6}$	$S_{C_3H_6}$	$S_{C_3H_8}$	$S_{C_4H_{10}}$	$S_{C_5H_{12}}$	$S_{C_6H_{14}}$	$S_{C_7H_{16}}$	$S_{C_{5+}}$
Test-01	Experiment	78.04	4.52	7.063	0.028	0.554	0.655	0.346	0.175	0.100	0.090	0.047	91.18
	Prediction	83.85	4.75	7.76	0.026	0.573	0.596	0.325	0.187	0.105	0.085	0.040	90.533
Test-02	Experiment	79.34	4.46	16.588	0.075	1.390	1.892	0.893	0.342	0.258	0.155	0.132	78.82
	Prediction	76.47	3.45	16.4	0.072	1.310	1.980	0.780	0.371	0.227	0.143	0.134	79.087
Test-03	Experiment	66.55	2.63	11.170	0.095	1.422	2.085	0.817	1.576	0.120	0.085	0.013	82.84
	Prediction	66.55	2.63	11.1	0.102	1.430	2.080	0.914	1.505	0.113	0.089	0.013	82.869
Test-05	Experiment	93.03	14.1	23.271	0.042	2.235	1.282	1.856	0.873	0.443	0.186	0.077	70.44
	Prediction	93.00	12.35	23.99	0.047	2.500	1.150	1.758	0.978	0.486	0.192	0.084	69.577
Test-06	Experiment	99.15	14.68	10.962	0.012	1.041	0.548	0.927	0.334	0.154	0.069	0.022	86.18
	Prediction	95.00	12.63	10.9	0.012	1.080	0.507	1.050	0.348	0.165	0.075	0.021	86.103
Test-07	Experiment	92.52	10.25	24.383	0.060	2.316	1.579	1.898	1.172	0.407	0.269	0.120	68.59
	Prediction	88.00	9.24	22.5	0.058	2.010	1.438	1.978	1.188	0.389	0.255	0.110	70.828
Test-10	Experiment	96.81	17.05	38.249	0.080	3.812	1.393	3.268	1.174	0.475	0.352	0.170	52.02
	Prediction	94.78	17.05	38.68	0.077	3.890	1.480	3.025	1.168	0.465	0.348	0.181	51.6804
Test-11	Experiment	99.96	20.7	21.549	0.010	2.044	0.479	2.054	0.382	0.085	0.066	0.044	73.48
	Prediction	96.80	17.17	21.43	0.011	2.120	0.514	2.010	0.329	0.091	0.062	0.050	73.5857
Test-12	Experiment	99.74	18.34	28.254	0.008	2.770	0.862	2.660	0.647	0.277	0.178	0.100	64.80
	Prediction	97.58	17.15	28.46	0.008	2.450	0.980	3.056	0.599	0.240	0.172	0.105	64.4474
Test-13	Experiment	93.95	21.01	39.656	0.078	3.660	1.753	2.854	1.026	0.346	0.223	0.145	50.97
	Prediction	86.00	26.85	41.53	0.076	3.800	1.650	3.140	1.150	0.319	0.213	0.145	48.654
Test-14	Experiment	99.74	24.75	35.888	0.018	3.433	0.449	3.192	0.549	0.318	0.125	0.027	56.47
	Prediction	97.12	26.12	37.5	0.017	3.350	0.470	3.627	0.526	0.331	0.138	0.029	54.51
Test-15	Experiment	99.59	25.36	55.817	0.021	5.404	0.451	5.068	0.701	0.427	0.073	0.024	32.56
	Prediction	98.23	26.03	55.89	0.023	4.650	0.440	5.540	0.687	0.465	0.077	0.022	32.793

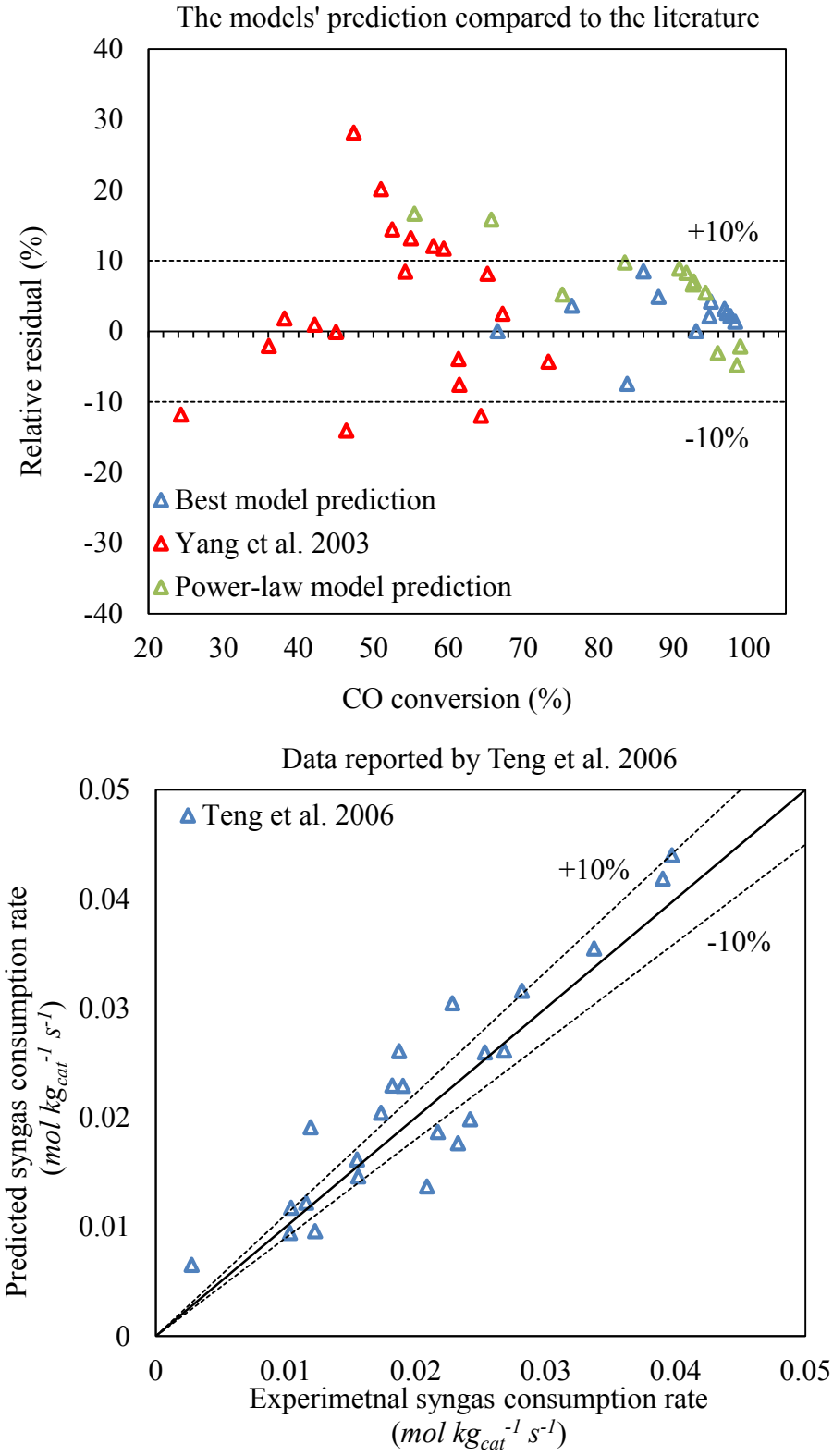

Figure 5-9 Comparison of calculated and experimental CO conversion obtained by the FT−III (RDS-2)/WGS-VII (RDS-4) mechanistic model, developed empirical power-law model, and those reported by Yang *et al.* [133] and Teng *et al.* [123, 175].

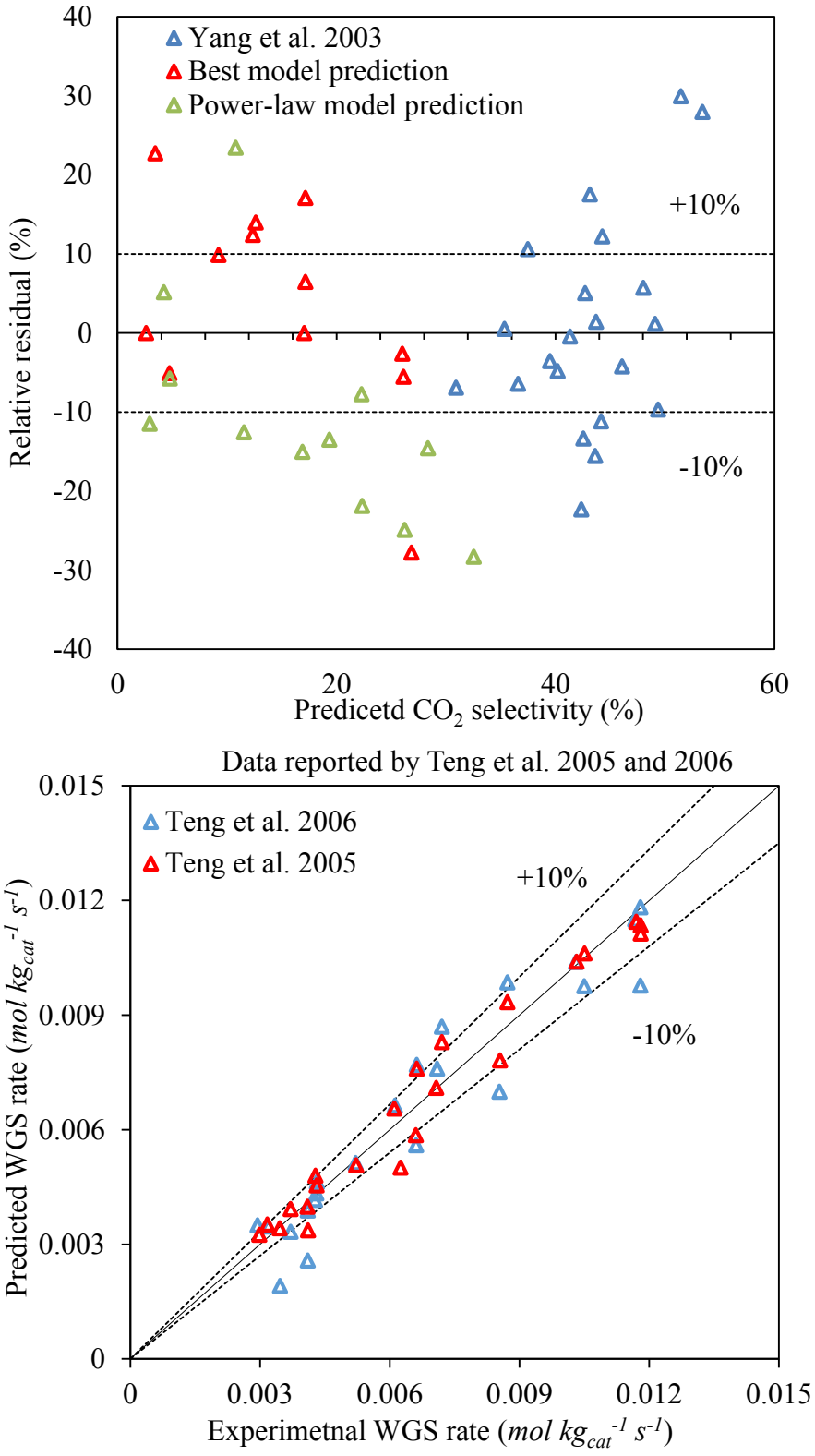

Figure 5-10 Comparison of calculated and experimental CO_2 selectivity obtained by the FT−III (RDS-2)/WGS-VII (RDS-4) model, power-law model, and those reported by Yang *et al.* [133] and Teng *et al.* [123, 175].

5.2.2.3. *ASF Deviation*

In addition, the details of product selectivities were predicted by the developed model which are illustrated in Figure 5-11, Figure 5-12, and Figure 5-13 for all experimental runs performed at different operating conditions with respect to temperature, pressure and space velocity. These figures show the model's fit in terms of n-paraffins and α-olefins with carbon atom number in the range of available hydrocarbons obtained from quantitative analysis of experimental studies. The model's fit was compared to an ASF product distribution model and the deviations of the experimental results in term of n-paraffin and α-olefins from the ASF model are clearly shown; while a satisfactory agreement with the developed kinetic model FT−III (RDS-2) with WGS-VII (RDS-4) is signified. Indeed, the change of the ASF slope with a growing carbon atoms number, as well as the high selectivity to methane and low ethylene selectivity, were the main causes of the typical deviations of the experimental distribution from the ASF model (see in Figure 5-11, Figure 5-12, and Figure 5-13). In contrast, the postulated mechanism and rate models could overcome the deviations of the experimental data, by adopting separate reaction sequences for methane and ethylene formation, and by postulating the combined alkyl/alkenyl mechanisms, in which the alkyl represents the paraffinic compounds and the alkenyl expressing the olefin hydrocarbons. As a consequence, separate rate constants (i.e. k_{meth} and k_{eth}) were defined for the reaction sequences that were responsible for the formation of these two components; while only one representative rate constants was introduced for the termination steps of both n-paraffin and α-olefin (i.e. $k_{t,par}$ and $k_{t,olef}$). These values are listed in Table 5-7 and will be discussed in detail in section 5.2.2.4.

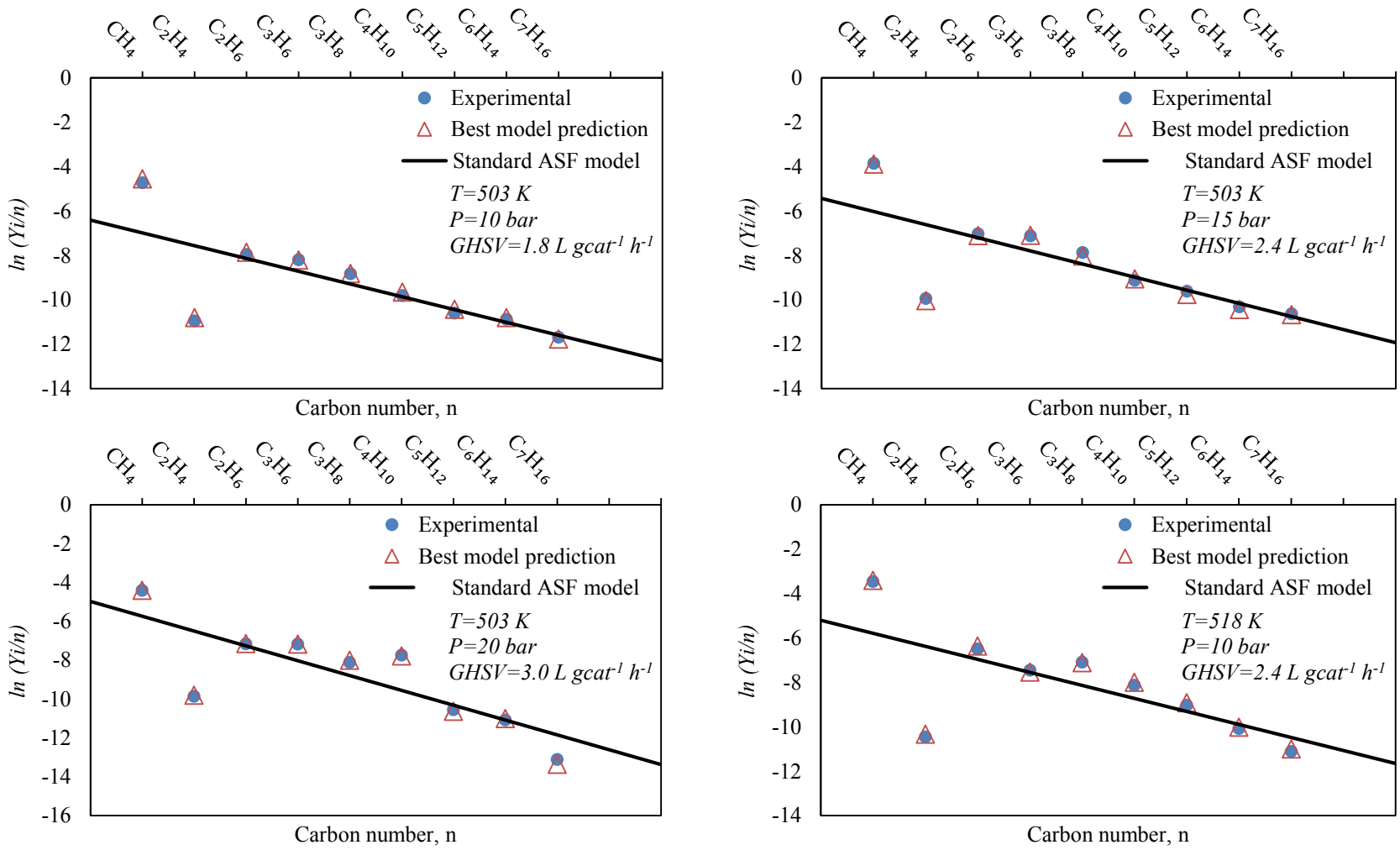

Figure 5-11 Product distribution comparison between FT−III (RDS-2)/WGS-VII (RDS-4) model prediction, standard ASF model, and the experimental results, logarithmic of mole-fraction (Y_i) to carbon number (n) ratio versus n; a): Test-01, b): Test-02, c): Test-03, d): Test-05.

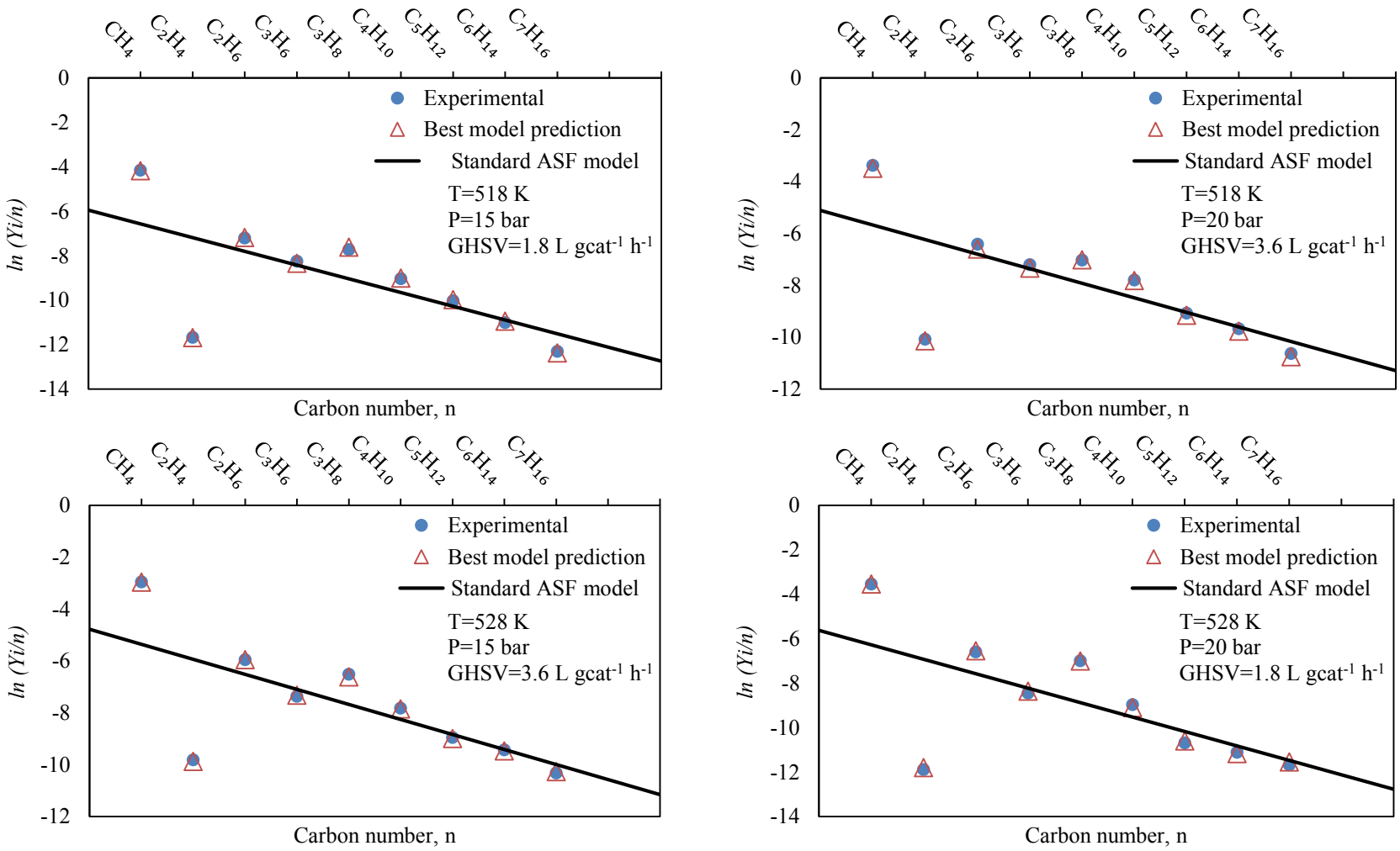

Figure 5-12 Product distribution comparison between FT−III (RDS-2)/WGS-VII (RDS-4) model prediction, standard ASF model, and the experimental results, logarithmic of mole-fraction (Y_i) to carbon number (n) ratio versus n; a): Test-06, b): Test-07, c): Test-10, d): Test-11.

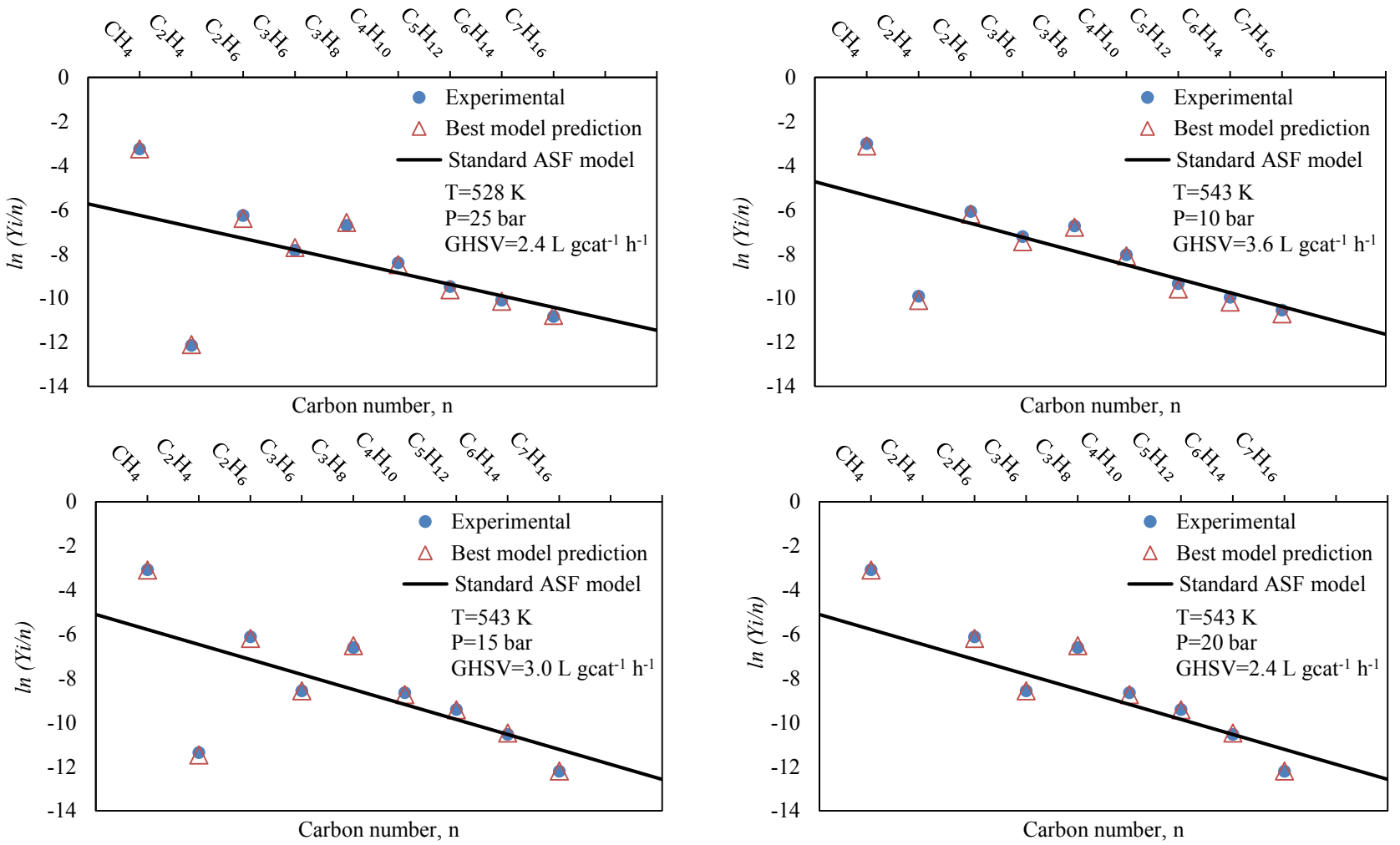

Figure 5-13 Product distribution comparison between FT−III (RDS-2)/WGS-VII (RDS-4) model prediction, standard ASF model, and the experimental results, logarithmic of mole-fraction (Y_i) to carbon number (n) ratio versus n; a): Test-12, b): Test-13, c): Test-14, d): Test-15.

5.2.2.4. *Evaluated Kinetic Parameters*

The estimated kinetic parameters for the comprehensive (combined) FT−III (RDS-2) with WGS-VII (RDS-4) kinetic model over a Co/SiO_2 catalyst, assuming that the slowest paths (RDSs) in the FT reaction model are steps 4, 8-15 and that of the WGS reaction is step 4, are listed in Table 5-7. Referring to section 4.8.2.1, it is worth noting that the numerical value of each parameter in this work, in addition to obtaining a satisfactory fit of the experimental data, was physically relevant and in good agreement with the expectations and literature studies. For instance, the adsorption equilibrium constant of hydrogen (K_{H_2}) was obtained three orders of magnitude lower than that of carbon monoxide (K_{CO}), which is comparable with the data reported by [176] with K_{CO}/K_{H_2} of $1.78/4.81\times10^{-3}$ (K_{CO} was three order of magnitude higher than K_{H_2}). This is related to the strong CO adsorption over a Co catalyst which was also indicated by the negative reaction order for CO partial pressure, as shown in section 5.2.1 by the empirical power-law rate expressions.

In addition, both the rate of reaction and the rate constant ($R_{i,par}$ and $k_{i,par}$) of step 8 in the FT−III (RDS-2) rate model, representing the formation of surface methyl species (chain initiator) in the chain initiation step, were found to be few orders of magnitude lower than the similar parameters (R_4 and k_4) for the reaction step 4, leading to the formation of $CH_2-\psi$ species i.e. the chain growth monomer. This signifies the fact that the latter reaction step is faster than the former reaction; therefore the chain initiation step was a more kinetically-relevant step than the CO activation process for the overall reaction scheme. However, $R_{i,par}$ and $k_{i,par}$ were found to be three orders of magnitude higher than those of ($R_{g,par}$ and $k_{g,par}$) in the propagation step (step 12); which in fact depended on the carbon atom number of the

growing intermediate ($C_nH_{2n+1}-\psi$). Indeed, the paraffins and olefins' formation rates ($R_{paraffins}$ and $R_{olefins}$) were found to be slower than the rate of formation of chain growth (by one order of magnitude), implying that the products' formation steps (steps 13 and 15) are the RDSs in the overall FT process over a Co/SiO_2 catalyst. To sum up, it can be concluded that:

$$k_4 \gg k_8 = k_{CH_3} = k_{i,par} =\gg k_{12} = k_{g,par} \gg k_{13} = k_{paraffins} \;\&\; k_{15} = k_{olefins}$$

$$R_4 \gg R_8 = R_{CH_3} = R_{i,par} =\gg R_{12} = R_{g,par} \gg R_{13} = R_{paraffins} \;\&\; R_{15} = R_{olefins}$$

The activation energies of the chain initiation, propagation and termination steps for the alkyl route, leading to the formation of paraffins, were significantly lower than those of the alkenyl route, leading to the formation of olefins. This is in line with the expectations as the paraffins formation rates were significantly higher than those of the olefins (considering the same carbon atom number) obtained at all experiment conditions. The activation energy for the chain growth step of the alkyl route ($E_{g,par}$) was predicted to be 82.57 $kJ\ mol^{-1}$. This was lower than the activation energies for that of the alkenyl route ($E_{g,olef} = 88.31$ kJ mol^{-1}) and the activation energies for the chain initiation ($E_{i,par} = 90.22\ kJ\ mol^{-1}$ and $E_{i,olef} = 95.34\ kJ\ mol^{-1}$) and termination ($E_{t,par} = 95.63\ kJ\ mol^{-1}$ and $E_{t,olef} = 100.22\ kJ\ mol^{-1}$) steps. The higher activation energies for the chain termination steps indicate that the assumptions related to RDSs for the product formation are reasonable. The relatively higher activation energy barriers of the olefins' ($E_{t,olef}$) formation compared to those of the paraffins ($E_{t,par}$), signifies the higher paraffins' selectivities over the Co/SiO_2 catalyst. Again, the rate of formation of the paraffins with ''n'' carbon atoms ($R^n_{paraffins}$) was found to be higher than

the rate of formation of the corresponding olefins ($R^{n}_{olefins}$), suggesting the preferred formation of saturated products (i.e. paraffinic compounds) in the FT synthesis over a Co/SiO_2 catalyst. The activation energy of CH_4 formation (E_{meth}) was found to be significantly lower (76.5 $kJ\ mol^{-1}$) than that of lower carbon atom number formation, suggesting the considerably higher rate of formation as well as selectivity for CH_4 than those of other paraffins and olefins, in line with that reported by the literature [133, 169, 175, 177] and significantly lower than those obtained in the case of Co, Fe-and Ni catalysts by other investigators [163-167, 172]. In addition, the pre-exponential factor for methane formation ($k_{0,meth}$) was estimated to be one order of magnitude greater than the same coefficient for desorption of heavier paraffins ($k_{0,t,par}$). The above statements, together with the higher surface coverage of $CH_3-\psi$ intermediate relative to the other growing species ($C_nH_{2n+1}-\psi$; $n \geq 2$), signifies the main justifications of a higher selectivity to methane than those of other FT synthesis products. The estimated rate constant for ethylene (k_{eth}) was two orders of magnitude smaller than that of the other olefins ($k_{t,olef}$) in order to guarantee a good fit of the product distribution data, which are characterized by a low selectivity to ethylene, as shown in previous sections. Additionally, the activation energy of the ethylene (E_{eth}) was higher than those of olefins, paraffins, and methane which led to its lower rate of formation and productivity. The activation energy barriers of the WGS reaction were found to be 83.6 $kJ\ mol^{-1}$, in line with the expectations regarding the considerable selectivity to CO_2 co-products and in the range of the reported values by other investigators (28–125 $kJ\ mol^{-1}$) [7, 120, 121, 133, 175, 178]. This value was higher than that of CH_4, in line with the activation energies for chain growth steps and considerably lower than that for olefins and paraffins' formation steps, which justifies the relatively higher selectivities to CO_2 formation in the present study at specified operating conditions for FT synthesis over a Co/SiO_2 catalyst.

Table 5-7 Optimum values of estimated kinetic parameters of comprehensive combined FT−III (RDS-2) and WGS-VII (RDS-4)

Kinetic parameter	Unit	Value	t_{value}	Kinetic parameter	Unit	Value	t_{value}
$k_{0,meth}$	$mol\ kg^{-1}\ s^{-1}$	5.10×10^{7}	162.84	$k_{0,4}$	$mol\ kg^{-1}\ s^{-1}$	9.25×10^{6}	62.10
E_{meth}	$kJ\ mol^{-1}$	76.54	179.98	E_4	$kJ\ mol^{-1}$	74.98	154.63
$k_{0,eth}$	$mol\ kg^{-1}\ s^{-1}$	2.03×10^{4}	223.40	$k_{0,WGS}$	$mol\ kg^{-1}\ s^{-1}$	6.89×10^{5}	130.64
E_{eth}	$kJ\ mol^{-1}$	125.28	49.48	E_{WGS}	$kJ\ mol^{-1}$	83.59	299.32
$k_{0,i,par}$	$mol\ kg^{-1}\ s^{-1}$	1.14×10^{7}	327.70	$K_1(K_{CO})$	bar^{-1}	1.78	381.40
$E_{i,par}$	$kJ\ mol^{-1}$	90.22	248.64	$K_2(K_{H_2})$	bar^{-1}	4.81×10^{-3}	230.29
$k_{0,g,par}$	$mol\ kg^{-1}\ s^{-1}$	3.04×10^{3}	95.79	$K_3(K_{HCO})$	–	5.53	356.09
$E_{g,par}$	$kJ\ mol^{-1}$	82.57	282.68	$K_6(K_{OH})$	–	5.12×10^{-2}	137.05
$k_{0,t,par}$	$mol\ kg^{-1}\ s^{-1}$	7.85×10^{3}	132.00	$K_5(K_{CH})$	–	2.19	348.80
$E_{t,par}$	$kJ\ mol^{-1}$	95.63	191.64	$K_7(K_{CH_2})$	–	4.36	301.85
$k_{0,i,olef}$	$mol\ kg^{-1}\ s^{-1}$	8.44×10^{6}	134.76	K_{W_1}	bar^{-1}	4.15×10^{-2}	367.16
$E_{i,olef}$	$kJ\ mol^{-1}$	95.34	252.90	K_{W_2}	bar^{-1}	7.84×10^{-2}	300.04
$k_{0,g,olef}$	$mol\ kg^{-1}\ s^{-1}$	7.56×10^{3}	45.04	K_{W_3}	–	2.67	390.72
$E_{g,olef}$	$kJ\ mol^{-1}$	88.31	181.78	K_{W_5}	bar	5.40×10^{1}	38.50
$k_{0,t,olef}$	$mol\ kg^{-1}\ s^{-1}$	1.75×10^{3}	75.39				
$E_{t,olef}$	$kJ\ mol^{-1}$	100.22	87.81	MAPD = 5.93%			

*Results of statistical analysis:
(i) F-test: $F_{\text{ratio}} = 921.75 > F_{critical}\ (n-m, m-1; 1-\alpha) = F_{critical}\ (144-30, 30-1; 1-0.01) = 2.14$
(ii) t-test: lowest t-value $= 38.5 > t_{critical}\ (n-m; 1-\alpha) = t_{critical}\ (144-30; 1-0.01) = 2.36$

5.3. Model Validation Results

This section provides the details of model validation. Model validation was carried out subsequent to completion of the model calibration and the estimation of proper kinetic parameters. The overall purpose of the validation study was to ensure that the model provides a robust and realistic assessment of all the parameters defined by the mathematical model e.g. kinetic parameters, rate of reactants' consumption and products' formation. In order to ensure the model is relevant to an appropriate level, it was assessed against experimental data at four different operating conditions (tabulated in Table 5-8), which were available for validation, with respect to: temperature; pressure; and space velocity; as well as at a constant H_2/Co molar ratio of 2. Table 5-8 shows the values of conversion and selectivities obtained from model validation and then compares them with those of the experiments at four different operating conditions (see Table 5-8 for process conditions). To verify whether or not a model is valid, the MAPD value between predictions and experiments was determined. The MAPD obtained between the variables was at 14.62% which indicates that the model was satisfactorily validated against the measured data.

Table 5-8 Results obtained by model validation against experimental data at four different operating conditions with respect to reaction temperature, total inlet pressure and space velocity, values of conversion and selectivities

	T	P_{tot}	GHSV	P_{H_2}	P_{CO}	X_{CO}	S_{CO_2}	S_{CH_4}	$S_{C_2H_4}$	$S_{C_2H_6}$	$S_{C_3H_6}$	$S_{C_3H_8}$	$S_{C_4H_{10}}$	$S_{C_5H_{12}}$	$S_{C_6H_{14}}$	$S_{C_7H_{16}}$	$S_{C_{5+}}$
	(K)	*(bar)*	*($Nm\ell$ (STP) g_{cat}^{-1} h^{-1})*	*(bar)*	*(bar)*	%	%	%	%	%	%	%	%	%	%	%	%
													Measured				
Test-04	503	25	3600	8.5	4.25	66.55	1.71	12.60	0.08	0.97	1.56	0.56	1.22	0.76	0.48	0.23	83.00
Test-08	518	25	3000	8.5	4.25	98.22	11.45	16.25	0.04	1.54	1.28	1.13	0.78	0.47	0.13	0.06	78.97
Test-09	528	10	3000	3.30	1.70	90.78	16.38	28.72	0.10	3.76	2.52	2.85	1.65	1.03	0.64	0.31	60.41
Test-16	543	25	1800	8.5	4.25	99.88	24.93	49.72	0.01	4.54	0.08	4.24	0.41	0.19	0.07	0.02	41.02
													Predicted				
Test-04						69.50	1.86	13.56	0.07	1.10	1.88	0.66	0.99	0.62	0.29	0.14	81.74
Test-08						91.26	10.94	19.60	0.03	1.68	1.12	1.25	0.65	0.39	0.13	0.07	75.67
Test-09						93.60	15.50	30.21	0.08	3.65	2.00	2.20	2.10	1.31	0.63	0.30	59.76
Test-16						95.50	24.00	48.60	0.02	4.54	1.50	3.99	0.51	0.17	0.06	0.01	40.84

5.4. Summary and Conclusions

In this chapter, the key characteristics of experimental facility, setup and procedure were highlighted. The experimental results at sixteen different process conditions were used for calibration and validation of the developed mathematical model and kinetics model. The kinetic models which were developed by the two approaches (i.e. power-law model and combined mechanistic FT/WGS mechanisms) described in Chapter 3, were assessed against the experimental data. Twelve out of sixteen of the experimental data were used for the calibration of the model. The results showed that the combined developed model FT–III with RDS-2/WGS-VII with RDS-4, exhibited excellent agreement with the measured data compared to the proposed power-law kinetic expression as well as the literature. The goodness of fit was assessed by mean absolute percentage deviation and statistically analysed by employing the *F*-statistic. In addition, it was shown that the obtained kinetic parameters were statistically significant by using the *t*-statistic. The F_{ratio} and t_{value} of 55.34 and 7.14 (the lowest t_{value}) were obtained respectively when the power-law model was taken into account and the cumulative probability of the F-distribution was 0.99. Similarly, the F_{ratio} and t_{value} of 921.75 and 38.50 (the lowest t_{value}) were attained when the model FT−III with RDS-2/WGS-VII with RDS-4 was postulated. Among different models, this was the highest F_{ratio}, hence it was considered as the best model and that it was statistically adequate. The MAPD of 13.23% by empirical power-law model was achieved; however, better agreement with measured data was predicted using developed model FT−III with RDS-2/WGS-VII with RDS-4 the MAPD of 5.93%. Such results highlight the potential of this combined mechanistic FT/WGS mechanism as well as reaction networks that can further improve the performance of FT synthesis. Consequently, such information can provide guidelines for the design of more active and selective catalyst materials.

CHAPTER 6

PARAMETRIC STUDIES AND OPTIMIZATION

6.1. Optimization Methodology

As discussed in the previous chapters, the performance of the reactor is characterized not by one but by several parameters such as reaction rates, reactant conversions as well as products' selectivities. Thus, such a feature requires multi-objective (opposed to single-objective) optimization of all performance parameters. Such an optimization problem is often complex especially if the objective functions (*OF*) are conflicting with respect to each other. These problems give rise to a set of trade-off optimal solutions, popularly known as Pareto-optimal solutions [179]. Therefore, due to the diversity in solutions, these problems can be solved effectively using evolutionary algorithms which utilize a population search approach and results are a group of optimal solutions rather than a single solution.

Among the evolutionary optimization algorithms, the genetic algorithm (GA) is one of the most efficient approaches. The GA is based on the biological evolution and it is started with

the creation of an initial population whose elements are randomly selected in the whole design space. Different procedures are then applied in order to successively generate a new population containing better elements. The performance of an individual is measured by its fitness. Pairs of individuals are selected from this population based on their objective function values. Then each pair of individuals undergoes a reproduction mechanism to generate a new population in such a way that fitter individuals will spread their genes with higher probability. The children replace their parents and as this proceeds, inferior traits in the pool die out due to the lack of reproduction. At the same time, strong traits tend to combine with other strong traits to produce children who perform better. This procedure is repeated for the next generation until the maximum specified number of generations is reached i.e. 5000 generations (see Table 6-3).

The GA can deal with complex optimization problems such as multi-dimensional, non-continuous, and non-linear problems. Moreover, the GA locates the global optimal values reliably from a population of solutions, even if many local optima exist and prevents the convergence to sub-optimal solutions. This distinguishes the GA from the traditional optimization techniques that are reliant on the initial guesses; while the GA is far less sensitive to the initial conditions enforced on it. The GA will eventually reject any solution that does not show enough promise; this helps to provide more flexibility and robustness during the optimization [180].

The most common and straightforward method of defining the objective functions in multi-objective optimization problems is based on the weighted sum approach. As the name manifests, such an approach scalarizes all objective functions into a single objective, by multiplying each objective with a user-specified weight as shown by Equation 6-1:

$$Minimize\ or\ Maximize \qquad F(x) = \sum_{m=1}^{M} w_m f_m(x), \qquad \text{Equation 6-1}$$

$$Subject\ to \quad g_j(x) \geq 0 \qquad j = 1,2,\dots,J \qquad \text{Equation 6-2}$$

$$where \quad x_i^{lower} \leq x_i \leq x_i^{upper} \qquad i = 1,2,\dots,n \qquad \text{Equation 6-3}$$

$$0 \leq w_m \leq 1 \qquad m = 1,2,\dots.,M \qquad \text{Equation 6-4}$$

Although simple, the outcome of the objectives' values with this approach is strongly reliant on the specified weight and also the scaling factor utilized to normalize all objective functions to the same order of magnitude.

To alleviate such deficiency, a NSGA–II (Non-dominated Sorting Genetic Algorithm-II) was employed to conduct the multi-objective optimization. The NSGA–II is an advanced version of the GA which attempts to find multiple Pareto-fronts with emphasis on non-dominated solutions and operates based on controlled elitism concepts [179]. Non-dominated solutions are the points on the first Pareto-front solution so that selecting any one of them in place of another will always sacrifice the quality of at least one objective, while improving at least one other. Such a feature is advantageous as it allows trade-off between wide ranges of optimal solutions before selecting the final one. The NSGA–II is a very fast and efficient search mechanism that utilizes crowding distance as the diversity mechanism and classifies the population into non-dominated fronts, using the Pareto-ranking approach introduced by [181]. In contrast to the weighted sum approach, in multi-objective optimization with the NSGA–II,

all objectives are specified individually to be either maximized or minimized as shown in the mathematical form below:

$$Minimize\ or\ Maximize \qquad f_m(x), \quad m = 1,2,\dots,M \tag{Equation 6-5}$$

$$Subject\ to \quad g_j(x) \geq 0 \qquad j = 1,2,\dots,J \tag{Equation 6-6}$$

$$where \quad x_i^{lower} \leq x_i \leq x_i^{upper} \qquad i = 1,2,\dots,n \tag{Equation 6-7}$$

The weighted sum approach formulated by Equation 6-1 only provides the best solution corresponding to the minimum or maximum value of the single-objective function that lumps all different objectives into one objective. Therefore, it cannot provides a set of alternative solutions for comparison of various objectives especially if they are conflicting. In contrast, the multi-objective optimization with NSGA–II is advantageous as it provide a wider range of alternative solutions and allows more flexibility during decision-making and selecting the optimal solution from the Pareto-front. Such a procedure can be performed based on higher-level information by evaluating the advantageous and drawbacks of each optimal solution from the Pareto-front. In the context of this thesis such information depends on the variation rate of objective functions on the Pareto-front charts (see Figure 6-21 to Figure 6-23 in section 6.3). Further details about NSGA-II can be found in [179, 182].

6.2. Parametric Studies

Prior to the optimization, it was vital to conduct comprehensive parametric studies using the developed model in order to investigate the effect of input variables (i.e. reaction temperature, total pressure, space velocity, and H_2/CO molar ratio) on the reactor's critical performance parameters (i.e. syngas conversions and products' selectivities), which are dependent variables of the model. Such parametric studies are based on variation of one input parameter in a defined range (see Table 6-1), while other inputs were kept constant and then plotting its effects on the performance parameters mentioned above. Such plots are then examined to identify those input parameters that have the most substantial effects on dependent variables.

Table 6-1 Range of variation of parameters defined for parametric study

Parameters	Reference	Unit	Temperature Effects Investigation	Pressure Effects Investigation	GHSV Effects Investigation	H_2/CO Effects Investigation
T	[114]	(*K*)	470-530	500	520	510
P	[114]	(*bar*)	15	1-30	10	10
GHSV	[114]	($Nm\ell$ *(STP)* g_{cat}^{-1} h^{-1})	7500	2400	1800-6000	4500
H_2/CO	[114]	(*mol/mol*)	2	2	2	1-3.2

6.2.1. Effects of Operating Temperature

Figure 6-1 shows the influences of the reaction temperature on CO and H_2 conversions, as well as the selectivities of CO_2, CH_4, and C_{5+} products at a constant total inlet pressure of 15

bar, H_2/CO ratio of 2 and gas hourly space velocity (GHSV) of 7500 $Nm\ell\ (STP)\ g_{cat}^{-1}\ h^{-1}$. The effects of temperature on the light paraffinic content (i.e. C_2-C_7) of the products are illustrated in Figure 6-2. In addition, the product olefins as well as the changes of olefin to paraffin ratio with respect to the temperature are depicted in Figure 6-3. Figure 6-1 manifests the significant growth of the catalyst's activity and its performance upon the raising of the reaction temperature in terms of the syngas components' conversion, suggesting that the temperature has positive effects on CO and H_2 conversion in which both quantities increase substantially from about 35% to 92% and 35% to 74% respectively, by increasing the temperature from 470 *K* to 530 *K*. The undesired CO_2 selectivity increases from about 0.04% to 13% upon the rising of the temperature. From Figure 6-1 to Figure 6-3, one can conclude that the increment of temperature results in a shift towards products with low molecular weight hydrocarbons on a Co/SiO_2 catalyst i.e. methane, olefins: C_2-C_3, paraffins: C_2-C_7. It is apparent that the formation of heavier hydrocarbons (C_{5+}) is favoured at lower temperatures; while at high temperatures, the reactor produces higher low molecular weight products (see Figure 6-1 to Figure 6-3). The total light hydrocarbon products with carbon atoms between C_2-C_7 increases from 2.75% to 10.31% and there are increases of methane from 3.7% to 20.3%, while the selectivity of C_{5+} decreases substantially from about 94% to 71%. Also, the results justify the decrease of the low molecular weight olefin to paraffin ratio upon increasing the temperature (see Figure 6-3). Hence, low temperatures favour the higher formation of heavy liquid products, the lower undesired CH_4 and CO_2 selectivities, as well as a higher olefin to paraffin ratio. In contrast, high temperatures are desirable to increase the conversion of syngas components (CO and H_2), the paraffin to olefin ratio, and for the production of light hydrocarbons, especially CH_4.

As shown in Chapter 5, methane has a higher temperature dependency compared to other hydrocarbons due to its lower activation barriers. As expected, methane and desired heavier

hydrocarbons had opposite variations with respect to temperature change. The question is why the effects of temperature on outlet liquid phase selectivity are different from methane selectivity and syngas conversion. As depicted in Figure 6-1, the positive effects of temperature on syngas conversion is due to the nature of the Arrhenius expression (i.e. the temperature dependency factor of Arrhenius expression is expressed as an exponent term: $e^{-E_a/RT}$) and reaction rate since both are temperature dependent and positively impact the conversion; all the reactions are enhanced with a greater temperature so more reactants are consumed. However, products' distribution is not directly proportional to the temperature. This can be explained by the nature of the chain growth probability (α). Indeed, α is defined by the rate of propagation (growth) and termination steps through Equation 6-8. Also, mole fraction, y_n, with n carbon atom number is equated to α through Equation 6-9. It is worth noting that when the value of alpha is high, it is proportional to y_n ($\alpha \propto y_n$). The α value is in the range of 0 to 1 and is closer to 1 when the desired FT products are heavy hydrocarbons. On the other hand, α is inversely proportional to the termination reaction rate (R_t), and that all reaction rates (e.g. R_g, R_t, and etc.) increases upon the increasing of the temperature. Therefore, at higher temperatures, the chain growth probability (considering heavy FT products) value would be lower, suggesting that the alpha value is inversely proportional to the temperature ($\alpha \propto 1/T$) and with the lower alpha value the mole fraction would be lower as well. This can justify why the increase of temperature decreases the selectivity of the liquid product, while that of light hydrocarbons grows. In other words, from the very different values of the activation energies (see Table 5-7), the C_{5+} products' formation is noticeably favoured over that of the light hydrocarbons upon the decrease of reaction temperature.

To sum up, the increase of temperature increases the rate constants and all reaction rates (through the Arrhenius equation), followed by the decrease of chain growth probability;

therefore this results in the decrease of the mole fraction of the liquid content of the products. The olefin to paraffin ratio can also be explained by the same reason and considering the greater reaction rate for the termination step of the paraffinic compounds ($R_{t,par}$) compared to that of the olefins ($R_{t,olef}$) due to lower activation energy barriers of the former compared to the latter (see Table 5-7). The lower activation barriers of the former causes the termination reaction rate to grow faster with an increase of temperature compared to the latter. Assuming a separate alpha value for paraffins (α_P) and olefins (α_O), the denominator of Equation 6-8 would be greater for α_P than that of the olefins, implying higher α_O compared to that of paraffins. Therefore, the mole fraction of the olefins would increase faster than for paraffins. In contrast to heavier hydrocarbon, the y_n value for lighter hydrocarbons has inverse proportionality to α value. In this case, since the α_O/α_P ratio increases upon the increment of reaction temperature, hence the y_O/y_P decreases due to their inverse proportionality. This justifies why the increase of temperature decreases the selectivity the olefins to paraffins ratio.

$$\alpha = \frac{R_g}{R_g + R_t} \qquad \text{Equation 6-8}$$

$$y_n = (1-\alpha)\alpha^{n-1} \qquad \text{Equation 6-9}$$

Figure 6-4 and Figure 6-5 indicate how the CO and H_2 conversions and mole fractions at the centreline of the reactor are influenced by the reaction temperature when the process conditions are set at constant total pressure of 25 *bar*, H_2/CO ratio of 2 and at two different high space velocity of 4500 $Nm\ell$ *(STP)* g_{cat}^{-1} h^{-1} (Figure 6-4) and 7500 $Nm\ell$ *(STP)* g_{cat}^{-1} h^{-1} (Figure 6-5). From these families of figures, it is apparent that the CO and H_2 mole fractions decrease, while their consumptions and conversions enhance significantly along the axial distance of the reactor bed length as the temperature rises, regardless of the syngas space velocity, as is

illustrated in Figure 6-4 (the case with the lower space velocity) and Figure 6-5 (the case with the higher space velocity). However, later it will be shown that the CO and H_2 are more sensitive to GHSV at lower temperature conditions. Generally, these figures imply that the consumption of syngas species increases faster and their mole fraction decreases drastically upon increasing the temperature.

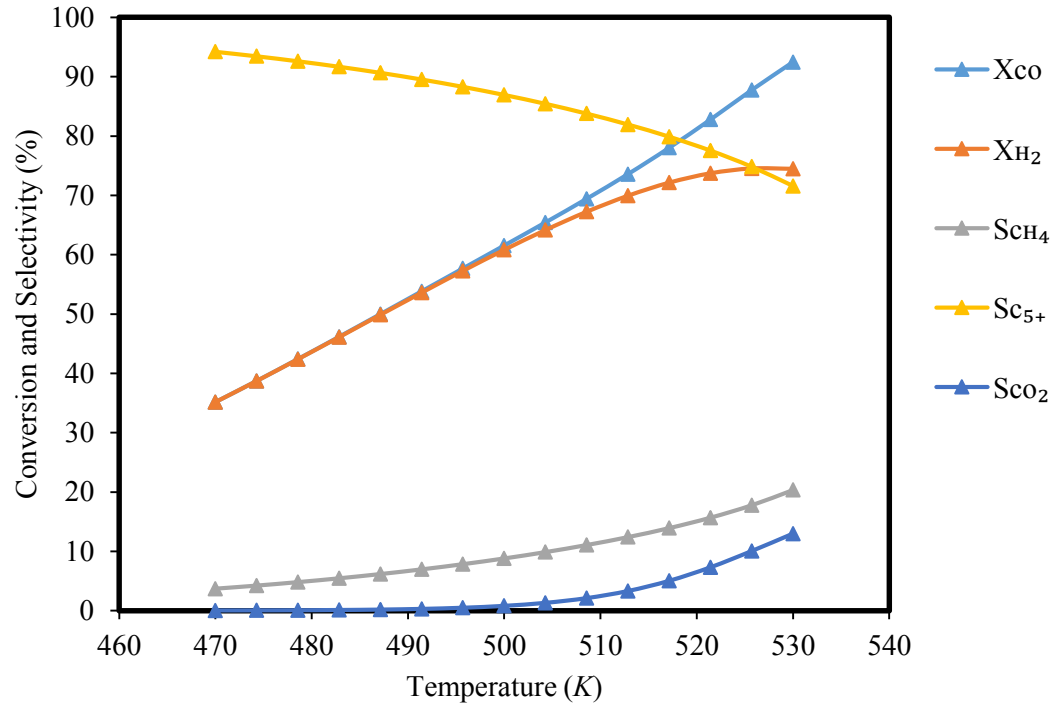

Figure 6-1 Effects of reaction temperatures on CO and H_2 conversions as well as the CO_2, CH_4, and C_{5+} products' selectivities at constant P = 15 *bar*, GHSV = 7500 $Nm\ell\ (STP)\ g_{cat}^{-1}\ h^{-1}$ and $H_2/CO = 2$.

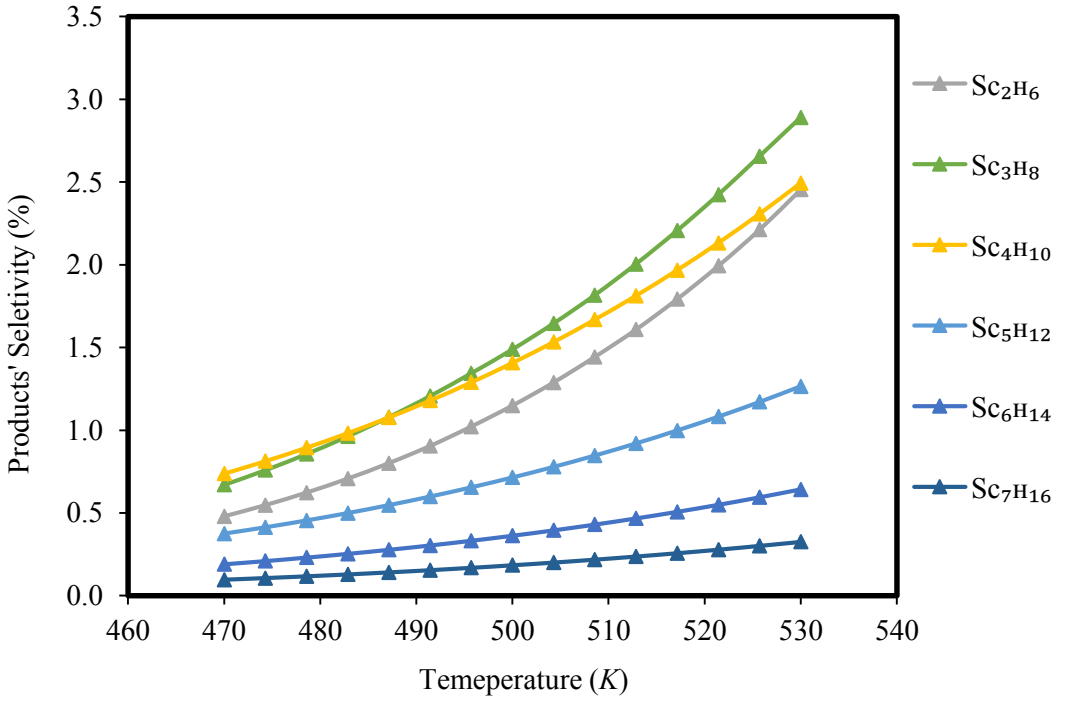

Figure 6-2 Effects of reaction temperature on the light paraffinic content (i.e. C_2-C_7) of the products at constant P= 15 *bar*, GHSV= 7500 $Nm\ell\ (STP)\ g_{cat}^{-1}\ h^{-1}$ and $H_2/CO = 2$.

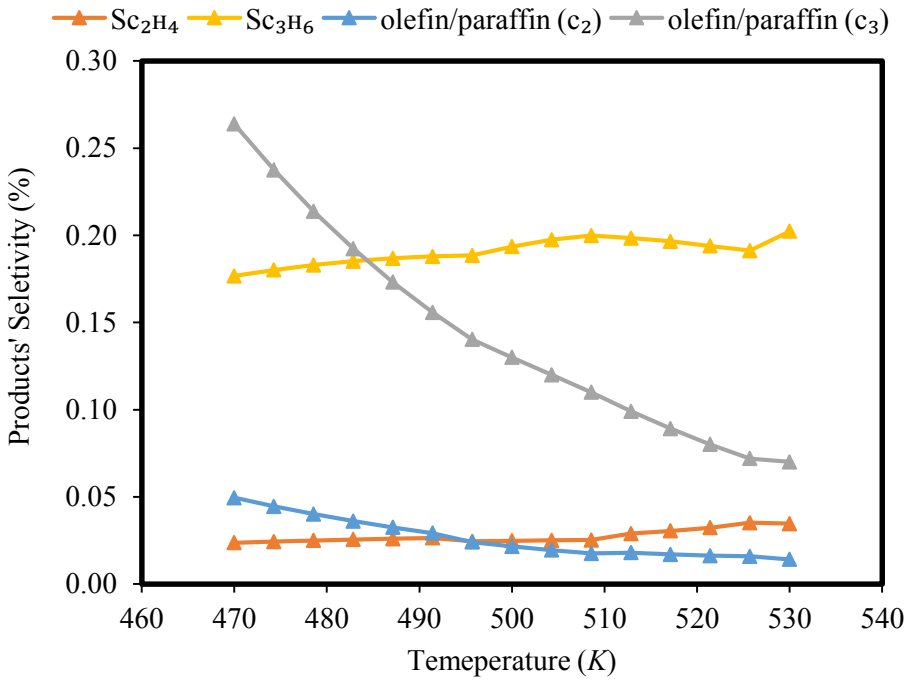

Figure 6-3 Effects of reaction temperature on the product olefins as well as the changes of olefin to paraffin ratio at constant P= 15 *bar*, GHSV= 7500 $Nm\ell\ (STP)\ g_{cat}^{-1}\ h^{-1}$ and H_2/CO= 2.

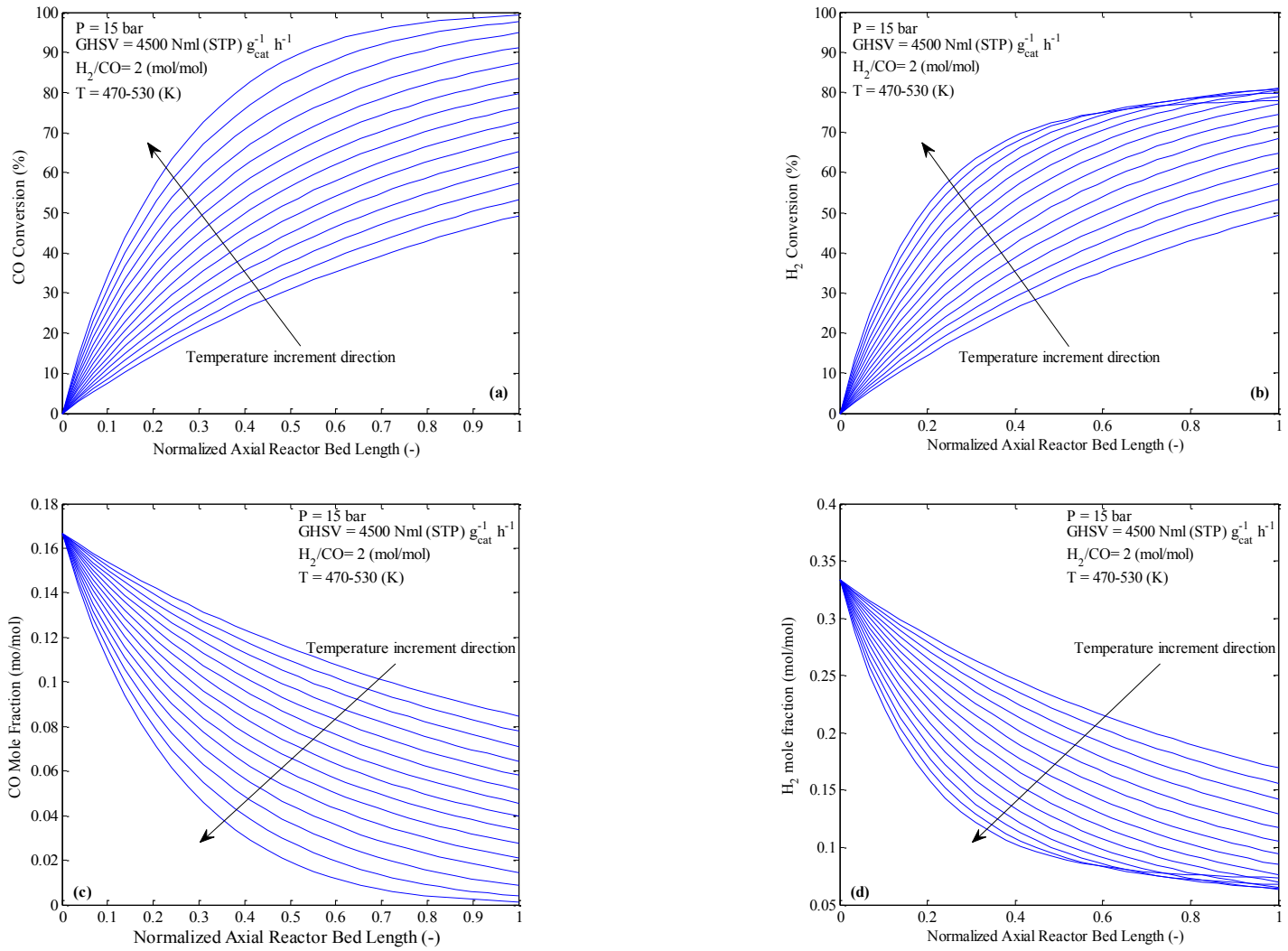

Figure 6-4 The changes of conversion of (a) CO and (b) H_2 and mole fraction of the same species (c) and (d) respectively along the normalized axial dimension of the reactor bed length, effects of temperatures on their behaviour at constant P= 15 *bar*, GHSV= 4500 $Nm\ell\ (STP)\ g_{cat}^{-1}\ h^{-1}$ and H_2/CO= 2.

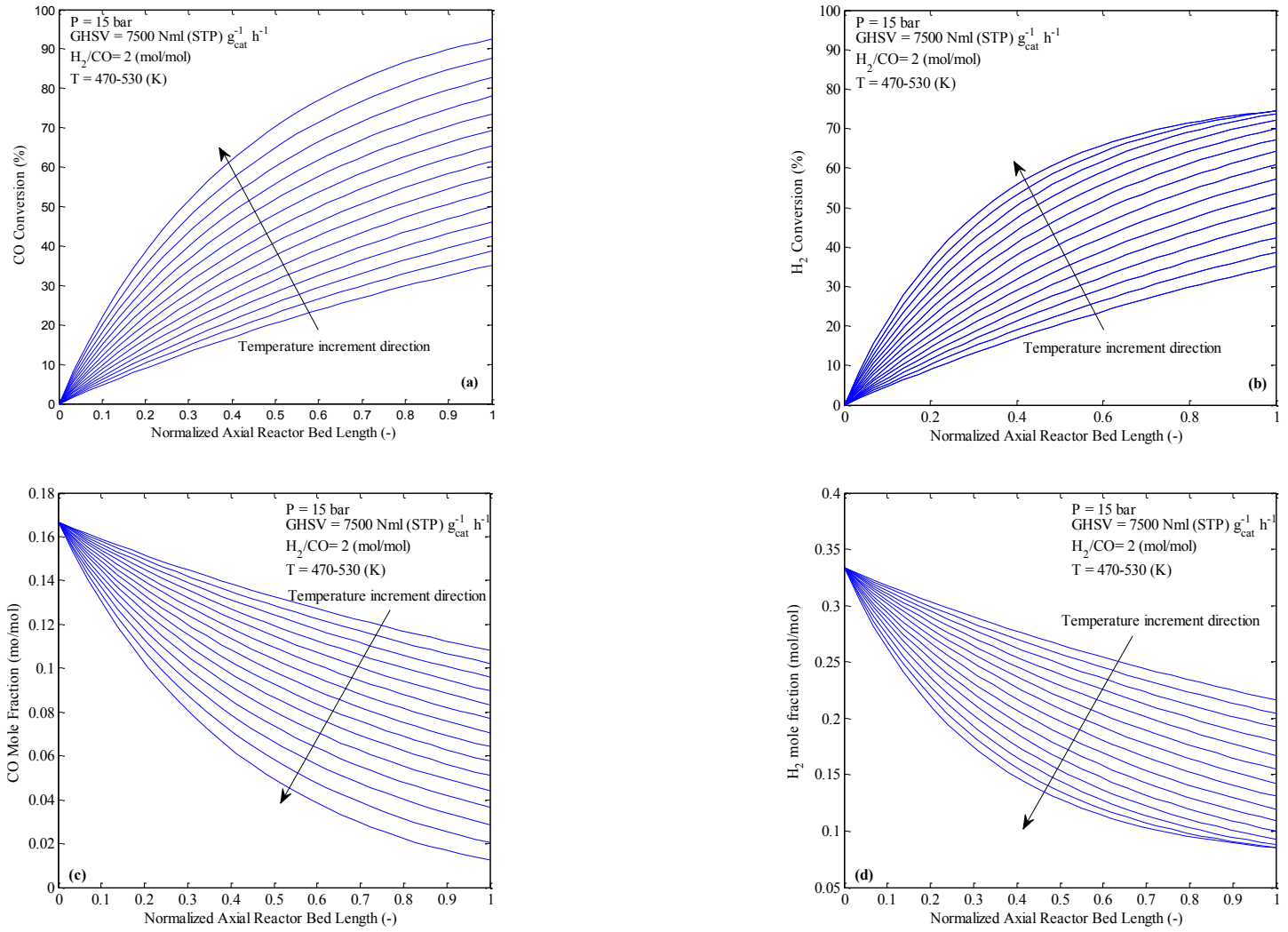

Figure 6-5 The changes of conversion of (a) CO and (b) H_2 and mole fraction of the same species (c) and (d) respectively along the normalized axial dimension of the reactor bed length, effects of temperatures on their behaviour at constant P= 15 *bar*, GHSV= 7500 $Nm\ell\ (STP)\ g_{cat}^{-1}\ h^{-1}$ and H_2/CO= 2.

6.2.2. Effects of Operating Space Velocity

The changes of CO and H_2 conversions, as well as, selectivities of CO_2, CH_4 and C_{5+} under different process conditions with respect to gas hourly space velocity (GHSV) on a Co/SiO_2 catalyst are illustrated in Figure 6-6. Their influences on selectivities of paraffins with carbon atom C_2-C_7 are also shown in Figure 6-7. In addition, the product olefins as well as the changes of olefin to paraffin ratio with respect to the GHSV are indicated in Figure 6-8. This study was performed at the constant reaction temperature, total inlet pressure, and H_2/CO molar ratio listed in Table 6-1.

From Figure 6-6, the highest conversion of both CO and H_2 were obtained at the lowest GHSV in the range of the studied process conditions. In fact, a low GHSV is associated with a high residence time so that the reactants have sufficient time to react and their concentrations subsequently decrease; this justifies that the CO and H_2 conversions increases upon decreasing the space velocity.

In addition, the results manifests the substantial increase of selectivity of heavy products and the decrease of that of methane upon increasing the space velocity, suggesting that the increase of space velocity leads to the elimination of mass transfer resistance so that the dominant effects of diffusional limitation yield the removal of hydrocarbons from the active sites at the surface of the catalyst. Therefore the increase of GHSV favours the production of long chain heavy hydrocarbon components, while CH_4 selectivity, as expected, goes in the opposite direction. The heavy products' selectivity increases from about 58% to 83% with the increasing of the GHSV from 1800 to 6000 $Nm\ell\ (STP)\ g_{cat}^{-1}\ h^{-1}$; whereas the undesired methane selectivity decreases from about 35% to 10%. It can be seen in Figure 6-7 and Figure

6-8, the lighter olefins (C_2-C_3) and paraffins (C_2-C_7) were nearly unchanged considering significant changes of space velocity in the range of 1800-6000 $Nm\ell\ (STP)\ g_{cat}^{-1}\ h^{-1}$. In general, the results show that the selectivities of heavy FT products were sensitive to space velocity changes on a Co/SiO_2 catalyst, while this parameter was the key element to attain the high conversion (CO and H_2) rates; hence, likewise the temperature factor had a significant impact on the catalytic activity, reaction kinetics and general performance of the reactor.

Figure 6-9 and Figure 6-10 indicate the changes of CO and H_2 conversions and mole fractions in the gaseous phase respectively, at the centreline of the reactor bed versus normalized axial distance of the reactor bed length for different values of GHSV changing from 1800 to 6000 $Nm\ell\ (STP)\ g_{cat}^{-1}\ h^{-1}$. Each figure includes a family curves for different space velocity. Figure 6-9 represents the results obtained at a temperature of 490 *K* while Figure 6-10 shows those at 520 *K*. It is apparent that the CO and H_2 consumptions are more sensitive to GHSV for the lower temperature's case. For instance, the increase of GHSV from 1800 to 6000 $Nm\ell\ (STP)\ g_{cat}^{-1}\ h^{-1}$ results in the reduction of CO and H_2 conversions from 82% and 83% to 51% and 53% at the lower temperature of 490 *K*, respectively; whereas, as it is apparent in Figure 6-10, the similar variables decreases from 99% and 82% to 81% and 73% respectively, at the higher temperature of 520 *K*.

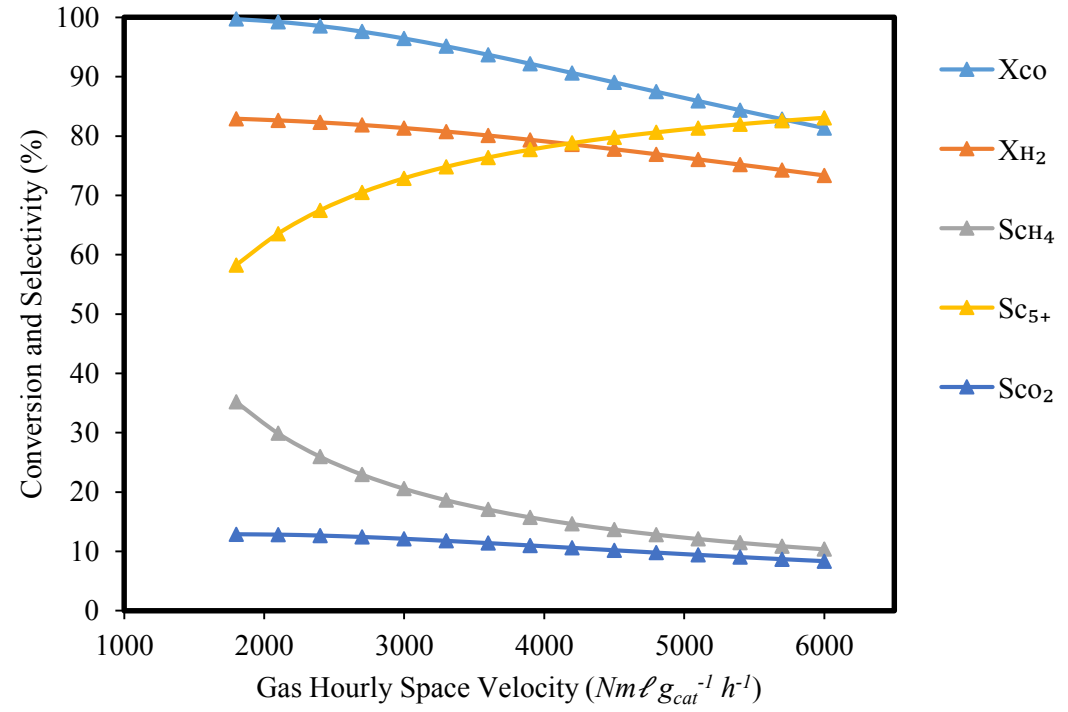

Figure 6-6 Effects of space velocity on CO and H_2 conversions as well as the CO_2, CH_4 and C_{5+} products' selectivities at constant P = 10 *bar*, H_2/CO = 2 and T = 520 *K*.

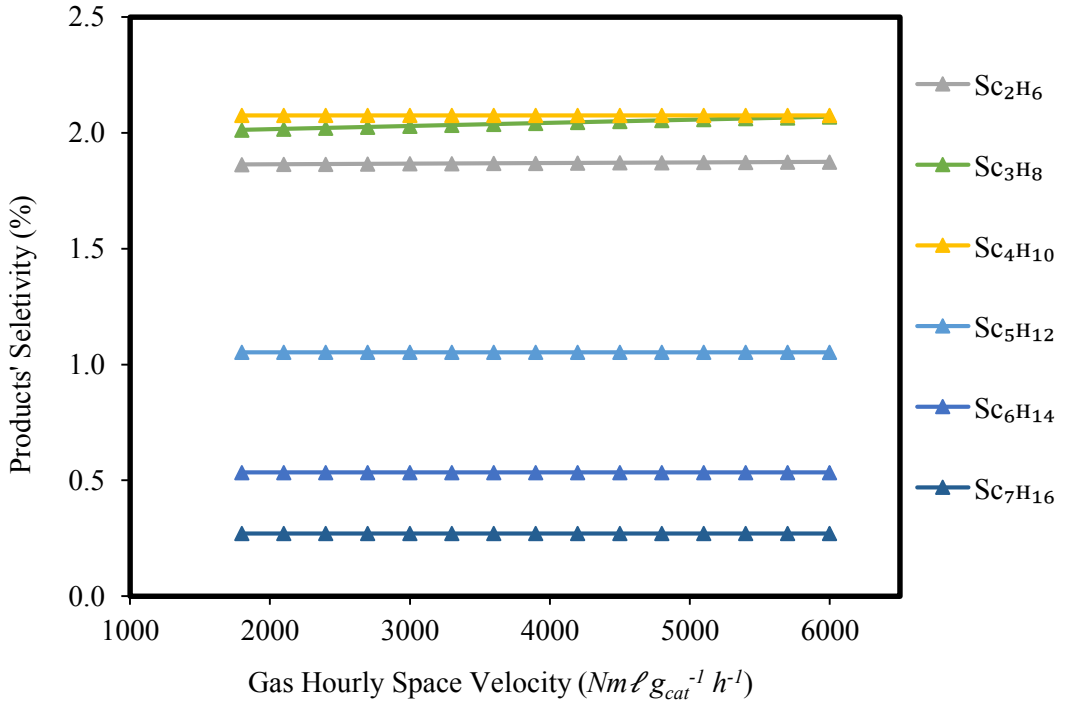

Figure 6-7 Effects of space velocity on the light paraffinic content (i.e. C_2-C_7) of the products at constant P = 10 *bar*, H_2/CO = 2 and T = 520 *K*.

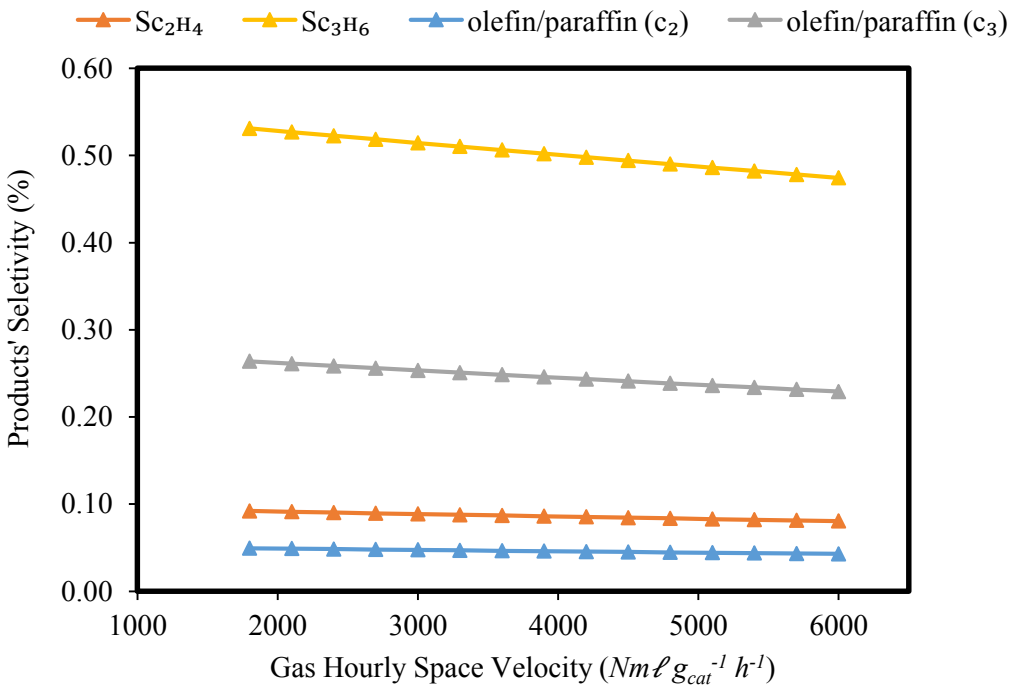

Figure 6-8 Effects of space velocity on the product olefins as well as the changes of olefin to paraffin ratio at constant P = 10 *bar*, $H_2/CO = 2$ and T = 520 *K*.

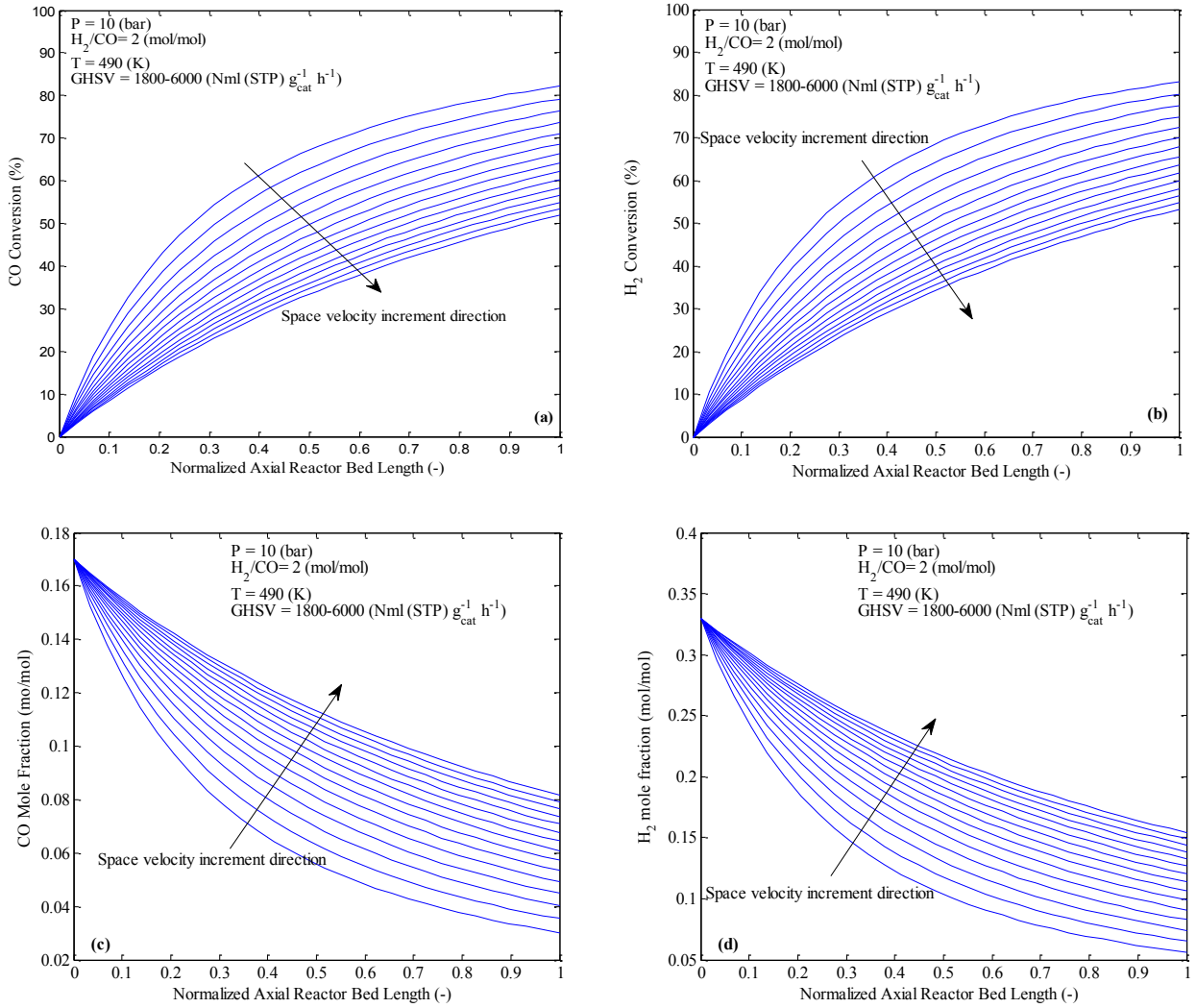

Figure 6-9 The changes of conversion of (a) CO and (b) H_2 and mole fraction of the same species (c) and (d) respectively along the normalized axial dimension of the reactor bed length, effects of GHSV on their behaviour at constant P= 10 *bar*, T= 490 *K* and H_2/CO= 2.

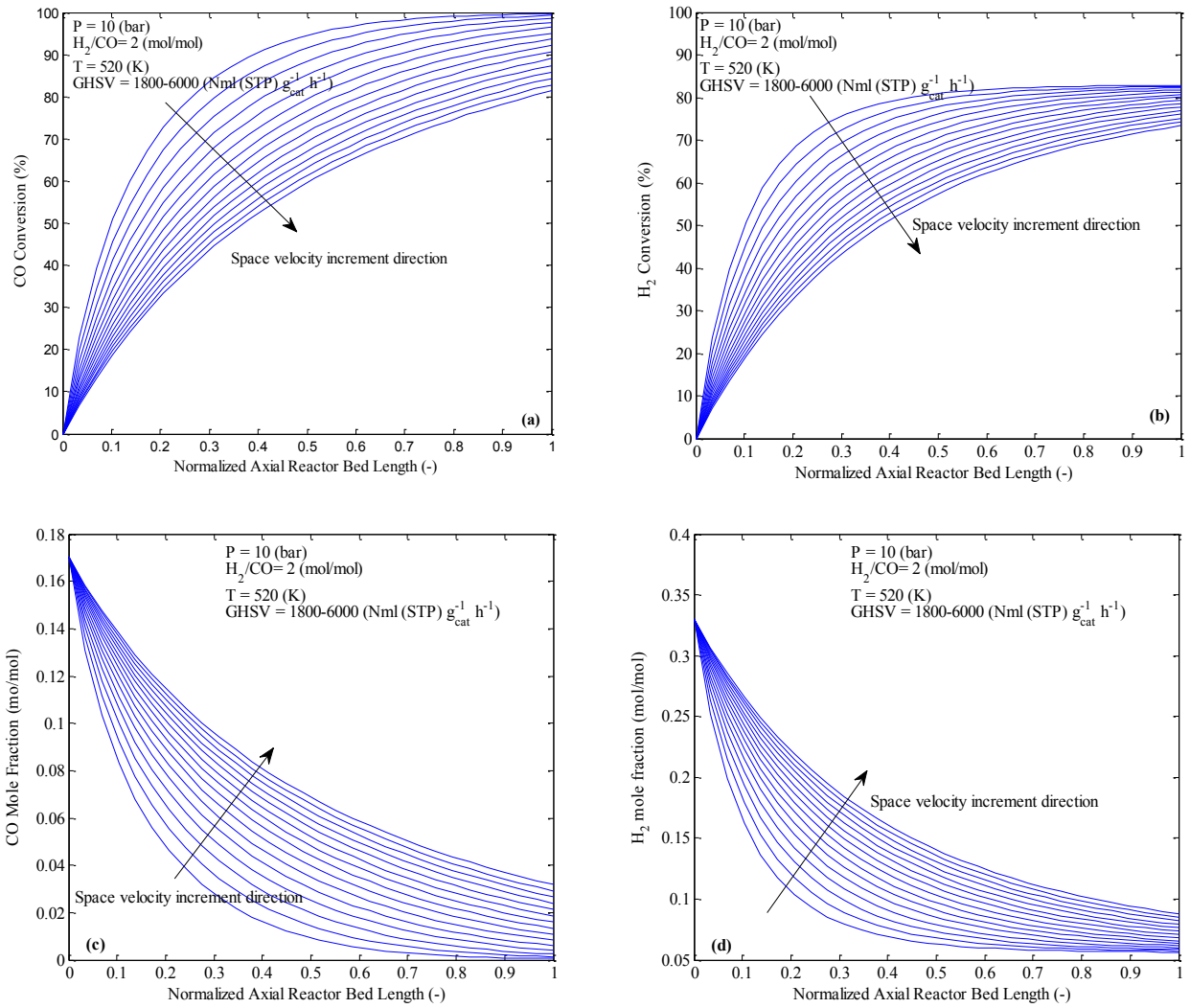

Figure 6-10 The changes of conversion of (a) CO and (b) H_2 and mole fraction of the same species (c) and (d) respectively along the normalized axial dimension of the reactor bed length, effects of GHSV on their behaviour at constant P= 10 *bar*, T= 520 *K* and H_2/CO= 2.

6.2.3. Effects of Operating Pressure

Figure 6-11 to Figure 6-13 manifest the pressure effects on syngas conversion as well as CO_2, CH_4 and C_{5+} products' selectivities, the selectivity of light paraffins, and the olefin to paraffin ratio as well as light olefin products, respectively. Typically, at low total pressures, the establishment of the thermodynamic equilibrium proceeds more gradually; whereas at equilibrium condition the products are mainly liquids. As shown in Figure 6-11, an increase in total pressure yields the product selectivities towards heavy products implying the condensation of hydrocarbons, which are normally in the gaseous state at atmospheric pressure. It is also important to notice that higher pressures typically lead to saturation of catalyst pores by liquid formation. From Figure 6-11, it is apparent that when the total pressure increases from 1 to 30 *bar*, the liquid products' selectivity significantly rises from about 36% to 92% at typical process conditions with respect to temperature, space velocity and H_2/CO molar ratio. As depicted in Figure 6-11, the changes of CO and H_2 conversions are proportional to the total pressure: increasing pressure results in the increment of CO and H_2 conversions from about 39% and 38% at 1 *bar* to 95% and 91% at 30 *bar*, respectively. Also, the selectivity C_2-C_7 paraffins decreases as the total pressure increases (see Figure 6-12). For instance, the selectivity of C_7H_{16} (heptane) decreases from 0.57% to 0.02% as the total pressure varies from 1 to 30 *bar*. Similarly, the selectivity of C_2H_6 (ethane) and C_3H_8 (propane) decrease from 3.49% and 4.15% to 0.12% and 0.14% respectively, which indicate the faster reduction of the hydrocarbon compounds with lower carbon atom number. Therefore, the increase of the total pressure would have adverse effect on tail gas and LPG productions which exhibits the increase of pressure condition is not desirable if the low chain hydrocarbons are preferable products. Similar behaviours were attained for light olefin components as it can be seen in Figure 6-13; whereas

the olefins to paraffins ratio were not changed. CH_4 selectivity decrease substantially with the increasing of the pressure, which is a favourable condition as this component is undesired FT products.

Figure 6-14 and Figure 6-15 indicate the influence of total pressure on syngas consumptions in terms of CO and H_2 conversions and mole fractions, at the centreline of the fixed bed reactor along the normalized axial dimension of the bed length, when the temperatures, space velocity and H_2/CO ratio are set at a constant 500 *K*, 2400 $Nm\ell\ (STP)\ g_{cat}^{-1}\ h^{-1}$ and 2 (*mol*/*mol*), respectively. From Figure 6-14 and Figure 6-15, one can deduce that the increase of pressure from 1 to 30 *bar* results in significant enhancement of catalytic activity in terms of syngas consumption. The CO and H_2 conversion increase faster at lower total pressure (e.g. 1-10 *bar*) compared to that of the higher range of 10-20 *bar*; suggesting that the syngas consumption rate is more sensitive to total pressure at its lower range. When pressure increases from 1 *bar* to 10 *bar* then CO and H_2 raise from about 39% and 38% to about 85% and 82%, respectively; whereas at a higher pressure range, these variables changes from 85% and 82% at 10 *bar* to 92% and 88% at 20 *bar*.

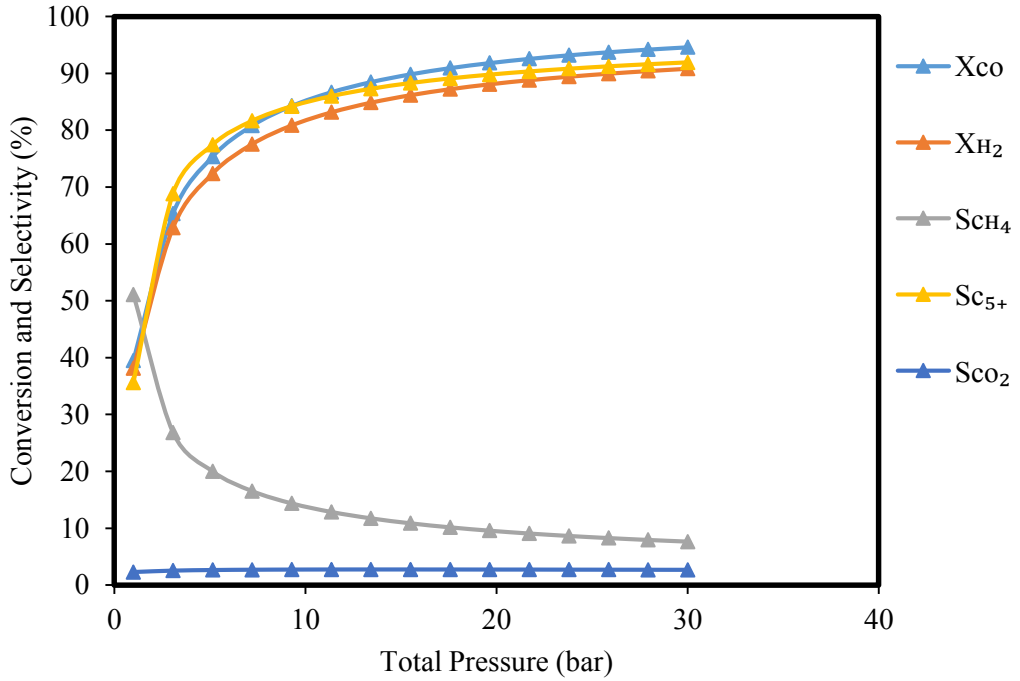

Figure 6-11 Effects of total pressure on CO and H_2 conversions as well as the CO_2, CH_4, and C_{5+} products' selectivities at constant T = 500 *K*, H_2/CO = 2 and GHSV = 2400 $Nm\ell$ *(STP)* g_{cat}^{-1} h^{-1}.

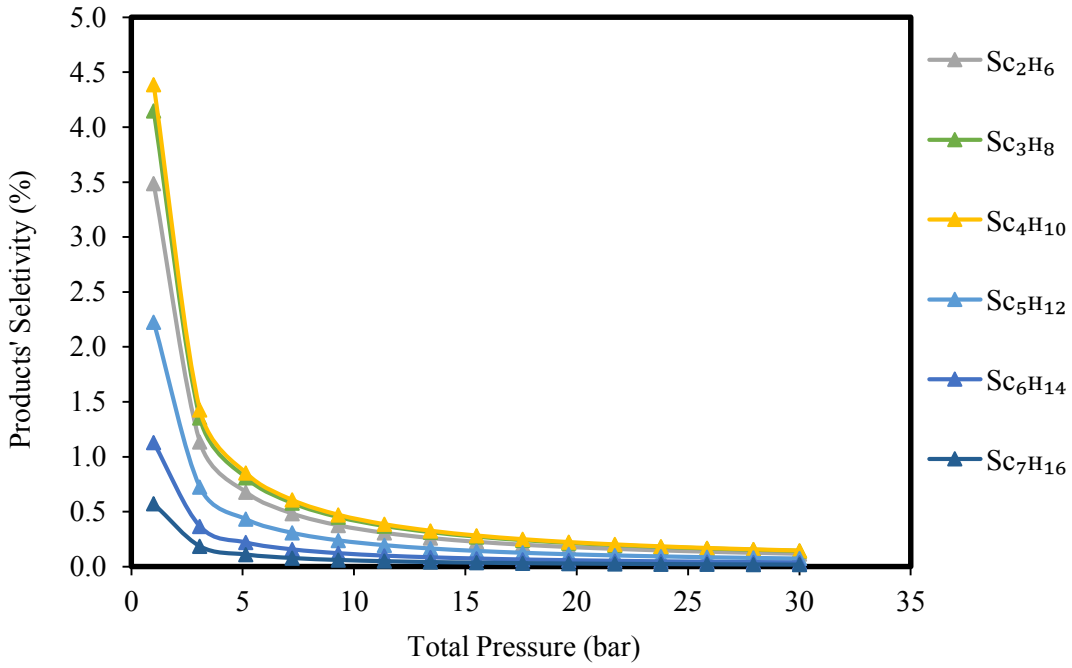

Figure 6-12 Effects of total pressure on the light paraffinic content (i.e. C_2-C_7) of the products at constant T = 500 *K*, H_2/CO = 2 and GHSV = 2400 $Nm\ell$ *(STP)* g_{cat}^{-1} h^{-1}.

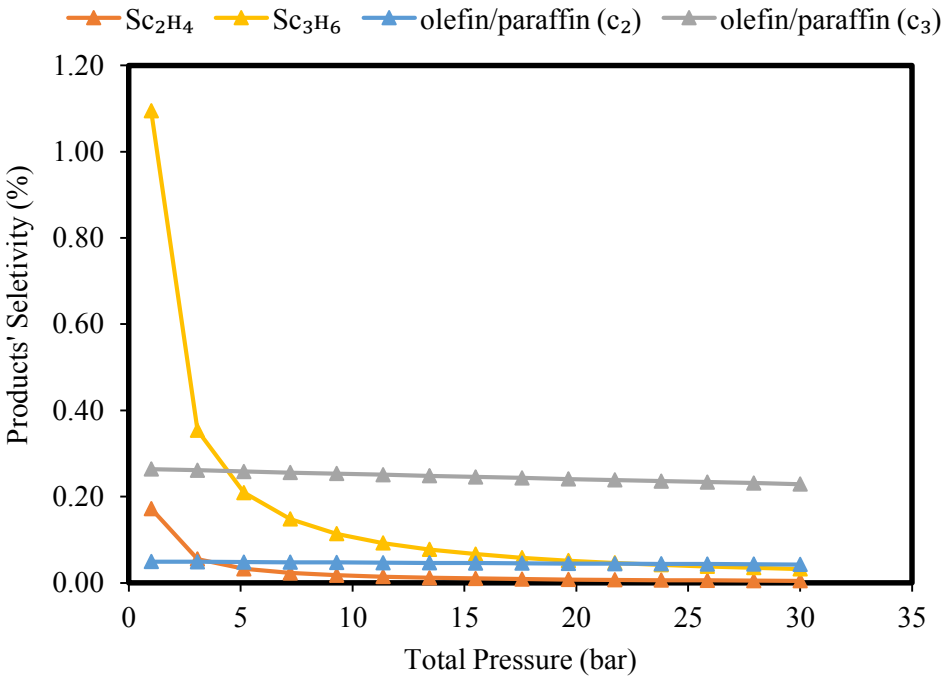

Figure 6-13 Effects of total pressure on the product olefins as well as the changes of olefin to paraffin ratio at constant T = 500 *K*, $H_2/CO = 2$ and GHSV = 2400 $Nm\ell\ (STP)\ g_{cat}^{-1}\ h^{-1}$.

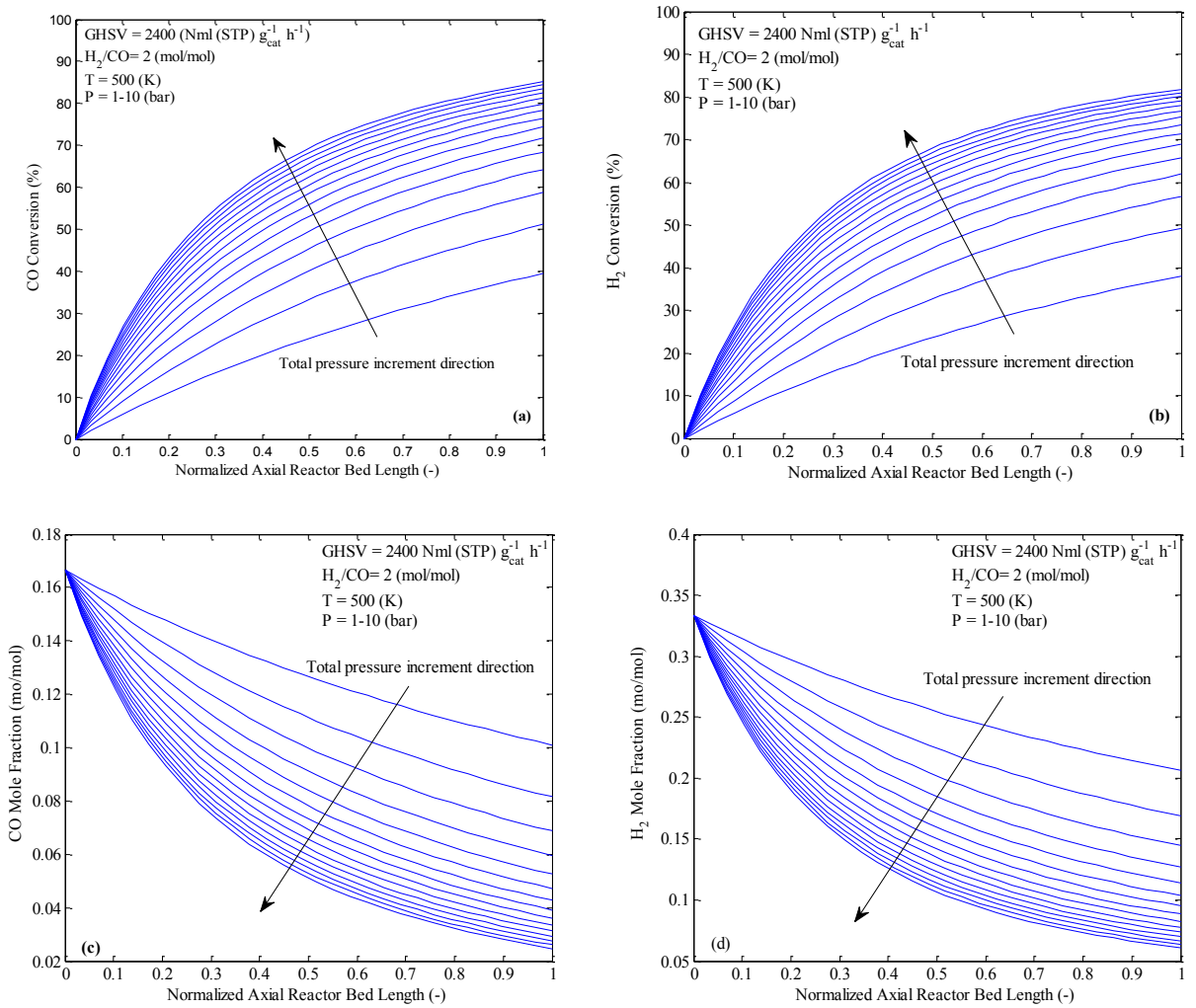

Figure 6-14 The changes of conversion of (a) CO and (b) H_2 and mole fraction of the same species (c) and (d) respectively along the normalized axial dimension of the reactor bed length, effects of total pressure (P=1-10 *bar*) on their behaviour at constant T= 500 *K*, GHSV= 2400 $Nm\ell\ (STP)\ g_{cat}^{-1}\ h^{-1}$ and H_2/CO= 2.

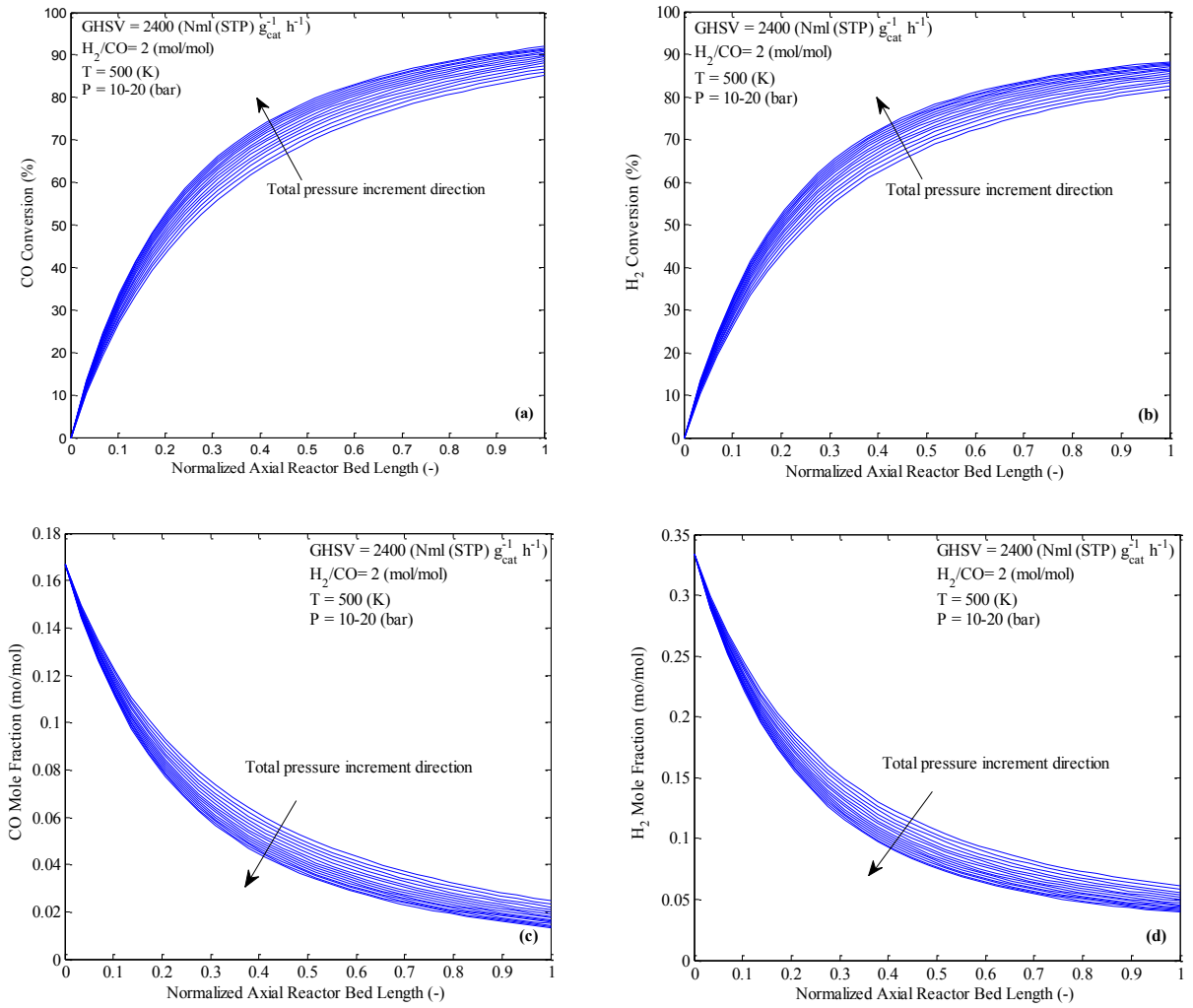

Figure 6-15 The changes of conversion of (a) CO and (b) H_2 and mole fraction of the same species (c) and (d) respectively along the normalized axial dimension of the reactor bed length, effects of total pressure (P=10-20 *bar*) on their behaviour at constant T= 500 *K*, GHSV= 2400 *Nmℓ (STP)* g_{cat}^{-1} h^{-1} and H_2/CO= 2.

6.2.4. Effects of Synthesis Gas Composition (H_2/CO Molar Ratio)

Figure 6-17 shows the influence of the hydrogen to carbon monoxide molar ratio on CO and H_2 conversions, as well as the selectivities of CO_2, CH_4 and C_{5+} when the temperature, pressure and space velocity are set at 510 *K*, 10 *bar*, and 4500 $Nm\ell\ (STP)\ g_{cat}^{-1}\ h^{-1}$, respectively. Their effects on selectivities of paraffins with carbon atom C_2-C_7 are also shown in Figure 6-18. In addition, the product olefins as well as the changes of olefin to paraffin ratio with respect to the H_2/CO ratio are demonstrated in Figure 6-19. The increase of the H_2/CO ratio leads to a different proportion of adsorbed hydrogen and surface carbon atoms as well as their partial pressures. As manifested from the final developed kinetic model, CO and H_2 have inhibiting and positive impacts on the rate of reaction respectively; suggesting that the consumption rate of CO increases with the rising of the H_2/CO ratio, while that of H_2 decreases upon the increment of the ratio. The increase of the H_2/CO ratio results in the enhanced hydrogen concentration on the active sites and increments the hydrogenation degree of highly concentrated monomers. At the same time, this accelerates the rate of chain termination step causing faster desorption of products rather than incorporating to the chain growth, which results in a reduction of selectivity of heavy FT products and a subsequent increase of light hydrocarbons (C_2-C_7) (see Figure 6-18). It is also evident from Figure 6-17 that the major loss of liquid (C_{5+}) formation was due to a methanation reaction in which the C_{5+} and methane selectivities changed from about 93% to 72% and 5% to 20% with the increasing of the H_2/CO ratio from 1 to 3.5 (*mol/mol*), respectively. As can be seen in Figure 6-19, the olefins/paraffins ratio slightly decreases upon the increasing of the ratio, while (from Figure 6-17) the CO_2 selectivity decreases from about 15% to 1%; which implies the slight water gas shift activity at low H_2/CO ratio. It was found from the kinetic model and governed equations in Chapter 3 (see

Table 3-18, model WGS-VII with RDS-4) that the water gas shift reaction rate is inversely proportional to the H_2/CO ratio and one can conclude that the partial pressures of both reactants as well as their proportion have substantial effects on the rate of CO_2 formation. In addition, this can be seen from Figure 6-16 which illustrates the trend of changes of R_{WGS} (water gas shift reaction rate) along the axial dimension of the tube length at different H_2/CO molar ratio in which the rate decreases from 1.4964×10^{-5} to 1.987×10^{-7} $mol\ g_{cat}^{-1}\ s^{-1}$ upon the increasing of the molar ratio from 1 to 3.5 *mol/mol*.

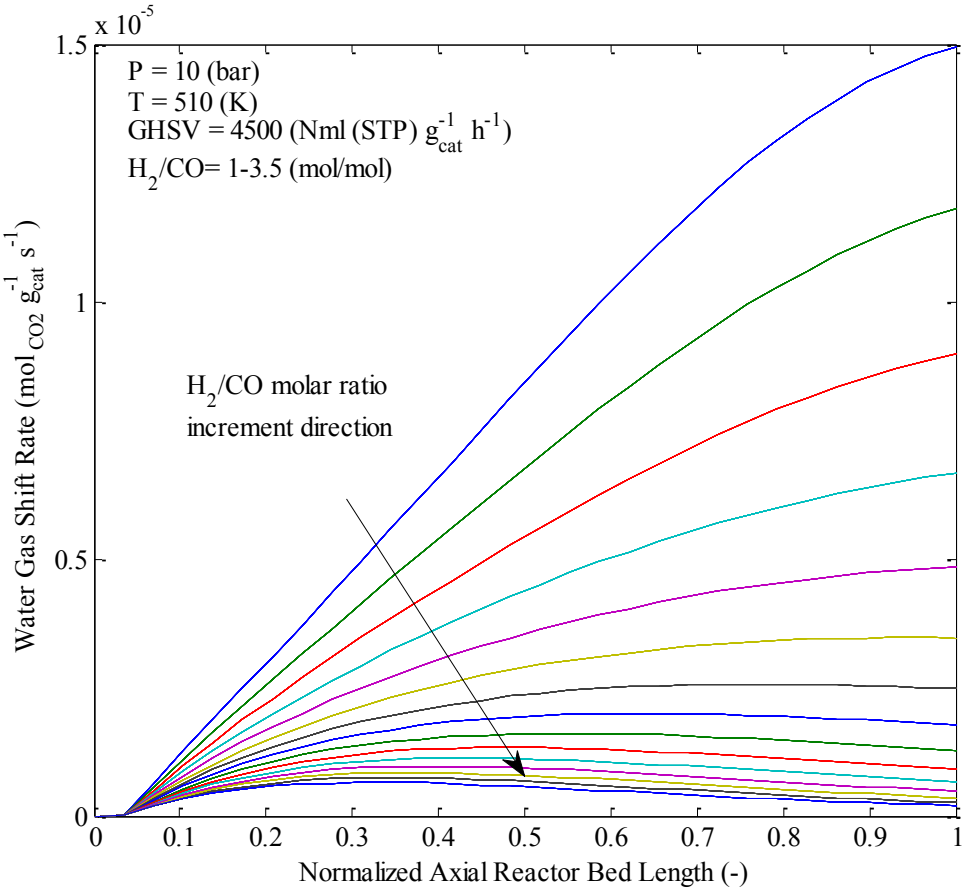

Figure 6-16 Effects of H_2/CO molar ratio on WGS reaction rate and its trend of changes along the normalized axial dimension of the reactor bed length, at constant T= 510 *K*, GHSV= 4500 $Nm\ell\ (STP)\ g_{cat}^{-1}\ h^{-1}$ and P= 10 *bar*.

Figure 6-20 (a) to (d) show how the CO, H_2, and syngas conversion and mole fraction at the centreline of the reactor are influenced by the input H_2/CO molar ratio when the process conditions are set at a constant temperature, pressure and GHSV of 510 *K,* 10 *bar* and 4500 $Nm\ell\ (STP)\ g_{cat}^{-1}\ h^{-1}$, respectively. In contrast to the previous figures of reactant consumption versus normalized axial distance, the inlet contents of CO mole fraction or H_2 mole fraction is not identical as the hydrogen to carbon monoxide fraction varies at the inlet of the reactor bed. From this figure, it is apparent that the increase of H_2/CO ratio leads to the increment of syngas consumption. Although this is a true manifestation, it would not be confirmed unless the comparison of syngas conversion is performed. From Figure 6-20, it can be deduced that the outlet CO conversion increases from 23% to 99% upon the increment of the ratio from 0.25 to 6. Overall, a high H_2/CO molar ratio would be suggested for increasing the catalytic activity and overall performance due to the considerable increase of CO conversion as well as significant reduction of CO_2 selectivity, though a low H_2/CO feed ratio would be preferable for the increased production of heavy hydrocarbons.

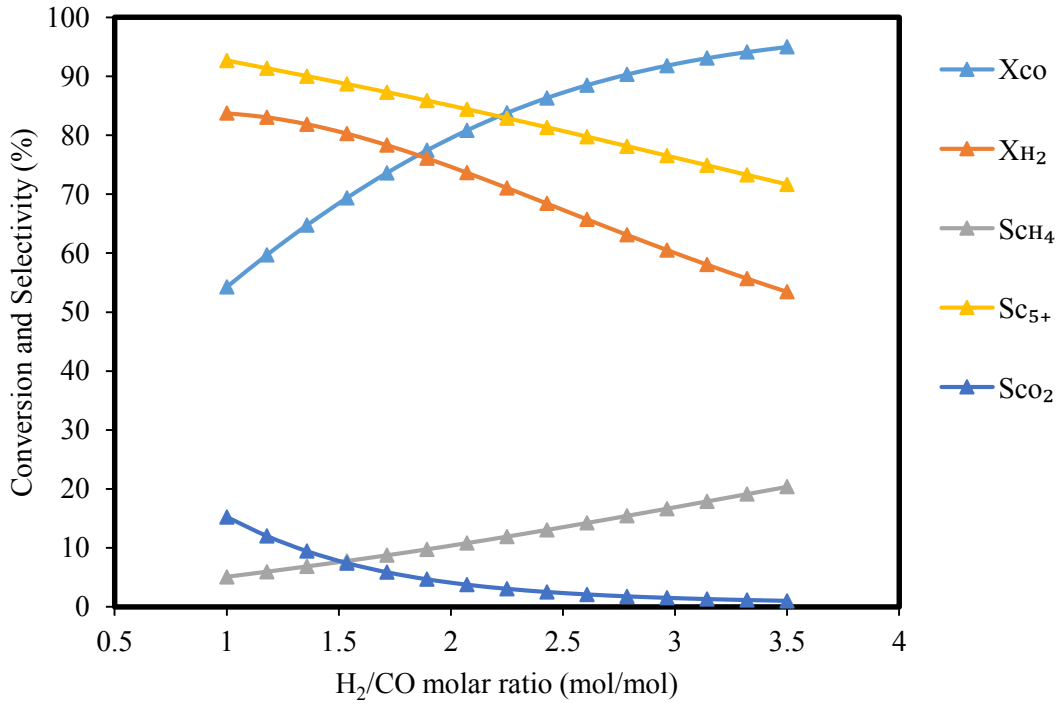

Figure 6-17 Effects of H_2/CO ratio on CO and H_2 conversions as well as the CO_2, CH_4, and C_{5+} products' selectivities at constant T = 510 *K*, P = 10 *bar* and GHSV = 4500 $m\ell$ *(STP)* g_{cat}^{-1} h^{-1}.

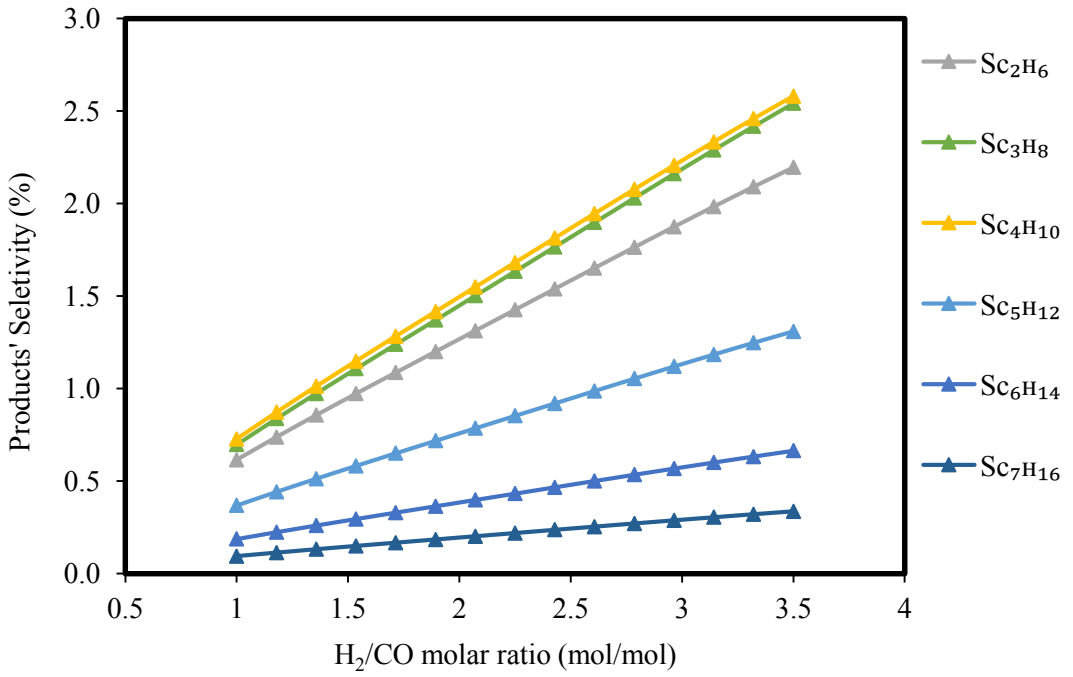

Figure 6-18 Effects of H_2/CO ratio on the light paraffinic content (i.e. C_2-C_7) of the products at constant T = 510 *K*, P = 10 *bar* and GHSV = 4500 $Nm\ell$ *(STP)* g_{cat}^{-1} h^{-1}.

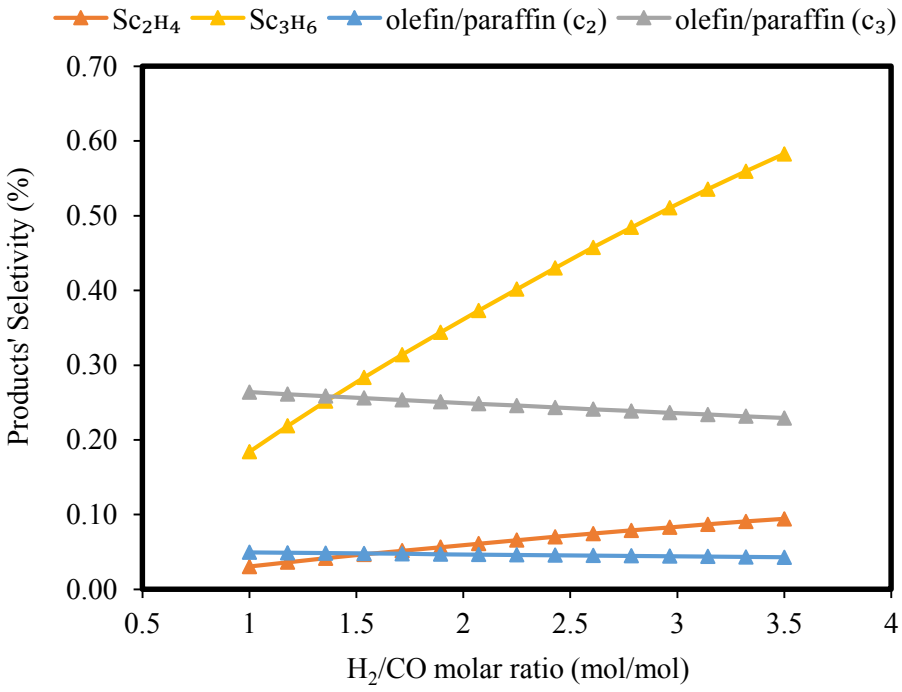

Figure 6-19 Effects of H_2/CO ratio on the product olefins as well as the changes of olefin to paraffin ratio at constant T = 510 *K*, P = 10 *bar* and GHSV = 4500 $Nm\ell\ (STP)\ g_{cat}^{-1}\ h^{-1}$.

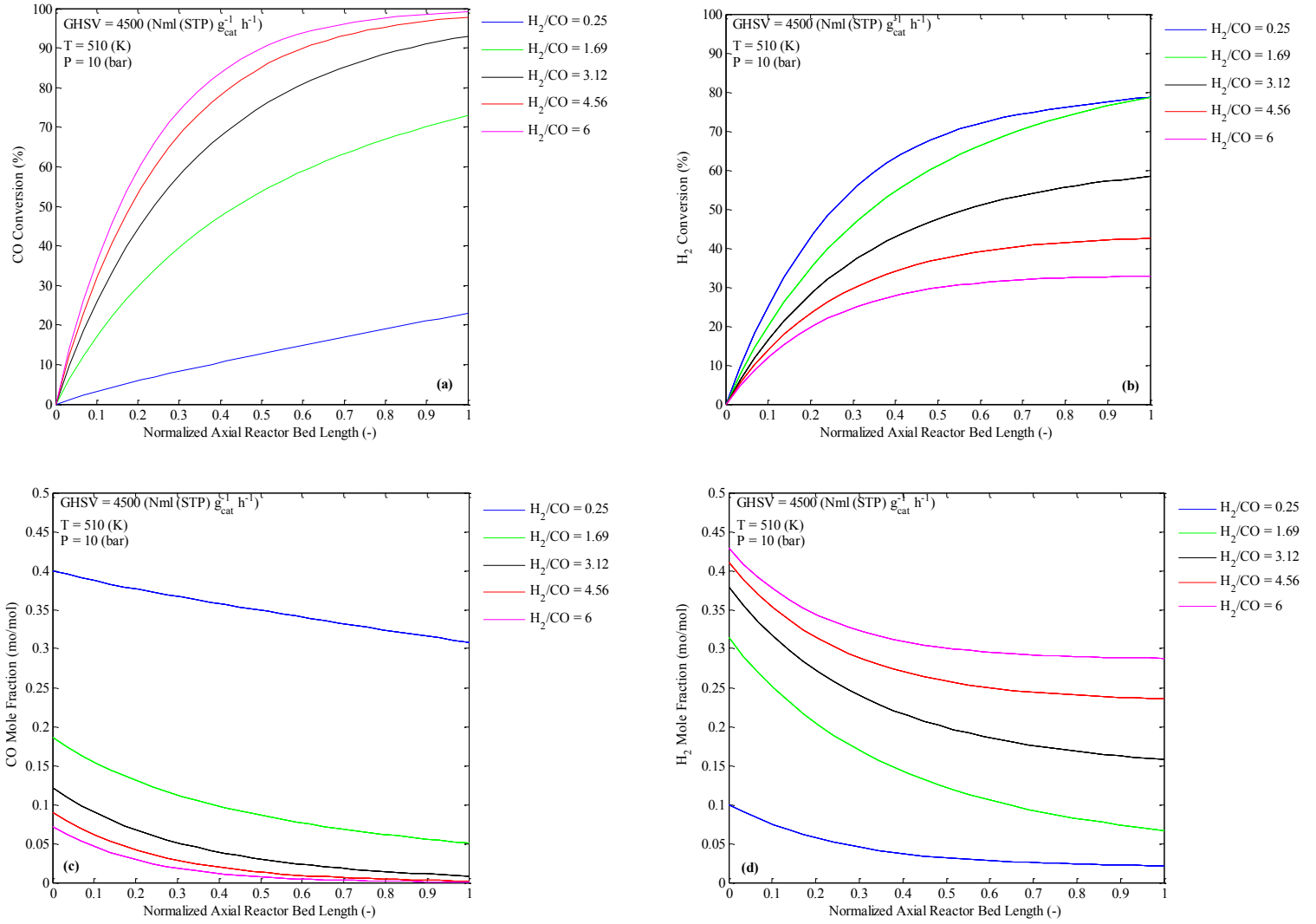

Figure 6-20 The changes of conversion of (a) CO and (b) H_2 and mole fraction of the same species (c) and (d) respectively along the normalized axial dimension of the reactor bed length, effects of H_2/CO on these plots at constant T= 510 *K*, GHSV= 4500 $Nm\ell\ (STP)\ g_{cat}^{-1}\ h^{-1}$ and P= 2 *bar*.

For the present study, the influences of critical process conditions i.e. reaction temperature, total pressure, space velocity, and H_2/CO inlet molar ratio on conversion of syngas compositions and FT products' selectivities, are summarized in Table 6-2.

Table 6-2 effects of operating conditions on FT products' selectivity and syngas components' conversion

Components		Temperature	Pressure	GHSV	H_2/CO molar ratio
H_2 conversion	x_{H_2}	↑	↑	↓	↓
CO conversion*	x_{CO}	↑	↑	↓	↑
CH_4 selectivity †	S_{CH_4}	↑	↓	↓	↑
CO_2 selectivity	S_{CO_2}	↑	↑§	↓	↓
Olefins selectivity	$S_{C_2-C_3}$	↑§	↓	↓§	↑
Olefin/paraffin ratio	S_O/S_P	↓	—	↓§	↓§
Light paraffins	$S_{C_2-C_7}$	↑	↓	—	↑
Liquid products	$S_{C_{5+}}$	↓	↑	↑	↓

*All the operating process conditions, except space velocity, have positive impact on CO conversion.

† The effects of all process conditions on CH_4 and C_{5+} products obtained completely in the opposite direction.

§ Slightly changed

6.3. Optimization Results:

The obtained results, based on the parametric studies, indicated that all the process parameters had significant impacts on output conversion and products' selectivity. Hence, all parameters were considered in the multi-objective optimization process using Non-dominated Sorting Genetic Algorithm (NSGA–II) to optimize the fitness functions (i.e. objective functions).

The target of the optimization study was to maximize the selectivity of desired products i.e. high molecular weight hydrocarbons, in general C_{5+} selectivity, to maximize the synthesis gaseous conversions (in particular CO conversion) and to minimize the formation of undesired products i.e. carbon dioxide and methane products. Accordingly, four objective functions comprised a multi-objective optimization process. Also, four control operators, as (1) the number of populations, (2) number of generations, (3) crossover and (4) mutation rate were used in the NSGA–II in which the first two were identified as the key elements. Table 6-3 lists the selected values of each of these operators and the best tried value of the operators in the optimization procedure. The optimizer terminates as the maximum number of generations is reached. The mutation and crossover rates were set to 0.2 and 0.8 respectively, as suggested in [180, 183]; however, different values were tried at different optimization runs to identify its impact on the optimization results. The crossover function specifies the fraction of the population at the next generation, excluding elite children, which is one of the reproduction options to specify how the genetic algorithm builds children for the succeeding generation [183]. Elite count is a positive integer specifying how many individuals in the current generation are guaranteed to survive to the next generation. The crossover enables the algorithm

to extract the best genes from different individuals and recombine them into potentially superior children. Mutation adds to the diversity of a population and thereby increases the likelihood that the algorithm will generate individuals with better fitness values. More information about the operators and the method of their selection can be found in the literature [183].

Table 6-3 Main control operators considered in the multi-objective optimization process using NSGA–II

	Number of population	Number of generation	Crossover	Mutation rate
Values tried	100 300 400 500	5000	0.8	0.2
	500	1000 3000 4000 5000	0.8	0.2
	500	5000	0.4 0.6 0.8 0.9	0.2
	500	5000	0.8	0.001 0.01 0.1 0.2
Best values	500	5000	0.8	0.2

The Pareto-front solutions can be plotted by 2D and 3D scatter between two and three objectives, respectively. Figure 6-21 to Figure 6-23 show the solutions plotted by 2D scatter between CO_2 selectivity vs. CO conversion; C_{5+} selectivity vs. CO conversion; and CH_4 selectivity vs. CO conversion, respectively. One of the key factors that determines the performance of the genetic algorithm is the diversity of the population. If the average distance between individuals is large, the diversity is high; if the average distance is small, the diversity

is low. Getting the right amount of diversity is a matter of trial and error. If the diversity is too high or too low, the genetic algorithm might not perform well. From (Figure 6-21 to Figure 6-23), it is apparent that the diversity of the populations are neither low nor high, which indicate that the values of crossover as well as mutation rate were perfectly defined for the current optimization; since these operators generally add to the diversity of the population and thereby increases the likelihood that the algorithm will generate individuals with better objective values [183].

The obtained Pareto frontiers reveal the conflict between the objective functions. For example any operating conditions that increases the CO conversion will evidently reduce C_{5+} selectivity as it is apparent from Figure 6-22. In other words, the point of maximum CO conversion (point A in Figure 6-22) corresponds to the minimum of C_{5+} selectivity (point B in Figure 6-22), while the maximum of the latter objective function leads to the minimum of the former which of course is not desirable. If the single-objective optimization would have been conducted for CO conversion then point "A" would be the solution of the optimization, while for C_{5+} selectivity it would be point "B". Moreover, any operating condition that increases the CO conversion increases the CH_4 selectivity which will lead to production of undesired lighter hydrocarbon compounds as can be seen from Figure 6-23. As it is evident, the point of maximum CO conversion (point C in Figure 6-23) corresponds to the maximum of CH_4 selectivity (point D in Figure 6-23), while the minimum of the latter objective function leads to the minimum of the former. Similarly, if the single-objective optimization would have been conducted for CO conversion then point "C" would be the solution of the optimization, while for CH_4 selectivity it would be point "D". Apparently, there is no combination of the operating conditions that can optimize all the objectives simultaneously. Each individual point on the Pareto frontier lines in Figure 6-21 to Figure 6-23 is an optimal solution and such results can

be utilized as a database of optimum solutions from which the selection of the optimum operating condition (independent variables) can be conducted from the higher-level information, experience as well as the importance of each objective function for a specific application.

Comparison of the experimental data overlaid on Figure 6-21 to Figure 6-23 with Pareto-frontier solutions reveals that, not all the experiments were conducted at optimum operating conditions that led to the best performance for all objective functions. Hence, the optimization results represented herein manifested the possibility of remarkable improvement in FT synthesis conversion and selectivities.

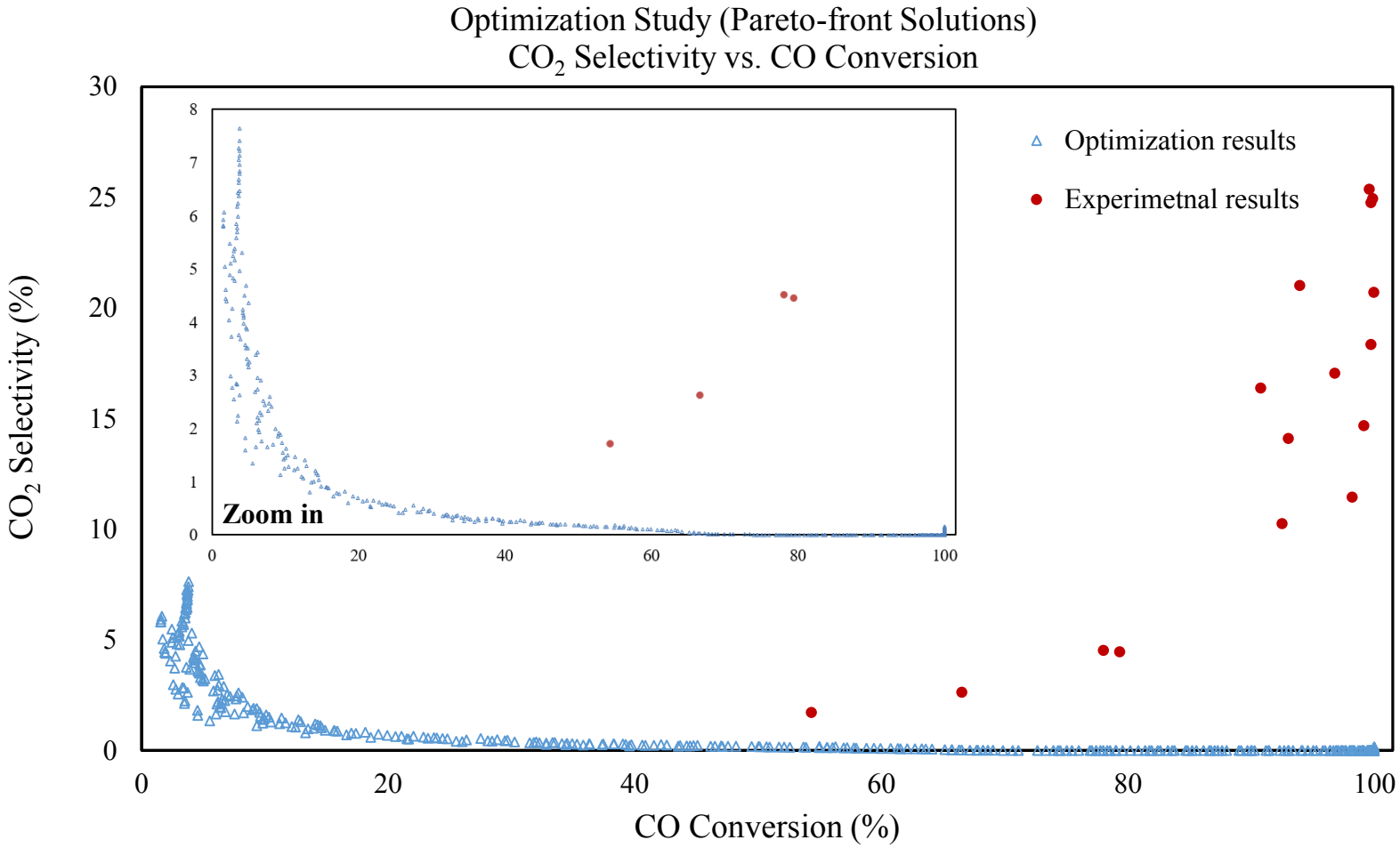

Figure 6-21 Pareto-front solutions obtained by optimization (between CO_2 selectivity and CO conversion) and its comparison with experimental data.

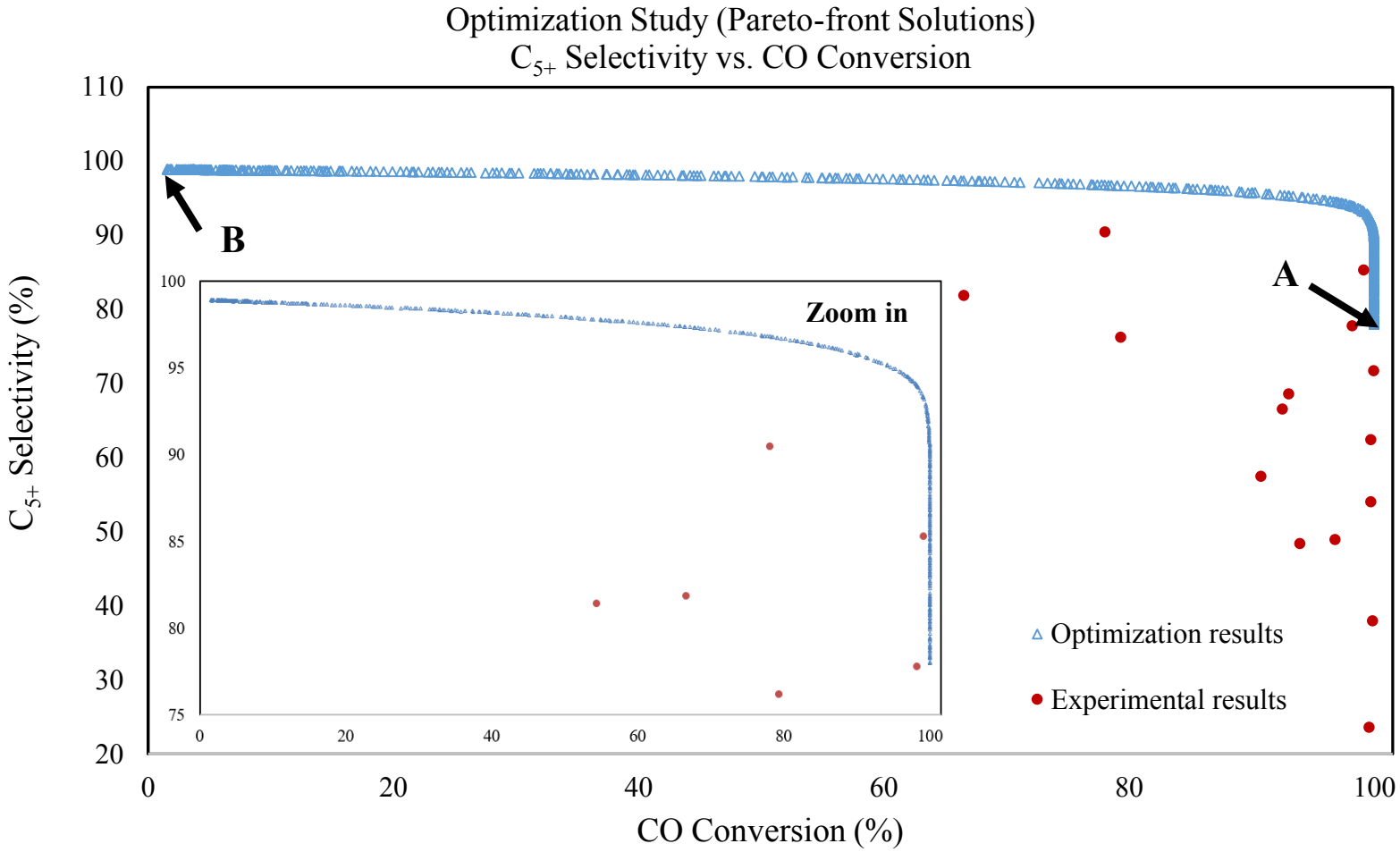

Figure 6-22 Pareto-front solutions obtained by optimization (between C_{5+} selectivity and CO conversion) and its comparison with experimental data.

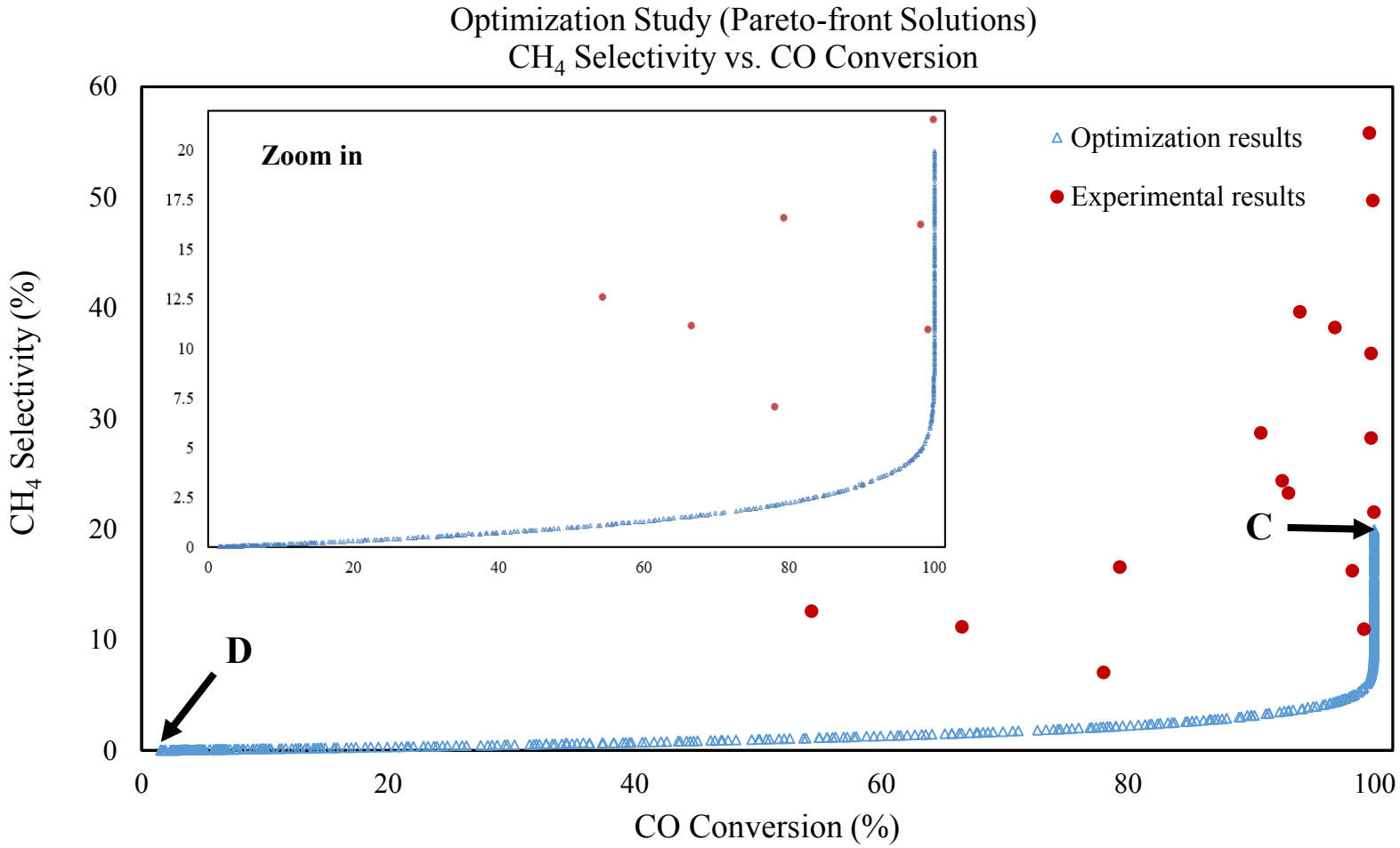

Figure 6-23 Pareto-front solutions obtained by optimization (between CH_4 selectivity and CO conversion) and its comparison with experimental data.

The boundary conditions of the process parameters considered for the optimization procedure are listed in Table 6-4. The best two experimental data in terms of selectivities of CH_4, CO_2 and C_{5+} products as well as CO conversion were selected for comparison with the optimization results. The pie charts (Figure 6-24 to Figure 6-26) show the results of selectivities at the selected runs as well as that obtained from the optimization procedure. Also, the values of CO conversion and CO_2 selectivity, together with the process operating conditions, were given in the chart for comparison. It can be seen that better outcomes were obtained from the optimization study for all the objectives compared to those of the experiments. In detail, the optimization study showed the optimum CO conversion at 94.26%, which is better than that of Exp. 01 at 78.04% but not as good as Exp. 06 at 99.15%. However, with regard to C_{5+} and CH_4 selectivities, the optimization case indicated the optimum selectivities were at 91.06% and 6.57%, respectively while C_{5+} selectivity was obtained at 90.45% and 85.30% for Exp. 01 and Exp. 06, and CH_4 selectivity was about 7.06% and 10.96%, respectively. Hence, the performance of the FT synthesis were improved with respect to the desired C_{5+} and undesired CH_4 selectivity. Last but not least, CO_2 selectivity determined from the optimization procedure was almost zero, while that of the optimum experiential runs measured CO_2 values at 4.52% and 14.68%. The optimum selected condition from the optimization data-set was achieved at T = 485 *K*, P = 30 *bar*, GHSV = 1800 Nmℓ (STP) g_{cat}^{-1} h^{-1} and H_2/CO = 2.6. It is apparent that better global output was attained at low temperature, space velocity, high pressure and inlet hydrogen-to-carbon monoxide molar ratio.

Table 6-4 Boundary conditions considered for optimization with respect to reaction temperature, total pressure and space velocity and carbon monoxide molar ratio

Temperature range (*K*)	Pressure range (*bar*)	Space velocity range ($Nm\ell\ (STP)\ g_{cat}^{-1}\ h^{-1}$)	H_2/CO range (*mol/mol*)
470-550	1-35	1800-5400	0.5-3.5

The trends herein reported, manifest that a compromise has to be found in the selection of the process conditions in order to find the optimal operating set-point. The developed model and overall kinetics mechanism reported, together with the optimization procedure presented herein, represented a key tool for such an investigation.

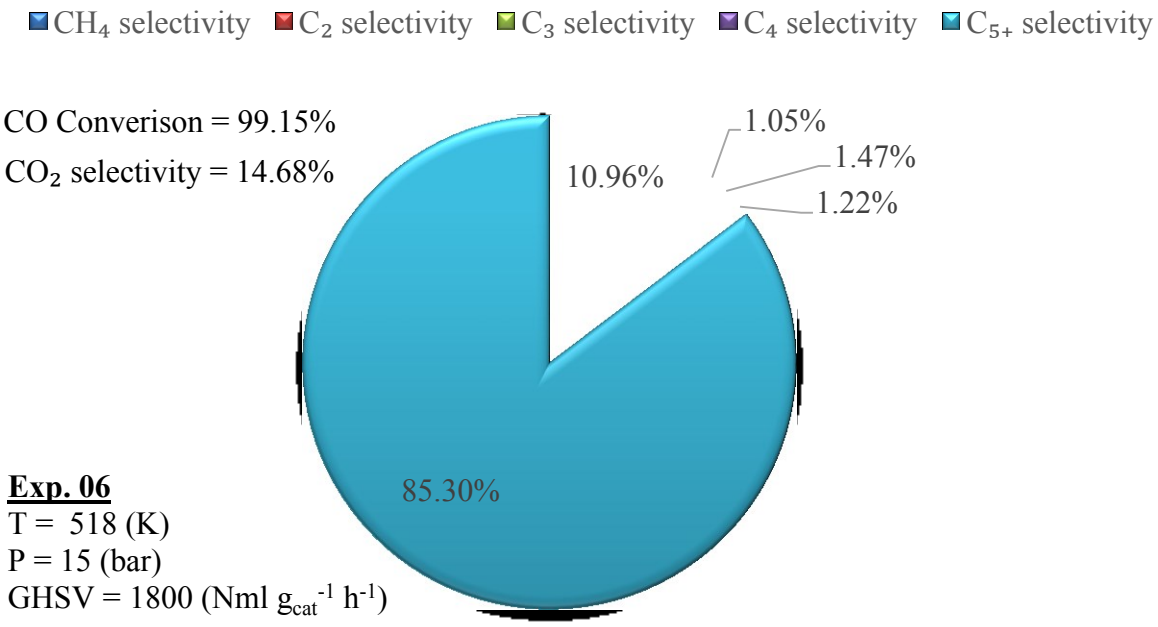

Figure 6-24 The first optimum experimental results.

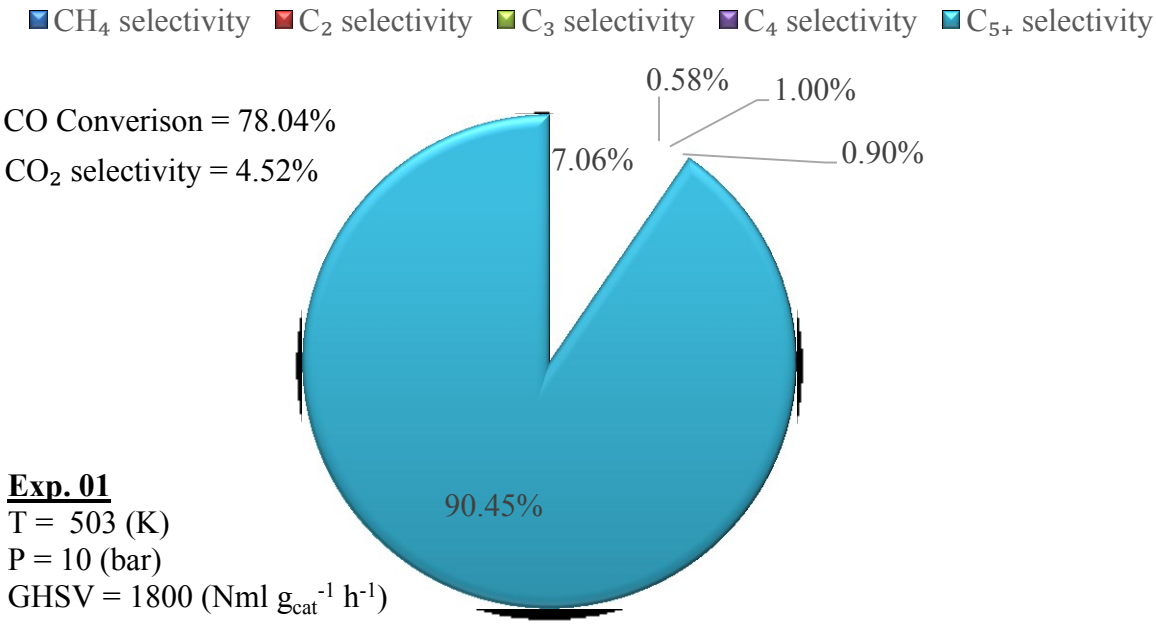

Figure 6-25 The second optimum experimental results.

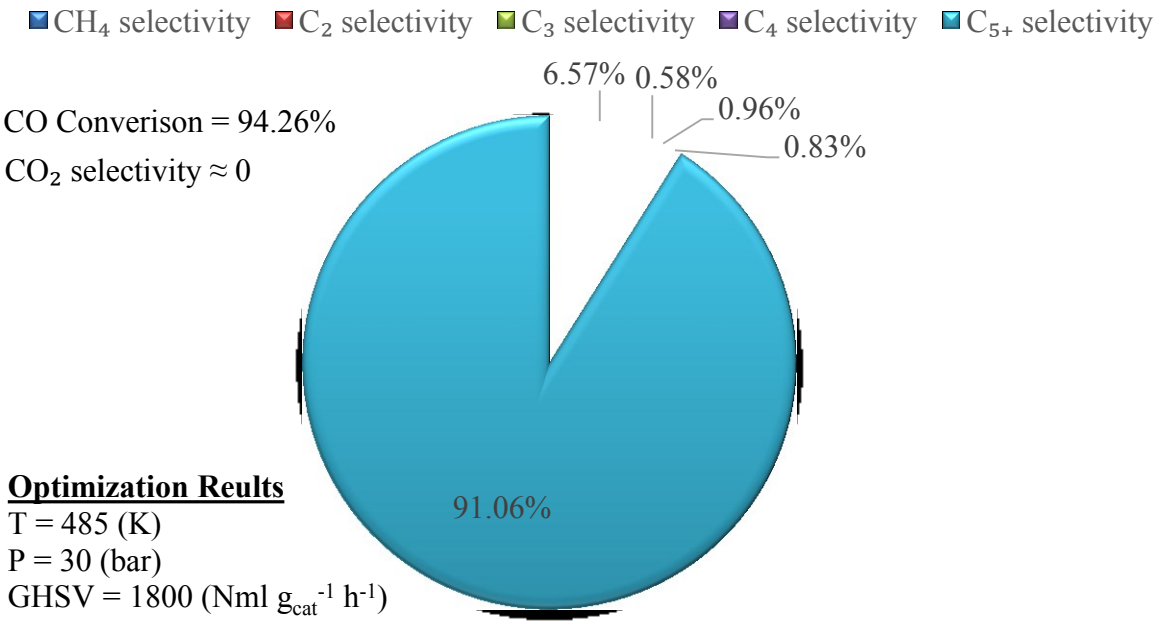

Figure 6-26 The optimum results obtained from multi-objective optimization (using NSGA–II).

6.4. Summary and Conclusions

The mathematical model developed in chapter 4 and calibrated and validated in chapter 5, was employed to conduct parametric studies (sensitivity analysis) as well as multi-objective optimization of FT synthesis global performance parameters using NSGA-II. Initially, the parametric studies were conducted to identify those input variables that have the most significant effect on CO conversion and selectivity of products species. The results indicated that reaction temperature, total pressure, space velocity and H_2/CO molar ratio had all substantial influence on the output parameters mentioned above and were then included in the optimization. Due to the conflicting objective functions, single values of the input variables could not satisfy all the objective functions simultaneously. Thus, the optimum solution were presented in the form of Pareto-fronts in which each individual points on these lines presented an optimum solution. The trends of Pareto-fronts were so that the selection of input variables for optimum performance required a compromise between different objectives. Such results serve as an optimal database that can be considerably helpful for the selection of the optimal operating conditions for maximum performance of FT process depending on the priority of the objective functions.

CHAPTER 7

CONCLUSIONS

7.1. Concluding Remarks

A mathematical model of a fixed bed reactor for Fischer-Tropsch (FT) synthesis on a cobalt-based catalyst was systematically developed. An in-depth understanding in terms of FT synthesis kinetics and water gas shift (WGS) reaction mechanisms was effectively accomplished. The model was capable of simulating the changes of reactants' conversion (CO and H_2), products' selectivity (CO_2, light olefins and paraffins as well as total liquid hydrocarbons) along the axial distance of rector bed length. A solution algorithm was presented that was effective in solving a single tube reactor model. Such a solution methodology can be applied to a wide variety of problems which require the solution of sets of coupled non-linear partial differential equations. The algorithm was applied after the decision was made about which numerical scheme to employ and the equations were reformulated in the appropriate manner. The algorithm was applied to a steady-state one-dimensional model; however, the methodology is easily extended to more spatial coordinates. The code can be enhanced into

transient (non-steady) condition by the addition of one nested loop into the core of the program. Clearly, this can be used to predict the behaviour of the reactor subject to the presence of catalyst deactivation.

The kinetics parameters were evaluated for each kinetics model developed herein, using an advanced optimization technique. Among different global optimization methods, the GlobalSearch algorithm was used as an alternative to avoid convergence to the local minima (sub-optimal solutions) during the search process and to surmount the difficulties existing in traditional (gradient-based) local optimization methods that fail to arrive at satisfactory global solutions. In addition, physical and statistical consistencies of the kinetics parameters were evaluated by various statistical analyses.

Based on the results obtained the limitations of power-law rate model were identified for the applications that wider range of operating conditions has to be selected. In contrast the advantages of LHHW for predicting a wider range of operating conditions were underlined. A comprehensive plausible mechanism-derived FT kinetics models with eight novel elementary reaction pathways along with seven novel WGS kinetics models were developed. The novel combined model FT−III with RDS-2/WGS-VII with RDS-4 was in excellent agreement with experimental results. The MAPD (mean absolute percentage deviation) value reported in this study was at 5.93% less than that of in the literature studies which highlights the significance, reliability and accuracy of the present model.

Model validation was carried out subsequent to completion of the model calibration and the estimation of proper kinetic parameters. The overall purpose of the validation study was to ensure that the model provides a robust and realistic assessment of all the parameters defined by the mathematical model e.g. kinetic parameters, rate of reactants' consumption and products

formation. In order to ensure that the model is precise to an appropriate level, the model was assessed against experimental data at four different operating conditions, which were available for validation, with respect to temperature, pressure, and space velocity. The MAPD obtained between the variables was 14.62% which indicates that the model is satisfactorily validated against measured data. Considering the results of conversion and selectivity, it can be concluded that the implementation of the reactor model, chemical kinetics, and product distribution have been successfully achieved.

The mathematical model reported, together with the developed kinetic model were used to investigate the influence of different process parameters i.e. reaction temperature, total inlet pressure, gas hourly space velocity (GHSV) and inlet hydrogen-to-carbon monoxide (H_2/CO) molar ratio, on catalytic activity and reactor performance. The results obtained from this study can be concluded as following:

Effects of reaction temperature: The results indicated that the increase of reaction temperature had positive influence on catalytic activity and its performance in terms of conversion of syngas compositions. However, increasing the temperature had also an adverse impact as it resulted in increased CO_2 selectivity and the shift toward low molecular weight hydrocarbons products (i.e. Methane, olefins: C_2-C_3, paraffins: C_2-C_7) over the Co/SiO_2 catalyst. In contrast, it was shown that the formation of heavier hydrocarbons (C_{5+}) was favoured at low temperatures. All the reaction rates were enhanced upon increasing temperature ($R_j \propto T$), hence more reactants were consumed and more products were formed. However, the results manifested that the products distributions were not directly proportional to the temperature (in the case of higher molecular weight) as it is explained by the nature of the chain growth probability (α) defined by the rate of propagation (growth) and termination steps. It was

shown that α was inversely proportional to termination reaction rate ($\alpha \propto 1/R_t$). Meanwhile, the mole and mass fraction of heavier hydrocarbons increased upon increasing the α value. This justified why the increase of temperature led to lower liquid product selectivity, while the higher light hydrocarbons formed. Moreover, methane had higher temperature dependency compared to other hydrocarbons due to its lower activation barriers and hence its production rate increased faster than other light hydrocarbons.

Effects of gas hourly space velocity (GHSV): The highest CO and H_2 conversions were obtained at the lowest GHSV values considered in the present thesis. This was true as a low GHSV is associated with a high residence time so that the reactants have sufficient time to react and subsequently their concentrations decrease. The results indicated that the selectivities of heavy FT products were sensitive to space velocity changes on Co/SiO_2 catalyst, while this parameter was the key element to attain the high conversion rates (of CO and H_2). GHSV, similarly to the temperature factor, had substantial impact on the catalytic activity, reaction kinetics and overall performance of the reactor. It was shown that the CO and H_2 consumptions are more sensitive to GHSV at lower temperature condition. For instance, the increase of GHSV from 1800 to 6000 $Nm\ell\ (STP)\ g_{cat}^{-1}\ h^{-1}$ resulted in the reduction of CO and H_2 conversions from 82% and 83% to 51% and 53% at the lower temperature of 490 *K*, respectively; whereas the similar variables decreased from 99% and 82% to 81% and 73% respectively, at the higher temperature of 520 *K*.

In addition, the results manifested the substantial increase of selectivity of heavy products and the decrease of that of methane upon increasing the space velocity, suggesting that the increase of space velocity leads to the elimination of mass transfer resistance so that the dominant effects of diffusional limitation yield the removal of hydrocarbons from the active

sites at the surface of the catalyst. Therefore the increase of GHSV favours the production of long chain heavy hydrocarbon components, while CH_4 selectivity, as expected, goes in the opposite direction. The heavy products' selectivity increases from about 58% to 83% with the increasing of the GHSV from 1800 to 6000 $Nm\ell\ (STP)\ g_{cat}^{-1}\ h^{-1}$; whereas the undesired methane selectivity decreases from about 35% to 10%. It was shown that the lighter olefins (C_2-C_3) and paraffins (C_2-C_7) were nearly unchanged considering significant changes of space velocity in the range of 1800-6000 $Nm\ell\ (STP)\ g_{cat}^{-1}\ h^{-1}$.

Effects of total pressure: Pressure effects were also considerable in that the increase in total pressure moved the product selectivities towards heavy products due to hydrocarbons condensation, which are normally in the gaseous state at atmospheric pressure. In fact, the saturation of catalyst pores by liquid formation happens at high pressure condition. As the total pressure increased from 1 to 30 *bar*, the liquid products' selectivity increased significantly from about 36% to 92%. The changes of CO and H_2 conversions were proportional to the total pressure: increasing pressure resulted in the increment of CO and H_2 conversions from about 39% and 38% at 1 *bar* to 95% and 91% at 30 *bar*, respectively. Also, the selectivity C_2-C_7 paraffins decreased upon increase of the total pressure. For instance, the selectivity of C_7H_{16} decreases from 0.57% to 0.02% as the total pressure varies from 1 to 30 *bar*. Similarly, the selectivity of C_2H_6 and C_3H_8 decreased from 3.49% and 4.15% to 0.12% and 0.14% respectively. Such variation manifested the faster reduction of the hydrocarbon compounds with lower carbon atom number. Hence, the increase of the total pressure had adverse effect on tail gas and LPG productions which exhibited the increase of pressure condition is not desirable if the low chain hydrocarbons are preferable products. Similar behaviours were observed for light olefin components; whereas the olefins to paraffins ratio were not changed. CH_4 selectivity decrease substantially with the increasing of the pressure, which is a favourable condition as

this component is undesired FT products. The CO and H_2 conversion increased faster at lower total pressure (e.g. 1-10 *bar*) compared to that of the higher range of 10-20 *bar*; suggesting that the syngas consumption rate is more sensitive to total pressure at its lower range. When pressure increased from 1 *bar* to 10 *bar* then CO and H_2 raised from about 39% and 38% to about 85% and 82%, respectively; whereas at a higher pressure range, these variables changed from 85% and 82% at 10 *bar* to 92% and 88% at 20 *bar*.

Effects of H_2/CO ratio: The increase of H_2/CO ratio in the inlet reactants led to different proportion of adsorbed hydrogen and surface carbon atoms. CO and H_2 had respectively inhibiting and positive impacts on the rate of reaction, suggesting that the CO consumption rate increases with rising the H_2/CO ratio whereas that of H_2 decreases upon the increase of the molar ratio. This also resulted in enhancing hydrogen concentration on the active sites and increasing the hydrogenation degree of highly concentrated monomers and accelerating the rate of chain termination step. This caused faster desorption of products rather than incorporating to the chain growth, which resulted in a substantial reduction of selectivity of heavy FT products and a subsequent increase of light hydrocarbons (C_2-C_7). Also, the results manifested that the major loss of liquid (C_{5+}) formation was due to methanation reaction in which the C_{5+} and methane selectivities changed from about 93% to 72% and 5% to 20% respectively with increasing the H_2/CO ratio from 1 to 3.5 (*mol/mol*).

The olefins/paraffins ratio slightly decreased upon the increasing of the H_2/CO molar ratio, while the CO_2 selectivity decreased from about 15% to 1%; which implied the slight water gas shift activity at low H_2/CO ratio. It was found from the kinetic model and governed equations in Chapter 3 (see Table 3-18, model WGS-VII with RDS-4) that the water gas shift reaction rate is inversely proportional to the H_2/CO ratio and one can conclude that the partial

pressures of both reactants as well as their proportion have substantial effects on the rate of CO_2 formation. In addition, the trend of changes of R_{WGS} (water gas shift reaction rate) along the axial dimension of the tube length at different H_2/CO molar ratio was illustrated in which the rate decreased from 1.4964×10^{-5} to 1.987×10^{-7} $mol\ g_{cat}^{-1}\ s^{-1}$ upon the increasing of the molar ratio from 1 to 3.5 *mol/mol*.

Optimization: The obtained results, based on parametric studies, indicated that all the process parameters had significant impacts on the output conversion and products selectivities. Hence, all parameters were considered in the multi-objective optimization process using Non-dominated Sorting Genetic Algorithm (NSGA–II) to optimize the fitness functions (i.e. objective functions). The obtained Pareto frontiers revealed the conflict between most of the defined objective functions. Any operating conditions that increased the CO conversion, reduced C_{5+} selectivity while increased the undesirable CH_4 selectivity. It was shown that there was no combination of the operating conditions that could simultaneously optimize all the defined objectives and necessitated the compromise between various objectives in order to find the optimum operating set-point. Comparison of the experimental data with Pareto-frontier solutions revealed that, not all the experiments were conducted at optimum operating conditions and manifested the possibility of remarkable improvement by utilizing the optimum operating conditions obtained from multi-objective optimization and employing those for conducting experiments. The Pareto-front solutions represented an optimal dynamic database that can be used for specific requirements. Different operating conditions can be selected from such database which privileges the optimization of a particular output (e.g. conversion and/or selectivities).

7.2. Future work and recommendations

This thesis studied various kinetics mechanisms for Co-based catalyst that have been used to develop the rate equations for FT reactions and WGS reaction. Nevertheless, more research can be conducted as following:

- The developed rate models proved to be effective for Co-based catalysts; however, it is recommended to investigate the accuracy and reliability of model for other types of catalysts especially iron-based catalysts. The results of such analysis can be used to compare the accuracy of the model for different types of catalysts.
- One of the advantages of this model is its capability for predicting the longer chain hydrocarbons products by expanding the chain growth probability defined by the model (both olefins and paraffins). Upon the availably of the experimental data for these hydrocarbons, the accuracy of the developed kinetic models can be assessed for the prediction of higher hydrocarbon number.
- The developed kinetic models were examined for the certain loaded amount of catalyst in the reactor (i.e. 15% Co/SiO_2 catalyst). It is suggested to conduct the experiments with different amount of catalyst loading to assess the reliability of the kinetic models and adjust the kinetic parameters if necessary.
- The optimized operating conditions achieved from the Pareto-front solutions can be utilized as inputs for conducting new experiments to compare the outcomes (i.e. selectivity and conversion) with the values suggested by the NSGA–II optimization and enhance the performance of FT synthesis.

- The optimization methodology manifested to be effective to improve the FT synthesis performance for a mini-scale reactor. It is suggested to advance and extend the proposed methodology to accommodate the characteristic of larger scale reactor to enhance the performance.

REFERENCES

[1] H. Mahmoudi, "Performance of cobalt-based eggshell catalyst in lowtemperature Fischer-Tropsch synthesis process to produce long-chain hydrocarbons from synthesis gas utilizing fixed-bed reactor technology," Ph.D. Thesis, School of Mechanical Engineering, University of Birmingham, 2015.

[2] M. S. Hadnađev-Kostić, T. J. Vulić, R. P. Marinković-Nedučin, A. D. Nikolić, and B. Jović, "Mg-Fe-mixed oxides derived from layered double hydroxides: a study of the surface properties," *Journal of the Serbian Chemical Society,* vol. 76, pp. 1661-1671, 2011.

[3] E. Lira, C. M. López, F. Oropeza, M. Bartolini, J. Alvarez, M. Goldwasser*, et al.*, "HMS mesoporous silica as cobalt support for the Fischer–Tropsch Synthesis: Pretreatment, cobalt loading and particle size effects," *Journal of Molecular Catalysis A: Chemical,* vol. 281, pp. 146-153, 2/18/ 2008.

[4] S. Gill, A. Tsolakis, K. Dearn, and J. Rodríguez-Fernández, "Combustion characteristics and emissions of Fischer–Tropsch diesel fuels in IC engines," *Progress in Energy and Combustion Science,* vol. 37, pp. 503-523, 2011.

[5] T. Fu, Y. Jiang, J. Lv, and Z. Li, "Effect of carbon support on Fischer–Tropsch synthesis activity and product distribution over Co-based catalysts," *Fuel Processing Technology,* vol. 110, pp. 141-149, 2013.

[6] G. P. van der Laan, *Kinetics, selectivity and scale up of the Fischer-Tropsch synthesis*: [University Library Groningen][Host], 1999.

[7] G. P. Van der Laan and A. A. Beenackers, "Intrinsic kinetics of the gas–solid Fischer–Tropsch and water gas shift reactions over a precipitated iron catalyst," *Applied Catalysis A: General,* vol. 193, pp. 39-53, 2000.

[8] A. Steynberg and M. Dry, *Fischer-Tropsch Technology*. The Netherlands: Elsevier, 2004.

[9] E.I.A, "International Energy Outlook with projection to 2040," *United States Energy Information Administration,* p. 312, July 2013.

[10] A. Abu-Jrai, J. Rodriguez-Fernandez, A. Tsolakis, A. Megaritis, K. Theinnoi, R. Cracknell*, et al.*, "Performance, combustion and emissions of a diesel engine operated with reformed EGR. Comparison of diesel and GTL fuelling," *Fuel,* vol. 88, pp. 1031-1041, 2009.

[11] P. Schaberg, J. Botha, M. Schnell, H.-O. Hermann, N. Pelz, and R. Maly, "Emissions performance of GTL diesel fuel and blends with optimized engine calibrations," SAE Technical Paper2005.

[12] A. Abu-Jrai, A. Tsolakis, K. Theinnoi, R. Cracknell, A. Megaritis, M. Wyszynski*, et al.*, "Effect of gas-to-liquid diesel fuels on combustion characteristics, engine emissions, and exhaust gas fuel reforming. Comparative study," *Energy & fuels,* vol. 20, pp. 2377-2384, 2006.

[13] F. Fischer and H. Tropsch, *Brennstoff Chem.,* vol. 4, pp. 276-285, 1923.

[14] F. Fischer and H. Tropsch, *Brennstoff Chem.,* vol. 5, pp. 201-208, 1924.

[15] F. Fischer and H. Tropsch, *Brennstoff Chem.,* vol. 7, pp. 97-104, 1926.

[16] J. L. Casci, C. M. Lok, and M. D. Shannon, "Fischer–Tropsch catalysis: The basis for an emerging industry with origins in the early 20th Century," *Catalysis Today,* vol. 145, pp. 38-44, 7/15/ 2009.

[17] D. Leckel, "Diesel production from Fischer− Tropsch: the past, the present, and new concepts," *Energy & Fuels,* vol. 23, pp. 2342-2358, 2009.

[18] R. Guettel, U. Kunz, and T. Turek, "Reactors for Fischer-Tropsch Synthesis," *Chemical Engineering & Technology,* vol. 31, pp. 746-754, 2008.

[19] H. Schulz, "Short history and present trends of Fischer–Tropsch synthesis," *Applied Catalysis A: General,* vol. 186, pp. 3-12, 1999.

[20] M. J. Overett, R. O. Hill, and J. R. Moss, "Organometallic chemistry and surface science: mechanistic models for the Fischer–Tropsch synthesis," *Coordination Chemistry Reviews,* vol. 206, pp. 581-605, 2000.

[21] E. van Steen and M. Claeys, "Fischer-Tropsch Catalysts for the Biomass-to-Liquid (BTL)-Process," *Chemical Engineering & Technology,* vol. 31, pp. 655-666, 2008.

[22] P. L. Spath and D. C. Dayton, "Preliminary screening-technical and economic assessment of synthesis gas to fuels and chemicals with emphasis on the potential for biomass-derived syngas," DTIC Document2003.

[23] C. N. Hamelinck, A. P. C. Faaij, H. den Uil, and H. Boerrigter, "Production of FT transportation fuels from biomass; technical options, process analysis and optimisation, and development potential," *Energy,* vol. 29, pp. 1743-1771, 9// 2004.

[24] T. Reddy Keshav and S. Basu, "Gas-to-liquid technologies: India's perspective," *Fuel Processing Technology,* vol. 88, pp. 493-500, 5// 2007.

[25] M. J. Tijmensen, A. P. Faaij, C. N. Hamelinck, and M. R. van Hardeveld, "Exploration of the possibilities for production of Fischer Tropsch liquids and power via biomass gasification," *Biomass and Bioenergy,* vol. 23, pp. 129-152, 2002.

[26] K. Göransson, U. Söderlind, J. He, and W. Zhang, "Review of syngas production via biomass DFBGs," *Renewable and Sustainable Energy Reviews,* vol. 15, pp. 482-492, 2011.

[27] H. Climate changeBoerrigter, H. P. Calis, D. J. Slort, and H. Bodenstaff, "Gas cleaning for integrated biomass gasification (BG) and Fischer-Tropsch (FT) systems; experimental demonstration of two BG-FT systems," in *Proceedings of the 2nd World Conference and Technology Exhibition on Biomass for Energy, Industry and Climate Protection*, 2004, pp. 51-56.

[28] K. Liu, C. Song, and V. Subramani, *Hydrogen and syngas production and purification technologies*: Wiley Online Library, 2010.

[29] T. Doss, "Low severity Fischer-Tropsch synthesis for the production of synthetic hydrocarbon fuels," Aston University, 2012.

[30] A. de Klerk and E. Furimsky, *Catalysis in the refining of Fischer-Tropsch Syncrude*: Royal Society of Chemistry, 2010.

[31] H.-J. Lee, "Optimization of Fischer-Tropsch plant," 2011.

[32] A. Raje, J. R. Inga, and B. H. Davis, "Fischer-Tropsch synthesis: process considerations based on performance of iron-based catalysts," *Fuel,* vol. 76, pp. 273-280, 1997.

[33] A. P. Raje and B. H. Davis, "Fischer-Tropsch synthesis over iron-based catalysts in a slurry reactor. Reaction rates, selectivities and implications for improving hydrocarbon productivity," *Catalysis today,* vol. 36, pp. 335-345, 1997.

[34] G. F. Froment, K. B. Bischoff, and J. De Wilde, *Chemical reactor analysis and design* vol. 2: Wiley New York, 1990.

[35] Y.-N. Wang, Y.-W. Li, L. Bai, Y.-L. Zhao, and B.-J. Zhang, "Correlation for gas–liquid equilibrium prediction in Fischer–Tropsch synthesis," *Fuel,* vol. 78, pp. 911-917, 1999.

[36] A. De Klerk, "Refining of Fischer–Tropsch syncrude: lessons from the past, Prepr," *Pap.-Am. Chem. Soc., Div. Petrol. Chem,* vol. 53, p. 105, 2008.

[37] A. De Klerk, "Gas-to-liquids conversion," in *Natural Gas Conversion Technologies Workshop of ARPA-E. US Department of Energy, Houston, TX*, 2012.

[38] R. Rapier. (2010). *Inside Shell's Bintulu GTL Plant*. Available: http://www.energytrendsinsider.com

[39] A. Di Fronzo and D. Roberto, "Biomass to Liquid Process: new kind of cobalt and iron based catalysts for the Fischer-Tropsch Synthesis."

[40] A. P. Steynberg, "Chapter 1 - Introduction to Fischer-Tropsch Technology," in *Studies in Surface Science and Catalysis*. vol. Volume 152, S. André and D. Mark, Eds., ed: Elsevier, 2004, pp. 1-63.

[41] J. A. Velasco, L. Lopez, M. Velásquez, M. Boutonnet, S. Cabrera, and S. Järås, "Gas to liquids: A technology for natural gas industrialization in Bolivia," *Journal of Natural Gas Science and Engineering,* vol. 2, pp. 222-228, 2010.

[42] M. Dry, "The Fischer-Tropsch Synthesis," *Catalysis science and technology,* vol. 1, pp. 159-255, 1981.

[43] J.-P. Wauquier, *Petroleum Refining: Crude oil, petroleum products, process flowsheets* vol. 1: Éditions Technip, 1995.

[44] B. Jager, "Developments in Fischer-Tropsch technology," *Studies in surface science and catalysis,* pp. 25-34, 1998.

[45] H. Boerrigter, H. den Uil, and H.-P. Calis, "Green diesel from biomass via Fischer-Tropsch synthesis: new insights in gas cleaning and process design," ed: CPL Press: Newbury, UK, 2003, pp. 371-383.

[46] M. J. A. Tijmensen, A. P. C. Faaij, C. N. Hamelinck, and M. R. M. van Hardeveld, "Exploration of the possibilities for production of Fischer Tropsch liquids and power via biomass gasification," *Biomass and Bioenergy,* vol. 23, pp. 129-152, 8// 2002.

[47] A. N. Pour, Y. Zamani, A. Tavasoli, S. M. Kamali Shahri, and S. A. Taheri, "Study on products distribution of iron and iron–zeolite catalysts in Fischer–Tropsch synthesis," *Fuel,* vol. 87, pp. 2004-2012, 2008.

[48] A. Steynberg and M. Dry, "Chemical concepts used for engineering purposes (edited by Steynberg A, Dry M)," *Stud Surf Sci Catal,* vol. 152, pp. 196-257, 2004.

[49] M. E. Dry, "The Fischer-Tropsch process-commercial aspects," *Catalysis Today,* vol. 6, pp. 183-206, 1990.

[50] R. B. Anderson and P. H. Emmett, *Catalysis: Hydrocarbon Synthesis, Hydrogenation and Cyclization*: Reinhold, 1956.

[51] Y. Liu, B.-T. Teng, X.-H. Guo, Y. Li, J. Chang, L. Tian*, et al.*, "Effect of reaction conditions on the catalytic performance of Fe-Mn catalyst for Fischer-Tropsch synthesis," *Journal of Molecular Catalysis A: Chemical,* vol. 272, pp. 182-190, 2007.

[52] B. H. Davis, "Fischer-Tropsch synthesis: relationship between iron catalyst composition and process variables," *Catalysis Today,* vol. 84, pp. 83-98, 2003.

[53] M. E. Dry, "The Fischer–Tropsch process: 1950–2000," *Catalysis today,* vol. 71, pp. 227-241, 2002.

[54] J. L. Casci, C. M. Lok, and M. D. Shannon, "Fischer–Tropsch catalysis: The basis for an emerging industry with origins in the early 20th Century," *Catalysis Today,* vol. 145, pp. 38-44, 2009.

[55] M. E. Dry, "The fischer-tropsch process - commercial aspects," *Catalysis Today,* vol. 6, pp. 183-206, 1// 1990.

[56] J.-K. Jeon, C.-J. Kim, Y.-K. Park, and S.-K. Ihm, "Catalytic properties of potassium-or lanthanum-promoted Co/γ-Al_2O_3 catalysts in carbon monoxide hydrogenation," *Korean Journal of Chemical Engineering,* vol. 21, pp. 365-369, 2004.

[57] A. N. Stranges, "A history of the fischer-tropsch synthesis in Germany 1926-45," *Studies in surface science and catalysis,* pp. 1-27, 2007.

[58] Y. H. Kim, K.-W. Jun, H. Joo, C. Han, and I. K. Song, "A simulation study on gas-to-liquid (natural gas to Fischer–Tropsch synthetic fuel) process optimization," *Chemical Engineering Journal,* vol. 155, pp. 427-432, 2009.

[59] A. De la Osa, A. De Lucas, A. Romero, J. Valverde, and P. Sánchez, "Influence of the catalytic support on the industrial Fischer–Tropsch synthetic diesel production," *Catalysis today,* vol. 176, pp. 298-302, 2011.

[60] R. Oukaci, A. H. Singleton, and J. G. Goodwin, "Comparison of patented Co F–T catalysts using fixed-bed and slurry bubble column reactors," *Applied Catalysis A: General,* vol. 186, pp. 129-144, 1999.

[61] E. Iglesia, S. L. Soled, R. A. Fiato, and G. H. Via, "Bimetallic synergy in cobalt ruthenium Fischer-Tropsch synthesis catalysts," *Journal of Catalysis,* vol. 143, pp. 345-368, 1993.

[62] E. Iglesia, S. L. Soled, R. A. Fiato, and G. H. Via, "Dispersion, support, and bimetallic effects in Fischer-Tropsch synthesis on cobalt catalysts," *Studies in Surface Science and Catalysis,* vol. 81, pp. 433-442, 1994.

[63] A. Bao, K. Liew, and J. Li, "Fischer–Tropsch synthesis on CaO-promoted Co/Al 2 O 3 catalysts," *Journal of Molecular Catalysis A: Chemical,* vol. 304, pp. 47-51, 2009.

[64] A. Y. Khodakov, "Fischer-Tropsch synthesis: Relations between structure of cobalt catalysts and their catalytic performance," *Catalysis Today,* vol. 144, pp. 251-257, 2009.

[65] S. Sie and R. Krishna, "Fundamentals and selection of advanced Fischer–Tropsch reactors," *Applied Catalysis A: General,* vol. 186, pp. 55-70, 1999.

[66] M. E. Dry, "Practical and theoretical aspects of the catalytic Fischer-Tropsch process," *Applied Catalysis A: General,* vol. 138, pp. 319-344, 1996.

[67] B. H. Davis, "Overview of reactors for liquid phase Fischer–Tropsch synthesis," *Catalysis Today,* vol. 71, pp. 249-300, 2002.

[68] R. Guettel and T. Turek, "Comparison of different reactor types for low temperature Fischer–Tropsch synthesis: A simulation study," *Chemical Engineering Science,* vol. 64, pp. 955-964, 3// 2009.

[69] J. De Swart, R. Krishna, and S. Sie, "Selection, design and scale up of the Fischer Tropsch slurry reactor," 1997.

[70] B. Jager, "Development of fischer tropsch reactors," in *Prepared for Presentation at the AIChE 2003 Spring National Meeting, New Orleans, LA*, 2003.

[71] C. N. Satterfield, G. A. Huff Jr, H. G. Stenger, J. L. Carter, and R. J. Madon, "A comparison of Fischer-Tropsch synthesis in a fixed-bed reactor and in a slurry reactor," *Industrial & engineering chemistry fundamentals,* vol. 24, pp. 450-454, 1985.

[72] B. Todic, V. V. Ordomsky, N. M. Nikacevic, A. Y. Khodakov, and D. B. Bukur, "Opportunities for intensification of Fischer-Tropsch synthesis through reduced formation of methane over cobalt catalysts in microreactors," *Catalysis Science & Technology,* vol. 5, pp. 1400-1411, 2015.

[73] W. Brötz, "Zur Systematik der Fischer-Tropsch-Katalyse," *Zeitschrift für Elektrochemie und angewandte physikalische Chemie,* vol. 53, pp. 301-306, 1949.

[74] C. C. Hall, D. Gall, and S. L. Smith, "A comparison on the fixed-bed, liquid-phase ("slurry") and fluidized-bed techniques in the Fischer-Tropsch synthesis," *J. Inst. Pet. Technologists,* vol. 38, pp. 845-875, 1952.

[75] R. Anderson, F. Karn, and J. Schulz, "US Bur. Mines," *Bull,* vol. 614, 1964.

[76] M. E. Dry, T. Shingles, and L. J. Boshoff, "Rate of the Fischer-Tropsch reaction over iron catalysts," *Journal of Catalysis,* vol. 25, pp. 99-104, 4// 1972.

[77] C.-H. Yang, F. E. Massoth, and A. G. Oblad, "Kinetics of CO + H_2 Reaction over Co-Cu-Al_2O_3 Catalyst," in *Hydrocarbon Synthesis from Carbon Monoxide and Hydrogen*. vol. 178, ed: American Chemical Society, 1979, pp. 35-46.

[78] G. Bub, M. Baerns, B. Büssemeier, and C. Frohning, "Prediction of the performance of catalytic fixed bed reactors for Fischer-Tropsch synthesis," *Chemical Engineering Science,* vol. 35, pp. 348-355, 1980.

[79] R. B. Pannell, C. L. Kibby, and T. P. Kobylinski, "Tokyo," pp. 447-459, 1980.

[80] J. Wang, " Ph.D. Thesis, Bringham Young University, Provo, UT," 1987.

[81] A. Jess, R. Popp, and K. Hedden, "Production of diesel oil and wax by Fischer-Tropsch-synthesis using a nitrogen-rich synthesis gas-Investigations on a semi-technical scale," *OIL GAS-EUROPEAN MAGAZINE,* vol. 24, pp. 34-43, 1998.

[82] R. Zennaro, M. Tagliabue, and C. H. Bartholomew, "Kinetics of Fischer–Tropsch synthesis on titania-supported cobalt," *Catalysis Today,* vol. 58, pp. 309-319, 2000.

[83] X. Zhan, H. J. Robota, and K. B. Arcuri, "Elucidation of Fischer-Tropsch reaction kinetics," *American Chemical Society, Division of Fuel Chemistry,* vol. 49, pp. 200-202, 2004.

[84] M. A. Marvast, M. Sohrabi, S. Zarrinpashne, and G. Baghmisheh, "Fischer-Tropsch Synthesis: Modeling and Performance Study for Fe-HZSM5 Bifunctional Catalyst," *Chemical Engineering & Technology,* vol. 28, pp. 78-86, 2005.

[85] T. K. Das, W. A. Conner, J. Li, G. Jacobs, M. E. Dry, and B. H. Davis, "Fischer-Tropsch synthesis: kinetics and effect of water for a Co/SiO_2 catalyst," *Energy & fuels,* vol. 19, pp. 1430-1439, 2005.

[86] S. Craxford and E. K. Rideal, "338. The mechanism of the synthesis of hydrocarbons from water gas," *J. Chem. Soc.,* pp. 1604-1614, 1939.

[87] W. Sachtler, "Elementary steps in the catalyzed conversion of synthesis gas," in *Proceedings of 8th International Congress on Catalysis, West Berlin*, 1984, pp. 151-173.

[88] A. T. Bell, "Surface chemistry of carbonaceous species," *Studies in Surface Science and Catalysis,* vol. 48, pp. 91-109, 1989.

[89] F. Fischer and H. Tropsch, "The preparation of synthetic oil mixtures (synthol) from carbon monoxide and hydrogen," *Brennstoff-Chem,* vol. 4, pp. 276-285, 1923.

[90] F. A. Fernandes, "Polymerization Kinetics of Fischer-Tropsch Reaction on Iron Based Catalysts and Product Grade Optimization," *Chemical engineering & technology,* vol. 28, pp. 930-938, 2005.

[91] B. Wojciechowski, "The kinetics of the Fischer-Tropsch synthesis," *Catalysis Reviews Science and Engineering,* vol. 30, pp. 629-702, 1988.

[92] R. C. Brady III and R. Pettit, "Mechanism of the Fischer-Tropsch reaction. The chain propagation step," *Journal of the American Chemical Society,* vol. 103, pp. 1287-1289, 1981.

[93] R. C. Brady and R. Pettit, "Reactions of diazomethane on transition-metal surfaces and their relationship to the mechanism of the Fischer-Tropsch reaction," *Journal of the American Chemical Society,* vol. 102, pp. 6181-6182, 1980/09/01 1980.

[94] P. M. Maitlis, A. Haynes, G. J. Sunley, and M. J. Howard, "Methanol carbonylation revisited: thirty years on," *Journal of the Chemical Society, Dalton Transactions,* pp. 2187-2196, 1996.

[95] P. M. Maitlis, R. Quyoum, H. C. Long, and M. L. Turner, "Towards a chemical understanding of the Fischer–Tropsch reaction: alkene formation," *Applied Catalysis A: General,* vol. 186, pp. 363-374, 10/4/ 1999.

[96] P. M. Maitlis, "A new view of the Fischer-Tropsch polymerisation reaction," in *Pure and Applied Chemistry* vol. 61, ed, 1989, p. 1747.

[97] H. H. Storch, R. A. Anderson, and N. Golumbic, *The Fischer-Tropsch and related syntheses* vol. 6: Wiley New York, 1951.

[98] T. Chang, "US consumption of alternative road fuels growing," *Oil & Gas Journal,* vol. 97, pp. 37-39, 1999.

[99] T.-S. Lee, "Numerical modeling and simulation of Fischer-Tropsch packed-bed reactor and its thermal management," University of Florida, 2011.

[100] A. Sternberg and J. Wender, in *Proc. Intern. Conf. Coordination Chem*, London, 1959.

[101] S. Z. Roginski, in *3rd Congress on Catalysis*, Amsterdam, 1965, p. 939.

[102] R. George, J.-A. M. Andersen, and J. R. Moss, "A comparison of the rates of alkyl migration in the complexes [CpM(CO)2R](M・Fe, Ru, Os; Cp = η5-C5H5)," *Journal of Organometallic Chemistry,* vol. 505, pp. 131-133, 12/13/ 1995.

[103] K. G. Anderson and J. G. Ekerdt, "Study of Fischer-Tropsch synthesis over FeSiO2: Effect of diethylamine on hydrocarbon and alcohol production," *Journal of Catalysis,* vol. 95, pp. 602-604, 10// 1985.

[104] A. O. I. Rautavuoma and H. S. van der Baan, "Kinetics and mechanism of the Fischer-Tropsch hydrocarbon synthesis on abobalt on alumina catalyst," *Appl. Catal.,* vol. 1, pp. 247-272, 1981.

[105] C. N. Satterfield and T. K. Sherwood, *The role of diffusion in catalysis*: Addison-Wesley ^ eMassachussets Massachussets, 1963.

[106] B. Sarup and B. W. Wojciechowski, "Studies of the fischer-tropsch synthesis on a cobalt catalyst II. Kinetics of carbon monoxide conversion to methane and to higher hydrocarbons," *The Canadian Journal of Chemical Engineering,* vol. 67, pp. 62-74, 1989.

[107] I. C. Yates and C. N. Satterfield, "Intrinsic kinetics of the Fischer-Tropsch synthesis on a cobalt catalyst," *Energy & Fuels,* vol. 5, pp. 168-173, 1991.

[108] M. A. Vannice, "The Catalytic Synthesis of Hydrocarbons from Carbon Monoxide and Hydrogen," *Catalysis Reviews,* vol. 14, pp. 153-191, 1976/01/01 1976.

[109] E. Iglesia, S. C. Reyes, R. J. Madon, and S. L. Soled, "Selectivity Control and Catalyst Design in the Fischer-Tropsch Synthesis: Sites, Pellets, and Reactors," in *Advances in Catalysis*. vol. Volume 39, H. P. D.D. Eley and B. W. Paul, Eds., ed: Academic Press, 1993, pp. 221-302.

[110] R. J. Madon and W. F. Taylor, "Fischer-Tropsch synthesis on a precipitated iron catalyst," *Journal of Catalysis,* vol. 69, pp. 32-43, 5// 1981.

[111] N. O. Elbashir, D. B. Borough, R. Gupta, and C. B. Roberts, "Reaction pathway and kinetic modeling of Fischer-Tropsch synthesis over an alumina supported cobalt catalyst in supercritical-hexane media," *C1 Chemistry for the Production of Ultra-Clean Liquid Transportation Fuels and Hydrogen,* p. 14, 2004.

[112] C. S. Kellner and A. T. Bell, "The kinetics and mechanism of carbon monoxide hydrogenation over alumina-supported ruthenium," *Journal of Catalysis,* vol. 70, pp. 418-432, 1981.

[113] F. G. Botes, B. van Dyk, and C. McGregor, "The Development of a Macro Kinetic Model for a Commercial Co/Pt/Al2O3 Fischer− Tropsch Catalyst," *Industrial & Engineering Chemistry Research,* vol. 48, pp. 10439-10447, 2009.

[114] H. Atashi, M. Mansouri, S. Hosseini, M. Khorram, A. Mirzaei, M. Karimi*, et al.*, "Intrinsic kinetics of the Fischer-Tropsch synthesis over an impregnated cobalt-potassium catalyst," *Korean Journal of Chemical Engineering,* vol. 29, pp. 304-309, 2012/03/01 2012.

[115] E. Iglesia, S. L. Soled, J. E. Baumgartner, and S. C. Reyes, "Synthesis and catalytic properties of eggshell cobalt catalysts for the Fischer-Tropsch synthesis," *Journal of catalysis,* vol. 153, pp. 108-122, 1995.

[116] G. P. v. d. Laan, "Kinetics, selectivity and scale up of the Fischer-Tropsch synthesis," University of Groningen, Groningen, 1999.

[117] D. S. Newsome, "The Water-Gas Shift Reaction," *Catalysis Reviews,* vol. 21, pp. 275-318, 1980/01/01 1980.

[118] M. E. Dry, "Advances in Fishcher-Tropsch Chemistry," *Product R&D,* vol. 15, pp. 282-286, 1976/12/01 1976.

[119] J. L. Feimer, P. L. Silveston, and R. R. Hudgins, "Steady-state study of the Fischer-Tropsch reaction," *Industrial & Engineering Chemistry Product Research and Development,* vol. 20, pp. 609-615, 1981/12/01 1981.

[120] W. H. Zimmerman and D. B. Bukur, "Reaction kinetics over iron catalysts used for the fischer-tropsch synthesis," *The Canadian Journal of Chemical Engineering,* vol. 68, pp. 292-301, 1990.

[121] E. S. Lox and G. F. Froment, "Kinetics of the Fischer-Tropsch reaction on a precipitated promoted iron catalyst. 2. Kinetic modeling," *Industrial & Engineering Chemistry Research,* vol. 32, pp. 71-82, 1993/01/01 1993.

[122] W. J. Shen, J. L. Zhou, and B. J. Zhang, "Kinetics of Fischer-Tropsch synthesis over precipitated iron catalyst," *J. Nat. Gas Chem.,* vol. 4, pp. 385-400, 1994.

[123] B.-T. Teng, J. Chang, J. Yang, G. Wang, C.-H. Zhang, Y.-Y. Xu*, et al.*, "Water gas shift reaction kinetics in Fischer–Tropsch synthesis over an industrial Fe–Mn catalyst," *Fuel,* vol. 84, pp. 917-926, 5// 2005.

[124] A. N. Pour, M. R. Housaindokht, S. F. Tayyari, and J. Zarkesh, "Kinetics of the water-gas shift reaction in Fischer-Tropsch synthesis over a nano-structured iron catalyst," *Journal of Natural Gas Chemistry,* vol. 19, pp. 362-368, 2010.

[125] D. G. Rethwisch and J. A. Dumesic, "Adsorptive and Catalytic Properties of Carbon Monoxide and Carbon Dioxide Over Supported Metal Oxides," in *Catalytic Activation of Carbon Dioxide*. vol. 363, ed: American Chemical Society, 1988, pp. 102-122.

[126] G. H. Graaf, J. G. M. Winkelman, E. J. Stamhuis, and A. A. C. M. Beenackers, "Kinetics of the three phase methanol synthesis," *Chemical Engineering Science,* vol. 43, pp. 2161-2168, // 1988.

[127] J. Kuo, F. Sanzo, W. Garwood, K. Gupte, C. Lang, T. Leib*, et al.*, "Slurry Fischer-Tropsch/Mobil Two-Stage Process of Converting Syngas to High Octane Gasoline," *Final report, DOE contract no. DE-AC22-80PC30022 (June 1983),* 1983.

[128] G. A. Huff and C. N. Satterfield, "Intrinsic kinetics of the Fischer-Tropsch synthesis on a reduced fused-magnetite catalyst," *Industrial & Engineering Chemistry Process Design and Development,* vol. 23, pp. 696-705, 1984/10/01 1984.

[129] S. Oki and R. Mezaki, "Identification of rate-controlling steps for the water-gas shift reaction over an iron oxide catalyst," *The Journal of Physical Chemistry,* vol. 77, pp. 447-452, 1973/02/01 1973.

[130] D. C. Grenoble, M. M. Estadt, and D. F. Ollis, "The chemistry and catalysis of the water gas shift reaction: 1. The kinetics over supported metal catalysts," *Journal of Catalysis,* vol. 67, pp. 90-102, 1// 1981.

[131] M. E. Dry, T. Shingles, L. J. Boshoff, and G. J. Oosthuizen, "Heats of chemisorption on promoted iron surfaces and the role of alkali in Fischer-Tropsch synthesis," *Journal of Catalysis,* vol. 15, pp. 190-199, 10// 1969.

[132] A. Haghtalab, M. Nabipoor, and S. Farzad, "Kinetic modeling of the Fischer–Tropsch synthesis in a slurry phase bubble column reactor using Langmuir–Freundlich isotherm," *Fuel Processing Technology,* vol. 104, pp. 73-79, 2012.

[133] J. Yang, Y. Liu, J. Chang, Y.-N. Wang, L. Bai, Y.-Y. Xu*, et al.*, "Detailed kinetics of Fischer-Tropsch synthesis on an industrial Fe-Mn catalyst," *Industrial & engineering chemistry research,* vol. 42, pp. 5066-5090, 2003.

[134] Y.-N. Wang, W.-P. Ma, Y.-J. Lu, J. Yang, Y.-Y. Xu, H.-W. Xiang*, et al.*, "Kinetics modelling of Fischer–Tropsch synthesis over an industrial Fe–Cu–K catalyst," *Fuel,* vol. 82, pp. 195-213, 2003.

[135] J. Chang, L. Bai, B. Teng, R. Zhang, J. Yang, Y. Xu*, et al.*, "Kinetic modeling of Fischer–Tropsch synthesis over Fe–Cu–K–SiO2 catalyst in slurry phase reactor," *Chemical Engineering Science,* vol. 62, pp. 4983-4991, 2007.

[136] N. Moazami, H. Mahmoudi, K. Rahbar, P. Panahifar, A. Tsolakis, and M. L. Wyszynski, "Catalytic performance of cobalt–silica catalyst for Fischer–Tropsch synthesis: Effects of reaction rates on efficiency of liquid synthesis," *Chemical Engineering Science,* vol. 134, pp. 374-384, 9/29/ 2015.

[137] N. Moazami, M. L. Wyszynski, H. Mahmoudi, A. Tsolakis, Z. Zou, P. Panahifar*, et al.*, "Modelling of a fixed bed reactor for Fischer–Tropsch synthesis of simulated N_2-rich syngas over Co/SiO_2: Hydrocarbon production," *Fuel,* vol. 154, pp. 140-151, 8/15/ 2015.

[138] N. Moazami, H. Mahmoudi, P. Panahifar, K. Rahbar, A. Tsolakis, and M. L. Wyszynski, "Mathematical Modeling and Performance Study of Fischer-tropsch Synthesis of Liquid Fuel over Cobalt-silica," *Energy Procedia,* vol. 75, pp. 62-71, 8// 2015.

[139] V. Ponec and W. A. van Barneveld, "The Role of Chemisorption of Fischer-Tropsch Synthesis," *Industrial & Engineering Chemistry Product Research and Development,* vol. 18, pp. 268-271, 1979/12/01 1979.

[140] A. Mosayebi and A. Haghtalab, "The comprehensive kinetic modeling of the Fischer–Tropsch synthesis over Co@Ru/γ-Al_2O_3 core–shell structure catalyst," *Chemical Engineering Journal,* vol. 259, pp. 191-204, 1/1/ 2015.

[141] M. Ojeda, R. Nabar, A. U. Nilekar, A. Ishikawa, M. Mavrikakis, and E. Iglesia, "CO activation pathways and the mechanism of Fischer–Tropsch synthesis," *Journal of Catalysis,* vol. 272, pp. 287-297, 6/15/ 2010.

[142] W. A. A. van Barneveld and V. Ponec, "Reactions of CHxCl4−x with hydrogen: Relation to the Fischer-Tropsch synthesis of hydrocarbons," *Journal of Catalysis,* vol. 88, pp. 382-387, 8// 1984.

[143] G. P. Van Der Laan and A. Beenackers, "Kinetics and selectivity of the Fischer–Tropsch synthesis: a literature review," *Catalysis Reviews,* vol. 41, pp. 255-318, 1999.

[144] R. E. Hayes and S. T. Kolaczkowski, *Introduction to catalytic combustion*: CRC Press, 1998.

[145] A. Michaelides and P. Hu, "Catalytic Water Formation on Platinum: A First-Principles Study," *Journal of the American Chemical Society,* vol. 123, pp. 4235-4242, 2001/05/01 2001.

[146] V. Perrichon, M. Pijolat, and M. Primet, "Surface species involved during the hydrogenation of CO or CO2 on iron-alumina catalysts," *Journal of Molecular Catalysis,* vol. 25, pp. 207-217, 7// 1984.

[147] G. Jacobs, E. Chenu, P. M. Patterson, L. Williams, D. Sparks, G. Thomas*, et al.*, "Water-gas shift: comparative screening of metal promoters for metal/ceria systems and role of the metal," *Applied Catalysis A: General,* vol. 258, pp. 203-214, 2/20/ 2004.

[148] L. J. Broadbelt and R. Q. Snurr, "Applications of molecular modeling in heterogeneous catalysis research," *Applied Catalysis A: General,* vol. 200, pp. 23-46, 8/28/ 2000.

[149] J. A. Dumesic, *The Microkinetics of heterogeneous catalysis*. Washington, DC: American Chemical Society, 1993.

[150] R. B. Bird, W. E. Stewart, and E. N. Lightfoot, *Transport Phenomena*: Wiley, 2007.

[151] A. Y. Khodakov, A. Griboval-Constant, R. Bechara, and V. L. Zholobenko, "Pore Size Effects in Fischer Tropsch Synthesis over Cobalt-Supported Mesoporous Silicas," *Journal of Catalysis,* vol. 206, pp. 230-241, 3/10/ 2002.

[152] C. G. Visconti, E. Tronconi, L. Lietti, P. Forzatti, S. Rossini, and R. Zennaro, "Detailed kinetics of the Fischer–Tropsch synthesis on cobalt catalysts based on H-assisted CO activation," *Topics in Catalysis,* vol. 54, pp. 786-800, 2011.

[153] D. van Herk, P. Castaño, M. Quaglia, M. T. Kreutzer, M. Makkee, and J. A. Moulijn, "Avoiding segregation during the loading of a catalyst–inert powder mixture in a packed micro-bed," *Applied Catalysis A: General,* vol. 365, pp. 110-121, 8/15/ 2009.

[154] U. Mann, *Principles of chemical reactor analysis and design: new tools for industrial chemical reactor operations*: John Wiley & Sons, 2009.

[155] D. Song and J. Li, "Effect of catalyst pore size on the catalytic performance of silica supported cobalt Fischer–Tropsch catalysts," *Journal of Molecular Catalysis A: Chemical,* vol. 247, pp. 206-212, 2006.

[156] D. M. Himmelblau, *Process analysis by statistical methods [by] David M. Himmelblau*. New York: Wiley, 1970.

[157] H. J. Berendsen, *A student's guide to data and error analysis*: Cambridge University Press, 2011.

[158] S. Trek. *F Distribution Calculator: Online Statistical Table*. Available: http://stattrek.com/online-calculator/f-distribution.aspx

[159] S. Trek. *T Distribution Calculator: Online Statistical Table*. Available: http://stattrek.com/online-calculator/t-distribution.aspx

[160] C. M. Van Den Bleek, K. Van Der Wiele, and P. J. Van Den Berg, "The effect of dilution on the degree of conversion in fixed bed catalytic reactors," *Chemical Engineering Science,* vol. 24, pp. 681-694, 4// 1969.

[161] C. Perego and P. Villa, "Catalyst preparation methods," *Catalysis Today,* vol. 34, pp. 281-305, 2/28/ 1997.

[162] N. Moazami, M. L. Wyszynski, H. Mahmoudi, A. Tsolakis, Z. Zou, P. Panahifar*, et al.*, "Modelling of a fixed bed reactor for Fischer–Tropsch synthesis of simulated N2-rich syngas over Co/SiO2: Hydrocarbon production," *Fuel,* vol. 154, pp. 140-151, 8/15/ 2015.

[163] W. H. Lee and C. H. Bartholomew, "Multiple reaction states in CO hydrogenation on alumina-supported cobalt catalysts," *Journal of Catalysis,* vol. 120, pp. 256-271, 1989.

[164] C. H. Bartholomew and W.-H. Lee, "Effects of support on methane selectivity in cobalt-catalyzed Fischer-Tropsch synthesis: A kinetic model," *Studies in Surface Science and Catalysis,* vol. 130, pp. 1151-1156, 2000.

[165] M. A. Vannice, "The catalytic synthesis of hydrocarbons from H_2-CO mixtures over the group VIII metals: II. The kinetics of the methanation reaction over supported metals," *Journal of Catalysis,* vol. 37, pp. 462-473, 6/6 1975.

[166] R. A. Dictor and A. T. Bell, "Fischer-Tropsch synthesis over reduced and unreduced iron oxide catalysts," *Journal of Catalysis,* vol. 97, pp. 121-136, 1986.

[167] J. G. Ekerdt and A. T. Bell, "Synthesis of hydrocarbons from CO and H 2 over silica-supported Ru: reaction rate measurements and infrared spectra of adsorbed species," *Journal of Catalysis,* vol. 58, pp. 170-187, 1979.

[168] S. Shetty, A. Jansen, and R. A. van Santen, "Methane formation on corrugated Ru surfaces," *The Journal of Physical Chemistry C,* vol. 114, pp. 22630-22635, 2010.

[169] B. Todic, T. Bhatelia, G. F. Froment, W. Ma, G. Jacobs, B. H. Davis*, et al.*, "Kinetic Model of Fischer–Tropsch Synthesis in a Slurry Reactor on Co–Re/Al_2O_3 Catalyst," *Industrial & Engineering Chemistry Research,* vol. 52, pp. 669-679, 2013/01/16 2012.

[170] C. G. Visconti, E. Tronconi, L. Lietti, R. Zennaro, and P. Forzatti, "Development of a complete kinetic model for the Fischer–Tropsch synthesis over Co/Al_2O_3 catalysts," *Chemical Engineering Science,* vol. 62, pp. 5338-5343, 2007.

[171] J. Yang, D. Chen, and A. Holmen, "Understanding the kinetics and Re promotion of carbon nanotube supported cobalt catalysts by SSITKA," *Catalysis Today,* vol. 186, pp. 99-108, 2012.

[172] W. Ma, G. Jacobs, T. K. Das, C. M. Masuku, J. Kang, V. R. R. Pendyala*, et al.*, "Fischer–Tropsch Synthesis: Kinetics and Water Effect on Methane Formation over 25% Co/γ-Al_2O_3 Catalyst," *Industrial & Engineering Chemistry Research,* vol. 53, pp. 2157-2166, 2014.

[173] W. H. Hung and S. L. Bernasek, "Adsorption and decomposition of ethylene and acetylene on Fe(100)," *Surface Science,* vol. 339, pp. 272-290, 10/1/ 1995.

[174] A. A. Mirzaei, B. Shirzadi, H. Atashi, and M. Mansouri, "Modeling and operating conditions optimization of Fischer–Tropsch synthesis in a fixed-bed reactor," *Journal of Industrial and Engineering Chemistry,* vol. 18, pp. 1515-1521, 2012.

[175] B.-T. Teng, J. Chang, C.-H. Zhang, D.-B. Cao, J. Yang, Y. Liu*, et al.*, "A comprehensive kinetics model of Fischer–Tropsch synthesis over an industrial Fe–Mn catalyst," *Applied Catalysis A: General,* vol. 301, pp. 39-50, 2/10/ 2006.

[176] W. Qian, H. Zhang, W. Ying, and D. Fang, "The comprehensive kinetics of Fischer–Tropsch synthesis over a Co/AC catalyst on the basis of CO insertion mechanism," *Chemical Engineering Journal,* vol. 228, pp. 526-534, 7/15/ 2013.

[177] S. Storsæter, D. Chen, and A. Holmen, "Microkinetic modelling of the formation of C_1 and C_2 products in the Fischer–Tropsch synthesis over cobalt catalysts," *Surface science,* vol. 600, pp. 2051-2063, 2006.

[178] N. Park, J.-R. Kim, Y. Yoo, J. Lee, and M.-J. Park, "Modeling of a pilot-scale fixed-bed reactor for iron-based Fischer–Tropsch synthesis: Two-dimensional approach for optimal tube diameter," *Fuel,* vol. 122, pp. 229-235, 4/15/ 2014.

[179] K. Deb, *Multi-Objective Optimization using Evolutionary Algorithms*: John Wiley & sons Ltd, 2001.

[180] M. Gen and R. Cheng, *Genetic Algorithms and Engineering Optimizations*, 1st ed ed. Canada: John Wiley and sons, 2000.

[181] D. E. Goldberg, *Genetic Algorithms in Search, Optimization and Machine Learning*: Addison-Wesley Longman Publishing Co., Inc., 1989.

[182] A. Konak, D. W. Coit, and A. E. Smith, "Multi-objective optimization using genetic algorithms: A tutorial," *Reliability Engineering & System Safety,* vol. 91, pp. 992-1007, 9// 2006.

[183] G. O. T. U. s. Guide, "The MathWorks, Inc.," R2013b, Ed., Version 3.2.4 ed, 2013.

APPENDIX

APPENDIX

Table A. 1 Reaction pathway and LHHW rate expressions developed for model FT−I based on unassisted CO dissociation mechanism

No.	General Reaction Path	Kinetic parameter	Rate Equations
1	$CO + \psi \rightleftarrows CO - \psi$	K_1	$K_1 P_{CO} \psi = \psi_{CO}$
2	$H_2 + 2\psi \rightleftarrows 2H - \psi$	K_2	$K_2 P_{H_2} \psi^2 = \psi_H^2$
3	$CO - \psi + \psi \rightleftarrows C - \psi + O - \psi$	K_3	$K_3 \psi_{CO} \psi = \psi_C \psi_O$
4	$O - \psi + H - \psi \rightleftarrows OH - \psi + \psi$	K_4	$K_4 \psi_O \psi_H = \psi_{OH} \psi$
5	$OH - \psi + H - \psi \rightleftarrows H_2O + 2\psi$	K_5	$k_5 \psi_{OH} \psi_H = P_{H_2O} \psi^2$
6	$C - \psi + H - \psi \rightleftarrows CH - \psi + \psi$	K_6	$K_6 \psi_C \psi_H = \psi_{CH} \psi$
7	$CH - \psi + H - \psi \rightleftarrows CH_2 - \psi + \psi$	K_7	$K_7 \psi_{CH} \psi_H = \psi_{CH_2} \psi$
8	$CH_2 - \psi + H - \psi \rightarrow CH_3 - \psi + \psi$	$k_{i,par}$	$R_{FT} = k_{i,par} \psi_{CH_2} \psi_H$ $\frac{d\psi_{CH_3}}{dt} = 0 \Rightarrow +R_8 - R_9 - R_{12} = 0 \Rightarrow + k_{i,par} \psi_{CH_2} \psi_H - k_{meth} \psi_{CH_3} \psi_H - k_{g,par} \psi_{CH_3} \psi_{CH_2} = 0$ $\Rightarrow$ $\psi_{CH_3} = \frac{k_{i,par} \psi_{CH_2} \psi_H}{k_{g,par} \psi_{CH_2} + k_{meth} \psi_H}$
9	$CH_3 - \psi + H - \psi \rightarrow CH_4 + 2\psi$	k_{meth}	$R_{CH_4} = k_{meth} \psi_{CH_3} \psi_H$
10	$CH_2 - \psi + CH_2 - \psi \rightarrow C_2H_4 + 2\psi$	k_{eth}	$R_{C_2H_4} = k_{eth} {\psi_{CH_2}}^2$
11	$CH_2 - \psi + CH - \psi \rightarrow C_2H_3 - \psi + \psi$	$k_{i,olef}$	$\frac{d\psi_{C_2H_3}}{dt} = 0 \Rightarrow +R_{11} - R_{14} = 0 \Rightarrow + k_{i,olef} \psi_{CH_2} \psi_{CH} - k_{g,olef} \psi_{CH_2} \psi_{C_2H_3} = 0 \Rightarrow$ $\psi_{C_2H_3} = \frac{k_{i,olef} \psi_{CH}}{k_{g,olef}}$
12	$C_{n-1}H_{2n-1} - \psi + CH_2 - \psi \rightarrow C_nH_{2n+1} - \psi + \psi\ ;\ n \geq 3$	$k_{g,par}$	$\frac{d\psi_{C_nH_{2n+1}}}{dt} = 0 \Rightarrow +R_{12} - R'_{12} - R_{13} = 0$ $\Rightarrow + k_{g,par} \psi_{C_{n-1}H_{2n-1}} \psi_{CH_2} - k_{g,par} \psi_{C_nH_{2n+1}} \psi_{CH_2} - k_{t,par} \psi_{C_nH_{2n+1}} \psi_H = 0$ $\Rightarrow$ $\psi_{C_nH_{2n+1}} = \frac{k_{g,par} \psi_{C_{n-1}H_{2n-1}} \psi_{CH_2}}{k_{g,par} \psi_{CH_2} + k_{t,par} \psi_H}$
13	$C_nH_{2n+1} - \psi + H - \psi \rightarrow C_nH_{2n+2} + 2\psi$	$k_{t,par}$	$R_{parffins} = k_{t,par} \psi_{C_nH_{2n+1}} \psi_H$
14	$\mathrm{C_{n-1}H_{2n-3}} - \psi + \mathrm{CH_2} - \psi \rightarrow \mathrm{C_nH_{2n-1}} - \psi + \psi\ ;\ \mathrm{n} \geq 3$	$k_{g,olef}$	$\frac{d\psi_{C_nH_{2n-1}}}{dt} = 0 \Rightarrow +R_{14} - R'_{14} - R_{15} = 0$ $\Rightarrow + k_{g,olef} \psi_{C_{n-1}H_{2n-3}} \psi_{CH_2} - k_{g,olef} \psi_{C_nH_{2n-1}} \psi_{CH_2} - k_{t,olef} \psi_{C_nH_{2n-1}} \psi_H = 0$ $\Rightarrow$ $\psi_{C_nH_{2n-1}} = \frac{k_{g,olef} \psi_{C_{n-1}H_{2n-3}} \psi_{CH_2}}{k_{g,olef} \psi_{CH_2} + k_{t,olef} \psi_H}$

15	$C_nH_{2n-1} - \psi + H - \psi \rightarrow C_nH_{2n} + 2\psi$	$k_{t,olef}$	$R_{olefins} = k_{t,olef}\psi_{C_nH_{2n-1}}\psi_H$	

Table A. 2 Kinetic model FT−I assuming steps 5 and 8–15 are the rate-determining steps (RDS-1)

No.	FT–I (RDS-1: 5, 8–15)	Rate Equations
1	$CO + \psi \rightleftarrows CO - \psi$	$K_1 P_{CO}\psi = \psi_{CO}$
2	$H_2 + 2\psi \rightleftarrows 2H - \psi$	$\psi_H = \sqrt{K_2 P_{H2}^{0.5}}\psi$
3	$CO - \psi + \psi \rightleftarrows C - \psi + O - \psi$	$\psi_C = \frac{K_3\psi_{CO}\psi}{\psi_O} = \frac{K_3(K_1 P_{CO}\psi)\psi}{\frac{R_{FT}}{k_5 K_4 K_2 P_{H_2}\psi}} = k_5 K_4 K_2 K_3 K_1 \frac{P_{H_2}P_{CO}\psi^3}{R_{FT}} = k_5 K_4 K_2 K_3 K_1 \frac{P_{H_2}P_{CO}\psi^3}{\left(k_{i,par}k_5 K_1 K_2^{2.5} K_3 K_4 K_6 K_7\right)^{0.5} P_{H_2}^{1.25} P_{CO}^{0.5}\psi^2} \Rightarrow$ $\psi_C = \frac{(k_5 K_4 K_3 K_1)^{0.5}}{K_2^{0.25}\left(k_{i,par}K_6 K_7\right)^{0.5}} P_{H_2}^{-0.25} P_{CO}^{0.5}\psi$
4	$O - \psi + H - \psi \rightleftarrows OH - \psi + \psi$	$\psi_O = \frac{\psi_{OH}\psi}{K_4\psi_H} = \frac{\left(\frac{R_{FT}}{k_5\psi_H}\right)\psi}{K_4\psi_H} = \frac{R_{FT}}{k_5 K_4 \psi_H^2}\psi = \frac{R_{FT}}{k_5 K_4 K_2 P_{H_2}\psi^2}\psi = \frac{R_{FT}}{k_5 K_4 K_2 P_{H_2}\psi} = \frac{\left(k_{i,par}k_5 K_1 K_2^{2.5} K_3 K_4 K_6 K_7\right)^{0.5} P_{H_2}^{1.25} P_{CO}^{0.5}\psi^2}{k_5 K_4 K_2 P_{H_2}\psi} \Rightarrow$ $\psi_O \frac{K_2^{0.25}\left(k_{i,par}K_1 K_3 K_6 K_7\right)^{0.5}}{(k_5 K_4)^{0.5}} P_{H_2}^{0.25} P_{CO}^{0.5}\psi$
5	$OH - \psi + H - \psi \rightarrow H_2O + 2\psi$	$R_{FT} = k_5\psi_{OH}\psi_H$ $\psi_{OH} = \frac{R_{FT}}{k_5\psi_H} = \frac{R_{FT}}{k_5\sqrt{K_2}P_{H2}^{0.5}\psi} = \frac{\left(k_{i,par}k_5 K_1 K_2^{2.5} K_3 K_4 K_6 K_7\right)^{0.5} P_{H_2}^{1.25} P_{CO}^{0.5}\psi^2}{k_5\sqrt{K_2}P_{H2}^{0.5}\psi} = \frac{K_2^{0.75}\left(k_{i,par}K_1 K_3 K_4 K_6 K_7\right)^{0.5}}{k_5^{0.5}} P_{H_2}^{0.75} P_{CO}^{0.5}\psi$
6	$C - \psi + H - \psi \rightleftarrows CH - \psi + \psi$	$\psi_{CH} = \frac{K_6\psi_C\psi_H}{\psi} = \frac{K_6\left(k_5 K_4 K_2 K_3 K_1 \frac{P_{H_2}P_{CO}\psi^3}{R_{FT}}\right)\left(\sqrt{K_2}P_{H2}^{0.5}\psi\right)}{\psi} = K_6 k_5 K_4 K_2^{1.5} K_3 K_1 \frac{P_{H_2}^{1.5}P_{CO}\psi^3}{\left(k_{i,par}k_5 K_1 K_2^{2.5} K_3 K_4 K_6 K_7\right)^{0.5} P_{H_2}^{1.25} P_{CO}^{0.5}\psi^2} \Rightarrow$ $\psi_{CH} = \frac{K_2^{0.25}(k_5 K_1 K_3 K_4 K_6)^{0.5}}{\left(k_{i,par}K_7\right)^{0.5}} P_{H_2}^{0.25} P_{CO}^{0.5}\psi$
7	$CH - \psi + H - \psi \rightleftarrows CH_2 - \psi + \psi$	$\psi_{CH_2} = \frac{K_7\psi_{CH}\psi_H}{\psi} = \frac{K_7\left(K_6 k_5 K_4 K_2^{1.5} K_3 K_1 \frac{P_{H_2}^{1.5}P_{CO}\psi^3}{R_{FT}}\right)\left(\sqrt{K_2}P_{H2}^{0.5}\psi\right)}{\psi} = K_7 K_6 k_5 K_4 K_2^2 K_3 K_1 \frac{P_{H_2}^2 P_{CO}\psi^3}{\left(k_{i,par}k_5 K_1 K_2^{2.5} K_3 K_4 K_6 K_7\right)^{0.5} P_{H_2}^{1.25} P_{CO}^{0.5}\psi^2} \Rightarrow$ $\psi_{CH_2} = \frac{K_2^{0.75}(K_7 K_6 k_5 K_4 K_3 K_1)^{0.5}}{k_{i,par}^{0.5}} P_{H_2}^{0.75} P_{CO}^{0.5}\psi$
8	$CH_2 - \psi + H - \psi \rightarrow CH_3 - \psi + \psi$	$R_{FT} = k_{i,par}\psi_{CH_2}\psi_H = k_{i,par}\left(K_7 K_6 k_5 K_4 K_2^2 K_3 K_1 \frac{P_{H_2}^2 P_{CO}\psi^3}{R_{FT}}\right)\left(\sqrt{K_2}P_{H2}^{0.5}\psi\right) = k_{i,par}K_7 K_6 k_5 K_4 K_2^{2.5} K_3 K_1 \frac{P_{H_2}^{2.5}P_{CO}}{R_{FT}}\psi^4 \Rightarrow$ $R_{FT} = \left(k_{i,par}K_7 K_6 k_5 K_4 K_2^{2.5} K_3 K_1 P_{H_2}^{2.5} P_{CO}\psi^4\right)^{1/2} = \left(k_{i,par}k_5 K_1 K_2^{2.5} K_3 K_4 K_6 K_7\right)^{0.5} P_{H_2}^{1.25} P_{CO}^{0.5}\psi^2$

Total Surface Coverage	$\psi + \psi_{CO} + \psi_H + \psi_C + \psi_O + \psi_{OH} + \psi_{CH} + \psi_{CH_2} = 1$	$\psi = \frac{1}{\left(\begin{array}{c} 1 + K_1 P_{CO} + \sqrt{K_2} P_{H2}^{0.5} + \frac{(k_5 K_4 K_3 K_1)^{0.5}}{K_2^{0.25}\left(k_{i,par} K_6 K_7\right)^{0.5}} P_{H_2}^{-0.25} P_{CO}^{0.5} + \cdots \\ \frac{K_2^{0.25}\left(k_{i,par} K_1 K_3 K_6 K_7\right)^{0.5}}{(k_5 K_4)^{0.5}} P_{H_2}^{0.25} P_{CO}^{0.5} + \frac{K_2^{0.75}\left(k_{i,par} K_1 K_3 K_4 K_6 K_7\right)^{0.5}}{k_5^{0.5}} P_{H_2}^{0.75} P_{CO}^{0.5} + \cdots \\ \frac{K_2^{0.25}(k_5 K_1 K_3 K_4 K_6)^{0.5}}{\left(k_{i,par} K_7\right)^{0.5}} P_{H_2}^{0.25} P_{CO}^{0.5} + \frac{K_2^{0.75}(k_5 K_7 K_6 K_4 K_3 K_1)^{0.5}}{k_{i,par}^{0.5}} P_{H_2}^{0.75} P_{CO}^{0.5} \end{array}\right)}$

Table A. 3 Kinetic model FT−I assuming steps 3 and 8–15 are the rate-determining steps (RDS-2)

No.	FT–I (RDS-2: 3, 8–15)	Rate Equations
1	$CO + \psi \ \rightleftarrows CO - \psi$	$K_1 P_{CO} \psi = \psi_{CO}$
2	$H_2 + 2\psi \ \rightleftarrows 2H - \psi$	$\psi_H = \sqrt{K_2 P_{H_2}} \psi$
3	$CO - \psi + \psi \rightarrow C - \psi + O - \psi$	$R_{FT} = k_3 \psi_{CO} \psi = k_3 K_1 P_{CO} \psi^2$
4	$O - \psi + H - \psi \rightleftarrows OH - \psi + \psi$	$\psi_O = \frac{\psi_{OH} \psi}{K_4 \psi_H} = \frac{\left(\frac{P_{H_2O} \psi^2}{K_5 \psi_H}\right) \psi}{K_4 \psi_H} = \frac{P_{H_2O} \psi^3}{K_5 K_4 K_2 P_{H_2} \psi^2} = \frac{1}{K_5 K_4 K_2} \frac{P_{H_2O}}{P_{H_2}} \psi$
5	$OH - \psi + H - \psi \rightleftarrows H_2O + 2\psi$	$\psi_{OH} = \frac{P_{H_2O} \psi^2}{K_5 \psi_H} = \frac{P_{H_2O}}{K_5 \sqrt{K_2} P_{H2}^{0.5}} \psi = \frac{1}{K_5 \sqrt{K_2}} \frac{P_{H_2O}}{P_{H2}^{0.5}} \ \psi$
6	$C - \psi + \ H - \psi \rightleftarrows CH - \psi + \ \psi$	$\psi_C = \frac{\psi_{CH} \psi}{K_6 \psi_H} = \frac{\frac{R_{FT} \psi}{k_{i,par} K_7 \psi_H^2} \psi}{K_6 \psi_H} = \frac{R_{FT} \psi^2}{k_{i,par} K_7 K_6 \psi_H^3} = \frac{k_3 K_1 P_{CO} \psi^4}{k_{i,par} K_7 K_6 \left(\sqrt{K_2} P_{H2}^{0.5} \psi\right)^3} = \frac{k_3 K_1}{k_{i,par} K_7 K_6 K_2^{1.5}} \frac{P_{CO}}{P_{H_2}^{1.5}} \psi$
7	$CH - \psi + H - \psi \rightleftarrows CH_2 - \psi + \psi$	$\psi_{CH} = \frac{\psi_{CH_2} \psi}{K_7 \psi_H} = \frac{\frac{R_{FT}}{k_{i,par} \psi_H} \psi}{K_7 \psi_H} = \frac{k_3 K_1 P_{CO} \psi^3}{k_{i,par} K_7 \left(\sqrt{K_2} P_{H2}^{0.5} \psi\right)^2} = \frac{k_3 K_1}{k_{i,par} K_7 K_2} \frac{P_{CO}}{P_{H_2}} \psi$
8	$CH_2 - \psi + H - \psi \rightarrow CH_3 - \psi + \ \psi$	$R_{FT} = k_{i,par} \psi_{CH_2} \psi_H$ $\psi_{CH_2} = \frac{k_3 K_1 P_{CO} \psi^2}{k_{i,par} \sqrt{K_2} P_{H2}^{0.5} \psi} = \frac{k_3 K_1}{k_{i,par} \sqrt{K_2}} \frac{P_{CO}}{P_{H2}^{0.5}} \psi$
Total Surface Coverage	$\psi + \psi_{CO} + \psi_H + \psi_O + \psi_{OH} + \psi_C + \psi_{CH} + \psi_{CH_2} = 1$	$\psi = \frac{1}{\left(\begin{array}{c} 1 + K_1 P_{CO} + \sqrt{K_2 P_{H_2}} + \frac{1}{K_5 K_4 K_2} \frac{P_{H_2O}}{P_{H_2}} + \cdots \\ \frac{1}{K_5 \sqrt{K_2}} \frac{P_{H_2O}}{P_{H2}^{0.5}} + \frac{k_3 K_1}{k_{i,par} K_7 K_6 K_2^{1.5}} \frac{P_{CO}}{P_{H_2}^{1.5}} + \frac{k_3 K_1}{k_{i,par} K_7 K_2} \frac{P_{CO}}{P_{H_2}} + \frac{k_3 K_1}{k_{i,par} \sqrt{K_2}} \frac{P_{CO}}{P_{H2}^{0.5}} \end{array}\right)}$

Table A. 4 Kinetic model FT−I assuming steps 8–15 are the rate-determining steps (RDS-3)

No.	FT–I (RDS-3: 8–15)	Rate Equations
1	$CO + \psi \rightleftarrows CO - \psi$	$K_1 P_{CO} \psi = \psi_{CO}$
2	$H_2 + 2\psi \rightleftarrows 2H - \psi$	$\psi_H = \sqrt{K_2 P_{H_2}}\psi$
3	$CO - \psi + \psi \rightleftarrows C - \psi + O - \psi$	$\psi_C = \frac{K_3 \psi_{CO} \psi}{\psi_O} = \frac{K_3 K_1 P_{CO} \psi \psi}{\frac{P_{H_2O}}{K_5 K_4 K_2 P_{H_2}}\psi} = \frac{K_5 K_4 K_3 K_2 K_1 P_{CO} P_{H_2}}{P_{H_2O}}\psi$
4	$O - \psi + H - \psi \rightleftarrows OH - \psi + \psi$	$\psi_O = \frac{\psi_{OH}\psi}{K_4 \psi_H} = \frac{\frac{P_{H_2O}}{k_5\sqrt{K_2}P_{H2}^{0.5}}\psi\psi}{K_4\sqrt{K_2}P_{H2}^{0.5}\psi} = \frac{P_{H_2O}}{K_5 K_4 K_2 P_{H_2}}\psi$
5	$OH - \psi + H - \psi \rightleftarrows H_2O + 2\psi$	$\psi_{OH} = \frac{P_{H_2O}\psi^2}{K_5 \psi_H} = \frac{P_{H_2O}}{K_5\sqrt{K_2}P_{H2}^{0.5}}\psi$
6	$C - \psi + H - \psi \rightleftarrows CH - \psi + \psi$	$\psi_{CH} = \frac{K_6 \psi_C \psi_H}{\psi} = \frac{K_6 \frac{K_5 K_4 K_3 K_2 K_1 P_{CO} P_{H_2}}{P_{H_2O}}\psi\left(\sqrt{K_2 P_{H_2}}\psi\right)}{\psi} = K_6 K_5 K_4 K_3 K_2^{1.5} K_1 \frac{P_{CO}}{P_{H_2O}} P_{H_2}^{1.5}\psi$
7	$CH - \psi + H - \psi \rightleftarrows CH_2 - \psi + \psi$	$\psi_{CH_2} = \frac{K_7 \psi_{CH} \psi_H}{\psi} = \frac{K_7 K_6 K_5 K_4 K_3 K_2^{1.5} K_1 \frac{P_{CO}}{P_{H_2O}} P_{H_2}^{1.5}\psi\sqrt{K_2}P_{H2}^{0.5}\psi}{\psi} = K_7 K_6 K_5 K_4 K_3 K_2^2 K_1 \frac{P_{CO}}{P_{H_2O}} P_{H_2}^2 \psi$
8	$CH_2 - \psi + H - \psi \rightarrow CH_3 - \psi + \psi$	$R_{FT} = k_{i,par}\psi_{CH_2}\psi_H = k_{i,par}\left(K_7 K_6 K_5 K_4 K_3 K_2^2 K_1 \frac{P_{CO}}{P_{H_2O}} P_{H_2}^2 \psi\right)\sqrt{K_2}P_{H2}^{0.5}\psi \Rightarrow R_{FT} = k_{i,par} K_7 K_6 K_5 K_4 K_3 K_2^{2.5} K_1 \frac{P_{CO}}{P_{H_2O}} P_{H2}^{2.5}\psi^2$

APPENDIX

Total Surface Coverage	$\psi + \psi_{CO} + \psi_H + \psi_O + \psi_{OH} + \psi_C + \psi_{CH} + \psi_{CH_2} = 1$	$\psi = \dfrac{1}{\left(\begin{array}{c} 1 + K_1 P_{CO} + \sqrt{K_2 P_{H_2}} + \dfrac{P_{H_2O}}{K_5 K_4 K_2 P_{H_2}} + \dfrac{P_{H_2O}}{K_5 \sqrt{K_2} P_{H2}^{0.5}} + \cdots \\ \dfrac{K_5 K_4 K_3 K_2 K_1 P_{CO} P_{H_2}}{P_{H_2O}} + K_6 K_5 K_4 K_3 K_2^{1.5} K_1 \dfrac{P_{CO}}{P_{H_2O}} P_{H_2}^{1.5} + \cdots \\ K_7 K_6 K_5 K_4 K_3 K_2^2 K_1 \dfrac{P_{CO}}{P_{H_2O}} P_{H_2}^2 \end{array}\right)}$

Table A. 5 Reaction pathway and LHHW rate expressions developed for model FT−II based on H-assisted (first route) CO dissociation mechanism

No.	General Reaction Path	Kinetic parameter	Rate Equations
1	$CO + \psi \rightleftarrows CO - \psi$	K_1	$K_1 P_{CO} \psi = \psi_{CO}$
2	$H_2 + 2\psi \rightleftarrows 2H - \psi$	K_2	$K_2 P_{H_2} \psi^2 = \psi_H^2$
3	$CO - \psi + H - \psi \rightleftarrows COH - \psi + \psi$	K_3	$K_3 \psi_{CO} \psi_H = \psi_{COH} \psi$
4	$COH - \psi + \psi \rightleftarrows C - \psi + OH - \psi$	K_4	$K_4 \psi_{COH} = \psi_C \psi_{OH}$
5	$OH - \psi + H - \psi \rightleftarrows H_2O + 2\psi$	K_6	$k_6 \psi_{OH} \psi_H = P_{H_2O} \psi^2$
6	$C - \psi + H - \psi \rightleftarrows CH - \psi + \psi$	K_5	$K_5 \psi_C \psi_H = \psi_{CH} \psi$
7	$CH - \psi + H - \psi \rightleftarrows CH_2 - \psi + \psi$	K_7	$K_7 \psi_{CH} \psi_H = \psi_{CH_2} \psi$
8	$CH_2 - \psi + H - \psi \rightarrow CH_3 - \psi + \psi$	$k_{i,par}$	$R_{FT} = k_{i,par} \psi_{CH_2} \psi_H$ $\dfrac{d\psi_{CH_3}}{dt} = 0 \Rightarrow +R_8 - R_9 - R_{12} = 0 \Rightarrow + k_{i,par} \psi_{CH_2} \psi_H - k_{meth} \psi_{CH_3} \psi_H - k_{g,par} \psi_{CH_3} \psi_{CH_2} = 0 \Rightarrow$ $\psi_{CH_3} = \dfrac{k_{i,par} \psi_{CH_2} \psi_H}{k_{g,par} \psi_{CH_2} + k_{meth} \psi_H}$
9	$CH_3 - \psi + H - \psi \rightarrow CH_4 + 2\psi$	k_{meth}	$R_{CH_4} = k_{meth} \psi_{CH_3} \psi_H$
10	$CH_2 - \psi + CH_2 - \psi \rightarrow C_2H_4 + 2\psi$	k_{eth}	$R_{C_2H_4} = k_{eth} {\psi_{CH_2}}^2$
11	$CH_2 - \psi + CH - \psi \rightarrow C_2H_3 - \psi + \psi$	$k_{i,olef}$	$\dfrac{d\psi_{C_2H_3}}{dt} = 0 \Rightarrow +R_{11} - R_{14} = 0 \Rightarrow + k_{i,olef} \psi_{CH_2} \psi_{CH} - k_{g,olef} \psi_{CH_2} \psi_{C_2H_3} = 0 \Rightarrow$ $\psi_{C_2H_3} = \dfrac{k_{i,olef} \psi_{CH}}{k_{g,olef}}$

12	$C_{n-1}H_{2n-1}-\psi+CH_2-\psi \rightarrow C_nH_{2n+1}-\psi+\psi\,;\ n\geq 3$	$k_{g,par}$	$\frac{d\psi_{C_nH_{2n+1}}}{dt}=0\Rightarrow +R_{12}-R'_{12}-R_{13}=0\Rightarrow +k_{g,par}\psi_{C_{n-1}H_{2n-1}}\psi_{CH_2}-k_{g,par}\psi_{C_nH_{2n+1}}\psi_{CH_2}-k_{t,par}\psi_{C_nH_{2n+1}}\psi_H=0\Rightarrow \psi_{C_nH_{2n+1}}=\frac{k_{g,par}\psi_{C_{n-1}H_{2n-1}}\psi_{CH_2}}{k_{g,par}\psi_{CH_2}+k_{t,par}\psi_H}$
13	$C_nH_{2n+1}-\psi+H-\psi \rightarrow C_nH_{2n+2}+2\psi$	$k_{t,par}$	$R_{parffins}=k_{t,par}\psi_{C_nH_{2n+1}}\psi_H$
14	$CH_2-\psi+C_{n-1}H_{2n-3}-\psi \rightarrow C_nH_{2n-1}-\psi+\ \psi;\ n\geq 3$	$k_{g,olef}$	$\frac{d\psi_{C_nH_{2n-1}}}{dt}=0\Rightarrow +R_{14}-R'_{14}-R_{15}=0\Rightarrow +k_{g,olef}\psi_{C_{n-1}H_{2n-3}}\psi_{CH_2}-k_{g,olef}\psi_{C_nH_{2n-1}}\psi_{CH_2}-k_{t,olef}\psi_{C_nH_{2n-1}}\psi_H=0\Rightarrow \psi_{C_nH_{2n-1}}=\frac{k_{g,olef}\psi_{C_{n-1}H_{2n-3}}\psi_{CH_2}}{k_{g,olef}\psi_{CH_2}+k_{t,olef}\psi_H}$
15	$C_nH_{2n-1}-\psi+H-\psi \rightarrow C_nH_{2n}+2\psi$	$k_{t,olef}$	$R_{olefins}=k_{t,olef}\psi_{C_nH_{2n-1}}\psi_H$

Table A. 6 Kinetic model FT−II assuming steps 5 and 8–15 are the rate-determining steps (RDS-1)

No.	FT–II (RDS-1: 5, 8–15)	Rate Equations
1	$CO+\psi\ \rightleftarrows CO-\psi$	$\psi_{CO}=K_1P_{CO}\psi$
2	$H_2+2\psi\ \rightleftarrows 2H-\psi$	$\psi_H=\sqrt{K_2P_{H_2}}\psi$
3	$CO-\psi+H-\psi\rightleftarrows COH-\psi+\psi$	$\psi_{COH}=\frac{K_3\psi_{CO}\psi_H}{\psi}=\frac{K_3K_1P_{CO}\psi\sqrt{K_2}P_{H2}^{0.5}\psi}{\psi}=K_3K_1\sqrt{K_2}P_{CO}P_{H2}^{0.5}\psi$
4	$COH-\psi+\psi\rightleftarrows C-\psi+\ OH-\psi$	$\psi_C=\frac{K_4\psi_{COH}\psi}{\psi_{OH}}=\frac{K_4\frac{K_3\psi_{CO}\psi_H}{\psi}\psi}{\psi_{OH}}=\frac{K_4K_3K_1P_{CO}^{0.5}k_5^{0.5}}{\sqrt{k_{i,par}K_1K_2^{1.5}K_3K_4K_6K_7P_{H_2}^{0.25}}}\psi=\frac{k_5^{0.5}K_4K_3K_1P_{CO}^{0.5}}{\sqrt{k_{i,par}K_1K_2^{1.5}K_3K_4K_6K_7P_{H_2}^{0.25}}}$
5	$OH-\psi+H-\psi\rightarrow H_2O+2\psi$	$R_{FT}=k_5\psi_{OH}\psi_H$ $\psi_{OH}=\frac{R_{FT}}{k_5\psi_H}=\frac{\sqrt{k_{i,par}k_5K_1K_2^{2.5}K_3K_4K_6K_7P_{CO}^{0.5}P_{H_2}^{1.25}\psi^2}}{k_5\psi_H}=\sqrt{k_{i,par}K_1K_2^2K_3K_4K_6K_7\frac{P_{CO}^{0.5}P_{H_2}^{0.75}}{k_5^{0.5}}}\psi$
6	$C-\psi+H-\psi\rightleftarrows CH-\psi+\psi$	$\psi_{CH}=\frac{K_6\psi_C\psi_H}{\psi}=\frac{K_6\left(K_4\frac{K_3\psi_{CO}\psi_H}{\psi}\psi\right)\sqrt{K_2P_{H_2}}\psi}{\psi}=\sqrt{K_2}K_3K_4K_6\frac{\psi_{CO}\psi_H}{\frac{R_{FT}}{k_5\psi_H}}\sqrt{P_{H_2}}=\sqrt{K_2}K_3K_4K_6k_5\frac{\psi_{CO}\psi_H^2}{R_{FT}}\sqrt{P_{H_2}}$

APPENDIX

7	$CH-\psi+H-\psi \rightleftarrows CH_2-\psi+\psi$	$\psi_{CH_2}=\frac{K_7\psi_{CH}\psi_H}{\psi}=\frac{K_7\sqrt{K_2}K_3K_4K_6k_5\frac{\psi_{CO}\psi_H^2}{R_{FT}}\sqrt{P_{H_2}}\psi_H}{\psi}=K_1\sqrt{K_2}K_3K_4K_6K_7k_5\frac{P_{CO}\sqrt{P_{H_2}}\psi_H^3}{R_{FT}}=K_1K_2^2K_3K_4K_6K_7k_5\frac{P_{CO}P_{H_2}^2\psi^3}{R_{FT}}$
8	$CH_2-\psi+H-\psi \rightarrow CH_3-\psi+\psi$	$R_{FT}=k_{i,par}\psi_{CH_2}\psi_H=k_{i,par}K_1K_2^2K_3K_4K_6K_7k_5\frac{P_{CO}P_{H_2}^2\psi^3}{R_{FT}}\sqrt{K_2P_{H_2}}\psi=k_{i,par}k_5K_1K_2^{2.5}K_3K_4K_6K_7\frac{P_{CO}P_{H_2}^{2.5}}{R_{FT}}\psi^4$ $R_{FT}=\sqrt{k_{i,par}k_5K_1K_2^{2.5}K_3K_4K_6K_7}P_{CO}^{0.5}P_{H_2}^{1.25}\psi^2$
Total Surface Coverage	$\psi+\psi_{CO}+\psi_H+\psi_{COH}+\psi_{OH}+\psi_C+\psi_{CH}+\psi_{CH_2}=1$	$\psi=\frac{1}{\left(\begin{array}{c}1+K_1P_{CO}+\sqrt{K_2P_{H_2}}+K_3K_1\sqrt{K_2}P_{CO}P_{H2}^{0.5}\psi+\sqrt{K_2}K_3K_4K_6k_5\frac{\psi_{CO}\psi_H^2}{R_{FT}}\sqrt{P_{H_2}}+\cdots\\ K_1K_2^2K_3K_4K_6K_7k_5\frac{P_{CO}P_{H_2}^2}{R_{FT}}+\sqrt{k_{i,par}K_1K_2^2K_3K_4K_6K_7}\frac{P_{CO}^{0.5}P_{H_2}^{0.75}}{k_5^{0.5}}+\frac{k_5^{0.5}K_4K_3K_1P_{CO}^{0.5}}{\sqrt{k_{i,par}K_1K_2^{1.5}K_3K_4K_6K_7P_{H_2}^{0.25}}}\end{array}\right)}$

Table A. 7 Kinetic model FT−II assuming steps 4 and 8–15 are the rate-determining steps (RDS-2)

No.	FT–II (RDS-2: 4, 8–15)	Rate Equations
1	$CO+\psi \rightleftarrows CO-\psi$	$\psi_{CO}=K_1P_{CO}\psi$
2	$H_2+2\psi \rightleftarrows 2H-\psi$	$\psi_H=\sqrt{K_2P_{H_2}}\psi$
3	$CO-\psi+H-\psi \rightleftarrows COH-\psi+\psi$	$\psi_{COH}=\frac{K_3\psi_{CO}\psi_H}{\psi}=\frac{K_3K_1P_{CO}\psi\sqrt{K_2}P_{H2}^{0.5}\psi}{\psi}=K_3K_1\sqrt{K_2}P_{CO}P_{H2}^{0.5}\psi$
4	$COH-\psi+\psi \rightarrow C-\psi+OH-\psi$	$R_{FT}=k_4\psi_{COH}\psi=k_4K_3K_1\sqrt{K_2}P_{CO}P_{H2}^{0.5}\psi^2$
5	$OH-\psi+H-\psi \rightleftarrows H_2O+2\psi$	$\psi_{OH}=\frac{P_{H_2O}\psi^2}{K_5\psi_H}=\frac{P_{H_2O}\psi^2}{K_5\sqrt{K_2P_{H_2}}\psi}=\frac{P_{H_2O}}{K_5\sqrt{K_2P_{H_2}}}\psi$
6	$C-\psi+H-\psi \rightleftarrows CH-\psi+\psi$	$\psi_C=\frac{\psi\psi_{CH}}{K_6\psi_H}=\frac{\psi^2P_{H_2O}}{K_6\sqrt{K_2P_{H_2}}\psi}=\frac{P_{H_2O}}{K_6\sqrt{K_2P_{H_2}}}\psi$
7	$CH-\psi+H-\psi \rightleftarrows CH_2-\psi+\psi$	$\psi_{CH}=\frac{\psi_{CH_2}\psi}{K_7\psi_H}=\frac{\left(\frac{R_{FT}}{k_{i,par}\psi_H}\right)\psi}{K_7\psi_H}=\frac{R_{FT}}{K_7k_{i,par}\psi_H^2}\psi=\frac{k_4K_3K_1\sqrt{K_2}P_{CO}P_{H2}^{0.5}\psi^2}{K_7k_{i,par}K_2P_{H_2}\psi^2}\psi=\frac{k_4K_1K_3}{K_2^{0.5}k_{i,par}K_7}\frac{P_{CO}}{P_{H2}^{0.5}}\psi$ $R_{FT}=k_8\psi_{CH_2}\psi_H$
8	$CH_2-\psi+H-\psi \rightarrow CH_3-\psi+\psi$	$\psi_{CH_2}=\frac{R_{FT}}{k_{i,par}\psi_H}=\frac{k_4K_3K_1\sqrt{K_2}P_{CO}P_{H2}^{0.5}\psi^2}{k_{i,par}\sqrt{K_2P_{H_2}}\psi}=\frac{k_4K_1K_3}{k_{i,par}}P_{CO}\psi$

Total Surface Coverage	$\psi + \psi_{CO} + \psi_H + \psi_{COH} + \psi_{OH} + \psi_C + \psi_{CH} + \psi_{CH_2} = 1$	$\psi = \frac{1}{\left(1 + K_1 P_{CO} + \sqrt{K_2 P_{H_2}} + K_3 K_1 \sqrt{K_2} P_{CO} P_{H2}^{0.5} + \frac{P_{H_2O}}{K_5 \sqrt{K_2 P_{H_2}}} + \frac{P_{H_2O}}{K_6 \sqrt{K_2 P_{H_2}}} + \frac{k_4 K_1 K_3}{K_2^{0.5} k_{i,par} K_7} \frac{P_{CO}}{P_{H2}^{0.5}} + \frac{k_4 K_1 K_3}{k_{i,par}} P_{CO}\right)}$

Table A. 8 Kinetic model FT–II assuming steps 8–15 are the rate-determining steps (RDS-3)

No.	FT–II (RDS-3: 8–15)	Rate Equations
1	$CO + \psi \rightleftarrows CO - \psi$	$\psi_{CO} = K_1 P_{CO} \psi$
2	$H_2 + 2\psi \rightleftarrows 2H - \psi$	$\psi_H = \sqrt{K_2 P_{H_2}}\,\psi$
3	$CO - \psi + H - \psi \rightleftarrows COH - \psi + \psi$	$\psi_{COH} = \frac{K_3 \psi_{CO} \psi_H}{\psi} = \frac{K_3 K_1 P_{CO} \psi \sqrt{K_2} P_{H2}^{0.5} \psi}{\psi} = K_3 K_1 \sqrt{K_2} P_{CO} P_{H2}^{0.5} \psi$
4	$COH - \psi + \psi \rightleftarrows C - \psi + OH - \psi$	$\psi_C = \frac{K_4 \psi_{COH} \psi}{\psi_{OH}} = \frac{K_4 \left(K_3 K_1 \sqrt{K_2} P_{CO} P_{H2}^{0.5} \psi\right) \psi}{\frac{P_{H_2O} \psi}{K_5 \sqrt{K_2 P_{H_2}}}} = K_4 \left(K_5 K_3 K_1 K_2 \frac{P_{CO} P_{H_2}}{P_{H_2O}} \psi \right)$
5	$OH - \psi + H - \psi \rightleftarrows H_2O + 2\psi$	$\psi_{OH} = \frac{P_{H_2O} \psi^2}{K_5 \psi_H} = \frac{P_{H_2O} \psi}{K_5 \sqrt{K_2 P_{H_2}}}$
6	$C - \psi + H - \psi \rightleftarrows CH - \psi + \psi$	$\psi_{CH} = \frac{\psi_C \psi_H}{K_6 \psi} = \frac{K_4 \left(K_5 K_3 K_1 K_2 \frac{P_{CO} P_{H_2}}{P_{H_2O}} \psi \right) \sqrt{K_2 P_{H_2}} \psi}{K_6 \psi} = \frac{K_1 K_2^{1.5} K_3 K_4 K_5}{K_6} \frac{P_{CO} P_{H_2}^{1.5}}{P_{H_2O}} \psi$
7	$CH - \psi + H - \psi \rightleftarrows CH_2 - \psi + \psi$	$\psi_{CH_2} = \frac{K_7 \psi_{CH} \psi_H}{\psi} = \frac{K_7 \frac{K_1 K_2^{1.5} K_3 K_4 K_5}{K_6} \frac{P_{CO} P_{H_2}^{1.5}}{P_{H_2O}} \psi \sqrt{K_2 P_{H_2}} \psi}{\psi} = \frac{K_1 K_2^2 K_3 K_4 K_5 K_7}{K_6} \frac{P_{CO} P_{H_2}^2}{P_{H_2O}} \psi$
8	$CH_2 - \psi + H - \psi \rightarrow CH_3 - \psi + \psi$	$R_{FT} = k_{i,par} \psi_{CH_2} \psi_H = k_{i,par} \frac{K_1 K_2^2 K_3 K_4 K_5 K_7}{K_6} \frac{P_{CO} P_{H_2}^2}{P_{H_2O}} \psi \left(\sqrt{K_2 P_{H_2}} \psi \right) = k_{i,par} \frac{K_1 K_2^{2.5} K_3 K_4 K_5 K_7}{K_6} \frac{P_{CO} P_{H_2}^{2.5}}{P_{H_2O}} \psi^2$
Total Surface Coverage	$\psi + \psi_{CO} + \psi_H + \psi_{COH} + \psi_{OH} + \psi_C + \psi_{CH} + \psi_{CH_2} = 1$	$\psi = \frac{1}{\left(1 + K_1 P_{CO} + \sqrt{K_2 P_{H_2}} + \frac{P_{H_2O}}{K_6 \sqrt{K_2 P_{H_2}}} + K_3 K_1 \sqrt{K_2} P_{CO} P_{H2}^{0.5} + K_4 \left(K_5 K_3 K_1 K_2 \frac{P_{CO} P_{H_2}}{P_{H_2O}} \right) + \frac{P_{H_2O}}{K_5 \sqrt{K_2 P_{H_2}}} + \cdots \right.$ $\left. \frac{K_1 K_2^{1.5} K_3 K_4 K_5}{K_6} \frac{P_{CO} P_{H_2}^{1.5}}{P_{H_2O}} + \frac{K_1 K_2^2 K_3 K_4 K_5 K_7}{K_6} \frac{P_{CO} P_{H_2}^2}{P_{H_2O}} \right)}$

APPENDIX

Table A. 9 Reaction pathway and LHHW rate expressions developed for model FT–III based on H-assisted (second route) CO dissociation mechanism

No.	General Reaction Path	Kinetic parameter	Rate Equations
1	$CO + \psi \rightleftarrows CO - \psi$	K_1	$K_1 P_{CO} \psi = \psi_{CO}$
2	$H_2 + 2\psi \rightleftarrows 2H - \psi$	K_2	$K_2 P_{H_2} \psi^2 = \psi_H^2$
3	$CO - \psi + H - \psi \rightleftarrows HCO - \psi + \psi$	K_3	$K_3 \psi_{CO} \psi_H = \psi_{HCO} \psi$
4	$HCO - \psi + H - \psi \rightleftarrows HCOH - \psi + \psi$	K_4	$K_4 \psi_{HCO} \psi_H = \psi_{HCOH} \psi$
5	$HCOH - \psi + \psi \rightleftarrows CH - \psi + OH - \psi$	K_5	$K_5 \psi_{HCOH} \psi = \psi_{CH} \psi_{OH}$
6	$OH - \psi + H - \psi \rightleftarrows H_2O + 2\psi$	K_6	$k_6 \psi_{OH} \psi_H = P_{H_2O} \psi^2$
7	$CH - \psi + H - \psi \rightleftarrows CH_2 - \psi + \psi$	K_7	$K_7 \psi_{CH} \psi_H = \psi_{CH_2} \psi$ $R_{FT} = k_{i,par} \psi_{CH_2} \psi_H$
8	$CH_2 - \psi + H - \psi \rightarrow CH_3 - \psi + \psi$	$k_{i,par}$	$\frac{d\psi_{CH_3}}{dt} = 0 \Rightarrow +R_8 - R_9 - R_{12} = 0 \Rightarrow + k_{i,par} \psi_{CH_2} \psi_H - k_{meth} \psi_{CH_3} \psi_H - k_{g,par} \psi_{CH_3} \psi_{CH_2} = 0$ $\psi_{CH_3} = \frac{k_{i,par} \psi_{CH_2} \psi_H}{k_{g,par} \psi_{CH_2} + k_{meth} \psi_H}$
9	$CH_3 - \psi + H - \psi \rightarrow CH_4 + 2\psi$	k_{meth}	$R_{CH_4} = k_{meth} \psi_{CH_3} \psi_H$
10	$CH_2 - \psi + CH_2 - \psi \rightarrow C_2H_4 + 2\psi$	k_{eth}	$R_{C_2H_4} = k_{eth} \psi_{CH_2}{}^2$
11	$CH_2 - \psi + CH - \psi \rightarrow C_2H_3 - \psi + \psi$	$k_{i,olef}$	$\frac{d\psi_{C_2H_3}}{dt} = 0 \Rightarrow +R_{11} - R_{14} = 0 \Rightarrow + k_{i,olef} \psi_{CH_2} \psi_{CH} - k_{g,olef} \psi_{CH_2} \psi_{C_2H_3} = 0$ $\psi_{C_2H_3} = \frac{k_{i,olef} \psi_{CH}}{k_{g,olef}}$
12	$C_{n-1}H_{2n-1} - \psi + CH_2 - \psi \rightarrow C_nH_{2n+1} - \psi + \psi \; ; \; n \geq 3$	$k_{g,par}$	$\frac{d\psi_{C_nH_{2n+1}}}{dt} = 0 \Rightarrow +R_{12} - R'_{12} - R_{13} = 0 \Rightarrow + k_{g,par} \psi_{C_{n-1}H_{2n-1}} \psi_{CH_2} - k_{g,par} \psi_{C_nH_{2n+1}} \psi_{CH_2} - k_{t,par} \psi_{C_nH_{2n+1}} \psi_H = 0$ $\psi_{C_nH_{2n+1}} = \frac{k_{g,par} \psi_{C_{n-1}H_{2n-1}} \psi_{CH_2}}{k_{g,par} \psi_{CH_2} + k_{t,par} \psi_H}$
13	$C_nH_{2n+1} - \psi + H - \psi \rightarrow C_nH_{2n+2} + 2\psi$	$k_{t,par}$	$R_{parffins} = k_{t,par} \psi_{C_nH_{2n+1}} \psi_H$
14	$CH_2 - \psi + C_{n-1}H_{2n-3} - \psi \rightarrow C_nH_{2n-1} - \psi + \psi; \; n \geq 3$	$k_{g,olef}$	$\frac{d\psi_{C_nH_{2n-1}}}{dt} = 0 \Rightarrow +R_{14} - R'_{14} - R_{15} = 0 \Rightarrow + k_{g,olef} \psi_{C_{n-1}H_{2n-3}} \psi_{CH_2} - k_{g,olef} \psi_{C_nH_{2n-1}} \psi_{CH_2} - k_{t,olef} \psi_{C_nH_{2n-1}} \psi_H = 0$ $\psi_{C_nH_{2n-1}} = \frac{k_{g,olef} \psi_{C_{n-1}H_{2n-3}} \psi_{CH_2}}{k_{g,olef} \psi_{CH_2} + k_{t,olef} \psi_H}$
15	$C_nH_{2n-1} - \psi + H - \psi \rightarrow C_nH_{2n} + 2\psi$	$k_{t,olef}$	$R_{olefins} = k_{t,olef} \psi_{C_nH_{2n-1}} \psi_H$

APPENDIX

Table A. 10 Kinetic model FT–III assuming steps 6 and 8–15 are the rate-determining steps (RDS-1)

No.	FT–III (RDS-1: 6, 8–15)	Rate Equations
1	$CO + \psi \rightleftarrows CO - \psi$	$\psi_{CO} = K_1 P_{CO} \psi$
2	$H_2 + 2\psi \rightleftarrows 2H - \psi$	$\psi_H = \sqrt{K_2 P_{H_2}}\psi$
3	$CO - \psi + H - \psi \rightleftarrows HCO - \psi + \psi$	$\psi_{HCO} = \frac{K_3 \psi_{CO} \psi_H}{\psi} = \frac{K_3 K_1 P_{CO} \psi \sqrt{K_2} P_{H2}^{0.5} \psi}{\psi} = K_3 K_1 \sqrt{K_2} P_{CO} P_{H2}^{0.5} \psi$
4	$HCO - \psi + H - \psi \rightleftarrows HCOH - \psi + \psi$	$\psi_{HCOH} = \frac{K_4 \psi_{HCO} \psi_H}{\psi} = \frac{K_4 \frac{K_3 \psi_{CO} \psi_H}{\psi} \psi_H}{\psi} = \frac{K_4 K_3 \psi_{CO} \psi_H^2}{\psi^2} = \frac{K_4 K_3 K_1 P_{CO} \psi K_2 P_{H2} \psi^2}{\psi^2} = K_1 K_2 K_3 K_4 P_{CO} P_{H2} \psi$
		$\psi_{CH} = \frac{K_5 \psi_{HCOH} \psi}{\psi_{OH}} = \frac{(K_5 K_1 K_2 K_3 K_4 P_{CO} P_{H2} \psi)\psi}{\frac{R_{FT}}{k_6 \psi_H}} = k_6 K_5 K_1 K_2^{1.5} K_3 K_4 \frac{P_{CO} P_{H2}^{1.5}}{R_{FT}} \psi^3$
5	$HCOH - \psi + \psi \rightleftarrows CH - \psi + OH - \psi$	$\psi_{CH} = \frac{k_6 K_5 K_1 K_2^{1.5} K_3 K_4}{\sqrt{k_{i,par} k_6 K_7 K_5 K_1 K_2^{2.5} K_3 K_4}} P_{CO}^{0.5} P_{H2}^{0.25} \psi = K_2^{0.25} \sqrt{\frac{k_6 K_1 K_3 K_4 K_5}{k_{i,par} K_7}} P_{CO}^{0.5} P_{H2}^{0.25} \psi$
		$R_{FT} = k_6 \psi_{OH} \psi_H$
6	$OH - \psi + H - \psi \rightarrow H_2O + 2\psi$	$\psi_{OH} = \frac{R_{FT}}{k_6 \psi_H} = \frac{\sqrt{k_{i,par} K_7 k_6 K_5 K_1 K_2^{2.5} K_3 K_4} P_{CO}^{0.5} P_{H2}^{1.25} \psi^2}{k_6 \sqrt{K_2} P_{H2}^{0.5} \psi} = K_2^{0.75} \sqrt{\frac{k_{i,par} K_7 K_5 K_1 K_3 K_4}{k_6}} P_{CO}^{0.5} P_{H2}^{0.75} \psi$
		$\psi_{CH_2} = \frac{K_7 \psi_{CH} \psi_H}{\psi} = \frac{K_7 k_6 K_5 K_1 K_2^{1.5} K_3 K_4 \frac{P_{CO} P_{H2}^{1.5}}{R_{FT}} \psi^3 \sqrt{K_2} P_{H2}^{0.5} \psi}{\psi} = k_6 K_7 K_5 K_1 K_2^2 K_3 K_4 \frac{P_{CO} P_{H2}^2}{R_{FT}} \psi^3$
7	$CH - \psi + H - \psi \rightleftarrows CH_2 - \psi + \psi$	$\psi_{CH_2} = \frac{k_6 K_7 K_5 K_1 K_2^2 K_3 K_4 \frac{P_{CO} P_{H2}^2}{R_{FT}} \psi^3}{\sqrt{k_{i,par} k_6 K_7 K_5 K_1 K_2^{2.5} K_3 K_4 P_{CO}^{0.5} P_{H2}^{1.25} \psi^2}} = \sqrt{\frac{k_6 K_7 K_5 K_1 K_2^{1.5} K_3 K_4}{k_{i,par}}} P_{CO}^{0.5} P_{H2}^{0.75} \psi$
8	$CH_2 - \psi + H - \psi \rightarrow CH_3 - \psi + \psi$	$R_{FT} = k_{i,par} \psi_{CH_2} \psi_H = k_{i,par} k_6 K_7 K_5 K_1 K_2^{2.5} K_3 K_4 \frac{P_{CO} P_{H2}^{2.5}}{R_{FT}} \psi^4$
		$R_{FT} = \sqrt{k_{i,par} K_7 k_6 K_5 K_1 K_2^{2.5} K_3 K_4} P_{CO}^{0.5} P_{H2}^{1.25} \psi^2$
Total Surface Coverage	$\psi + \psi_{CO} + \psi_H + \psi_{OH} + \psi_{HCO} + \psi_{HCOH} + \psi_{CH} + \psi_{CH_2} = 1$	$\psi = \frac{1}{\left(\begin{array}{c} 1 + K_1 P_{CO} + \sqrt{K_2 P_{H_2}} + K_2^{0.75} \sqrt{\frac{k_{i,par} K_7 K_5 K_1 K_3 K_4}{k_6}} P_{CO}^{0.5} P_{H2}^{0.75} + \\ K_3 K_1 \sqrt{K_2} P_{CO} P_{H2}^{0.5} + K_1 K_2 K_3 K_4 P_{CO} P_{H2} + \\ K_2^{0.25} \sqrt{\frac{k_6 K_1 K_3 K_4 K_5}{k_{i,par} K_7}} P_{CO}^{0.5} P_{H2}^{0.25} + \sqrt{\frac{K_7 k_6 K_5 K_1 K_2^{1.5} K_3 K_4}{k_{i,par}}} P_{CO}^{0.5} P_{H2}^{0.75} \end{array}\right)}$

Table A. 11 Kinetic model FT–III assuming steps 4 and 8–15 are the rate-determining steps (RDS-2)

No.	FT–III (RDS-2: 4, 8–15)	Rate Equations
1	$CO + \psi \rightleftarrows CO - \psi$	$\psi_{CO} = K_1 P_{CO} \psi$
2	$H_2 + 2\psi \rightleftarrows 2H - \psi$	$\psi_H = \sqrt{K_2 P_{H_2}}\,\psi$
3	$CO - \psi + H - \psi \rightleftarrows HCO - \psi + \psi$	$\psi_{HCO} = \frac{K_3 \psi_{CO} \psi_H}{\psi} = \frac{K_3 K_1 P_{CO} \psi \sqrt{K_2} P_{H2}^{0.5} \psi}{\psi} = K_3 K_1 \sqrt{K_2} P_{CO} P_{H2}^{0.5} \psi$
4	$HCO - \psi + H - \psi \rightarrow HCOH - \psi + \psi$	$R_{FT} = k_4 \psi_{HCO} \psi_H = k_4 \left(K_3 K_1 \sqrt{K_2} P_{CO} P_{H2}^{0.5} \psi\right) \left(\sqrt{K_2 P_{H_2}}\,\psi\right) = k_4 K_1 K_2 K_3 P_{CO} P_{H_2} \psi^2$
5	$HCOH - \psi + \psi \rightleftarrows CH - \psi + OH - \psi$	$\psi_{HCOH} = \frac{\psi_{OH} \psi_{CH}}{K_5 \psi} = \frac{\left(\frac{P_{H_2O}}{K_6 \sqrt{K_2 P_{H_2}}} \psi\right) \left(\frac{k_4 K_1 K_2^{0.5} K_3}{k_{i,par} K_7} P_{CO} P_{H_2}^{0.5} \psi\right)}{K_5 \psi} = \frac{k_4 K_1 K_3}{k_{i,par} K_5 K_6 K_7} P_{H_2O} P_{CO} \psi$
6	$OH - \psi + H - \psi \rightleftarrows H_2O + 2\psi$	$\psi_{OH} = \frac{\psi^2 P_{H_2O}}{K_6 \psi_H} = \frac{\psi^2 P_{H_2O}}{K_6 \sqrt{K_2 P_{H_2}} \psi} = \frac{P_{H_2O}}{K_6 \sqrt{K_2 P_{H_2}}} \psi$
7	$CH - \psi + H - \psi \rightleftarrows CH_2 - \psi + \psi$	$\psi_{CH} = \frac{\psi_{CH_2} \psi}{K_7 \psi_H} = \frac{\left(\frac{R_{FT}}{k_{i,par} \psi_H}\right) \psi}{K_7 \psi_H} = \frac{R_{FT}}{K_7 k_{i,par} \psi_H^2} \psi = \frac{k_4 K_1 K_2 K_3 P_{CO} P_{H_2} \psi^2}{K_7 k_{i,par} K_2 P_{H_2} \psi^2} \psi = \frac{k_4 K_1 K_2^{0.5} K_3}{k_{i,par} K_7} P_{CO} P_{H_2}^{0.5} \psi$
8	$CH_2 - \psi + H - \psi \rightarrow CH_3 - \psi + \psi$	$R_{FT} = k_{k_{i,par}} \psi_{CH_2} \psi_H$ $\psi_{CH_2} = \frac{R_{FT}}{k_{i,par} \psi_H} = \frac{k_4 K_1 K_2 K_3 P_{CO} P_{H_2} \psi^2}{k_{i,par} \sqrt{K_2 P_{H_2}} \psi} = \frac{k_4 K_1 K_2^{0.5} K_3}{k_{i,par}} P_{CO} P_{H_2}^{0.5} \psi$
Total Surface Coverage	$\psi + \psi_{CO} + \psi_H + \psi_{OH} + \psi_{HCO} + \psi_{HCOH} + \psi_{CH} + \psi_{CH_2} = 1$	$\psi = \frac{1}{\left(\begin{array}{c} 1 + K_1 P_{CO} + \sqrt{K_2 P_{H_2}} + \frac{P_{H_2O}}{K_6 \sqrt{K_2 P_{H_2}}} + K_3 K_1 \sqrt{K_2} P_{CO} P_{H2}^{0.5} + \\ \frac{k_4 K_1 K_3}{k_{i,par} K_5 K_6 K_7} P_{H_2O} P_{CO} + \frac{k_4 K_1 K_2^{0.5} K_3}{k_{i,par} K_7} P_{CO} P_{H_2}^{0.5} + \frac{k_4 K_1 K_2^{0.5} K_3}{k_{i,par}} P_{CO} P_{H_2}^{0.5} \end{array}\right)}$

Table A. 12 Kinetic model FT–III assuming steps 8–15 are the rate-determining steps (RDS-3)

No.	FT–III (RDS-3: 8–15)	Rate Equations
1	$CO + \psi \rightleftarrows CO - \psi$	$\psi_{CO} = K_1 P_{CO} \psi$
2	$H_2 + 2\psi \rightleftarrows 2H - \psi$	$\psi_H = \sqrt{K_2 P_{H_2}}\,\psi$
3	$CO - \psi + H - \psi \rightleftarrows HCO - \psi + \psi$	$\psi_{HCO} = \frac{K_3 \psi_{CO} \psi_H}{\psi} = \frac{K_3 K_1 P_{CO} \psi \sqrt{K_2} P_{H2}^{0.5} \psi}{\psi} = K_3 K_1 \sqrt{K_2} P_{CO} P_{H2}^{0.5} \psi$
4	$HCO - \psi + H - \psi \rightleftarrows HCOH - \psi + \psi$	$\psi_{HCOH} = \frac{K_4 \psi_{HCO} \psi_H}{\psi} = \frac{K_4 \left(K_3 K_1 \sqrt{K_2} P_{CO} P_{H2}^{0.5} \psi\right) \sqrt{K_2 P_{H_2}} \psi}{\psi} = K_1 K_2 K_3 K_4 P_{CO} P_{H_2} \psi$
5	$HCOH - \psi + \psi \rightleftarrows CH - \psi + OH - \psi$	$\psi_{CH} = \frac{K_5 \psi_{HCOH} \psi}{\psi_{OH}} = \frac{K_5 \left(K_1 K_2 K_3 K_4 P_{CO} P_{H_2} S\right) \psi}{\frac{P_{H_2O}}{K_6 \sqrt{K_2 P_{H_2}}} \psi} = K_5 K_1 K_2^{1.5} K_3 K_4 K_6 \frac{P_{CO} P_{H_2}^{1.5}}{P_{H_2O}} \psi$
6	$OH - \psi + H - \psi \rightleftarrows H_2O + 2\psi$	$\psi_{OH} = \frac{\psi^2 P_{H_2O}}{K_6 \psi_H} = \frac{\psi^2 P_{H_2O}}{K_6 \sqrt{K_2 P_{H_2}} \psi} = \frac{P_{H_2O}}{K_6 \sqrt{K_2 P_{H_2}}} \psi$
7	$CH - \psi + H - \psi \rightleftarrows CH_2 - \psi + \psi$	$\psi_{CH_2} = \frac{K_7 \psi_{CH} \psi_H}{\psi} = \frac{K_7 K_5 K_1 K_2^{1.5} K_3 K_4 K_6 \frac{P_{CO} P_{H_2}^{1.5}}{P_{H_2O}} \psi \sqrt{K_2 P_{H_2}} \psi}{\psi} = K_7 K_5 K_1 K_2^2 K_3 K_4 K_6 \frac{P_{CO} P_{H_2}^2}{P_{H_2O}} \psi$
8	$CH_2 - \psi + H - \psi \rightarrow CH_3 - \psi + \psi$	$R_{FT} = k_{i,par} \psi_{CH_2} \psi_H = k_{i,par} K_7 K_5 K_1 K_2^{2.5} K_3 K_4 K_6 \frac{P_{CO} P_{H_2}^{2.5}}{P_{H_2O}} \psi^2$
Total Surface Fraction Coverage	$\psi + \psi_{CO} + \psi_H + \psi_{OH} + \psi_{HCO} + \psi_{HCOH} + \psi_{CH} + \psi_{CH_2} = 1$	$\psi = \frac{1}{\left(\begin{array}{c} 1 + K_1 P_{CO} + \sqrt{K_2 P_{H_2}} + \frac{P_{H_2O}}{K_6 \sqrt{K_2 P_{H_2}}} + K_3 K_1 \sqrt{K_2} P_{CO} P_{H2}^{0.5} + \\ K_1 K_2 K_3 K_4 P_{CO} P_{H_2} + K_5 K_1 K_2^{1.5} K_3 K_4 K_6 \frac{P_{CO} P_{H_2}^{1.5}}{P_{H_2O}} + \\ K_7 K_5 K_1 K_2^2 K_3 K_4 K_6 \frac{P_{CO} P_{H_2}^2}{P_{H_2O}} \end{array}\right)}$

APPENDIX

Table A. 13 Reaction pathway and LHHW rate expressions developed for model FT–IV based on H-assisted (third route) CO dissociation mechanism

No.	General Reaction Path	Kinetic parameter	Rate Equations
1	$CO + \psi \rightleftarrows CO - \psi$	K_1	$K_1 P_{CO} \psi = \psi_{CO}$
2	$H_2 + 2\psi \rightleftarrows 2H - \psi$	K_2	$K_2 P_{H_2} \psi^2 = \psi_H^2$
3	$CO - \psi + H - \psi \rightleftarrows HCO - \psi + \psi$	K_3	$K_3 \psi_{CO} \psi_H = \psi_{HCO} \psi$
4	$HCO - \psi + \psi \rightleftarrows CH - \psi + O - \psi$	K_4	$K_4 \psi_{HCO} \psi = \psi_{CH} \psi_O$
5	$O - \psi + H - \psi \rightleftarrows OH - \psi + \psi$	K_5	$K_5 \psi_O \psi_H = \psi_{OH} \psi$
6	$OH - \psi + H - \psi \rightleftarrows H_2O + 2\psi$	K_6	$K_6 \psi_{OH} \psi_H = P_{H_2O} \psi^2$
7	$CH - \psi + H_2 \rightarrow CH_3 - \psi$	$k_{i,par}$	$R_{FT} = k_{i,par} \psi_{CH} P_{H_2}$ $\frac{d\psi_{CH_3}}{dt} = 0 \Rightarrow +R_7 - R_8 - R_{11} = 0 \Rightarrow + k_{i,par} \psi_{CH} P_{H_2} - k_{meth} \psi_{CH_3} \psi_H - k_{g,par} \psi_{CH_3} \psi_H \psi_{CH} = 0 \Rightarrow$ $\psi_{CH_3} = \frac{k_{i,par} \psi_{CH} P_{H_2}}{k_{g,par} \psi_H \psi_{CH} + k_{meth} \psi_H}$
8	$CH_3 - \psi + H - \psi \rightarrow CH_4 + 2\psi$	k_{meth}	$R_{CH_4} = k_{meth} \psi_{CH_3} \psi_H$
9	$CH - \psi + CH - \psi + 2H - \psi \rightarrow C_2H_4 + 2\psi$	k_{eth}	$R_{C_2H_4} = k_{eth} \psi_{CH}{}^2 \psi_H{}^2$
10	$CH - \psi + CH - \psi + H - \psi \rightarrow C_2H_3 - \psi + \psi$	$k_{i,olef}$	$\frac{d\psi_{C_2H_3}}{dt} = 0 \Rightarrow +R_{10} - R_{13} = 0 \Rightarrow + k_{i,olef} \psi_H \psi_{CH}^2 - k_{g,olef} \psi_H \psi_{CH} \psi_{C_2H_3} = 0 \Rightarrow \psi_{C_2H_3} = \frac{k_{i,olef} \psi_{CH}}{k_{g,olef}}$
11	$C_{n-1}H_{2n-1} - \psi + CH - \psi + H - \psi \rightarrow C_nH_{2n+1} - \psi + \psi\ ;\ n \geq 3$	$k_{g,par}$	$\frac{d\psi_{C_nH_{2n+1}}}{dt} = 0 \Rightarrow +R_{11} - R'_{11} - R_{12} = 0 \Rightarrow + k_{g,par} \psi_{C_{n-1}H_{2n-1}} \psi_H \psi_{CH} - k_{g,par} \psi_{C_nH_{2n+1}} \psi_H \psi_{CH} - k_{t,par} \psi_{C_nH_{2n+1}} \psi_H = 0 \Rightarrow$ $\psi_{C_nH_{2n+1}} = \frac{k_{g,par} \psi_{C_{n-1}H_{2n-1}} \psi_H \psi_{CH}}{k_{g,par} \psi_H \psi_{CH} + k_{t,par} \psi_H}$
12	$C_nH_{2n+1} - \psi + H - \psi \rightarrow C_nH_{2n+2} + 2\psi$	$k_{t,par}$	$R_{parffins} = k_{t,par} \psi_{C_nH_{2n+1}} \psi_H$
13	$CH - \psi + H - \psi + C_{n-1}H_{2n-3} - \psi \rightarrow C_nH_{2n-1} - \psi + \psi;\ n \geq 3$	$k_{g,olef}$	$\frac{d\psi_{C_nH_{2n-1}}}{dt} = 0 \Rightarrow +R_{13} - R'_{13} - R_{14} = 0 \Rightarrow +k_{g,olef} \psi_{C_{n-1}H_{2n-3}} \psi_H \psi_{CH} - k_{g,olef} \psi_{C_nH_{2n-1}} \psi_H \psi_{CH} - k_{t,olef} \psi_{C_nH_{2n-1}} \psi_H = 0 \Rightarrow$ $\psi_{C_nH_{2n-1}} = \frac{k_{g,olef} \psi_{C_{n-1}H_{2n-3}} \psi_H \psi_{CH}}{k_{g,olef} \psi_H \psi_{CH} + k_{t,olef} \psi_H}$
14	$C_nH_{2n-1} - \psi + H - \psi \rightarrow C_nH_{2n} + 2\psi$	$k_{t,olef}$	$R_{olefins} = k_{t,olef} \psi_{C_nH_{2n-1}} \psi_H$

Table A. 14 Kinetic model FT–IV assuming steps 6 and 7–14 are the rate-determining steps (RDS-1)

No.	FT–IV (RDS-1: 6, 7–14)	Rate Equations
1	$CO + \psi \rightleftarrows CO - \psi$	$\psi_{CO} = K_1 P_{CO} \psi$
2	$H_2 + 2\psi \rightleftarrows 2H - \psi$	$\psi_H = \sqrt{K_2 P_{H_2}} \psi$
3	$CO - \psi + H - \psi \rightleftarrows HCO - \psi + \psi$	$\psi_{HCO} = \frac{K_3 \psi_{CO} \psi_H}{\psi} = \frac{K_3 K_1 P_{CO} \psi \sqrt{K_2} P_{H2}^{0.5} \psi}{\psi} = K_3 K_1 \sqrt{K_2} P_{CO} P_{H2}^{0.5} \psi$
4	$HCO - \psi + \psi \rightleftarrows CH - \psi + O - \psi$	$\psi_{CH} = \frac{K_4 \psi_{HCO} \psi}{\psi_O} = \frac{K_4 K_3 K_1 \sqrt{K_2} P_{CO} P_{H2}^{0.5} \psi \psi}{\frac{R_{FT}}{k_6^2 K_5 K_2^{1.5} P_{H_2}^{1.5} \psi}} = \frac{k_6^2 K_4 K_3 K_1 K_2^2 K_5 P_{CO} P_{H2}^2 \psi}{R_{FT}} = \frac{k_6^2 K_4 K_3 K_1 K_2^2 K_5 P_{CO} P_{H2}^2 \psi}{\sqrt{k_{i,par} k_6^2 K_4 K_3 K_1 K_2^2 K_5 P_{CO}^{0.5}} P_{H2}^{1.25} \psi^{0.5}}$
5	$O - \psi + H - \psi \rightleftarrows OH - \psi + \psi$	$\psi_O = \frac{\psi_{OH} \psi}{K_5 \psi_H} = \frac{\frac{R_{FT}}{k_6 \sqrt{K_2 P_{H_2}} \psi} \psi}{k_6 K_5 K_2 P_{H_2} \psi} = \frac{R_{FT}}{k_6^2 K_5 K_2^{1.5} P_{H_2}^{1.5} \psi} = \frac{\sqrt{k_{i,par} k_6^2 K_4 K_3 K_1 K_2^2 K_5 P_{CO}^{0.5}} P_{H2}^{1.25} \psi^{0.5}}{k_6^2 K_5 K_2^{1.5} P_{H_2}^{1.5} \psi}$
6	$OH - \psi + H - \psi \rightarrow H_2O + 2\psi$	$R_{FT} = k_6 \psi_{OH} \psi_H$ $\psi_{OH} = \frac{R_{FT}}{k_6 \psi_H} = \frac{R_{FT}}{k_6 \sqrt{K_2 P_{H_2}} \psi} = \frac{\sqrt{k_{i,par} k_6^2 K_4 K_3 K_1 K_2^2 K_5 P_{CO}^{0.5}} P_{H2}^{1.25} \psi^{0.5}}{k_6 \sqrt{K_2 P_{H_2}} \psi}$
7	$CH - \psi + H_2 \rightarrow CH_3 - \psi$	$R_{FT} = k_{i,par} \psi \psi_{CH} P_{H_2} = k_{i,par} \frac{k_6^2 K_4 K_3 K_1 K_2^2 K_5 P_{CO} P_{H2}^2 \psi}{R_{FT}} P_{H_2} = k_{i,par} \frac{k_6^2 K_4 K_3 K_1 K_2^2 K_5 P_{CO} P_{H2}^2 \psi}{R_{FT}} P_{H_2}$ $R_{FT} = \sqrt{k_{i,par} k_6^2 K_4 K_3 K_1 K_2^2 K_5 P_{CO}^{0.5}} P_{H2}^{1.25} \psi^{0.5}$
Total Surface Coverage	$\psi + \psi_{CO} + \psi_H + \psi_{HCO} = 1$	$\psi = \frac{1}{\left(1 + K_1 P_{CO} + \sqrt{K_2 P_{H_2}} + K_3 K_1 \sqrt{K_2} P_{CO} P_{H2}^{0.5} + K_1 K_2 K_3 K_4 P_{CO} P_{H_2}\right)}$

Table A. 15 Kinetic model FT–IV assuming steps 4 and 7–14 are the rate-determining steps (RDS-2)

No.	FT–IV (RDS-2: 4, 7–14)	Rate Equations
1	$\mathrm{CO} + \psi \rightleftarrows \mathrm{CO} - \psi$	$\psi_{CO} = K_1 P_{CO} \psi$
2	$\mathrm{H_2} + 2\psi \rightleftarrows 2\mathrm{H} - \psi$	$\psi_H = \sqrt{K_2 P_{H_2}}\,\psi$
3	$\mathrm{CO} - \psi + \mathrm{H} - \psi \rightleftarrows \mathrm{HCO} - \psi + \psi$	$\psi_{HCO} = \frac{K_3 \psi_{CO} \psi_H}{\psi} = \frac{K_3 K_1 P_{CO} \psi \sqrt{K_2} P_{H2}^{0.5} \psi}{\psi} = K_3 K_1 \sqrt{K_2} P_{CO} P_{H2}^{0.5} \psi$
4	$\mathrm{HCO} - \psi + \psi \rightarrow \mathrm{CH} - \psi + \mathrm{O} - \psi$	$R_{FT} = k_4 \psi_{HCO} \psi = k_4 K_3 K_1 \sqrt{K_2} P_{CO} P_{H2}^{0.5} \psi^2$
5	$\mathrm{O} - \psi + \mathrm{H} - \psi \rightleftarrows \mathrm{OH} - \psi + \psi$	$\psi_O = \frac{\psi_{\mathrm{OH}} \psi}{K_5 \psi_H} = \frac{\frac{P_{H_2O}}{K_7 \sqrt{K_2 P_{H_2}}} \psi \psi}{K_5 \sqrt{K_2 P_{H_2}}\,\psi} = \frac{P_{H_2O}}{K_6 K_2 K_5 P_{H_2}} \psi$
6	$\mathrm{OH} - \psi + \mathrm{H} - \psi \rightleftarrows \mathrm{H_2O} + 2\psi$	$\psi_{OH} = \frac{P_{H_2O} \psi^2}{K_6 \psi_H} = \frac{P_{H_2O} \psi^2}{K_6 \sqrt{K_2 P_{H_2}}\,\psi} = \frac{P_{H_2O}}{K_6 \sqrt{K_2 P_{H_2}}} \psi$
7	$\mathrm{CH} - \psi + \mathrm{H_2} \rightarrow \mathrm{CH_3} - \psi$	$R_{FT} = k_{i,par} \psi_{CH} P_{H_2}$ $\psi_{CH} = \frac{R_{FT}}{k_{i,par} P_{H_2}} = \frac{k_4 K_3 K_1 \sqrt{K_2} P_{CO} P_{H2}^{0.5} \psi^2}{k_{i,par} P_{H_2}} = \frac{k_4 K_3 K_1 \sqrt{K_2}}{k_{i,par}} P_{CO} P_{H2}^{1.5} \psi^2$
Total Surface Coverage	$\psi + \psi_{\mathrm{CO}} + \psi_{\mathrm{H}} + \psi_{\mathrm{HCO}} + \psi_{\mathrm{OH}} + \psi_{\mathrm{O}} = 1$	$\psi = \frac{1}{\left(1 + K_1 P_{CO} + \sqrt{K_2 P_{H_2}} + K_3 K_1 \sqrt{K_2} P_{CO} P_{H2}^{0.5} + \frac{P_{H_2O}}{K_7 K_2 K_5 P_{H_2}} + \frac{P_{H_2O}}{K_6 \sqrt{K_2 P_{H_2}}}\right)}$

Table A. 16 Kinetic model FT–IV assuming steps 7–14 are the rate-determining steps (RDS-3)

No.	FT–IV (RDS-3: 7–14)	Rate Equations
1	$CO + \psi \rightleftarrows CO - \psi$	$\psi_{CO} = K_1 P_{CO} \psi$
2	$H_2 + 2\psi \rightleftarrows 2H - \psi$	$\psi_H = \sqrt{K_2 P_{H_2}}\,\psi$
3	$CO - \psi + H - \psi \rightleftarrows HCO - \psi + \psi$	$\psi_{HCO} = \frac{K_3 \psi_{CO} \psi_H}{\psi} = \frac{K_3 K_1 P_{CO} \psi \sqrt{K_2} P_{H2}^{0.5} \psi}{\psi} = K_3 K_1 \sqrt{K_2} P_{CO} P_{H2}^{0.5} \psi$
4	$HCO - \psi + \psi \rightleftarrows CH - \psi + O - \psi$	$\psi_{CH} = \frac{K_4 \psi_{HCO} \psi}{\psi_O} = \frac{K_4 K_3 K_1 \sqrt{K_2} P_{CO} P_{H2}^{0.5} \psi \psi}{\frac{P_{H_2O}}{K_6 K_2 K_5 P_{H_2}} \psi} = K_6 K_2^{1.5} K_5 K_4 K_3 K_1 \frac{P_{CO} P_{H2}^{1.5}}{P_{H_2O}} \psi$
5	$O - \psi + H - \psi \rightleftarrows OH - \psi + \psi$	$\psi_O = \frac{\psi_{OH} \psi}{K_5 \psi_H} = \frac{\frac{P_{H_2O}}{K_6 \sqrt{K_2 P_{H_2}}} \psi \psi}{K_5 \sqrt{K_2 P_{H_2}} \psi} = \frac{P_{H_2O}}{K_6 K_2 K_5 P_{H_2}} \psi$
6	$OH - \psi + H - \psi \rightleftarrows H_2O + 2\psi$	$\psi_{OH} = \frac{P_{H_2O} \psi^2}{K_6 \psi_H} = \frac{P_{H_2O} \psi^2}{K_6 \sqrt{K_2 P_{H_2}} \psi} = \frac{P_{H_2O}}{K_6 \sqrt{K_2 P_{H_2}}} \psi$
7	$CH - \psi + H_2 \rightarrow CH_3 - \psi$	$R_{FT} = k_{i,par} \psi_{CH} P_{H_2} = k_{i,par} K_6 K_2^{1.5} K_5 K_4 K_3 K_1 \frac{P_{CO} P_{H2}^{1.5}}{P_{H_2O}} \psi P_{H_2} \Rightarrow$ $R_{FT} = k_{i,par} K_6 K_2^{1.5} K_5 K_4 K_3 K_1 \frac{P_{CO} P_{H2}^{2.5}}{P_{H_2O}} \psi$
Total Surface Coverage	$\psi + \psi_{CO} + \psi_H + \psi_{HCO} + \psi_{CH} + \psi_O + \psi_{OH} = 1$	$\psi = \frac{1}{\left(1 + K_1 P_{CO} + \sqrt{K_2 P_{H_2}} + K_3 K_1 \sqrt{K_2} P_{CO} P_{H2}^{0.5} + K_6 K_2^{1.5} K_5 K_4 K_3 K_1 \frac{P_{CO} P_{H2}^{1.5}}{P_{H_2O}} \right.$ $\left. \frac{P_{H_2O}}{K_6 K_2 K_5 P_{H_2}} + \frac{P_{H_2O}}{K_6 \sqrt{K_2 P_{H_2}}} \right)}$

APPENDIX

Table A. 17 Reaction pathway and LHHW rate expressions developed for model FT–V based on H-assisted (fourth route) CO dissociation mechanism

No.	General Reaction Path	Kinetic parameter	Rate Equations
1	$CO + \psi \rightleftarrows CO - \psi$	K_1	$K_1 P_{CO} \psi = \psi_{CO}$
2	$H_2 + 2\psi \rightleftarrows 2H - \psi$	K_2	$K_2 P_{H_2} \psi^2 = \psi_H^2$
3	$CO - \psi + H - \psi \rightleftarrows HCO - \psi + \psi$	K_3	$K_3 \psi_{CO} \psi_H = \psi_{HCO} \psi$
4	$HCO - \psi + H - \psi \rightleftarrows CH_2O - \psi + \psi$	K_4	$K_4 \psi_{HCO} \psi_H = \psi_{CH_2O} \psi$
5	$CH_2O - \psi + \psi \rightleftarrows CH_2 - \psi + O - \psi$	K_5	$K_5 \psi_{CH_2O} \psi = \psi_{CH_2} \psi_O$
6	$O - \psi + H - \psi \rightleftarrows OH - \psi + \psi$	K_6	$K_6 \psi_O \psi_H = \psi_{OH} \psi$
7	$OH - \psi + H - \psi \rightleftarrows H_2O + 2\psi$	K_7	$K_7 \psi_{OH} \psi_H = P_{H_2O} \psi^2$
8	$CH_2 - \psi + H - \psi \rightarrow CH_3 - \psi$	$k_{i,par}$	$R_{FT} = k_{i,par} \psi_{CH_2} \psi_H$ $\frac{d\psi_{CH_3}}{dt} = 0 \Rightarrow +R_8 - R_9 - R_{12} = 0 \Rightarrow + k_{i,par} \psi_{CH_2} \psi_H - k_{meth} \psi_{CH_3} \psi_H - k_{g,par} \psi_{CH_3} \psi_{CH_2} = 0 \Rightarrow$ $\psi_{CH_3} = \frac{k_{i,par} \psi_{CH_2} \psi_H}{k_{g,par} \psi_{CH_2} + k_{meth} \psi_H}$
9	$CH_3 - \psi + H - \psi \rightarrow CH_4 + 2\psi$	k_{meth}	$R_{CH_4} = k_{meth} \psi_{CH_3} \psi_H$
10	$CH_2 - \psi + CH_2 - \psi \rightarrow C_2H_4 + 2\psi$	k_{eth}	$R_{C_2H_4} = k_{eth} {\psi_{CH_2}}^2$
11	$CH_2 - \psi + CH - \psi \rightarrow C_2H_3 - \psi + \psi$	$k_{i,olef}$	$\frac{d\psi_{C_2H_3}}{dt} = 0 \Rightarrow +R_{11} - R_{14} = 0 \Rightarrow + k_{i,olef} \psi_{CH_2} \psi_{CH} - k_{g,olef} \psi_{CH_2} \psi_{C_2H_3} = 0 \Rightarrow \psi_{C_2H_3} = \frac{k_{i,olef} \psi_{CH}}{k_{g,olef}}$
12	$C_{n-1}H_{2n-1} - \psi + CH_2 - \psi \rightarrow C_nH_{2n+1} - \psi + \psi\ ;\ n \geq 3$	$k_{g,par}$	$\frac{d\psi_{C_nH_{2n+1}}}{dt} = 0 \Rightarrow +R_{12} - R'_{12} - R_{13} = 0 \Rightarrow + k_{g,par} \psi_{C_{n-1}H_{2n-1}} \psi_{CH_2} - k_{g,par} \psi_{C_nH_{2n+1}} \psi_{CH_2} - k_{t,par} \psi_{C_nH_{2n+1}} \psi_H = 0 \Rightarrow$ $\psi_{C_nH_{2n+1}} = \frac{k_{g,par} \psi_{C_{n-1}H_{2n-1}} \psi_{CH_2}}{k_{g,par} \psi_{CH_2} + k_{t,par} \psi_H}$
13	$C_nH_{2n+1} - \psi + H - \psi \rightarrow C_nH_{2n+2} + 2\psi$	$k_{t,par}$	$R_{parffins} = k_{t,par} \psi_{C_nH_{2n+1}} \psi_H$
14	$CH_2 - \psi + C_{n-1}H_{2n-3} - \psi \rightarrow C_nH_{2n-1} - \psi + \psi;\ n \geq 3$	$k_{g,olef}$	$\frac{d\psi_{C_nH_{2n-1}}}{dt} = 0 \Rightarrow +R_{14} - R'_{14} - R_{15} = 0 \Rightarrow +k_{g,olef} \psi_{C_{n-1}H_{2n-3}} \psi_{CH_2} - k_{g,olef} \psi_{C_nH_{2n-1}} \psi_{CH_2} - k_{t,olef} \psi_{C_nH_{2n-1}} \psi_H = 0 \Rightarrow$ $\psi_{C_nH_{2n-1}} = \frac{k_{g,olef} \psi_{C_{n-1}H_{2n-3}} \psi_{CH_2}}{k_{g,olef} \psi_{CH_2} + k_{t,olef} \psi_H}$
15	$C_nH_{2n-1} - \psi + H - \psi \rightarrow C_nH_{2n} + 2\psi$	$k_{t,olef}$	$R_{olefins} = k_{t,olef} \psi_{C_nH_{2n-1}} \psi_H$

APPENDIX

Table A. 18 Kinetic model FT–V assuming steps 7 and 8–15 are the rate-determining steps (RDS-1)

No.	FT–V (RDS-1: 7, 8–15)	Rate Equations
1	$CO + \psi \rightleftarrows CO - \psi$	$\psi_{CO} = K_1 P_{CO} \psi$
2	$H_2 + 2\psi \rightleftarrows 2H - \psi$	$\psi_H = \sqrt{K_2 P_{H_2}}\psi$
3	$CO - \psi + H - \psi \rightleftarrows HCO - \psi + \psi$	$\psi_{HCO} = \frac{K_3 \psi_{CO} \psi_H}{\psi} = \frac{K_3 K_1 P_{CO} \psi \sqrt{K_2} P_{H2}^{0.5} \psi}{\psi} = K_3 K_1 \sqrt{K_2} P_{CO} P_{H2}^{0.5} \psi$
4	$HCO - \psi + H - \psi \rightleftarrows CH_2O - \psi + \psi$	$\psi_{CH_2O} = \frac{K_4 \psi_{HCO} \psi_H}{\psi} = \frac{K_4 \frac{K_3 \psi_{CO} \psi_H}{\psi} \psi_H}{\psi} = K_1 K_2 K_3 K_4 P_{CO} P_{H_2} \psi$
5	$CH_2O - \psi + \psi \rightleftarrows CH_2 - \psi + O - \psi$	$\psi_{\mathrm{CH_2}} = \frac{\psi_{CH_2O}\psi}{K_5 \psi_O} = \frac{\left(K_1 K_2 K_3 K_4 P_{CO} P_{H_2} \psi\right)\psi}{K_5 \frac{R_{FT}}{k_7 K_6 K_2 P_{H_2} \psi}} = \frac{(k_7 K_6 K_1 K_2^2 K_3 K_4)}{K_5} \frac{P_{CO} P_{H_2}^2}{R_{FT}} \psi^3 = \frac{(k_7 K_6 K_1 K_2^2 K_3 K_4)}{K_5} \frac{P_{CO} P_{H_2}^2}{\sqrt{k_{i,par} \frac{\left(k_7 K_6 K_1 K_2^{2.5} K_3 K_4\right)}{K_5} P_{CO} P_{H_2}^{1.25} \psi^2}} \psi^3$ $\psi_{\mathrm{CH_2}} = \frac{\left(\sqrt{k_7 K_6 K_1 K_3 K_4} K_2^{0.75}\right)}{\sqrt{K_5}} \frac{P_{CO} P_{H_2}^{0.75}}{\sqrt{k_{i,par}}} \psi$
6	$O - \psi + H - \psi \rightleftarrows OH - \psi + \psi$	$\psi_O = \frac{\frac{R_{FT}}{k_7 \sqrt{K_2 P_{H_2}} \psi} \psi}{K_6 \psi_H} = \frac{\sqrt{k_{i,par} \frac{\left(k_7 K_6 K_1 K_2^{2.5} K_3 K_4\right)}{K_5}} P_{CO} P_{H_2}^{1.25} \psi^2}{k_7 K_6 K_2 P_{H_2} \psi} = \frac{\sqrt{k_{i,par} \left(K_1 K_2^{0.25} K_3 K_4\right)} P_{CO} P_{H_2}^{0.25}}{K_5 \sqrt{k_7 K_6}} \psi$ $R_{FT} = k_7 \psi_{OH} \psi_H$
7	$OH - \psi + H - \psi \rightarrow H_2O + 2\psi$	$\psi_{OH} = \frac{R_{FT}}{k_7 \psi_H} = \frac{R_{FT}}{k_7 \sqrt{K_2 P_{H_2}} \psi} = \sqrt{k_{i,par} \frac{(K_6 K_1 K_2^2 K_3 K_4)}{K_5}} \frac{P_{CO} P_{H_2}^{0.5}}{k_7^{0.5}} \psi$
8	$CH_2 - \psi + H - \psi \rightarrow CH_3 - \psi$	$R_{FT} = k_{i,par} \psi_{CH_2} \psi_H = k_{i,par} \frac{(k_7 K_6 K_1 K_2^2 K_3 K_4)}{K_5} \frac{P_{CO} P_{H_2}^2}{R_{FT}} \psi^3 \sqrt{K_2 P_{H_2}} \psi = k_{i,par} \frac{\left(k_7 K_6 K_1 K_2^{2.5} K_3 K_4\right)}{K_5} \frac{P_{CO} P_{H_2}^{2.5}}{R_{FT}} \psi^4$ $R_{FT} = \sqrt{k_{i,par} \frac{\left(k_7 K_6 K_1 K_2^{2.5} K_3 K_4\right)}{K_5}} P_{CO} P_{H_2}^{1.25} \psi^2$
Total Surface Coverage	$\psi + \psi_{CO} + \psi_H + \psi_{HCO} + \psi_{OH} + \psi_{CH_2O} + \psi_O + \psi_{CH_2} = 1$	$\psi = \frac{1}{\left(\begin{array}{c} 1 + K_1 P_{CO} + \sqrt{K_2 P_{H_2}} + K_3 K_1 \sqrt{K_2} P_{CO} P_{H2}^{0.5} + K_1 K_2 K_3 K_4 P_{CO} P_{H_2} \\ \frac{\left(\sqrt{k_7 K_6 K_1 K_3 K_4} K_2^{0.75}\right)}{\sqrt{K_5}} \frac{P_{CO} P_{H_2}^{0.75}}{\sqrt{k_{i,par}}} + \frac{\sqrt{k_{i,par} \left(K_1 K_2^{0.25} K_3 K_4\right)} P_{CO} P_{H_2}^{0.25}}{K_5 \sqrt{k_7 K_6}} + \sqrt{k_{i,par} \frac{(K_6 K_1 K_2^2 K_3 K_4)}{K_5}} \frac{P_{CO} P_{H_2}^{0.5}}{k_7^{0.5}} \end{array}\right)}$

Table A. 19 Kinetic model FT–V assuming steps 4 and 8–15 are the rate-determining steps (RDS-2)

No.	FT–V (RDS-2: 4, 8–15)	Rate Equations
1	$CO + \psi \rightleftarrows CO - \psi$	$\psi_{CO} = K_1 P_{CO} \psi$
2	$H_2 + 2\psi \rightleftarrows 2H - \psi$	$\psi_H = \sqrt{K_2 P_{H_2}}\,\psi$
3	$CO - \psi + H - \psi \rightleftarrows HCO - \psi + \psi$	$\psi_{HCO} = \frac{K_3 \psi_{CO} \psi_H}{\psi} = \frac{K_3 K_1 P_{CO} \psi \sqrt{K_2} P_{H2}^{0.5} \psi}{\psi} = K_3 K_1 \sqrt{K_2} P_{CO} P_{H2}^{0.5} \psi$
4	$HCO - \psi + H - \psi \rightarrow CH_2O - \psi + \psi$	$R_{FT} = k_4 \psi_{HCO} \psi_H = k_4 K_3 K_1 \sqrt{K_2} P_{CO} P_{H2}^{0.5} \psi \sqrt{K_2 P_{H_2}}\,\psi = k_4 K_3 K_1 K_2 P_{CO} P_{H_2} \psi^2$
5	$CH_2O - \psi + \psi \rightleftarrows CH_2 - \psi + O - \psi$	$\psi_{CH_2O} = \frac{\psi_{\mathrm{CH_2}} \psi_O}{K_5 \psi} = \frac{\psi_{\mathrm{CH_2}} \frac{P_{H_2O}}{K_7 K_2 K_5 P_{H_2}} \psi}{K_5 \psi} = \frac{\frac{k_4 K_3 K_1 K_2^{0.5} P_{CO} P_{H_2}^{0.5}}{k_{i,par}} \psi \frac{P_{H_2O}}{K_7 K_2 K_5 P_{H_2}} \psi}{K_5 \psi} = \frac{k_4 K_3 K_1 K_2^{0.5}}{k_{i,par} K_7 K_2 K_5 K_5} P_{CO} \frac{P_{H_2O}}{P_{H_2}^{0.5}} \psi$
6	$O - \psi + H - \psi \rightleftarrows OH - \psi + \psi$	$\psi_O = \frac{\psi_{\mathrm{OH}} \psi}{K_5 \psi_H} = \frac{\frac{P_{H_2O}}{K_7 \sqrt{K_2 P_{H_2}}} \psi \psi}{K_5 \sqrt{K_2 P_{H_2}}\,\psi} = \frac{P_{H_2O}}{K_7 K_2 K_5 P_{H_2}} \psi$
7	$OH - \psi + H - \psi \rightleftarrows H_2O + 2\psi$	$\psi_{OH} = \frac{P_{H_2O} \psi^2}{K_7 \psi_H} = \frac{P_{H_2O} \psi^2}{K_7 \sqrt{K_2 P_{H_2}}\,\psi} = \frac{P_{H_2O}}{K_7 \sqrt{K_2 P_{H_2}}} \psi$
8	$CH_2 - \psi + H - \psi \rightarrow CH_3 - \psi$	$R_{FT} = k_{i,par} \psi_{CH_2} \psi_H$ $\psi_{CH_2} = \frac{R_{FT}}{k_{i,par} \psi_H} = \frac{k_4 K_3 K_1 K_2 P_{CO} P_{H_2} \psi^2}{k_{i,par} \psi_H} = \frac{k_4 K_3 K_1 K_2^{0.5} P_{CO} P_{H_2}^{0.5}}{k_{i,par}} \psi$
Total Surface Coverage	$\psi + \psi_{CO} + \psi_H + \psi_{HCO} + \psi_{OH} + \psi_{CH_2O} + \psi_O + \psi_{CH_2} = 1$	$\psi = \frac{1}{\left(\begin{array}{c} 1 + K_1 P_{CO} + \sqrt{K_2 P_{H_2}} + K_3 K_1 \sqrt{K_2} P_{CO} P_{H2}^{0.5} + K_1 K_2 K_3 K_4 P_{CO} P_{H_2} \\ \frac{k_4 K_3 K_1 K_2^{0.5}}{k_{i,par} K_7 K_2 K_5 K_5} P_{CO} \frac{P_{H_2O}}{P_{H_2}^{0.5}} + \frac{P_{H_2O}}{K_7 K_2 K_5 P_{H_2}} + \frac{P_{H_2O}}{K_7 \sqrt{K_2 P_{H_2}}} + \frac{k_4 K_3 K_1 K_2^{0.5} P_{CO} P_{H_2}^{0.5}}{k_{i,par}} \end{array}\right)}$

Table A. 20 Kinetic model FT–V assuming steps 8–15 are the rate-determining steps (RDS-3)

No.	FT–V (RDS-3: 8–15)	Rate Equations
1	$CO + \psi \rightleftarrows CO - \psi$	$\psi_{CO} = K_1 P_{CO} \psi$
2	$H_2 + 2\psi \rightleftarrows 2H - \psi$	$\psi_H = \sqrt{K_2 P_{H_2}}\,\psi$
3	$CO - \psi + H - \psi \rightleftarrows HCO - \psi + \psi$	$\psi_{HCO} = \frac{K_3 \psi_{CO} \psi_H}{\psi} = \frac{K_3 K_1 P_{CO} \psi \sqrt{K_2} P_{H2}^{0.5} \psi}{\psi} = K_3 K_1 \sqrt{K_2} P_{CO} P_{H2}^{0.5} \psi$
4	$HCO - \psi + H - \psi \rightleftarrows CH_2O - \psi + \psi$	$\psi_{CH_2O} = \frac{K_4 \psi_{HCO} \psi_H}{\psi} = \frac{K_4 \frac{K_3 \psi_{CO} \psi_H}{\psi} \psi_H}{\psi} = K_1 K_2 K_3 K_4 P_{CO} P_{H_2} \psi$
5	$CH_2O - \psi + \psi \rightleftarrows CH_2 - \psi + O - \psi$	$\psi_{CH_2} = \frac{\psi_{CH_2O} \psi}{K_5 \psi_O} = \frac{\left(K_1 K_2 K_3 K_4 P_{CO} P_{H_2} \psi\right)\psi}{\frac{P_{H_2O}}{K_7 K_2 K_5 P_{H_2}} \psi} = K_1 K_2^2 K_3 K_4 K_7 K_5 \frac{P_{CO} P_{H_2}^2}{P_{H_2O}} \psi$
6	$O - \psi + H - \psi \rightleftarrows OH - \psi + \psi$	$\psi_O = \frac{\psi_{OH} \psi}{K_5 \psi_H} = \frac{\frac{P_{H_2O}}{K_7 \sqrt{K_2 P_{H_2}}} \psi \psi}{K_5 \sqrt{K_2 P_{H_2}} \psi} = \frac{P_{H_2O}}{K_7 K_2 K_5 P_{H_2}} \psi$
7	$OH - \psi + H - \psi \rightleftarrows H_2O + 2\psi$	$\psi_{OH} = \frac{P_{H_2O} \psi^2}{K_7 \psi_H} = \frac{P_{H_2O} \psi^2}{K_7 \sqrt{K_2 P_{H_2}} \psi} = \frac{P_{H_2O}}{K_7 \sqrt{K_2 P_{H_2}}} \psi$
8	$CH_2 - \psi + H - \psi \rightarrow CH_3 - \psi$	$R_{FT} = k_{i,par} \psi_{CH_2} \psi_H = k_{i,par} K_1 K_2^{2.5} K_3 K_4 K_7 K_5 \frac{P_{CO} P_{H_2}^{2.5}}{P_{H_2O}} \psi^2$
Total Surface Coverage	$\psi + \psi_{CO} + \psi_H + \psi_{HCO} + \psi_{OH} + \psi_{CH_2O} + \psi_O + \psi_{CH_2} = 1$	$\psi = \frac{1}{\left(\begin{array}{c} 1 + K_1 P_{CO} + \sqrt{K_2 P_{H_2}} + K_3 K_1 \sqrt{K_2} P_{CO} P_{H2}^{0.5} + K_1 K_2 K_3 K_4 P_{CO} P_{H_2} \\ \frac{k_4 K_3 K_1 K_2^{0.5}}{k_{i,par} K_7 K_2 K_5 K_5} P_{CO} \frac{P_{H_2O}}{P_{H_2}^{0.5}} + \frac{P_{H_2O}}{K_7 K_2 K_5 P_{H_2}} + \frac{P_{H_2O}}{K_7 \sqrt{K_2 P_{H_2}}} + \frac{k_4 K_3 K_1 K_2^{0.5} P_{CO} P_{H_2}^{0.5}}{k_{i,par}} \end{array}\right)}$

APPENDIX

Table A. 21 Reaction pathway and rate equations developed based on model FT–VI: molecular hydrogen assisted CO dissociation

No.	General Reaction Path	Kinetic parameter	Rate Equations
1	$CO + \psi \rightleftarrows CO - \psi$	K_1	$K_1 P_{CO} \psi = \psi_{CO}$
2	$H_2 + 2\psi \rightleftarrows 2H - \psi$	K_2	$K_2 P_{H_2} \psi^2 = \psi_H^2$
3	$CO - \psi + H_2 \rightleftarrows C - \psi + H_2O$	K_3	$k_3 \psi_{CO} P_{H_2} = \psi_C P_{H_2O}$
4	$C - \psi + H - \psi \rightleftarrows CH - \psi + \psi$	K_4	$K_4 \psi_C \psi_H = \psi_{CH} \psi$
5	$CH - \psi + H - \psi \rightleftarrows CH_2 - \psi + \psi$	K_5	$K_5 \psi_{CH} \psi_H = \psi_{CH_2} \psi$ $R_{FT} = k_{i,par} \psi_{CH_2} \psi_H$
6	$CH_2 - \psi + H - \psi \rightarrow CH_3 - \psi + \psi$	$k_{i,par}$	$\frac{d\psi_{CH_3}}{dt} = 0 \Rightarrow +R_6 - R_7 - R_{10} = 0 \Rightarrow + k_{i,par} \psi_{CH_2} \psi_H - k_{meth} \psi_{CH_3} \psi_H - k_{g,par} \psi_{CH_3} \psi_{CH_2} = 0 \Rightarrow$ $\psi_{CH_3} = \frac{k_{i,par} \psi_{CH_2} \psi_H}{k_{g,par} \psi_{CH_2} + k_{meth} \psi_H}$
7	$CH_3 - \psi + H - \psi \rightarrow CH_4 + 2\psi$	k_{meth}	$R_{CH_4} = k_{meth} \psi_{CH_3} \psi_H$
8	$CH_2 - \psi + CH_2 - \psi \rightarrow C_2H_4 + 2\psi$	k_{eth}	$R_{C_2H_4} = k_{eth} {\psi_{CH_2}}^2$
9	$CH_2 - \psi + CH - \psi \rightarrow C_2H_3 - \psi + \psi$	$k_{i,olef}$	$\frac{d\psi_{C_2H_3}}{dt} = 0 \Rightarrow +R_9 - R_{12} = 0 \Rightarrow + k_{i,olef} \psi_{CH_2} \psi_{CH} - k_{g,olef} \psi_{CH_2} \psi_{C_2H_3} = 0 \Rightarrow$ $\psi_{C_2H_3} = \frac{k_{i,olef} \psi_{CH}}{k_{g,olef}}$
10	$C_{n-1}H_{2n-1} - \psi + CH_2 - \psi \rightarrow C_nH_{2n+1} - \psi + \psi\,;\ n \geq 3$	$k_{g,par}$	$\frac{d\psi_{C_nH_{2n+1}}}{dt} = 0 \Rightarrow +R_{10} - R'_{10} - R_{11} = 0 \Rightarrow + k_{g,par} \psi_{C_{n-1}H_{2n-1}} \psi_{CH_2} - k_{g,par} \psi_{C_nH_{2n+1}} \psi_{CH_2} - k_{t,par} \psi_{C_nH_{2n+1}} \psi_H = 0 \Rightarrow$ $\psi_{C_nH_{2n+1}} = \frac{k_{g,par} \psi_{C_{n-1}H_{2n-1}} \psi_{CH_2}}{k_{g,par} \psi_{CH_2} + k_{t,par} \psi_H}$
11	$C_nH_{2n+1} - \psi + H - \psi \rightarrow C_nH_{2n+2} + 2\psi$	$k_{t,par}$	$R_{parffins} = k_{t,par} \psi_{C_nH_{2n+1}} \psi_H$
12	$CH_2 - \psi + C_{n-1}H_{2n-3} - \psi \rightarrow C_nH_{2n-1} - \psi + \psi;\ n \geq 3$	$k_{g,olef}$	$\frac{d\psi_{C_nH_{2n-1}}}{dt} = 0 \Rightarrow +R_{12} - R'_{12} - R_{13} = 0 \Rightarrow +k_{g,olef} \psi_{C_{n-1}H_{2n-3}} \psi_{CH_2} - k_{g,olef} \psi_{C_nH_{2n-1}} \psi_{CH_2} - k_{t,olef} \psi_{C_nH_{2n-1}} \psi_H = 0 \Rightarrow$ $\psi_{C_nH_{2n-1}} = \frac{k_{g,olef} \psi_{C_{n-1}H_{2n-3}} \psi_{CH_2}}{k_{g,olef} \psi_{CH_2} + k_{t,olef} \psi_H}$
13	$C_nH_{2n-1} - \psi + H - \psi \rightarrow C_nH_{2n} + 2\psi$	$k_{t,olef}$	$R_{olefins} = k_{t,olef} \psi_{C_nH_{2n-1}} \psi_H$

Table A. 22 Kinetic model FT–VI assuming steps 3 and 6–13 are the rate-determining steps (RDS-1)

No.	FT–VI (RDS-1: 3, 6–13)	Rate Equations
1	$CO + \psi \rightleftarrows CO - \psi$	$K_1 P_{CO} \psi = \psi_{CO}$
2	$H_2 + 2\psi \rightleftarrows 2H - \psi$	$\sqrt{K_2 P_{H_2}}\psi = \psi_H$
3	$CO - \psi + H_2 \rightarrow C - \psi + H_2O$	$R_{FT} = k_3 \psi_{CO} P_{H_2} = k_3 K_1 P_{CO} P_{H_2} \psi = \frac{k_3 K_1 P_{CO} P_{H_2}}{\left(1 + K_1 P_{CO} + \sqrt{K_2 P_{H_2}}\right)}$
4	$C - \psi + H - \psi \rightleftarrows CH - \psi + \psi$	$\psi_C = \frac{\psi_{CH}\psi}{K_4 \psi_H} = \frac{\frac{k_3 K_1}{k_{i,par} K_2 K_5} P_{CO} \psi}{K_4 \sqrt{K_2 P_{H_2}} \psi} = \frac{k_3 K_1}{k_{i,par} K_2^{1.5} K_5 K_4} \frac{P_{CO}}{\sqrt{P_{H_2}}}$
5	$CH - \psi + H - \psi \rightleftarrows CH_2 - \psi + \psi$	$\psi_{CH} = \frac{\psi_{CH_2}\psi}{K_5 \psi_H} = \frac{\frac{k_3 K_1 P_{CO} P_{H_2}^{0.5}}{k_{i,par}\sqrt{K_2}} \psi}{K_5 \sqrt{K_2 P_{H_2}} \psi} = \frac{k_3 K_1}{k_{i,par} K_2 K_5} P_{CO}$
6	$CH_2 - \psi + H - \psi \rightarrow CH_3 - \psi + \psi$	$R_{FT} = k_{i,par} \psi_{CH_2} \psi_H$ $\psi_{CH_2} = \frac{R_{FT}}{k_{i,par} \psi_H} = \frac{k_3 K_1 P_{CO} P_{H_2} \psi}{k_{i,par} \psi_H} = \frac{k_3 K_1 P_{CO} P_{H_2}^{0.5}}{k_{i,par}\sqrt{K_2}}$
Total Surface Coverage	$\psi + \psi_{CO} + \psi_H = 1$	$\psi = \frac{1}{\left(1 + K_1 P_{CO} + \sqrt{K_2 P_{H_2}}\right)}$

Table A. 23 Kinetic model FT–VI assuming steps 4 and 6–13 are the rate-determining steps (RDS-2)

No.	FT–VI (RDS-2: 4, 6–13)	Rate Equations
1	$CO + \psi \rightleftarrows CO - \psi$	$K_1 P_{CO} \psi = \psi_{CO}$
2	$H_2 + 2\psi \rightleftarrows 2H - \psi$	$\sqrt{K_2 P_{H_2}}\psi = \psi_H$
3	$CO - \psi + H_2 \rightleftarrows C - \psi + H_2O$	$\psi_C = \frac{K_3 \psi_{CO} P_{H_2}}{P_{H_2O}} = \frac{K_3 K_1 P_{CO} \psi P_{H_2}}{P_{H_2O}} = K_3 K_1 \frac{P_{CO} P_{H_2}}{P_{H_2O}} \psi$
4	$C - \psi + H - \psi \rightarrow CH - \psi + \psi$	$R_{FT} = k_4 \psi_C \psi_H = k_4 \left(K_3 K_1 \frac{P_{CO} P_{H_2}}{P_{H_2O}} \psi \right) \left(\sqrt{K_2 P_{H_2}} \psi \right) = k_4 K_3 K_1 \sqrt{K_2} \frac{P_{CO} P_{H_2}^{1.5}}{P_{H_2O}} \psi^2$
5	$CH - \psi + H - \psi \rightleftarrows CH_2 - \psi + \psi$	$\psi_{CH} = \frac{\psi_{CH_2} \psi}{K_5 \psi_H} = \frac{\left(\frac{k_4 K_3 K_1}{k_{i,par}} \frac{P_{CO} P_{H_2}}{P_{H_2O}} \psi \right) \psi}{K_5 \sqrt{K_2 P_{H_2}} \psi} = \frac{k_4 K_3 K_1}{k_{i,par} K_5 \sqrt{K_2}} \frac{P_{CO} P_{H_2}^{0.5}}{P_{H_2O}} \psi$ $R_{FT} = k_{i,par} \psi_{CH_2} \psi_H$
6	$CH_2 - \psi + H - \psi \rightarrow CH_3 - \psi + \psi$	$\psi_{CH_2} = \frac{R_{FT}}{k_{i,par} \psi_H} = \frac{k_4 K_3 K_1 \sqrt{K_2} \frac{P_{CO} P_{H_2}^{1.5}}{P_{H_2O}} \psi^2}{k_{i,par} \sqrt{K_2 P_{H_2}} \psi} = \frac{k_4 K_3 K_1}{k_{i,par}} \frac{P_{CO} P_{H_2}}{P_{H_2O}} \psi$
Total Surface Coverage	$\psi + \psi_{CO} + \psi_H + \psi_C + \psi_{CH} + \psi_{CH_2} = 1$	$\psi = \frac{1}{\left(1 + K_1 P_{CO} + \sqrt{K_2 P_{H_2}} + K_3 K_1 \frac{P_{CO} P_{H_2}}{P_{H_2O}} + \frac{k_4 K_3 K_1}{k_{i,par} K_5 \sqrt{K_2}} \frac{P_{CO} P_{H_2}^{0.5}}{P_{H_2O}} + \frac{k_4 K_3 K_1}{k_{i,par}} \frac{P_{CO} P_{H_2}}{P_{H_2O}} \right)}$

Table A. 24 Kinetic model FT–VI assuming steps 6–13 are the rate-determining steps (RDS-3)

No.	FT–VI (RDS-3: 6–13)	Rate Equations
1	$CO + \psi \rightleftarrows CO - \psi$	$K_1 P_{CO} \psi = \psi_{CO}$
2	$H_2 + 2\psi \rightleftarrows 2H - \psi$	$\sqrt{K_2 P_{H_2}}\psi = \psi_H$
3	$CO - \psi + H_2 \rightleftarrows C - \psi + H_2O$	$\psi_C = \frac{K_3 \psi_{CO} P_{H_2}}{P_{H_2O}} = \frac{K_3 K_1 P_{CO} \psi P_{H_2}}{P_{H_2O}} = K_3 K_1 \frac{P_{CO} P_{H_2}}{P_{H_2O}} \psi$
4	$C - \psi + H - \psi \rightleftarrows CH - \psi + \psi$	$\psi_{CH} = \frac{K_4 \psi_C \psi_H}{\psi} = \frac{K_4 K_3 K_1 \frac{P_{CO} P_{H_2}}{P_{H_2O}} \psi \sqrt{K_2 P_{H_2}}\psi}{\psi} = K_1 \sqrt{K_2} K_3 K_4 \frac{P_{CO} P_{H_2}^{1.5}}{P_{H_2O}} \psi$
5	$CH - \psi + H - \psi \rightleftarrows CH_2 - \psi + \psi$	$\psi_{CH_2} = \frac{K_5 \psi_{CH} \psi_H}{\psi} = \frac{K_5 \left(K_1 \sqrt{K_2} K_3 K_4 \frac{P_{CO} P_{H_2}^{1.5}}{P_{H_2O}} \psi \right) \sqrt{K_2 P_{H_2}}\psi}{\psi} = K_1 K_2 K_3 K_4 K_5 \frac{P_{CO} P_{H_2}^2}{P_{H_2O}} \psi$
6	$CH_2 - \psi + H - \psi \rightarrow CH_3 - \psi + \psi$	$R_{FT} = k_{i,par} \psi_{CH_2} \psi_H \Rightarrow R_{FT} = k_{i,par} K_1 K_2 K_3 K_4 K_5 \frac{P_{CO} P_{H_2}^2}{P_{H_2O}} \psi \sqrt{K_2 P_{H_2}}\psi = k_{i,par} K_1 K_2^{1.5} K_3 K_4 K_5 \frac{P_{CO} P_{H_2}^{2.5}}{P_{H_2O}} \psi^2$
Total Surface Coverage	$\psi + \psi_{CO} + \psi_H + \psi_C + \psi_{CH} + \psi_{CH_2} = 1$	$\psi = \frac{1}{\left(1 + K_1 P_{CO} + \sqrt{K_2 P_{H_2}} + K_3 K_1 \frac{P_{CO} P_{H_2}}{P_{H_2O}} + K_1 \sqrt{K_2} K_3 K_4 \frac{P_{CO} P_{H_2}^{1.5}}{P_{H_2O}} + K_1 K_2 K_3 K_4 K_5 \frac{P_{CO} P_{H_2}^2}{P_{H_2O}} \right)}$

APPENDIX

Table A. 25 Reaction pathway and rate equations developed based on model FT–VII: molecular hydrogen assisted CO dissociation

No.	General Reaction Path	Kinetic parameter	Rate Equations
1	$CO + \psi \rightleftarrows CO - \psi$	K_1	$K_1 P_{CO} \psi = \psi_{CO}$
2	$H_2 + 2\psi \rightleftarrows 2H - \psi$	K_2	$K_2 P_{H_2} \psi^2 = \psi_H^2$
3	$CO - \psi + H_2 \rightleftarrows HCOH - \psi$	K_3	$K_3 \psi_{CO} P_{H_2} = \psi_{HCOH}$
4	$HCOH - \psi + H - \psi \rightleftarrows CH - \psi + H_2O - \psi$	K_4	$K_4 \psi_{HCOH} \psi_H = \psi_{CH} \psi_{H_2O}$
5	$H_2O - \psi \rightleftarrows H_2O + \psi$	K_5	$k_5 \psi_{H_2O} = P_{H_2O} \psi$
6	$CH - \psi + H - \psi \rightleftarrows CH_2 - \psi + \psi$	K_6	$K_6 \psi_{CH} \psi_H = \psi_{CH_2} \psi$
7	$CH_2 - \psi + H - \psi \rightarrow CH_3 - \psi + \psi$	$k_{i,par}$	$R_{FT} = k_{i,par} \psi_{CH_2} \psi_H$ $\frac{d\psi_{CH_3}}{dt} = 0 \Rightarrow +R_7 - R_8 - R_{11} = 0 \Rightarrow + k_{i,par} \psi_{CH_2} \psi_H - k_{meth} \psi_{CH_3} \psi_H - k_{g,par} \psi_{CH_3} \psi_{CH_2} = 0$ $\psi_{CH_3} = \frac{k_{i,par} \psi_{CH_2} \psi_H}{k_{g,par} \psi_{CH_2} + k_{meth} \psi_H}$
8	$CH_3 - \psi + H - \psi \rightarrow CH_4 + 2\psi$	k_{meth}	$R_{CH_4} = k_{meth} \psi_{CH_3} \psi_H$
9	$CH_2 - \psi + CH_2 - \psi \rightarrow C_2H_4 + 2\psi$	k_{eth}	$R_{C_2H_4} = k_{eth} \psi_{CH_2}{}^2$
10	$CH_2 - \psi + CH - \psi \rightarrow C_2H_3 - \psi + \psi$	$k_{i,olef}$	$\frac{d\psi_{C_2H_3}}{dt} = 0 \Rightarrow +R_{10} - R_{13} = 0 \Rightarrow + k_{i,olef} \psi_{CH_2} \psi_{CH} - k_{g,olef} \psi_{CH_2} \psi_{C_2H_3} = 0$ $\psi_{C_2H_3} = \frac{k_{i,olef} \psi_{CH}}{k_{g,olef}}$
11	$C_{n-1}H_{2n-1} - \psi + CH_2 - \psi \rightarrow C_nH_{2n+1} - \psi + \psi\ ;\ n \geq 3$	$k_{g,par}$	$\frac{d\psi_{C_nH_{2n+1}}}{dt} = 0 \Rightarrow +R_{11} - R'_{11} - R_{12} = 0 \Rightarrow + k_{g,par} \psi_{C_{n-1}H_{2n-1}} \psi_{CH_2} - k_{g,par} \psi_{C_nH_{2n+1}} \psi_{CH_2} - k_{t,par} \psi_{C_nH_{2n+1}} \psi_H = 0$ $\psi_{C_nH_{2n+1}} = \frac{k_{g,par} \psi_{C_{n-1}H_{2n-1}} \psi_{CH_2}}{k_{g,par} \psi_{CH_2} + k_{t,par} \psi_H}$
12	$C_nH_{2n+1} - \psi + H - \psi \rightarrow C_nH_{2n+2} + 2\psi$	$k_{t,par}$	$R_{parffins} = k_{t,par} \psi_{C_nH_{2n+1}} \psi_H$
13	$CH_2 - \psi + C_{n-1}H_{2n-3} - \psi \rightarrow C_nH_{2n-1} - \psi + \psi;\ n \geq 3$	$k_{g,olef}$	$\frac{d\psi_{C_nH_{2n-1}}}{dt} = 0 \Rightarrow +R_{13} - R'_{13} - R_{14} = 0 \Rightarrow + k_{g,olef} \psi_{C_{n-1}H_{2n-3}} \psi_{CH_2} - k_{g,olef} \psi_{C_nH_{2n-1}} \psi_{CH_2} - k_{t,olef} \psi_{C_nH_{2n-1}} \psi_H = 0$ $\psi_{C_nH_{2n-1}} = \frac{k_{g,olef} \psi_{C_{n-1}H_{2n-3}} \psi_{CH_2}}{k_{g,olef} \psi_{CH_2} + k_{t,olef} \psi_H}$
14	$C_nH_{2n-1} - \psi + H - \psi \rightarrow C_nH_{2n} + 2\psi$	$k_{t,olef}$	$R_{olefins} = k_{t,olef} \psi_{C_nH_{2n-1}} \psi_H$

Table A. 26 Kinetic model FT–VII assuming steps 5 and 7–14 are the rate-determining steps (RDS-1)

No.	FT–VII (RDS-1: 5, 7–14)	Rate Equations
1	$CO + \psi \rightleftarrows CO - \psi$	$K_1 P_{CO} \psi = \psi_{CO}$
2	$H_2 + 2\psi \rightleftarrows 2H - \psi$	$\sqrt{K_2 P_{H_2}}\psi = \psi_H$
3	$CO - \psi + H_2 \rightleftarrows HCOH - \psi$	$\psi_{HCOH} = K_1 K_3 P_{CO} P_{H_2} \psi$
4	$HCOH - \psi + H - \psi \rightleftarrows CH - \psi + H_2O - \psi$	$\psi_{H_2O} = \frac{K_4 \psi_{HCOH} \psi_H}{\psi_{CH}} = \frac{K_4 K_1 K_3 P_{CO} P_{H_2} \psi \sqrt{K_2 P_{H_2}} \psi}{\left(\frac{R_{FT}}{k_{i,par} K_6 K_2 P_{H_2} \psi}\right)} = \frac{k_{i,par} K_1 K_2^{1.5} K_3 K_4 K_6 P_{CO} P_{H_2}^{2.5}}{R_{FT}} \psi^3$
5	$H_2O - \psi + \psi \rightarrow H_2O + 2\psi$	$\psi_{H_2O} = \frac{k_{i,par} K_1 K_2^{1.5} K_3 K_4 K_6 P_{CO} P_{H_2}^{2.5}}{\sqrt{k_5 k_{i,par} K_1 K_2^{1.5} K_3 K_4 K_6 P_{CO} P_{H_2}^{2.5}} \psi^2} \psi^3 = \sqrt{\frac{k_{i,par} K_1 K_2^{1.5} K_3 K_4 K_6}{k_5}} P_{CO}^{0.5} P_{H_2}^{1.25} \psi$
6	$CH - \psi + H - \psi \rightleftarrows CH_2 - \psi + \psi$	$R_{FT} = k_5 \psi_{H_2O} \psi = k_5 \frac{k_{i,par} K_1 K_2^{1.5} K_3 K_4 K_6 P_{CO} P_{H_2}^{2.5}}{R_{FT}} \psi^4 \Rightarrow \; R_{FT} = \sqrt{k_5 k_{i,par} K_1 K_2^{1.5} K_3 K_4 K_6 P_{CO} P_{H_2}^{2.5}} \psi^2$
7	$CH_2 - \psi + H - \psi \rightarrow CH_3 - \psi + \psi$	$\psi_{CH} = \frac{\psi_{CH_2} \psi}{K_6 \psi_H} = \frac{\left(\frac{R_{FT}}{k_{i,par}\sqrt{K_2 P_{H_2}}\psi}\right)\psi}{K_6 \sqrt{K_2 P_{H_2}}\psi} = \frac{R_{FT}}{k_{i,par} K_6 K_2 P_{H_2} \psi} = \frac{\sqrt{k_5 k_{i,par} K_1 K_2^{1.5} K_3 K_4 K_6 P_{CO} P_{H_2}^{2.5}} \psi^2}{k_{i,par} K_6 K_2 P_{H_2} \psi}$ $= \frac{\sqrt{k_5 K_1 K_2^{1.5} K_3 K_4}}{K_2^{0.25} \sqrt{k_{i,par} K_6}} P_{CO}^{0.5} P_{H_2}^{0.25} \psi$
Total Surface Coverage	$\psi + \psi_{CO} + \psi_{HCOH} + \psi_{CH} + \psi_{H_2O} + \psi_{CH_2} + \psi_{CH} = 1$	$R_{FT} = k_{i,par} \psi_{CH_2} \psi_H \Rightarrow \quad \psi_{CH_2} = \frac{R_{FT}}{k_{i,par} \psi_H} = \frac{\sqrt{k_5 k_{i,par} K_1 K_2^{1.5} K_3 K_4 K_6 P_{CO} P_{H_2}^{2.5}} \psi^2}{k_{i,par}\sqrt{K_2 P_{H_2}}\psi} = \frac{\sqrt{k_5 K_1 K_2^{0.5} K_3 K_4 K_6}}{k_{i,par}^{0.5}} \sqrt{P_{CO}} P_{H_2}^{0.75} \psi$ $\psi = \frac{1}{\left(1 + K_1 P_{CO} + \sqrt{K_2 P_{H_2}} + K_1 K_3 P_{CO} P_{H_2} + \frac{\sqrt{\frac{k_5 K_1 K_2^{1.5} K_3 K_4}{k_{i,par} K_6}}}{K_2^{0.25}} P_{CO}^{0.5} P_{H_2}^{0.25} + \sqrt{\frac{k_{i,par} K_1 K_2^{1.5} K_3 K_4 K_6}{k_5}} P_{CO}^{0.5} P_{H_2}^{1.25} + \frac{\sqrt{k_5 K_1 K_2^{0.5} K_3 K_4 K_6}}{k_{i,par}^{0.5}} \sqrt{P_{CO}} P_{H_2}^{0.75}\right)}$

Table A. 27 Kinetic model FT–VII assuming steps 3 and 7–14 are the rate-determining steps (RDS-2)

No.	FT–VII (RDS-2: 3, 7–14)	Rate Equations
1	$CO + \psi \rightleftarrows CO - \psi$	$K_1 P_{CO} \psi = \psi_{CO}$
2	$H_2 + 2\psi \rightleftarrows 2H - \psi$	$\sqrt{K_2 P_{H_2}}\psi = \psi_H$
3	$CO - \psi + H_2 \rightarrow HCOH - \psi$	$R_{FT} = k_3 K_1 P_{CO} P_{H_2} \psi$ $R_{FT} = \dfrac{k_3 K_1 P_{CO} P_{H_2}}{\left(1 + K_1 P_{CO} + \sqrt{K_2 P_{H_2}} + \dfrac{P_{H_2O}}{K_5}\right)}$
4	$HCOH - \psi + H - \psi \rightleftarrows CH - \psi + H_2O - \psi$	$\psi_{HCOH} = \dfrac{\psi_{CH}\psi_{H_2O}}{K_4 \psi_H} = \dfrac{\left(\dfrac{k_3 K_1}{k_{i,par} K_2 K_6} P_{CO}\right)\left(\dfrac{P_{H_2O}\psi}{K_5}\right)}{K_4\left(\sqrt{K_2 P_{H_2}}\psi\right)} = \dfrac{k_3 K_1}{k_{i,par} K_2^{1.5} K_5 K_6 K_4} \dfrac{P_{H_2O} P_{CO}}{\sqrt{P_{H_2}}}$
5	$H_2O - \psi + \psi \rightleftarrows H_2O + 2\psi$	$\psi_{H_2O} = \dfrac{P_{H_2O}\psi}{K_5}$
6	$CH - \psi + H - \psi \rightleftarrows CH_2 - \psi + \psi$	$\psi_{CH} = \dfrac{\dfrac{k_3 K_1 P_{CO} P_{H_2}^{0.5}}{k_{i,par}\sqrt{K_2}}\psi}{K_6 \psi_H} = \dfrac{\dfrac{k_3 K_1 P_{CO} P_{H_2}^{0.5}}{k_{i,par}\sqrt{K_2}}\psi}{K_6\sqrt{K_2 P_{H_2}}\psi} = \dfrac{k_3 K_1}{k_{i,par} K_2 K_6} P_{CO}$
7	$CH_2 - \psi + H - \psi \rightarrow CH_3 - \psi + \psi$	$R_{FT} = k_{i,par}\psi_{CH_2}\psi_H$ $\psi_{CH_2} = \dfrac{k_3 K_1 P_{CO} P_{H_2}\psi}{k_{i,par}\sqrt{K_2 P_{H_2}}\psi} = \dfrac{k_3 K_1 P_{CO} P_{H_2}^{0.5}}{k_{i,par}\sqrt{K_2}}$
Total Surface Coverage	$\psi + \psi_{CO} + \psi_H + \psi_{H2O} = 1$	$\psi = \dfrac{1}{\left(1 + K_1 P_{CO} + \sqrt{K_2 P_{H_2}} + \dfrac{P_{H_2O}}{K_5}\right)}$

Table A. 28 Kinetic model FT–VII assuming steps 7–14 are the rate-determining steps (RDS-3)

No.	FT–VII (RDS-3: 7–14)	Rate Equations
1	$CO + \psi \rightleftarrows CO - \psi$	$\psi_{CO} = K_1 P_{CO} \psi$
2	$H_2 + 2\psi \rightleftarrows 2H - \psi$	$\psi_H = \sqrt{K_2 P_{H_2}}\,\psi$
3	$CO - \psi + H - \psi \rightleftarrows HCO - \psi + \psi$	$\psi_{HCO} = \frac{K_3 \psi_{CO} \psi_H}{\psi} = \frac{K_3 K_1 P_{CO} \psi \sqrt{K_2} P_{H2}^{0.5} \psi}{\psi} = K_3 K_1 \sqrt{K_2} P_{CO} P_{H2}^{0.5} \psi$
4	$HCO - \psi + H - \psi \rightleftarrows HCOH - \psi + \psi$	$\psi_{HCOH} = \frac{K_4 \psi_{HCO} \psi_H}{\psi} = \frac{K_4 \left(K_3 K_1 \sqrt{K_2} P_{CO} P_{H2}^{0.5} \psi\right) \sqrt{K_2 P_{H_2}} \psi}{\psi} = K_1 K_2 K_3 K_4 P_{CO} P_{H_2} \psi$
5	$HCOH - \psi + \psi \rightleftarrows CH - \psi + OH - \psi$	$\psi_{CH} = \frac{K_5 \psi_{HCOH} \psi}{\psi_{OH}} = \frac{K_5 \left(K_1 K_2 K_3 K_4 P_{CO} P_{H_2} \psi\right) \psi}{\frac{P_{H_2O}}{K_6 \sqrt{K_2 P_{H_2}}} \psi} = K_5 K_1 K_2^{1.5} K_3 K_4 K_6 \frac{P_{CO} P_{H_2}^{1.5}}{P_{H_2O}} \psi$
6	$OH - \psi + H - \psi \rightleftarrows H_2O + 2\psi$	$\psi_{OH} = \frac{\psi^2 P_{H_2O}}{K_6 \psi_H} = \frac{\psi^2 P_{H_2O}}{K_6 \sqrt{K_2 P_{H_2}} \psi} = \frac{P_{H_2O}}{K_6 \sqrt{K_2 P_{H_2}}} \psi$
7	$CH - \psi + H - \psi \rightleftarrows CH_2 - \psi + \psi$	$\psi_{CH_2} = \frac{K_7 \psi_{CH} \psi_H}{\psi} = \frac{K_7 K_5 K_1 K_2^{1.5} K_3 K_4 K_6 \frac{P_{CO} P_{H_2}^{1.5}}{P_{H_2O}} \psi \sqrt{K_2 P_{H_2}} \psi}{\psi} = K_7 K_5 K_1 K_2^2 K_3 K_4 K_6 \frac{P_{CO} P_{H_2}^2}{P_{H_2O}} \psi$
8	$CH_2 - \psi + H - \psi \rightarrow CH_3 - \psi + \psi$	$R_{FT} = k_{i,par} \psi_{CH_2} \psi_H = k_{i,par} K_7 K_5 K_1 K_2^{2.5} K_3 K_4 K_6 \frac{P_{CO} P_{H_2}^{2.5}}{P_{H_2O}} \psi^2$
Total Surface Coverage	$\psi + \psi_{CO} + \psi_H + \psi_{OH} + \psi_{HCO} + \psi_{HCOH} + \psi_{CH} + \psi_{CH_2} = 1$	$\psi = \frac{1}{\left(\begin{array}{c} 1 + K_1 P_{CO} + \sqrt{K_2 P_{H_2}} + \frac{P_{H_2O}}{K_6 \sqrt{K_2 P_{H_2}}} + K_3 K_1 \sqrt{K_2} P_{CO} P_{H2}^{0.5} + \\ K_1 K_2 K_3 K_4 P_{CO} P_{H_2} + K_5 K_1 K_2^{1.5} K_3 K_4 K_6 \frac{P_{CO} P_{H_2}^{1.5}}{P_{H_2O}} + \\ K_7 K_5 K_1 K_2^2 K_3 K_4 K_6 \frac{P_{CO} P_{H_2}^2}{P_{H_2O}} \end{array}\right)}$

Table A. 29 Reaction pathway and rate equations developed based on model FT–VIII: molecular hydrogen assisted CO dissociation

No.	General Reaction Path	Kinetic parameter	Rate Equations
1	$CO + \psi \rightleftarrows CO - \psi$	K_1	$K_1 P_{CO} \psi = \psi_{CO}$
2	$H_2 + 2\psi \rightleftarrows 2H - \psi$	K_2	$K_2 P_{H_2} \psi^2 = \psi_H^2$
3	$CO - \psi + H_2 \rightleftarrows HCOH - \psi$	K_3	$K_3 \psi_{CO} P_{H_2} = \psi_{HCOH}$
4	$HCOH - \psi + H_2 \rightleftarrows CH_2 - \psi + H_2O$	K_4	$K_4 \psi_{HCOH} P_{H_2} = \psi_{CH_2} P_{H_2O}$
5	$CH_2 - \psi + H - \psi \rightarrow CH_3 - \psi + \psi$	$k_{i,par}$	$R_{FT} = k_{i,par} \psi_{CH_2} \psi_H$ $\frac{d\psi_{CH_3}}{dt} = 0 \Rightarrow +R_5 - R_6 - R_9 = 0 \Rightarrow + k_{i,par} \psi_{CH_2} \psi_H - k_{meth} \psi_{CH_3} \psi_H - k_{g,par} \psi_{CH_3} \psi_{CH_2} = 0$ $\psi_{CH_3} = \frac{k_{i,par} \psi_{CH_2} \psi_H}{k_{g,par} \psi_{CH_2} + k_{meth} \psi_H}$
6	$CH_3 - \psi + H - \psi \rightarrow CH_4 + 2\psi$	k_{meth}	$R_{CH_4} = k_{meth} \psi_{CH_3} \psi_H$
7	$CH_2 - \psi + CH_2 - \psi \rightarrow C_2H_4 + 2\psi$	k_{eth}	$R_{C_2H_4} = k_{eth} {\psi_{CH_2}}^2$
8	$CH_2 - \psi + CH_2 - \psi \rightarrow C_2H_3 - \psi + H - \psi$	$k_{i,olef}$	$\frac{d\psi_{C_2H_3}}{dt} = 0 \Rightarrow +R_8 - R_{11} = 0 \Rightarrow + k_{i,olef} \psi_{CH_2} \psi_{CH_2} - k_{g,olef} \psi_{CH_2} \psi_{C_2H_3} = 0$ $\psi_{C_2H_3} = \frac{k_{i,olef} \psi_{CH_2}}{k_{g,olef}}$
9	$C_{n-1}H_{2n-1} - \psi + CH_2 - \psi \rightarrow C_nH_{2n+1} - \psi + \psi\ ;\ n \geq 2$	$k_{g,par}$	$\frac{d\psi_{C_nH_{2n+1}}}{dt} = 0 \Rightarrow +R_9 - R_9' - R_{10} = 0$ $\Rightarrow + k_{g,par} \psi_{C_{n-1}H_{2n-1}} \psi_{CH_2} - k_{g,par} \psi_{C_nH_{2n+1}} \psi_{CH_2} - k_{t,par} \psi_{C_nH_{2n+1}} \psi_H = 0$ $\psi_{C_nH_{2n+1}} = \frac{k_{g,par} \psi_{C_{n-1}H_{2n-1}} \psi_{CH_2}}{k_{g,par} \psi_{CH_2} + k_{t,par} \psi_H}$
10	$C_nH_{2n+1} - \psi + H - \psi \rightarrow C_nH_{2n+2} + 2\psi$	$k_{t,par}$	$R_{parffins} = k_{t,par} \psi_{C_nH_{2n+1}} \psi_H$
11	$CH_2 - \psi + C_{n-1}H_{2n-3} - \psi \rightarrow C_nH_{2n-1} - \psi + \psi;\ n \geq 3$	$k_{g,olef}$	$\frac{d\psi_{C_nH_{2n-1}}}{dt} = 0 \Rightarrow +R_{11} - R_{11}' - R_{12} = 0$ $\Rightarrow +k_{g,olef} \psi_{C_{n-1}H_{2n-3}} \psi_{CH_2} - k_{g,olef} \psi_{C_nH_{2n-1}} \psi_{CH_2} - k_{t,olef} \psi_{C_nH_{2n-1}} \psi_H = 0$ $\psi_{C_nH_{2n-1}} = \frac{k_{g,olef} \psi_{C_{n-1}H_{2n-3}} \psi_{CH_2}}{k_{g,olef} \psi_{CH_2} + k_{t,olef} \psi_H}$
12	$C_nH_{2n-1} - \psi + H - \psi \rightarrow C_nH_{2n} + 2\psi$	$k_{t,olef}$	$R_{olefins} = k_{t,olef} \psi_{C_nH_{2n-1}} \psi_H$

Table A. 30 Kinetic model FT–VIII assuming steps 4, 5–12 are the rate-determining steps (RDS-1)

No.	FT–VIII (RDS-1: 4, 5–12)	Rate Equations
1	$CO + \psi \rightleftarrows CO - \psi$	$K_1 P_{CO} \psi = \psi_{CO}$
2	$H_2 + 2\psi \rightleftarrows 2H - \psi$	$\sqrt{K_2 P_{H_2}} \psi = \psi_H$
3	$CO - \psi + H_2 \rightleftarrows HCOH - \psi$	$\psi_{HCOH} = K_1 K_3 P_{CO} P_{H_2} \psi$
4	$HCOH - \psi + H_2 \rightarrow CH_2 - \psi + H_2O$	$R_{FT} = k_4 \psi_{HCOH} P_{H_2} = k_4 K_1 K_3 P_{CO} P_{H_2} \psi P_{H_2}$ $R_{FT} = \frac{K_1 K_3 k_4 P_{CO} P_{H_2}^2}{\left(1 + K_1 P_{CO} + \sqrt{K_2 P_{H_2}} + K_1 K_3 P_{CO} P_{H_2}\right)}$
5	$CH_2 - \psi + H - \psi \rightarrow CH_3 - \psi + \psi$	$R_{FT} = k_{i,par} \psi_{CH_2} \psi_H$ $\psi_{CH_2} = \frac{R_{FT}}{k_{i,par} \psi_H} = \frac{R_{FT}}{k_{i,par} \sqrt{K_2 P_{H_2}} \psi} = \frac{k_4 \psi_{HCOH} P_{H_2}}{k_{i,par} \sqrt{K_2 P_{H_2}} \psi} = \frac{k_4 K_1 K_3 P_{CO} P_{H_2} \psi P_{H_2}}{k_{i,par} \sqrt{K_2 P_{H_2}} \psi} = k_{i,par} \frac{K_1 K_3 k_4}{\sqrt{K_2}} P_{CO} P_{H_2}^{1.5}$
Total Surface Coverage	$\psi + \psi_{CO} + \psi_H + \psi_{HCOH} = 1$	$\psi = \frac{1}{\left(1 + K_1 P_{CO} + \sqrt{K_2 P_{H_2}} + K_1 K_3 P_{CO} P_{H_2}\right)}$

Table A. 31 Kinetic model FT–VIII assuming steps 3, 5–12 are the rate-determining steps (RDS-2)

No.	FT–VIII (RDS-2: 3, 5–12)	Rate Equations
1	$CO + \psi \rightleftarrows CO - \psi$	$K_1 P_{CO} \psi = \psi_{CO}$
2	$H_2 + 2\psi \rightleftarrows 2H - \psi$	$\sqrt{K_2 P_{H_2}}\psi = \psi_H$
3	$CO - \psi + H_2 \rightarrow HCOH - \psi$	$R_{FT} = k_3 \psi_{CO} P_{H_2} = K_1 k_3 P_{CO} P_{H_2} \psi$ $R_{FT} = \frac{K_1 k_3 P_{CO} P_{H_2}}{\left(1 + K_1 P_{CO} + \sqrt{K_2 P_{H_2}}\right)}$
4	$HCOH - \psi + H_2 \rightleftarrows CH_2 - \psi + H_2O$	$K_4 \psi_{HCOH} P_{H_2} = \psi_{CH_2} P_{H_2O}$ $\psi_{HCOH} = \frac{\psi_{CH_2} P_{H_2O}}{K_4 P_{H_2}} = \frac{\frac{R_{FT}}{k_{i,par}\sqrt{K_2 P_{H_2}}\psi} P_{H_2O}}{K_4 P_{H_2}} = \frac{K_1 k_3}{k_{i,par}\sqrt{K_2} K_4} \frac{\frac{P_{CO} P_{H_2} \psi}{\sqrt{P_{H_2}}\psi} P_{H_2O}}{P_{H_2}}$
5	$CH_2 - \psi + H - \psi \rightarrow CH_3 - \psi + \psi$	$R_{FT} = k_{i,par} \psi_{CH_2} \psi_H$ $\psi_{CH_2} = \frac{R_{FT}}{k_{i,par}\sqrt{K_2 P_{H_2}}\psi} = -\frac{K_1 k_3 P_{CO} P_{H_2} \psi}{k_{i,par}\sqrt{K_2 P_{H_2}}\psi}$
Total Surface Coverage	$\psi + \psi_{CO} + \psi_H = 1$	$\psi = \frac{1}{\left(1 + K_1 P_{CO} + \sqrt{K_2 P_{H_2}}\right)}$

Table A. 32 Kinetic model FT–VIII assuming steps 5–12 are the rate-determining steps (RDS-3)

No.	FT–VIII (RDS-3: 5–12)	Rate Equations
1	$CO + \psi \rightleftarrows CO - \psi$	$K_1 P_{CO} \psi = \psi_{CO}$
2	$H_2 + 2\psi \rightleftarrows 2H - \psi$	$\sqrt{K_2 P_{H_2}}\psi = \psi_H$
3	$CO - \psi + H_2 \rightleftarrows HCOH - \psi$	$\psi_{HCOH} = K_1 K_3 P_{CO} P_{H_2} \psi$
4	$HCOH - \psi + H_2 \rightleftarrows CH_2 - \psi + H_2O$	$K_4 \psi_{HCOH} P_{H_2} = \psi_{CH_2} P_{H_2O}$ $\psi_{CH_2} = \frac{K_4 \psi_{HCOH} P_{H_2}}{P_{H_2O}} = \frac{K_4 K_1 K_3 P_{CO} P_{H_2} \psi P_{H_2}}{P_{H_2O}} = \frac{K_1 K_3 K_4 P_{CO} P_{H_2}^2}{P_{H_2O}} \psi$ $R_{FT} = k_{i,par} \psi_{CH_2} \psi_H = k_{i,par} \frac{K_1 K_3 K_4 P_{CO} P_{H_2}^2}{P_{H_2O}} \psi \sqrt{K_2 P_{H_2}} \psi$
5	$CH_2 - \psi + H - \psi \rightarrow CH_3 - \psi + \psi$	$R_{FT} = \frac{k_{i,par} K_1 K_3 K_4 \sqrt{K_2} \frac{P_{CO} P_{H_2}^{2.5}}{P_{H_2O}}}{\left(1 + K_1 P_{CO} + \sqrt{K_2 P_{H_2}} + K_1 K_3 P_{CO} P_{H_2} + \frac{K_1 K_3 K_4 P_{CO} P_{H_2}^2}{P_{H_2O}}\right)^2}$
Total Surface Coverage	$\psi + \psi_{CO} + \psi_H + \psi_{HCOH} + \psi_{CH_2} = 1$	$\psi = \frac{1}{\left(1 + K_1 P_{CO} + \sqrt{K_2 P_{H_2}} + K_1 K_3 P_{CO} P_{H_2} + \frac{K_1 K_3 K_4 P_{CO} P_{H_2}^2}{P_{H_2O}}\right)}$

Table A. 33 Reaction pathway and rate equations developed based on model WGS-I: with (RDS-3: 3) direct oxidation mechanism (redox mechanism)

No.	WGS–I (RDS-3: 3)	Constants	Rate Equations
1	$CO + \sigma \rightleftarrows CO - \sigma$	K_{W_1}	$\sigma_{CO} = K_{W_1} P_{CO} \sigma$
2	$H_2O + 2\sigma \rightleftarrows OH - \sigma + H - \sigma$	K_{W_2}	$\sigma_{OH} = \frac{K_{W_2} P_{H_2O}}{\sigma_H} \sigma^2 = \frac{K_{W_2} P_{H_2O}}{\sqrt{\frac{P_{H_2}}{K_{W_5}}} \sigma} \sigma^2 = K_{W_5}^{0.5} K_{W_2} \frac{P_{H_2O}}{P_{H_2}^{0.5}} \sigma$
			$R_{WGS} = \left(k_{WGS_3} \sigma_{OH} \sigma - k_{WGS_{-3}} \sigma_O \sigma_H\right)$ $= \left(k_{WGS_3} \left(K_{W_5} K_{W_2} \frac{P_{H_2O}}{P_{H_2}} \sigma \right) \sigma - k_{WGS_{-3}} \left(\frac{P_{CO_2}}{K_{W_4} K_{W_1} P_{CO}} \sigma \right) \left(\sqrt{\frac{P_{H_2}}{K_{W_5}}} \sigma \right) \right)$
3	$OH - \sigma + \sigma \rightarrow O - \sigma + H - \sigma$	k_{WGS_3}	$R_{WGS} = \frac{\left(k_{WGS_3} K_{W_5} K_{W_2} \frac{P_{H_2O}}{P_{H_2}} - k_{WGS_{-3}} \frac{P_{CO_2} P_{H_2}^{0.5}}{K_{W_4} K_{W_1} K_{W_5}^{0.5} P_{CO}} \right)}{\left(1 + K_{W_1} P_{CO} + \sqrt{\frac{P_{H_2}}{K_{W_5}}} + \frac{P_{CO_2}}{K_{W_4} K_{W_1} P_{CO}} + K_{W_5}^{0.5} K_{W_2} \frac{P_{H_2O}}{P_{H_2}^{0.5}} \right)^2}$
4	$CO - \sigma + O - \sigma \rightleftarrows CO_2 + 2\sigma$	K_{W_4}	$\sigma_O = \frac{P_{CO_2}}{K_{W_4} \sigma_{CO}} \sigma^2 = \frac{P_{CO_2}}{K_{W_4} K_{W_1} P_{CO}} \sigma$
5	$2H - \sigma \rightleftarrows H_2 + 2\sigma$	K_{W_5}	$\sigma_H = \sqrt{\frac{P_{H_2}}{K_{W_5}}} \sigma$
Total Surface Coverage	$\sigma + \sigma_{CO} + \sigma_H + \sigma_O + \sigma_{OH} = 1$		$\sigma = \frac{1}{\left(1 + K_{W_1} P_{CO} + \sqrt{\frac{P_{H_2}}{K_{W_5}}} + \frac{P_{CO_2}}{K_{W_4} K_{W_1} P_{CO}} + K_{W_5}^{0.5} K_{W_2} \frac{P_{H_2O}}{P_{H_2}^{0.5}} \right)}$

Table A. 34 Reaction pathway and rate equations developed based on model WGS-I: with (RDS-4: 4) direct oxidation mechanism (redox mechanism)

No.	WGS–I (RDS-4: 4)	Constants	Rate Equations
1	$CO + \sigma \rightleftarrows CO - \sigma$	K_{W_1}	$\sigma_{CO} = K_1 P_{CO} \sigma$
2	$H_2O + 2\sigma \rightleftarrows H_2 - \sigma + O - \sigma$	K_{W_2}	$\sigma_O = \frac{K_2 P_{H2O}}{\sigma_{H2}}\sigma^2 = \frac{K_2 P_{H2O}}{\frac{P_{H2}}{K_5}\sigma}\sigma^2 = K_5 K_2 \frac{P_{H2O}}{P_{H2}}\sigma$
3	$CO - \sigma + O - \sigma \rightleftarrows CO_2 - \sigma + \sigma$	K_{W_3}	$\sigma_{CO2} = \frac{K_3 \sigma_{CO}\sigma_O}{\sigma} = \frac{K_3 K_1 P_{CO}\, \sigma K_5 K_2 \frac{P_{H2O}}{P_{H2}}\sigma}{\sigma} = K_1 K_2 K_3 K_5 \frac{P_{CO}P_{H2O}}{P_{H2}}\sigma$
4	$CO_2 - \sigma \rightleftarrows CO_2 + \sigma$	k_{WGS_4}	$R_{WGS} = \left(k_{WGS_4}\sigma_{CO2} - k_{WGS_{-4}}P_{CO2}\sigma\right) = \left(k_{WGS_4}\left(K_1K_2K_3K_5\frac{P_{CO}P_{H2O}}{P_{H2}}\sigma\right) - k_{WGS_{-4}}P_{CO2}\sigma\right)$ $R_{WGS} = \frac{\left(k_{WGS_4}K_{W_1}K_{W_2}K_{W_3}K_{W_5}\frac{P_{CO}P_{H_2O}}{P_{H_2}} - k_{WGS_{-4}}P_{CO_2}\right)}{\left(1 + K_{W_1}P_{CO} + K_{W_5}K_{W_2}\frac{P_{H_2O}}{P_{H_2}} + K_{W_1}K_{W_2}K_{W_3}K_{W_5}\frac{P_{CO}P_{H_2O}}{P_{H_2}} + \frac{P_{H_2}}{K_{W_5}}\right)}$
5	$H_2 - \sigma \rightleftarrows H_2 + \sigma$	K_{IW_5}	$\sigma_{H2} = \frac{P_{H2}}{K_5}\sigma$
Total Surface Coverage	$\sigma + \sigma_{CO} + \sigma_O + \sigma_{H2} + \sigma_{CO2} = 1$		$\sigma = \frac{1}{\left(1 + K_1 P_{CO} + K_5K_2\frac{P_{H2O}}{P_{H2}} + K_1K_2K_3K_5\frac{P_{CO}P_{H2O}}{P_{H2}} + \frac{P_{H2}}{K_6}\right)}$

Table A. 35 Reaction pathway and rate equations developed based on model WGS-II: with (RDS-3: 3) direct oxidation mechanism (redox mechanism)

	WGS–II (RDS-3: 3)	Constants	Rate Equations
1	$CO + \sigma \rightleftarrows CO - \sigma$	K_{W_1}	$\sigma_{CO} = K_{W_1} P_{CO} \sigma$
2	$H_2O + 2\sigma \rightleftarrows OH - \sigma + H - \sigma$	K_{W_2}	$\sigma_{OH} = \frac{K_{W_2} P_{H_2O} \sigma^2}{\sigma_H} = \frac{K_{W_2} P_{H_2O} \sigma^2}{\sqrt{\frac{P_{H_2}}{K_{W_6}}}\sigma} = K_{W_2} K_{W_6}^{0.5} \frac{P_{H_2O}}{\sqrt{P_{H_2}}} \sigma$
3	$OH - \sigma + \sigma \rightarrow O - \sigma + H - \sigma$	k_{WGS}	$R_{WGS} = k_{WGS_3} \sigma_{OH} \sigma - k_{WGS_{-3}} \sigma_O \sigma_H = k_{WGS_3} K_{W_2} K_{W_6}^{0.5} \frac{P_{H_2O}}{\sqrt{P_{H_2}}} \sigma\theta - k_{WGS_{-3}} \frac{1}{K_{W_1} K_{W_5}} \frac{P_{CO_2}}{P_{CO}} \sigma \sqrt{\frac{P_{H_2}}{K_{W_6}}} \sigma$ $R_{WGS} = \frac{\left(k_{WGS_3} K_{W_2} K_{W_6}^{0.5} \frac{P_{H_2O}}{\sqrt{P_{H_2}}} - k_{WGS_{-3}} \frac{1}{K_{W_1} K_{W_5} K_{W_6}^{0.5}} \frac{P_{CO_2} P_{H_2}^{0.5}}{P_{CO}} \right)}{\left(1 + K_{W_1} P_{CO} + \sqrt{\frac{P_{H_2}}{K_{W_6}}} + \frac{1}{K_{W_1} K_{W_5}} \frac{P_{CO_2}}{P_{CO}} + K_{W_2} K_{W_6}^{0.5} \frac{P_{H_2O}}{\sqrt{P_{H_2}}} + \frac{P_{CO_2}}{K_{W_5}} \right)^2}$
4	$CO - \sigma + O - \sigma \rightleftarrows CO_2 - \sigma + \sigma$	K_{W_4}	$\sigma_O = \frac{\sigma_{CO_2} \sigma}{K_{W_4} \sigma_{CO}} = \frac{\frac{P_{CO_2}}{K_{W_5}} \sigma\theta}{K_{W_1} P_{CO} \sigma} = \frac{1}{K_{W_1} K_{W_5}} \frac{P_{CO_2}}{P_{CO}} \sigma$
5	$CO_2 - \sigma \rightleftarrows CO_2 + \sigma$	K_{W_5}	$\sigma_{CO_2} = \frac{P_{CO_2}}{K_{W_5}} \sigma$
6	$2H - \sigma \rightleftarrows H_2 + 2\sigma$	K_{W_6}	$\sigma_H = \sqrt{\frac{P_{H_2}}{K_{W_6}}} \sigma$
Total Surface Coverage	$\sigma + \sigma_{CO} + \sigma_H + \sigma_O + \sigma_{OH} + \sigma_{CO_2} = 1$		$\sigma = \frac{1}{\left(1 + K_{W_1} P_{CO} + \sqrt{\frac{P_{H_2}}{K_{W_6}}} + \frac{1}{K_{W_1} K_{W_5}} \frac{P_{CO_2}}{P_{CO}} + K_{W_2} K_{W_6}^{0.5} \frac{P_{H_2O}}{\sqrt{P_{H_2}}} + \frac{P_{CO_2}}{K_{W_5}} \right)}$

Table A. 36 Reaction pathway and rate equations developed based on model WGS-II: with (RDS-4: 4) direct oxidation mechanism (redox mechanism)

	WGS–II (RDS-4: 4)	Constants	Rate Equations
1	$CO + \sigma \rightleftarrows CO - \sigma$	K_{W_1}	$\sigma_{CO} = K_{W_1} P_{CO} \sigma$
2	$H_2O + 2\sigma \rightleftarrows OH - \sigma + H - \sigma$	K_{W_2}	$\sigma_{OH} = \frac{K_{W_2} P_{H_2O} \sigma^2}{\sigma_H} = \frac{K_{W_2} P_{H_2O} \sigma^2}{\sqrt{\frac{P_{H_2}}{K_{W_6}}}\sigma} = K_{W_2} K_{W_6}^{0.5} \frac{P_{H_2O}}{\sqrt{P_{H_2}}} \sigma$
3	$OH - \sigma + \sigma \rightleftarrows O - \sigma + H - \sigma$	K_{W_3}	$\sigma_O = \frac{K_{W_3} \sigma_{OH} \sigma}{\sigma_H} = \frac{K_{W_3} \left(K_{W_2} K_{W_6}^{0.5} \frac{P_{H_2O}}{\sqrt{P_{H_2}}} \sigma \right) \sigma}{\sqrt{\frac{P_{H_2}}{K_{W_6}}}\sigma} = K_{W_2} K_{W_3} K_{W_6} \frac{P_{H_2O}}{P_{H_2}} \sigma$
4	$CO - \sigma + O - \sigma \rightarrow CO_2 - \sigma + \sigma$	k_{WGS}	$R_{WGS} = k_{WGS_4} \sigma_{CO} \sigma_O - k_{WGS_{-4}} \sigma_{CO_2} \sigma = k_{WGS_4} \left(K_{W_1} P_{CO} \sigma \right) \left(K_{W_2} K_{W_3} K_{W_6} \frac{P_{H_2O}}{P_{H_2}} \sigma \right) - k_{WGS_{-4}} \frac{P_{CO_2}}{K_{W_5}} \sigma\theta$ $R_{WGS} = \frac{\left(k_{WGS_4} K_{W_1} K_{W_2} K_{W_3} K_{W_6} \frac{P_{CO} P_{H_2O}}{P_{H_2}} - k_{WGS_{-4}} \frac{P_{CO_2}}{K_{W_5}} \right)}{\left(1 + K_{W_1} P_{CO} + \sqrt{\frac{P_{H_2}}{K_{W_6}}} + K_{W_2} K_{W_3} K_{W_6} \frac{P_{H_2O}}{P_{H_2}} + K_{W_2} K_{W_6}^{0.5} \frac{P_{H_2O}}{\sqrt{P_{H_2}}} + \frac{P_{CO_2}}{K_{W_5}} \right)^2}$
5	$CO_2 - \sigma \rightleftarrows CO_2 + \sigma$	K_{W_5}	$\sigma_{CO_2} = \frac{P_{CO_2}}{K_{W_5}} \sigma$
6	$2H - \sigma \rightleftarrows H_2 + 2\sigma$	K_{W_6}	$\sigma_H = \sqrt{\frac{P_{H_2}}{K_{W_6}}} \sigma$
Total Surface Coverage	$\sigma + \sigma_{CO} + \sigma_O + \sigma_{OH} + \sigma_{CO_2} + \sigma_H = 1$		$\sigma = \frac{1}{\left(1 + K_{W_1} P_{CO} + \sqrt{\frac{P_{H_2}}{K_{W_6}}} + K_{W_2} K_{W_3} K_{W_6} \frac{P_{H_2O}}{P_{H_2}} + K_{W_2} K_{W_6}^{0.5} \frac{P_{H_2O}}{\sqrt{P_{H_2}}} + \frac{P_{CO_2}}{K_{W_5}} \right)}$

Table A. 37 Reaction pathway and rate equations developed based on model WGS-II: with (RDS-5: 5) direct oxidation mechanism (redox mechanism)

	WGS–II (RDS-5: 5)	Constants	Rate Equations
1	$CO + \sigma \rightleftarrows CO - \sigma$	K_{W_1}	$\sigma_{CO} = K_{W_1} P_{CO} \sigma$
2	$H_2O + 2\sigma \rightleftarrows OH - \sigma + H - \sigma$	K_{W_2}	$\sigma_{OH} = \frac{K_{W_2} P_{H_2O} \sigma^2}{\sigma_H} = \frac{K_{W_2} P_{H_2O} \sigma^2}{\sqrt{\frac{P_{H_2}}{K_{W_6}}}\sigma} = K_{W_2} K_{W_6}^{0.5} \frac{P_{H_2O}}{\sqrt{P_{H_2}}} \sigma$
3	$OH - \sigma + \sigma \rightleftarrows O - \sigma + H - \sigma$	K_{W_3}	$\sigma_O = \frac{K_{W_3} \sigma_{OH} \sigma}{\sigma_H} = \frac{K_{W_3} \left(K_{W_2} K_{W_6}^{0.5} \frac{P_{H_2O}}{\sqrt{P_{H_2}}} \sigma \right) \sigma}{\sqrt{\frac{P_{H_2}}{K_{W_6}}}\sigma} = K_{W_2} K_{W_3} K_{W_6} \frac{P_{H_2O}}{P_{H_2}} \sigma$
4	$CO - \sigma + O - \sigma \rightleftarrows CO_2 - \sigma + \sigma$	K_{W_4}	$\sigma_{CO_2} = \frac{K_{W_4} \sigma_{CO} \sigma_O}{\sigma} = \frac{K_{W_4} \left(K_{W_1} P_{CO} \sigma \right) \left(K_{W_2} K_{W_3} K_{W_6} \frac{P_{H_2O}}{P_{H_2}} \sigma \right)}{\sigma} = K_{W_1} K_{W_2} K_{W_3} K_{W_4} K_{W_6} \frac{P_{CO} P_{H_2O}}{P_{H_2}} \sigma$
5	$CO_2 - \sigma \rightarrow CO_2 + \sigma$	k_{WGS}	$R_{WGS} = k_{WGS_5} \sigma_{CO_2} - k_{WGS_{-5}} P_{CO_2} \sigma = k_{WGS_5} K_{W_1} K_{W_2} K_{W_3} K_{W_4} K_{W_6} \frac{P_{CO} P_{H_2O}}{P_{H_2}} \sigma - k_{WGS_{-5}} P_{CO_2} \sigma$ $R_{WGS} = \frac{k_{WGS_5} K_{W_1} K_{W_2} K_{W_3} K_{W_4} K_{W_6} \frac{P_{CO} P_{H_2O}}{P_{H_2}} - k_{WGS_{-5}} P_{CO_2}}{\left(1 + K_{W_1} P_{CO} + \sqrt{\frac{P_{H_2}}{K_{W_6}}} + K_{W_2} K_{W_3} K_{W_6} \frac{P_{H_2O}}{P_{H_2}} + K_{W_2} K_{W_6}^{0.5} \frac{P_{H_2O}}{\sqrt{P_{H_2}}} + K_{W_1} K_{W_2} K_{W_3} K_{W_4} K_{W_6} \frac{P_{CO} P_{H_2O}}{P_{H_2}} \sigma \right)}$
6	$2H - \sigma \rightleftarrows H_2 + 2\sigma$	K_{W_6}	$\sigma_H = \sqrt{\frac{P_{H_2}}{K_{W_6}}} \sigma$

Total Surface Coverage	$\sigma + \sigma_{CO} + \sigma_H + \sigma_O + \sigma_{OH} + \sigma_{CO_2} = 1$	$\sigma = \dfrac{1}{\left(1 + K_{W_1}P_{CO} + \sqrt{\dfrac{P_{H_2}}{K_{W_6}}} + K_{W_2}K_{W_3}K_{W_6}\dfrac{P_{H_2O}}{P_{H_2}} + K_{W_2}K_{W_6}^{0.5}\dfrac{P_{H_2O}}{\sqrt{P_{H_2}}} + K_{W_1}K_{W_2}K_{W_3}K_{W_4}K_{W_6}\dfrac{P_{CO}P_{H_2O}}{P_{H_2}}\sigma\right)}$

Table A. 38 Reaction pathway and rate equations developed based on model WGS-III: with (RDS-3: 3) direct oxidation mechanism (redox mechanism)

	WGS–III (RDS-3: 3)	Constants	Rate Equations
1	$CO + \sigma \rightleftarrows CO - \sigma$	K_{W_1}	$\sigma_{CO} = K_{W_1} P_{CO}\, \sigma$
2	$H_2O + 2\sigma \rightleftarrows H_2 - \sigma + O - \sigma$	K_{W_2}	$\sigma_O = \dfrac{K_{W_2}P_{H2O}}{\sigma_{H2}}\sigma^2 = \dfrac{K_{W_2}P_{H2O}}{\dfrac{P_{H2}}{K_{W_5}}\sigma}\sigma^2 = K_{W_5}K_{W_2}\dfrac{P_{H2O}}{P_{H2}}\sigma$
			$R_{WGS} = \left(k_{WGS_3}\sigma_{CO}\sigma_O - k_{WGS_{-3}}\sigma_{CO2}\sigma\right)$ $= \left(k_{WGS_3}\left(K_{W_1} P_{CO}\, \sigma\right)\left(K_{W_5}K_{W_2}\dfrac{P_{H2O}}{P_{H2}}\sigma\right) - k_{WGS_{-3}}\left(\dfrac{P_{CO2}}{K_{W_4}}\sigma\right)\sigma\right)$
3	$CO - \sigma + O - \sigma \rightleftarrows CO_2 - \sigma + \sigma$	k_{WGS}	$R_{WGS} = \dfrac{\left(k_{WGS_3}K_{W_1}K_{W_5}K_{W_2}\dfrac{P_{CO}P_{H2O}}{P_{H2}} - k_{WGS_{-3}}\dfrac{P_{CO2}}{K_{W_4}}\right)}{\left(1 + K_{W_1} P_{CO} + K_5K_{W_2}\dfrac{P_{H2O}}{P_{H2}} + \dfrac{P_{CO2}}{K_{W_4}} + \dfrac{P_{H2}}{K_{W_5}}\right)^2}$
			$R_{WGS} = \left(k_{WGS_3}K_{W_1}K_{W_5}K_{W_2}\dfrac{P_{CO}P_{H2O}}{P_{H2}} - k_{WGS_{-3}}\dfrac{P_{CO2}}{K_{W_4}}\right)\sigma^2$
4	$CO_2 - \sigma \rightleftarrows CO_2 + \sigma$	K_{W_4}	$\sigma_{CO2} = \dfrac{P_{CO2}}{K_{W_4}}\sigma$
5	$H_2 - \sigma \rightleftarrows H_2 + \sigma$	K_{W_5}	$\sigma_{H2} = \dfrac{P_{H2}}{K_{W_5}}\sigma$
Total Surface Coverage	$\sigma + \sigma_{CO} + \sigma_O + \sigma_{H2} + \sigma_{CO2} = 1$		$\sigma = \dfrac{1}{\left(1 + K_{W_1} P_{CO} + K_5K_{W_2}\dfrac{P_{H2O}}{P_{H2}} + \dfrac{P_{CO2}}{K_{W_4}} + \dfrac{P_{H2}}{K_{W_5}}\right)}$

Table A. 39 Reaction pathway and rate equations developed based on model WGS-III: with (RDS-4: 4) direct oxidation mechanism (redox mechanism)

	WGS–III (RDS-4: 4)	Constants	Rate Equations
1	$CO + \sigma \rightleftarrows CO - \sigma$	K_{W_1}	$\sigma_{CO} = K_{W_1} P_{CO}\, \sigma$
2	$H_2O + 2\sigma \rightleftarrows H_2 - \sigma + O - \sigma$	K_{W_2}	$\sigma_O = \frac{K_{W_2} P_{H2O}}{\sigma_{H2}}\sigma^2 = \frac{K_{W_2} P_{H2O}}{\frac{P_{H2}}{K_{W_5}}\sigma}\sigma^2 = K_{W_5} K_{W_2} \frac{P_{H2O}}{P_{H2}}\sigma$
3	$CO - \sigma + O - \sigma \rightleftarrows CO_2 - \sigma + \sigma$	K_{W_3}	$\sigma_{CO2} = \frac{K_{W_3}\sigma_{CO}\sigma_O}{\sigma} = \frac{K_{W_3}\left(K_{W_1} P_{CO}\, \sigma\right)\left(K_{W_5} K_{W_2} \frac{P_{H2O}}{P_{H2}}\sigma\right)}{\sigma} = K_{W_1} K_{W_2} K_{W_3} K_{W_5} \frac{P_{CO} P_{H2O}}{P_{H2}}\sigma$
			$R_{WGS} = \left(k_{WGS_4}\sigma_{CO2} - k_{WGS_{-4}} P_{CO2}\sigma\right) = \left(k_{WGS_4}\left(K_{W_1} K_{W_2} K_{W_3} K_{W_5} \frac{P_{CO} P_{H2O}}{P_{H2}}\sigma\right) - k_{WGS_{-4}} P_{CO2}\sigma\right)$
4	$CO_2 - \sigma \rightleftarrows CO_2 + \sigma$	k_{WGS}	$R_{WGS} = \left(k_{WGS_4} K_{W_1} K_{W_2} K_{W_3} K_{W_5} \frac{P_{CO} P_{H2O}}{P_{H2}} - k_{WGS_{-4}} P_{CO2}\right)\sigma$
			$R_{WGS} = \frac{\left(k_{WGS_4} K_{W_1} K_{W_2} K_{W_3} K_{W_5} \frac{P_{CO} P_{H2O}}{P_{H2}} - k_{WGS_{-4}} P_{CO2}\right)}{\left(1 + K_{W_1} P_{CO} + K_{W_5} K_{W_2} \frac{P_{H2O}}{P_{H2}} + K_{W_1} K_{W_2} K_{W_3} K_{W_5} \frac{P_{CO} P_{H2O}}{P_{H2}} + \frac{P_{H2}}{K_{W_5}}\right)}$
5	$H_2 - \sigma \rightleftarrows H_2 + \sigma$	K_{W_5}	$\sigma_{H2} = \frac{P_{H2}}{K_{W_5}}\sigma$
Total Surface Coverage	$\sigma + \sigma_{CO} + \sigma_O + \sigma_{H2} + \sigma_{CO2} = 1$		$\sigma = \frac{1}{\left(1 + K_{W_1} P_{CO} + K_{W_5} K_{W_2} \frac{P_{H2O}}{P_{H2}} + K_{W_1} K_{W_2} K_{W_3} K_{W_5} \frac{P_{CO} P_{H2O}}{P_{H2}} + \frac{P_{H2}}{K_{W_5}}\right)}$

Table A. 40 Reaction pathway and rate equations developed based on model WGS-IV: with (RDS-3: 3) direct oxidation mechanism (redox mechanism)

No.	WGS–IV (RDS-3: 3)	Constants	Rate Equations
1	$CO + \sigma \rightleftarrows CO - \sigma$	K_{W_1}	$\sigma_{CO} = K_{W_1} P_{CO}\, \sigma$
2	$H_2O + 2\sigma \rightleftarrows H_2 - \sigma + O - \sigma$	K_{W_2}	$\sigma_O = \frac{K_{W_2} P_{H2O}}{\frac{P_{H2}}{K_{W_4}}} \sigma^2 = \frac{K_{W_4} K_{W_2} P_{H2O}}{P_{H2}} \sigma$
3	$CO - \sigma + O - \sigma \rightleftarrows CO_2 + 2\sigma$	k_{WGS}	$R_{WGS} = k_{WGS_3} \sigma_{CO} \sigma_O - k_{WGS_{-3}} P_{CO2} \sigma^2 = k_{WGS_3} K_{W_1} P_{CO}\, \sigma \frac{K_{W_4} K_{W_2} P_{H2O}}{P_{H2}} \sigma - k_{WGS_{-3}} P_{CO2} \sigma^2$ $R_{WGS} = \left(k_{WGS_3} K_{W_1} K_{W_4} K_{W_2} \frac{P_{CO} P_{H2O}}{P_{H2}} - k_{WGS_{-3}} P_{CO2} \right) \sigma^2$ $R_{WGS} = \frac{\left(k_{WGS_3} K_{W_1} K_{W_4} K_{W_2} \frac{P_{CO} P_{H2O}}{P_{H2}} - k_{WGS_{-3}} P_{CO2} \right)}{\left(1 + K_{W_1} P_{CO} + \frac{K_{W_4} K_{W_2} P_{H2O}}{P_{H2}} + \frac{P_{H2}}{K_{W_4}} \right)^2}$
4	$H_2 - \sigma \rightleftarrows H_2 + \sigma$	K_{W_4}	$\sigma_{H2} = \frac{P_{H2}}{K_{W_4}} \sigma$
Total Surface Coverage	$\sigma + \sigma_{CO} + \sigma_O + \sigma_{H2} = 1$		$\sigma = \frac{1}{\left(1 + K_{W_1} P_{CO} + \frac{K_{W_4} K_{W_2} P_{H2O}}{P_{H2}} + \frac{P_{H2}}{K_{W_4}} \right)}$

Table A. 41 Reaction pathway and rate equations developed based on model WGS-V: with (RDS-3: 3) direct oxidation mechanism (redox mechanism)

	WGS–V (RDS-3: 3)	Constants	Rate Equations
1	$CO + \sigma \rightleftarrows CO - \sigma$	K_{W_1}	$\sigma_{CO} = K_{W_1} P_{CO}\, \sigma$
2	$H_2O + \sigma \rightleftarrows H_2 + O - \sigma$	K_{W_2}	$\sigma_O = \frac{K_{W_2} P_{H2O}}{P_{H2}} \sigma$
3	$CO - \sigma + O - \sigma \rightleftarrows CO_2 - \sigma + \sigma$	k_{WGS}	$R_{WGS} = k_{WGS_3}\sigma_{CO}\sigma_O - k_{WGS_2}\sigma_{CO2}\sigma = k_{WGS_1} K_{W_1} P_{CO}\, \sigma \frac{K_{W_2} P_{H2O}}{P_{H2}} \sigma - k_{WGS_{-3}} \frac{P_{CO2}}{K_{W_4}} \sigma\theta$ $R_{WGS} = \left(k_{WGS_3} K_{W_1} K_{W_2} \frac{P_{CO} P_{H2O}}{P_{H2}} - k_{WGS_{-3}} \frac{P_{CO2}}{K_{W_4}} \right) \sigma^2$ $R_{WGS} = \frac{\left(k_{WGS_3} K_{W_1} K_{W_2} \frac{P_{CO} P_{H2O}}{P_{H2}} - k_{WGS_{-3}} \frac{P_{CO2}}{K_{W_4}} \right)}{\left(1 + K_{W_1} P_{CO} + \frac{K_{W_2} P_{H2O}}{P_{H2}} + \frac{P_{CO2}}{K_{W_4}} \right)^2}$
4	$CO_2 - \sigma \rightleftarrows CO_2 + \sigma$	K_{W_4}	$\sigma_{CO2} = \frac{P_{CO2}}{K_{W_4}} \sigma$
Total Surface Coverage	$\sigma + \sigma_{CO} + \sigma_O + \sigma_{CO2} = 1$		$\sigma = \frac{1}{\left(1 + K_{W_1} P_{CO} + \frac{K_{W_2} P_{H2O}}{P_{H2}} + \frac{P_{CO2}}{K_{W_4}} \right)}$

Table A. 42 Reaction pathway and rate equations developed based on model WGS-V: with (RDS-4: 4) direct oxidation mechanism (redox mechanism)

	WGS–V (RDS-4: 4)	Constants	Rate Equations
1	$CO + \sigma \rightleftarrows CO - \sigma$	K_{W_1}	$\sigma_{CO} = K_{W_1} P_{CO}\, \sigma$
2	$H_2O + \sigma \rightleftarrows H_2 + O - \sigma$	K_{W_2}	$\sigma_O = \frac{K_{W_2} P_{H2O}}{P_{H2}} \sigma$
3	$CO - \sigma + O - \sigma \rightleftarrows CO_2 - \sigma + \sigma$	K_{W_3}	$\sigma_{CO2} = \frac{K_{W_3}\sigma_{CO}\sigma_O}{\sigma} = \frac{K_{W_3}K_{W_1} P_{CO}\, \sigma \frac{K_{W_2}P_{H2O}}{P_{H2}}\sigma}{\sigma} = K_{W_3}K_{W_1}K_{W_2}\frac{P_{CO}P_{H2O}}{P_{H2}}\sigma$
4	$CO_2 - \sigma \rightleftarrows CO_2 + \sigma$	k_{WGS}	$R_{WGS} = k_{WGS_1}\sigma_{CO2} - k_{WGS_2}P_{CO2}\sigma = k_{WGS_1}K_{W_3}K_{W_1}K_{W_2}\frac{P_{CO}P_{H2O}}{P_{H2}}\sigma - k_{WGS_2}P_{CO2}\sigma$ $R_{WGS} = \left(k_{WGS_1}K_{W_3}K_{W_1}K_{W_2}\frac{P_{CO}P_{H2O}}{P_{H2}} - k_{WGS_2}P_{CO2}\right)\sigma$ $R_{WGS} = \frac{\left(k_{WGS_1}K_{W_3}K_{W_1}K_{W_2}\frac{P_{CO}P_{H2O}}{P_{H2}} - k_{WGS_2}P_{CO2}\right)}{\left(1 + K_{W_1} P_{CO} + \frac{K_{W_2}P_{H2O}}{P_{H2}}\sigma + K_{W_3}K_{W_1}K_{W_2}\frac{P_{CO}P_{H2O}}{P_{H2}}\right)}$
Total Surface Coverage	$\sigma + \sigma_{CO} + \sigma_O + \sigma_{CO2} = 1$		$\sigma = \frac{1}{\left(1 + K_{W_1} P_{CO} + \frac{K_{W_2}P_{H2O}}{P_{H2}}\sigma + K_{W_3}K_{W_1}K_{W_2}\frac{P_{CO}P_{H2O}}{P_{H2}}\right)}$

Table A. 43 Reaction pathway and rate equations developed based on model WGS-VI: with (RDS-3: 3) direct oxidation mechanism (formate mechanism)

	WGS–VI (RDS-3: 3)	Constants	Rate Equations
1	$CO + \sigma \rightleftarrows CO - \sigma$	K_{W_1}	$\sigma_{CO} = K_{W_1} P_{CO}\, \sigma$
2	$H_2O + \sigma \rightleftarrows H_2O - \sigma$	K_{W_2}	$\sigma_{H2O} = K_{W_2} P_{H2O}\, \sigma$
3	$CO - \sigma + H_2O - \sigma \rightleftarrows CHO_2 - \sigma + H - \sigma$	k_{WGS}	$R_{WGS} = k_{WGS_3}\sigma_{CO}\sigma_{H2O} - k_{WGS_{-3}}\sigma_{CHO2}\sigma_H$ $= k_{WGS_3}\left(K_{W_1} P_{CO}\, \sigma\right)\left(K_{W_2} P_{H2O}\, \sigma\right) - k_{WGS_{-3}}\left(\frac{P_{CO2}\sqrt{P_{H2}}}{K_{W_4} K_{W_5}^{0.5}}\sigma\right)\sqrt{\frac{P_{H2}}{K_{W_5}}}\sigma$ $R_{WGS} = \frac{\left(k_{WGS_3} K_{W_1} K_{W_2} P_{CO} P_{H2O} - k_{WGS_{-3}}\left(\frac{P_{CO2}\, P_{H2}}{K_{W_4} K_{W_5}}\right)\right)}{\left(1 + K_{W_1} P_{CO} + \sqrt{\frac{P_{H2}}{K_{W_5}}} + K_{W_2} P_{H2O} + \frac{P_{CO2}\sqrt{P_{H2}}}{K_{W_4} K_{W_5}^{0.5}}\right)^2}$
4	$CHO_2 - \sigma \rightleftarrows CO_2 + H - \sigma$	K_{W_4}	$\sigma_{CHO2} = \frac{P_{CO2}\sigma_H}{K_{W_4}} = \frac{P_{CO2}\sqrt{P_{H2}}}{K_{W_4} K_{W_5}^{0.5}}\sigma$
5	$2H - \sigma \rightleftarrows H_2 + 2\sigma$	K_{W_5}	$\sigma_H = \sqrt{\frac{P_{H2}}{K_{W_5}}}\sigma$
Total Surface Coverage	$\sigma + \sigma_{CO} + \sigma_H + \sigma_{CHO2} + \sigma_{H2O} = 1$		$\sigma = \frac{1}{\left(1 + K_{W_1} P_{CO} + \sqrt{\frac{P_{H2}}{K_{W_5}}} + K_{W_2} P_{H2O} + \frac{P_{CO2}\sqrt{P_{H2}}}{K_{W_4} K_{W_5}^{0.5}}\right)}$

Table A. 44 Reaction pathway and rate equations developed based on model WGS-VI: with (RDS-4: 4) direct oxidation mechanism (formate mechanism)

	WGS–VI (RDS-4: 4)	Constants	Rate Equations
1	$CO + \sigma \rightleftarrows CO - \sigma$	K_{W_1}	$\sigma_{CO} = K_{W_1} P_{CO}\, \sigma$
2	$H_2O + \sigma \rightleftarrows H_2O - \sigma$	K_{W_2}	$\sigma_{H2O} = K_{W_2} P_{H2O}\, \sigma$
3	$CO - \sigma + H_2O - \sigma \rightleftarrows CHO_2 - \sigma + H - \sigma$	K_{W_3}	$\sigma_{CHO2} = \frac{K_{W_3}\sigma_{CO}\sigma_{H2O}}{\sigma_H} = \frac{K_{W_3}\left(K_{W_1} P_{CO}\, \sigma\right)\left(K_{W_2} P_{H2O}\, \sigma\right)}{\sqrt{\frac{P_{H2}}{K_{W_5}}}\sigma} = K_{W_3}K_{W_1}K_{W_2}K_{W_5}^{0.5}\frac{P_{CO}P_{H2O}}{\sqrt{P_{H2}}}\sigma$
			$R_{WGS} = k_{WGS_4}\sigma_{CHO2} - k_{WGS_{-4}}P_{CO2}\sigma_H$
			$= k_{WGS_4}K_{W_3}K_{W_1}K_{W_2}K_{W_5}^{0.5}\frac{P_{CO}P_{H2O}}{\sqrt{P_{H2}}}\sigma - k_{WGS_{-4}}P_{CO2}\sqrt{\frac{P_{H2}}{K_{W_5}}}\sigma$
4	$CHO_2 - \sigma \rightleftarrows CO_2 + H - \sigma$	k_{WGS}	$R_{WGS} = \frac{\left(k_{WGS_4}K_{W_3}K_{W_1}K_{W_2}K_{W_5}^{0.5}\frac{P_{CO}P_{H2O}}{\sqrt{P_{H2}}} - \frac{k_{WGS_{-4}}P_{CO2}\sqrt{P_{H2}}}{\sqrt{K_{W_5}}}\right)}{\left(1 + K_{W_1} P_{CO} + \sqrt{\frac{P_{H2}}{K_{W_5}}} + K_{W_2} P_{H2O} + K_{W_3}K_{W_1}K_{W_2}K_{W_5}^{0.5}\frac{P_{CO}P_{H2O}}{\sqrt{P_{H2}}}\right)}$
5	$2H - \sigma \rightleftarrows H_2 + 2\sigma$	K_{W_5}	$\sigma_H = \sqrt{\frac{P_{H2}}{K_{W_5}}}\sigma$
Total Surface Coverage	$\sigma + \sigma_{CO} + \sigma_H + \sigma_{CHO2} + \sigma_{H2O} = 1$		$\sigma = \frac{1}{\left(1 + K_{W_1} P_{CO} + \sqrt{\frac{P_{H2}}{K_{W_5}}} + K_{W_2} P_{H2O} + K_{W_3}K_{W_1}K_{W_2}K_{W_5}^{0.5}\frac{P_{CO}P_{H2O}}{\sqrt{P_{H2}}}\right)}$

Table A. 45 Reaction pathway and rate equations developed based on model WGS-VII: with (RDS-3: 3) direct oxidation mechanism (formate mechanism)

	WGS–VII (RDS-3: 3)	Constants	Rate Equations
1	$CO + \sigma \rightleftarrows CO - \sigma$	K_{W_1}	$\sigma_{CO} = K_{W_1} P_{CO}\, \sigma$
2	$H_2O + 2\sigma \rightleftarrows H - \sigma + OH - \sigma$	K_{W_2}	$\sigma_{OH} = \frac{K_{W_2} P_{H2O}}{\sigma_H}\sigma^2 = \frac{K_{W_2} P_{H2O}}{\sqrt{\frac{P_{H2}}{K_{W_5}}}\sigma}\sigma^2 = K_{W_2} K_{W_5}^{0.5} \frac{P_{H2O}}{P_{H2}^{0.5}}\sigma$
3	$CO - \sigma + OH - \sigma \rightleftarrows CHO_2 - \sigma + \sigma$	k_{WGS_3}	$R_{WGS} = k_{WGS_3}\sigma_{CO}\sigma_{OH} - k_{WGS_{-3}}\sigma_{CHO2}\sigma$ $= k_{WGS_3}\left(K_{W_1} P_{CO}\sigma\right)\left(K_{W_2} K_{W_5}^{0.5} \frac{P_{H2O}}{P_{H2}^{0.5}}\sigma\right) - k_{WGS_{-3}}\left(\frac{P_{CO2}\sqrt{P_{H2}}}{K_{W_4} K_{W_5}^{0.5}}\sigma\right)\sigma$ $R_{WGS} = \frac{\left(k_{WGS_3} K_{W_1} K_{W_2} K_{W_5}^{0.5} \frac{P_{CO} P_{H2O}}{P_{H2}^{0.5}} - k_{WGS_{-3}} \frac{P_{CO2}\sqrt{P_{H2}}}{K_{W_4} K_{W_5}^{0.5}}\right)}{\left(1 + K_{W_1} P_{CO} + \sqrt{\frac{P_{H2}}{K_{W_5}}} + \frac{P_{CO2}\sqrt{P_{H2}}}{K_{W_4} K_{W_5}^{0.5}} + K_{W_2} K_{W_5}^{0.5} \frac{P_{H2O}}{P_{H2}^{0.5}}\right)^2}$
4	$CHO_2 - \sigma \rightleftarrows H - \sigma + CO_2$	K_{W_4}	$\sigma_{CHO2} = \frac{P_{CO2}\sigma_H}{K_{W_4}} = \frac{P_{CO2}\sqrt{P_{H2}}}{K_{W_4} K_{W_5}^{0.5}}\sigma$
5	$2H - \sigma \rightleftarrows H_2 + 2\sigma$	K_{W_5}	$\sigma_H = \sqrt{\frac{P_{H2}}{K_{W_5}}}\sigma$
Total Surface Coverage	$\sigma + \sigma_{CO} + \sigma_H + \sigma_{CHO2} + \sigma_{OH} = 1$		$\sigma = \frac{1}{\left(1 + K_{W_1} P_{CO} + \sqrt{\frac{P_{H2}}{K_{W_5}}} + \frac{P_{CO2}\sqrt{P_{H2}}}{K_{W_4} K_{W_5}^{0.5}} + K_{W_2} K_{W_5}^{0.5} \frac{P_{H2O}}{P_{H2}^{0.5}}\right)}$

Table A. 46 Reaction pathway and rate equations developed based on model WGS-VII: with (RDS-4: 4) direct oxidation mechanism (formate mechanism)

	WGS–VII (RDS-4: 4)	Constants	Rate Equations
1	$CO + \sigma \rightleftarrows CO - \sigma$	K_{W_1}	$\sigma_{CO} = K_{W_1} P_{CO}\, \sigma$
2	$H_2O + 2\sigma \rightleftarrows H - \sigma + OH - \sigma$	K_{W_2}	$\sigma_{OH} = \frac{K_{W_2} P_{H2O}}{\sigma_H}\sigma^2 = \frac{K_{W_2} P_{H2O}}{\sqrt{\frac{P_{H2}}{K_5}}\sigma}\sigma^2 = K_{W_2} K_5^{0.5} \frac{P_{H2O}}{P_{H2}^{0.5}}\sigma$
3	$CO - \sigma + OH - \sigma \rightleftarrows CHO_2 - \sigma + \sigma$	K_{W_3}	$\sigma_{CHO2} = \frac{K_{W_3}\sigma_{CO}\sigma_{OH}}{\sigma} = \frac{K_{W_3}\left(K_{W_1} P_{CO}\, \sigma\right)\left(K_{W_2} K_5^{0.5} \frac{P_{H2O}}{P_{H2}^{0.5}}\sigma\right)}{\sigma} = K_{W_3} K_{W_1} K_{W_2} K_{W_5}^{0.5} \frac{P_{H2O}\, P_{CO}}{P_{H2}^{0.5}}\sigma$
			$R_{WGS} = k_{WGS_4}\sigma_{CHO2} - k_{WGS_{-4}} P_{CO_2}\sigma_H$
			$= k_{WGS_4} K_{W_3} K_{W_1} K_{W_2} K_{W_5}^{0.5} \frac{P_{H2O}\, P_{CO}}{P_{H2}^{0.5}}\sigma - k_{WGS_{-4}} P_{CO_2}\sqrt{\frac{P_{H2}}{K_{W_5}}}\sigma$
4	$CHO_2 - \sigma \rightleftarrows H - \sigma + CO_2$	k_{WGS_4}	$R_{WGS} = \frac{\left(k_{WGS_4} K_{W_3} K_{W_1} K_{W_2} K_{W_5}^{0.5} \frac{P_{H_2O}\, P_{CO}}{P_{H_2}^{0.5}} - k_{WGS_{-4}} P_{CO_2}\sqrt{\frac{P_{H_2}}{K_{W_5}}}\right)}{\left(1 + K_{W_1} P_{CO} + \sqrt{\frac{P_{H_2}}{K_{W_5}}} + K_{W_3} K_{W_1} K_{W_2} K_{W_5}^{0.5} \frac{P_{H_2O}\, P_{CO}}{P_{H_2}^{0.5}} + K_{W_2} K_{W_5}^{0.5} \frac{P_{H_2O}}{P_{H_2}^{0.5}}\right)}$
5	$2H - \sigma \rightleftarrows H_2 + 2\sigma$	K_{W_5}	$\sigma_H = \sqrt{\frac{P_{H2}}{K_{W_5}}}\sigma$
Total Surface Coverage	$\sigma + \sigma_{CO} + \sigma_H + \sigma_{CHO2} + \sigma_{OH} = 1$		$\sigma = \frac{1}{\left(1 + K_{W_1} P_{CO} + \sqrt{\frac{P_{H2}}{K_{W_5}}} + K_{W_3} K_{W_1} K_{W_2} K_{W_5}^{0.5} \frac{P_{H2O}\, P_{CO}}{P_{H2}^{0.5}} + K_{W_2} K_{W_5}^{0.5} \frac{P_{H2O}}{P_{H2}^{0.5}}\right)}$